MODEL ANALYSIS OF ADIPOSE TISSUE AND WHOLE BODY METABOLISM *IN VIVO*

by

JAEYEON KIM

Submitted in partial fulfillment of the requirements

for the degree of Doctor of Philosophy

Dissertation Advisers:

Gerald M. Saidel, Ph.D.

Satish C. Kalhan, M.D.

Department of Biomedical Engineering

CASE WESTERN RESERVE UNIVERSITY

August, 2008

CASE WESTERN RESERVE UNIVERSITY

SCHOOL OF GRADUATE STUDIES

We hereby approve the dissertation of

JAEYONE KIM

candidate for the Ph.D. Degree*.

(signed) Gerald M. Saidel

(chair of committee)

Satish C. Kalhan

Xin Yu

Faramarz Ismail-Beigi

Marco E. Cabrera

John P. Kirwan

(date) June 23 2008

*We also certify that written approval has been obtained for any proprietary material contained therein.

DEDICATION

To God for His mercy, patience, and grace,

and to my wife, Woojung for her love, encouragement, and sacrifice.

TABLE OF CONTENTS

LIST OF TABLES

LIST OF FIGURES

ACKNOWLEDGEMENTS

I would like to thank my academic adviser, Dr. Gerald M. Saidel for his encouragement, dedication to my work, and confidence in me. His enthusiasm for research and positive way of thinking have been my inspiration. I deeply thank my research adviser, Dr. Satish C. Kalhan for his thoughtful advice, support in every single aspect of my research, and of course, fatherly love. The way he analyzed experimental data was always impressive and enlightened me. In addition, he let me know that a sense of humor is one of the requisites to be a successful researcher. I am also grateful to my adviser, Dr. Marco E. Cabrera for his advice, encouragement, and trust in me. He showed me that a good personality and respect to other's work are the key factors for successful collaboration.

Special thanks are extended to my committee members, Drs. Faramartz Ismail-Beigi, John P. Kirwan and Xin Yu for their insightful critiques and guidance throughout my Ph.D. thesis studies. Especially, I thank to Dr. Kirwan for giving me an opportunity to participate in the hyperinsulinemic-euglycemic clamp experiments in humans.

I thank to my colleagues in the laboratories of Drs. Kalhan, Cabrera, and Kirwan for their willingness to share their expertise. I enjoyed working with them and truly appreciate their help. I am especially thankful to Dr. Ranjan Dash and Dr. Takhar Kasumov for the academic discussions we had and friendship. I also thank to Dr. Valerie O'Leary for her kindness to teach me various cell and molecular biology techniques.

I would like to thank my classmates and all the Korean students in the Department of Biomedical Engineering at Case Western Reserve University. All the good memories and friendship we had make me happy. I am also thankful to Pastor Kyung-soo Kim and all the brothers and sisters in the Korean Holiness Church of the Nazarene for their prayer and love. I would like to thank Je-deuk Woo, Dong-joo Shin, and Dr. Hyun-kil Shin for their encouragement and love. I thank to my best friend, Daewon Lee for his love and friendship. Even though he lives more than several thousand miles away, just thinking of him gives me strength and joy.

Finally, I am truly indebted to my family for their belief in me and priceless support. Although some of them cannot read or understand this work, I wish to be their proud son and brother. I would like to express my deepest gratitude to my wife for her sacrifice and devotion. Even though she struggled with her cancer, she did not cease to be my supporter. I have no idea of any word that can deliver the true appreciation to her. Without her prayer and loving support, I could have not finished this work. I also would like to share my pleasure with my lovely sons, Samuel and Daniel. They gave me the extra driving force to complete my work. I have tried to be a good father to them and promise that I will be.

This work was supported by a grant (P50-GM-66309) from the National Institute of General Medical Sciences (National Institutes of Health), a financial support from the Cleveland Clinic Foundation (S.C.K.), and a fellowship from the Kwanjeong Educational Foundation.

Model Analysis of Adipose Tissue and

Whole Body Metabolism *In Vivo*

ABSTRACT

by

JAEYEON KIM

Altered cellular metabolism can lead to metabolic disorders, such as insulin resistance, diabetes mellitus, and obesity. Quantitative analysis of cellular metabolic processes can provide insight into the regulatory mechanisms involved, which can lead to targets for the prevention and treatment of the metabolic abnormalities. Experimental studies of metabolic regulation *in vivo* accompanied by mechanistic mathematical modeling and simulation studies provide important insights into various physiological and pathophysiological states. In this study, metabolic regulation in adipose tissue and whole body was investigated by mathematical modeling and simulation related to *in vivo* experimental studies.

A multi-scale computational model of whole-body metabolism was developed to predict fuel homeostasis during exercise by incorporating hormonal regulation of cellular metabolic processes. The exercise induced changes in hormonal signals modulated metabolic flux rates of different tissues in a coordinated way in order to achieve glucose homeostasis. The model predicted the dynamic changes of hepatic glycogenolysis and gluconeogenesis. A higher contribution of glycogenolysis (~75%) to glucose production during exercise was predicted. In addition, the model provided dynamic information on

the relative contribution of carbohydrates and lipids to oxidative metabolism in skeletal muscle. Model simulations indicate that external fuel supplies from other tissue/organ systems to skeletal muscle become important for prolonged exercise emphasizing the significance of interaction among tissues.

A more detailed model of adipose tissue metabolism *in vivo* was developed to study regulation of triglyceride breakdown and synthesis. The model simulated and predicted physiological responses during intravenous epinephrine infusion and hyperinsulinemic-euglycemic clamp experiments. The model identified an active metabolic subdomain (~3% of total tissue volume) in adipose tissue. Model simulations indicated that lipolytic reactions are differentially stimulated by epinephrine and differentially suppressed by insulin to produce distinctive changes in the lipolytic intermediates (i.e., diglycerides and monoglycerides). By incorporating two separate pools of triose phosphates in the adipose tissue, model simulations showed that glyceroneogenesis is the dominant pathway for glycerol-3-phosphate synthesis in response to epinephrine and insulin. Simulations also predict responses from altered enzyme activities. These models that predict alterations in metabolism can be used to determine critical experiments for specific therapeutic interventions.

CHAPTER 1.

INTRODUCTION

Carbohydrates and lipids are primary sources of energy metabolism in living organism. Maintenance of physiological fluxes of these metabolic substrates is essential for energy metabolism. Perturbations in fuel homeostasis caused by nutrients and environment can result in changes in the expression levels and activities of genes and enzymes ultimately leading to disease states, such as insulin resistance, diabetes, and obesity. While each tissue/organ system has its own metabolic characteristics and functions, coordinated metabolic interactions among them is critical in order to achieve fuel homeostasis in whole body. Quantifying cellular metabolic processes associated with perturbed homeostasis can provide insight into the regulatory mechanism involved and help identify targets for the prevention and treatment of metabolic abnormalities (Shulman, 2004). Understanding the regulation of cellular metabolic pathways is fundamental for analyzing the metabolic responses of individual tissues/organs. Although appropriate changes in life style, exercise and nutritional regimens together with pharmacological interventions can reverse several impairments in fuel metabolism, no single approach is available to examine the impact of these interventions because of the complex interactions between various organs/tissues each regulated by nutrients, hormones and metabolic biochemical intermediates. Mathematical modeling of cellular metabolism can provide an alternative means of investigating regulatory mechanism and predicting physiological responses. It can be used as a valuable complement to

experimental studies *in vitro* and *in vivo*. Development of such a model requires the consideration of unique metabolic characteristics of individual organs/tissues and the integration of the data on enzyme kinetics, metabolic pathways and fluxes with their control mechanisms and inter-domain mass transport systems. The first part of this work deals with a computational model of whole body energy metabolism with reference to the fuel homeostasis during exercise. The second part deals with the development of a computational model of adipose tissue metabolism.

1.1. WHOLE BODY ENERGY METABOLISM

1.1.1. At rest

A sedentary healthy young adult man, 70kg body weight, consumes ~250ml/min of oxygen and produces ~200ml/min of carbon dioxide at rest resulting in a respiratory quotient (RQ) of 0.80 (Wahren et al., 1971). Such an RQ suggests that after an overnight fast (8~12hr) lipids are the major fuels comprising two thirds of the oxygen consumed by the whole body, whereas carbohydrates are responsible for the rest assuming a minimal contribution by proteins. Brain, liver, heart and skeletal muscle are the primary organs that oxidize circulating metabolic fuels (e.g., glucose, fatty acids, lactate) comprising more than 70% of the oxygen consumed by the whole body (Kim et al., 2007).

Most of the glucose produced (~95%) comes from liver with a minor contribution from the kidney (Gerich, 1993;Gerich, 2000;Ekberg et al., 1999). Almost half of glucose produced is utilized by brain, while skeletal muscle uses ~20%. Based on arterial and portal venous concentration differences measured in humans (Bjorkman et al., 1990) and dogs (Abumrad et al., 1982), the gut consumes ~10% of blood glucose. The glucose

utilization by heart and adipose tissue is relatively small (less than 5% each). Lactate, a product of glycolysis is produced in skeletal muscle, red blood cells and adipose tissue. Most of the circulating lactate (~90%) is taken up by the liver for gluconeogenesis.

Free fatty acids and glycerol are produced from lipolysis of triglycerides (TG) in the adipose tissue. The whole body rate of lipolysis rate is about two times greater than the rate of fatty acid oxidation in whole body. Isotopic tracer studies in humans show that ~50% of fatty acids are re-esterified to TG (Frayn et al., 1994;Klein and Wolfe, 1990). About 15% of the re-esterification occurs within the adipose tissue (Frayn et al., 1994) and the rest in the liver. Skeletal muscle, heart and liver utilize fatty acids as the main oxidative fuel. About half of the fatty acids taken up by liver are oxidized and half re-esterified to TG.

Since adipose tissue lacks glycerol kinase, glycerol produced via lipolysis cannot be re-utilized in adipose tissue for triglyceride synthesis (Reshef et al., 2003). Therefore, liver takes up majority of the glycerol produced in adipose tissue, and utilizes it as a precursor to synthesize glucose and TG.

Even though the contribution of proteins to energy metabolism is low compared to carbohydrates and lipids, certain amino acids such as alanine and glutamine are important precursors for nitrogen transport and synthesis of glucose in liver. Skeletal muscle is the major producer of amino acids, which are taken up primarily by liver and converted to glucose.

1.1.2. Exercise

Exercise is one of the most studied perturbations to increase the energy

metabolism in whole body. Depending on the intensity of exercise, the rate of oxygen consumption can increase more than 10 folds (Wahren et al., 1971). While the utilization of circulating fuels also increases, the relative contributions of carbohydrates and lipids to fuel oxidation varies depending upon the intensity of exercise (Brooks and Mercier, 1994). FFAs are the primary fuels oxidized in the whole body at rest and during low to moderate intensity exercise. Based upon the "crossover concept" of Brooks and Mercier (Brooks and Mercier, 1994), the contribution of lipids decreases with increasing exercise intensity, whereas that of carbohydrates increases. Thus, there is a crossover point in exercise intensity where carbohydrates become the major fuel for energy metabolism. Higher power output due to increase in exercise intensity requires altering the pattern of fiber type recruitment in the skeletal muscle. It results in the stimulation of fast twitch glycolytic fiber (i.e., Type II) and an increase in the breakdown of skeletal muscle glycogen. However, it has been known that endurance training can shift this point in favor of fat oxidation by muscular adaptation to enhance lipid oxidation and by decreasing sympathetic nervous system response (Brooks and Mercier, 1994). Therefore, the relative importance of carbohydrates and lipids in energy metabolism can be affected by higher exercise intensity, which induces responses favoring carbohydrate oxidation and by endurance training, which induces responses favoring lipid oxidation.

In addition to increasing the energy metabolism, exercise provides a useful tool for investigating glucose homeostasis because glucose production and utilization can be increased more than 3-4 folds in the absence of any change in the arterial glucose concentration. The highly coordinated interaction between muscle and liver works to prevent hypoglycemia during exercise (Wasserman and Cherrington, 1991). Most of the

increased glucose utilization during exercise is by the skeletal muscle, which increases glucose uptake ~10 fold (Bergman et al., 1999b). The plasma glucose utilization in other tissues remains almost constant. While the pyruvate flux changes from net uptake to net release by the skeletal muscle, lactate release keeps increasing (Henderson et al., 2004). Increased rate of lactate release from the skeletal muscle is accompanied by an increased uptake of lactate by liver and a high rate of glucose production by the liver via gluconeogenesis. During exercise, while the whole body rate of lipolysis increases 2-3 fold, whole body fatty acid oxidation increases 3-4 fold (Friedlander et al., 1999). Thus, the fraction of fatty acids re-esterified into TG during exercise decreases.

1.2. ENERGY METABOLISM IN INDIVIDUAL ORGAN SYSTEMS

Each organ/tissue has specialized metabolic functions and biochemical reactions, which dictate the exchange and distribution of metabolic fuels. The following is a brief summary of the characteristic metabolism of individual organ systems based upon available physiological data in humans.

Brain: As a major consumer of blood glucose, brain utilizes glucose as a primary source for energy metabolism. After an overnight fast, RQ=1 with a negligible contribution by FFA (Himwich and Nahum, 1932;Sokoloff, 1973). In the absence of an increase in the neuronal activity, the rate of glucose utilization by the brain is fairly constant despite changes in plasma glucose concentration because glucose transporter 3 (GLUT3) has a high affinity constant (i.e., low Km) (Arbuckle et al., 1996). However, during prolonged fasting, there is a decrease in plasma glucose concentration accompanied by a lower rate of hepatic glucose production and a higher rate of ketone

body production. Therefore, as a consequence of metabolic adaptive response to prolonged fasting, the brain gradually switches its primary fuel from glucose to ketone bodies (Sokoloff, 1973).

Liver: Even though liver comprises less than 2% of body weight, ~20% of the whole body oxygen uptake is consumed in the liver. While liver plays a critical role in various metabolic processes, the production of glucose and triglycerides (TG) in very large density lipoproteins (VLDL) is important with respect to fuel homeostasis in the whole body. At rest, the liver produces glucose via glycogenolysis and via gluconeogenesis with almost equal contribution of each (Hundal et al., 2000;Petersen et al., 1996;Petersen et al., 1999). Lactate, pyruvate, alanine and glycerol are the major gluconeogenic precursors. Since the concomitant oxidation of glucose is negligible, liver depends on the oxidation of FFA for energy metabolism. After an overnight fast, liver clears almost half of plasma FFA by VLDL-TG synthesis or β-oxidation. In response to prolonged fasting, the rate of FFA uptake by the liver and its oxidation increase resulting in the elevated production of ketone bodies. After an overnight fast, the RQ of the liver is ~0.7 (Mann and Boothby, 1928), but decreases to much below 0.7 during starvation increasing the production of ketone bodies.

Skeletal muscle and heart: Skeletal muscle is responsible for ~20% of the oxygen consumption of the body. Even though the metabolic rate of heart per tissue weight is high compared with other tissues/organs, its effect on the whole body energy metabolism is relatively small compared with that of the skeletal muscle (Kim et al., 2007). Lipids are the primary fuel in skeletal muscle and heart at rest, RQ=0.74~0.8 (Ahlborg et al., 1974). Since these organs are relatively inactive at rest, they have sufficient amount of substrate

delivered from circulation to be used for fuel oxidation. The breakdown of glycogen stores is negligible at rest, but becomes the dominant source of carbohydrate oxidation in response to exercise. As a primary source of blood lactate, skeletal muscle releases 30~40% of its glucose taken up from the circulation as lactate. In contrast, heart takes up plasma lactate as an additional source for fuel oxidation.

Adipose tissue: Adipose tissue comprises about 20% of body weight but its oxygen utilization rate in the basal state is less than 2% of the whole body oxygen utilization rate (Frayn et al., 1995). Although adipose tissue has an abundant supply of FFA, glucose appears to be the major fuel for the energy metabolism, RQ=~0.9 (Coppack et al., 1990). Approximately 50% of the glucose taken up by the adipose tissue is used for oxidative metabolism and about 20~40% is released as lactate (Frayn et al., 1995;Coppack et al., 1990). The uptake of glucose cannot account for the total oxygen consumption by the adipose tissue (Coppack et al., 1990). Although some FFA oxidation has been measured in the adipose tissue in rats (Harper and Saggerson, 1976), it has not been demonstrated *in vivo* in humans. Breakdown of glycogen is considered to be a negligible source for fuels in adipose tissue (Jurczak et al., 2007). Although acetoacetate and β-hydroxybutyrate are taken up by the adipose tissue *in vivo*, the oxidation of ketone bodies cannot account for the oxidative requirements. Another potential source of oxidative fuel for adipose tissue are amino acids (alanine and glutamine), which are released from adipose tissue in the fasting state (Patterson et al., 2002) with a net uptake of glutamate (Frayn et al., 1991). *In vitro* studies show the oxidation of amino acids in the adipose tissue, but their quantitative significance *in vivo* remains unclear.

1.3. ROLE OF ADIPOSE TISSUE METABOLISM AND ITS REGULATION

Adipose tissue is not just a metabolically quiescent storage depot for lipids, but an active organ that regulates plasma free fatty acid (FFA) levels and secretes several cytokines and hormones such as leptin, adiponectin, resistin, tumor necrosis factor (TNF)-α etc. (Frayn, 2002;Frayn et al., 2003;Trayhurn and Beattie, 2001). Despite its negligible contribution to energetics, it actively participates in whole body fuel homeostasis by regulating the production of plasma FFAs, which are potent modulator of insulin resistance. Regulation of breakdown (lipolysis) and synthesis (esterification) of TG in adipose tissue controls the fatty acid flux into circulation. The importance of quantitatively understanding adipose tissue metabolism and its regulation is underscored by its role in the development of insulin resistance, regulation of satiety, and other metabolic functions (Kahn et al., 2006;Frayn, 2001).

1.3.1. Obesity, insulin resistance and the role of adipose tissue

Obesity is associated with adverse health conditions including dyslipidemia, insulin resistance and type 2 diabetes mellitus. These metabolic abnormalities have even stronger correlation with regional adiposity (i.e., the visceral adiposity). Obese subjects have higher visceral adiposity, and FFAs released from the upper body obese subjects into the circulation are suppressed less by insulin (Jensen et al., 1989). FFAs from the visceral adipose depots are released into the portal vein so that the blood supplying the liver has higher levels of FFA. Therefore, visceral adiposity can have a critical effect on modulating hepatic metabolism leading to the development of insulin resistance.

Insulin resistance or impaired insulin action is a state that results in higher

requirements of insulin and higher insulin levels to elicit a normal response (Summers, 2006). Since insulin has an important effect on cellular metabolic processes including the disposal of plasma glucose and the suppression of lipolysis, any impairment in its action (i.e., insulin resistance) produces pathophysiological conditions leading to Type 2 diabetes mellitus, cardiovascular disease and ectopic fat deposition in liver, muscle and pancreas (Kahn et al., 2006). The glucose-fatty acid cycle (Randle et al., 1963), the classical concept of lipid-induced insulin resistance, describes the relationship between glucose and FFA metabolism. According to this concept, elevated FFA induces insulin resistance in muscle by increasing oxidation of fat relative to glucose, and results in accumulation of glucose-6-phosphate and lower insulin-stimulated glucose uptake. Human experiments using the hyperinsulinemic-euglycemic clamp with intralipid infusion show that lipid-induced insulin resistance is associated with the inhibition of glucose transport and phosphorylation (Boden et al., 1994). Furthermore, FFAs inhibit insulin-stimulated glucose disposal by affecting insulin signaling pathways (Belfort et al., 2005). Since adipose tissue is the major source of plasma FFA, it can actively participate in the regulation of whole body lipid flux. Consequently, impaired insulin action (i.e., insulin resistance) can result in dysregulation of the plasma levels of lipids and FFA, which alter metabolic regulation in other tissues/organs. Therefore, adipose tissue metabolism can play a critical role in whole body fuel homeostasis.

1.3.2. TG-FFA cycle

During fasting, adipose tissue releases FFA and glycerol into plasma as a result of increase in lipolysis. Since the amount of FFA released by adipose tissue is much greater

than that oxidized in the body, a significant portion of the released FFA is re-esterified in adipose tissue and other organs (Frayn et al., 1994). The overall consequence of TG lipolysis and re-esterification of FFA is the futile consumption of ATP. This futile TG-FFA cycle is composed of intra-tissue and extra-tissue cycles (Frayn et al., 1994). In the former, FFA is re-esterified within adipose tissue after being produced from TG hydrolysis, whereas in the latter, FFA released from adipose tissue is re-esterified in liver and released as very low density lipoprotein (VLDL)-TG. The released VLDL-TG is hydrolyzed by lipoprotein lipase (LPL) in the capillary wall of adipose tissue and then taken up as FFA (Figure 1.1).

Several roles of TG-FFA cycle have been suggested (Newsholme and Crabtree, 1976;Coppack et al., 1990). First, it can produce heat by increasing hydrolysis of ATP. However, thermogenesis is an important feature only for the brown adipose tissue which comprises only a small portion of body fat mass. Since the energy cost for TG-FFA cycle is less than 2% of the resting energy expenditure (Elia et al., 1987;Klein and Wolfe, 1990), thermogenesis is not important in white adipose tissue, which comprises most of body fat mass. Second, TG-FFA cycle can increase the sensitivity for control of lipid mobilization by producing high rates of breakdown and synthesis of TG with small net effect. Despite the large fluctuations in lipid utilization, plasma FFA and TG levels are maintained fairly constant by slightly altering the turnover rates of TG. Regulation of plasma lipid levels with increased sensitivity and flexibility on the regulation of whole body lipid metabolism are important roles of TG-FFA cycle.

Intra-tissue and extra-tissue TG-FFA cycles are under hormonal and substrate control. In overnight fasted humans, 40~60% of FFA release are recycled to TG at a rate

that increases with the starvation (Jensen et al., 2001;Elia et al., 1987;Klein and Wolfe, 1990). Control of lipid mobilization has apparently more sensitivity and is more significant during starvation. Insulin decreases the rate of TG-FFA cycling primarily by suppressing lipolysis (Boden et al., 1993), whereas epinephrine increases it by stimulating lipolysis (Miyoshi et al., 1988).

1.3.3. Regulation of lipolysis

The breakdown of TG is regulated via a complex mechanism involving several lipases and proteins. Until recently, hormone sensitive lipase (HSL) was considered the only rate limiting enzyme for lipolysis of TG in adipose tissue. Recent studies, however, show that HSL-deficient mice retain lipolysis rate in the basal state and respond to beta-adrenergic stimulation, although the response was quantitatively less than in normal controls (Okazaki et al., 2002;Zechner et al., 2005;Haemmerle et al., 2002). The accumulation of diglycerides (DG) in the adipose tissue of HSL knockout mice implies that HSL may be the rate-limiting enzyme for the hydrolysis of DG (Haemmerle et al., 2002). Adipose TG lipase (ATGL) has been suggested as the key enzyme involved in TG hydrolysis (Schweiger et al., 2006;Haemmerle et al., 2006;Zimmermann et al., 2004). In ATGL-deficient mice, TG lipolysis was severely impaired (Haemmerle et al., 2006).

Perilipin, a protein coating lipid droplets, plays an important role in the regulation of TG breakdown. The perilipin-null mice have elevated basal rate of lipolysis because the lack of perilipin allows intracellular lipases easy access to the TG stores in lipid droplets. Even with normal HSL activity, there is no beta-adrenergic stimulation of lipolysis in these mice (Sztalryd et al., 2003;Tansey et al., 2001). These data suggest that

perilipin is required not only to protect the TG stores in lipid droplets in the basal state, but also to facilitate the simulation of lipolysis by beta-adrenergic agonists.

Beta-adrenergic stimulation increases the rate of lipolysis by activating cyclic AMP (cAMP)-dependent protein kinase A (PKA), which affects various lipases and other proteins (Honnor et al., 1985). HSL is highly regulated by PKA. HSL activity increases on phosphorylation by PKA (Londos et al., 1999). In addition, perilipin undergoes conformational changes as a result of phosphorylation by PKA, which promotes lipolysis by facilitating the accessibility of intracellular lipases to TG stores (Miyoshi et al., 2007). Even though ATGL activity is only regulated transcriptionally, activation of perilipin increases the rate of lipolysis by ATGL by its interaction with comparative gene identification 58 (CGI-58) (Langin and Arner, 2006). In addition to the direct activation of HSL by PKA, the activation of perilipin facilitates HSL localization near the lipid droplets, increasing the HSL activity near TG stores (Sztalryd et al., 2003). In contrast, the breakdown of MG by HSL and by monoglyceride lipase (MGL) is not subject to the activity change via phosphorylation (Large et al., 2004;Zechner et al., 2005).

Insulin, the most potent antilipolytic hormone, suppresses lipolysis by inhibiting the phosphorylation of HSL and perilipin and promoting their dephosphorylation (Stralfors and Honnor, 1989). Insulin reduces the levels of cAMP and therefore, PKA activity by activating phosphodiesterase (PDB). In addition, it activates protein phosphatase 1 (PP1) resulting in the dephosphorylation of HSL and perilipin. While insulin can down-regulate ATGL activity transcriptionally (Kershaw et al., 2006), it can acutely suppress the reaction catalyzed by ATGL indirectly via dephosphorylation of perilipin.

1.3.4. Synthesis of glycerol-3-phosphate

Re-esterification of fatty acids requires a source of glycerol-3-phosphate (G3P). Since the activity of glycerol kinase is low in the adipose tissue (Edens et al., 1990b), it cannot form G3P from glycerol in significant quantities. Instead, glucose and/or pyruvate are utilized to produce G3P. The synthesis of G3P from sources other than glucose and glycerol is termed glyceroneogenesis (Reshef et al., 2003), which is an abbreviated version of gluconeogenesis. The arteriovenous gradients across the adipose tissue bed in humans show a net uptake of glucose and release of lactate (Coppack et al., 1990). The interstitial levels of lactate in the adipose tissue are substantially higher than those in the plasma and are even higher in obese compared with lean subjects (Qvisth et al., 2007). These data have been interpreted to suggest that adipose tissue utilizes glucose to produce lactate as well as G3P for TG synthesis. However, studies in rats (Nye et al., 2008) showed that lactate/pyruvate is the dominant carbon source for G3P in a variety of nutritional states and even in the presence of increased glucose uptake by the adipose tissue. In those studies, the contribution of glucose to G3P was negligible even when *de novo* lipogenesis from glucose was high. The *in vivo* formation of G3P from pyruvate via glyceroneogenesis has not been quantitatively evaluated in humans (Reshef et al., 2003).

Phosphoenolpyruvate carboxykinase (PEPCK) is a key regulatory enzyme for glyceroneogenesis, whose activity is regulated transcriptionally. PEPCK activity in adipose tissue of the rat was ~0.04 units/g in the postprandial state, but increases to ~0.18-0.28 in response to fasting (Reshef et al., 1969;Reshef and Hanson, 1972). Transgenic mice with over-expression of PEPCK in their adipose tissue are obese but

insulin sensitive due to the lower levels of circulating FFA (Franckhauser et al., 2002). These studies imply that the higher rate of intracellular re-esterification by increased expression of PEPCK is responsible for the lower FFA release from adipose tissue. Moreover, anti-diabetic drugs, thiazolidinediones (TZDs) increase the re-esterification of FFA in adipose tissue via the induction of PEPCK (Tordjman et al., 2003).

1.4. METHODS AND CHALLENGES IN INVESTIGATING ADIPOSE TISSUE METABOLISM

In vivo and *in vitro* methods have been applied to investigate adipose tissue metabolism: arteriovenous difference, microdialysis, and tissue analysis.

1.4.1. Substrate exchange across adipose tissue (by arteriovenous difference)

The fuel metabolism in a specific tissue can be examined by the net transport of substrates across a tissue/organ that can be quantitatively determined by measuring the differences in their arterial and venous concentrations and the blood flow. This assumes that a tissue has a unique artery (inflow) and vein (outflow). However, the venous drainage can often be contaminated with the contribution from other tissues or may not be accessible. In addition, determination of local blood flow often suffers from experimental difficulties. Even though this technique has been widely used to investigate *in vivo* metabolism, its application in human studies, particularly for adipose tissue, is limited (Arner and Bulow, 1993).

Since adipose tissue does not have a unique artery and vein, reliable *in vivo* data across this tissue are limited. In humans, the only location available for arteriovenous difference measurement is the subcutaneous fat bed in the abdominal wall (Samra et al.,

1996;Frayn et al., 1994;Coppack et al., 1990). Even here, the venous drainage could be contaminated by blood flow from skin. Furthermore, the heterogeneity of different adipose depots (subcutaneous vs. visceral) prevents generalizations based on data from a single depot (Jensen, 2002).

1.4.2. Interstitial levels of metabolic substrates (by microdialysis)

In vivo microdialysis has been extensively applied to study adipose tissue metabolism in humans. It measures the levels of diffusible metabolites in the interstitium by inserting a small semi-permeable probe, which is infused with an isotonic solvent (Arner and Bulow, 1993). The permeability of the membrane determines the type of biochemical substance that can be measured by microdialysis. In general, small hydrophilic molecules such as glucose, lactate, glycerol, amino acids and other pharmacological substances can be handled by the membranes with a molecular mass between 3000 and 20000 Da. The diffusible molecules cross the membrane and their concentrations are measured in the fluid leaving the microdialysis probe.

The microdialysis method was initiated to study subcutaneous adipose tissue metabolism in humans. However, it cannot be used to measure hydrophobic species such as free fatty acids or high molecular weight species such as proteins and hormones (Summers, 2006). Furthermore, microdialysis data are qualitative and cannot yield reliable estimates of the arteriovenous difference. Even though microdialysis can be used to determine intracellular lipolysis by changes in interstitial levels of glycerol, it cannot account for the production of glycerol in the capillary by LPL.

1.4.3. Tissue analysis

Tissue biopsy is the most reliable method for evaluating the intracellular processes *in vivo* from adipose tissue. To examine the dynamic information, however, multiple biopsy samples are required. Although a plethora of data are available from *in vitro* studies of tissue explants or isolated cells, these data may not correspond to *in vivo* conditions (Frayn et al., 2003). For example, *in vitro* studies ignore the effect of various regulatory factors such as blood flow (Summers, 2006). Consequently, the use of data from *in vitro* studies for application to *in vivo* processes is limited.

1.5. MATHEMATICAL MODELING AS AN ALTERNATIVE APPROACH

An important complement to *in vivo* experimental studies is a systems biology approach with analysis using computational modeling. This approach is appropriate for investigating complex multi-scale (i.e., molecular, cellular, tissue/organ levels) biological systems. Using this systems approach, computational models are developed by incorporating the information from different scales. The various components at each level can be evaluated in the context of the entire system. Simulations of an *in vivo* system with a computational model can provide the basis for quantitative analysis of biological control mechanisms and for prediction of system responses to physiological perturbations. A systems model combined with *in vivo* data can be used for testing hypotheses, validating predictions, designing critical experiments, and identifying targets of therapeutic interventions under pathophysiological conditions.

Modeling *in vivo* systems can involve bottom-up and/or top-down approaches (Michelson, 2006). The bottom-up approach starts with incremental addition of one gene

or protein function and its regulatory mechanism until it reaches the complexity of whole cell, organ/tissue, and finally whole organism to reproduce the physiological responses. A bottom-up approach can lead to a model with too many variables that have little effect on the key physiological aspects of *in vivo* systems. Since available experimental data are limited, knowledge gaps between different scales can be significant.

In contrast, the top-down approach begins with the physiological observations and incorporates data from different scales as needed. Thus, the parameterization of the model components is constrained by the overall systemic behavior ensuring the robustness (Michelson, 2006). Its usefulness is evident when data and knowledge about the system of interest are limiting. A mathematical model can overcome a knowledge gap by incorporating a phenomenological relationship to relate the variables in different scales. A mechanistically based model can reproduce the physiological responses as well as provide an insight into molecular mechanisms.

1.6. RESEARCH OBJECTIVES AND THESIS ORGANIZATION

The broad objective of this study is to investigate the regulatory mechanisms of *in vivo* fuel metabolism in the adipose tissue and in the whole body using mathematical modeling and simulation. Whole-body fuel homeostasis during exercise was studied with respect to the metabolic interaction of different tissues/organs. In addition, the regulation of TG breakdown and synthesis was examined in the adipose tissue. The following hypotheses are presented to investigate the metabolic regulations associated with these systems:

(1) Hormonal signals (e.g., insulin, glucagon, and epinephrine) provide interaction

and coordination among tissues/organs. With respect to glucose homeostasis during moderate intensity exercise, we hypothesize that *exercise-induced change in epinephrine affects the pancreatic secretion of glucagon and insulin; consequently, a change in the glucagon-to-insulin ratio (GIR = glucagon/insulin) can modulate the metabolic flux rates of different tissues in a coordinated way for the prevention of hypoglycemia*.

(2) The breakdown of TG is a complex mechanism involving the regulation of various lipases and other proteins. Data from transgenic mice studies (e.g., knockouts of ATGL and HSL) suggest that each enzyme has a distinctive role in the cumulative lipolytic responses. This leads to the hypothesis that *the lipolytic reactions catalyzed by various lipases are differentially regulated in the adipose tissue in response to physiological perturbations.*

(3) The synthesis of TG, however, requires sources of carbon to synthesize G3P, which can be formed either from glucose via glycolysis or from pyruvate via glyceroneogenesis. Obesity is associated with the induction of PEPCK, a regulatory enzyme for glyceroneogenesis, which is a major contributor to the synthesis of G3P in rats. This leads to the hypothesis that *glyceroneogenesis is the dominant pathway for the synthesis of G3P in human adipose tissue*.

To test these hypotheses, a multi-scale modeling framework is developed to study whole body metabolism by simulating the fuel homeostasis during a moderate intensity exercise. In addition, the mathematical model of adipose tissue metabolism *in vivo* is developed to simulate the physiological responses to infusions of epinephrine and insulin.

The fuel homeostasis during a moderate intensity exercise is examined using a

mathematical model of whole body metabolism (Chapter 2). Hormonal control by glucagon and insulin is incorporated into the model to coordinate the metabolic interaction among different tissues/organs. The efficacy of hormonal control is evaluated and the metabolic responses in each tissue are predicted during exercise.

A model of adipose tissue metabolism integrates physiological data and mechanisms associated with cellular reaction and mass transport, and is presented in Chapeter 3. Model simulations identify a localized cellular domain and investigate differential stimulation of TG and DG breakdown by intracellular lipases during intravenous epinephrine infusion. The relative importance of glucose and pyruvate to the synthesis of G3P is examined when the rate of TG-FFA cycle increased by epinephrine. The model predicts responses arising from the different expression levels of lipases.

In chapter 4, an enhanced model incorporates additional metabolic pathways and chemical species based on their significance in the fed state to simulate physiological responses to insulin. The suppression of lipolytic reactions by insulin is studied during hyperinsulinemic-euglycemic clamp experiment. The source of carbon to synthesize G3P is examined with increased glucose uptake by adipose tissue.

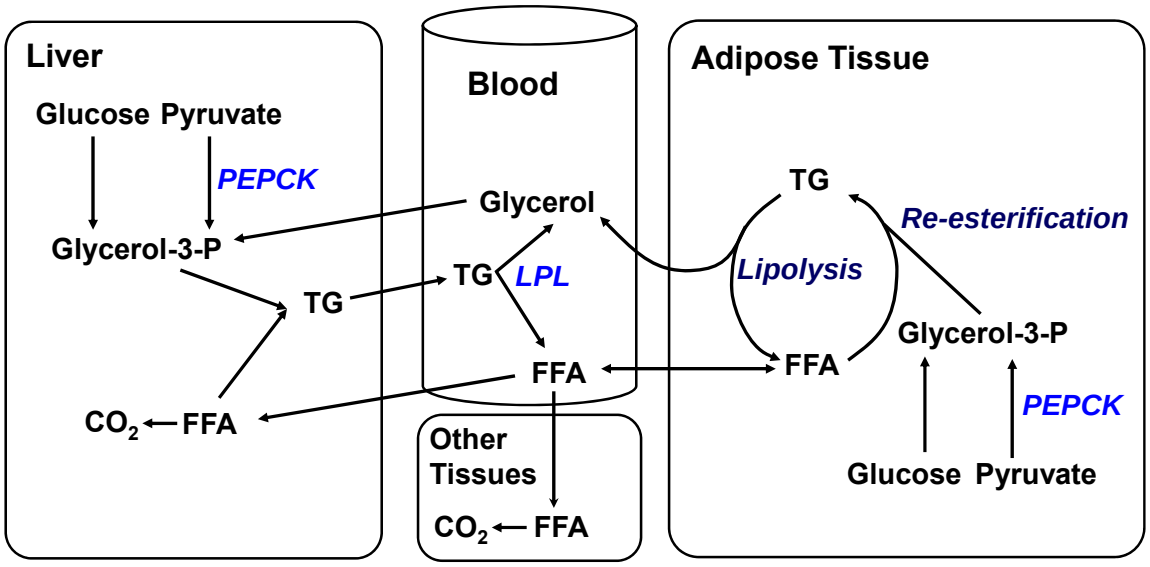

FIGURE 1.1. TG-FFA cycle in whole body

TG in adipose tissue is hydrolyzed by intracellular lipases releasing FFA into circulation (i.e., lipolysis). A part of FFA is re-utilized in the adipose tissue to synthesize TG (i.e., re-esterification) completing intratissue TG-FFA cycle. Since adipose tissue releases more FFA than what is required for oxidation, the additional FFA is re-esterified in liver and released as VLDL-TG into plasma, which is called extratissue TG-FFA cycle. The secreted VLDL-TG is hydrolyzed in the capillary by LPL, and then, FFA can be re-taken up by the adipose tissue. Since adipose tissue has a negligible activity of glycerol kinase, it cannot directly utilize glycerol for the synthesis of glycerol-3-phosphate. Thus, either glucose or pyruvate can be used for the carbon source of glyceride-glycerol. The pathway to use carbon source other than glucose and glycerol for the synthesis of glycerol-3-phosphate is called glyceroneogenesis, in which phosphoenolpyruvate carboxykinase (PEPCK) is the regulatory enzyme.

CHAPTER 2.

MULTI-SCALE COMPUTATIONAL MODEL OF FUEL HOMEOSTASIS DURING EXERCISE: EFFECT OF HORMONAL CONTROL

2.1. INTRODUCTION

Carbohydrates and lipids are primary fuel sources in a human body. To maintain normal levels of circulating fuels is essential to life because the persistent perturbation in fuel homeostasis of human body can induce the development of insulin resistance, leading to diabetes or obesity (Warram et al., 1990). However, quantifying the cellular metabolic processes associated with fuel homeostasis can provide a better understanding of regulatory mechanisms, and lead to targets for the prevention of those metabolic abnormalities (Shulman, 2004). Although appropriate exercise and nutritional regimens with pharmacological interventions can reverse impairments in fuel metabolism, no fundamental approach is available to optimize these interventions.

While exercise and diet are perturbations affecting whole-body metabolism, corresponding changes occur in cellular signaling pathways and metabolism. Integration of these multi-scale phenomena is essential to identify possible links between cellular processes and whole body responses, especially of those that are easily measurable. Experimental measurements of human metabolic responses of specific tissue-organs are limited, especially for obtaining dynamic responses. Therefore, a mathematical model that incorporates cellular metabolism of tissue/organ systems in whole-body responses is a necessary complement to experimental studies.

The goal of our study is to develop a multi-scale mathematical model that relates

cellular metabolism in tissue/organ systems connected via the circulation to whole body responses during exercise. The long-term goal of this model is to investigate mechanisms for promoting the adaptation to pathogenic conditions (insulin resistance) and reversing it with exercise and dietary intervention. In the initial phase of this work, however, we focused on the development of a model that includes the necessary tissue/organ subsystems and hormonal controllers to predict glucose homeostasis during a moderate intensity exercise bout in normal humans. Exercise provides a useful tool for investigating glucose homeostasis because glucose utilization and production can be increased more than 3-4 times without perturbing the arterial glucose concentration. The highly coordinated interaction between muscle and liver works to prevent hypoglycemia during exercise (Wasserman and Cherrington, 1991). While a few mathematical models have simulated the effects of increased metabolic rate in skeletal muscle during exercise, these models have dealt with limited metabolic pathways in muscle only (Lambeth and Kushmerick, 2002;Korzeniewski and Liguzinski, 2004) and none of them is comprehensive enough to include the effects of other organs and hormonal action on glucose homeostasis at the cellular, tissue/organ, and whole-body level.

In this study, we developed a computational model using the general framework and top-down approach of Cabrera et al. (Cabrera et al., 1998;Cabrera et al., 1999) that integrates cellular metabolic and transport processes in major tissue/organ systems. For the intended applications, the model must be significantly enhanced by incorporating additional tissue compartments, metabolic pathways, and substrates. In addition to metabolic regulation by ATP/ADP and $NADH/NAD^+$ at the cellular level, hormonal signals (insulin, glucagon, and epinephrine) provide interaction and coordination among

tissues/organs. With respect to glucose homeostasis during moderate intensity exercise, one hypothesis is that exercise-induced change in epinephrine affects the pancreatic secretion of glucagon and insulin, and consequently, a change in the glucagon-to-insulin ratio (GIR = glucagon/insulin) can modulate the metabolic flux rates of different tissues in a coordinated way for the prevention of hypoglycemia.

In addition to predicting the hormonal regulation for glucose homeostasis, the dynamics of fuel oxidation in skeletal muscle is simulated to quantify the relative importance of carbohydrates and lipids during exercise. Furthermore, model simulations can elucidate how other organ systems affect the fuel availability of skeletal muscle. In liver, glucose production via gluconeogenesis is affected by both the delivery of precursor in blood and altered enzyme activity induced by the GIR. We hypothesized that the dynamic change in hepatic glycogenolysis and gluconeogenesis rates during exercise can be predicted using a multi-scale whole body model if it is validated to give the correct representation of whole body glucose balance and arterial substrate concentration dynamics with the corresponding change in hormonal level.

2.2. MODEL DEVELOPMENT

The whole-body model consists of seven metabolically distinct tissue/organ compartments connected through the blood circulation (Figure 2.1): 1) brain, 2) heart, 3) skeletal muscle, 4) gastrointestinal (GI) tract, 5) liver, 6) adipose tissue, and 7) “other tissues”. The skeletal muscle compartment represents the lean muscles in the lower extremity. GI tract includes the splanchnic region (stomach, spleen, intestines) except for liver, and the visceral adipose tissue representing 10% of body fat mass. Adipose tissue

compartment is composed of the rest of body fat mass including subcutaneous and lower body fat (i.e., intermuscular fat). The "other tissues" compartment includes kidney, upper extremity muscles, and the rest of tissues. In addition to the hepatic artery, the blood input to the liver comes from venous blood of the GI tract. In this initial model, arterial oxygen and carbon dioxide concentrations are assumed to be constant. The pancreas serves as a controller of arterial glucagon and insulin concentrations, which depend on arterial glucose and epinephrine concentrations.

2.2.1. Subject characteristics and exercise intensity

As shown in Table 2.1, a typical healthy young adult man with 70 Kg body weight is used for our simulations of fuel metabolism during a moderate intensity exercise. The subject is in overnight fasted condition (8~12hr fast) with 5.5 L min^{-1} cardiac output, 250 ml min^{-1} oxygen consumption, and 0.8 Respiratory Quotient (RQ). It is assumed that the subject has a peak oxygen consumption (VO_{2max}) of 3.4 l/min (Hirsch et al., 1991). In this study, 60% VO_{2max} is used as an exercise intensity, which corresponds to the whole body oxygen consumption of 2.04 l/min with 150 W power output. In addition, it is assumed that 60% VO_{2max} is lower than the lactate threshold of the subject.

2.2.2. Fuel metabolism in tissues

Each tissue has specialized metabolic functions and biochemical reactions, which dictate the exchange and distribution of metabolic fuels. Figure 2.2 and 2.3 show the general and tissue-specific metabolic pathways of this model. The characteristics of fuel metabolism in each tissue are determined by its physiological behavior as found from

experimental studies.

Glucose: In an overnight fasted condition, most of glucose production (~95%) comes from liver with a minor contribution from the kidney (Gerich, 1993;Gerich, 2000;Ekberg et al., 1999). Liver produces glucose from two pathways (glycogenolysis and gluconeogenesis) with almost equal contribution at rest (Hundal et al., 2000;Petersen et al., 1996;Petersen et al., 1999). Lactate, pyruvate, alanine and glycerol are the major gluconeogenic precursors in liver. On the other hand, most glucose (50%) at rest is utilized by the brain, while skeletal muscle uses about 20%. Based on arterial and portal venous concentration differences conducted in humans (Bjorkman et al., 1990) and dogs (Abumrad et al., 1982) studies, the GI tract consumes only 10% of blood glucose. To consider the slowly falling blood glucose after an overnight fast, the whole body balance of glucose (i.e., sum of glucose production and utilization) at rest is set to -0.03mmol/min, which makes blood glucose level decrease at a rate of 0.005 mM/min.

During exercise, however, the whole body glucose turnover rate increases 3-4 fold according to the exercise intensity applied. According to the 'Glucose Shunt' concept, most of the increased glucose utilization is shunted to the essential tissue/organ during exercise (i.e., skeletal muscle) making glucose uptake by skeletal muscle increase by ~10 fold (Bergman et al., 1999b). Thus, the plasma glucose utilization in other tissues is kept almost constant.

Lactate and pyruvate: At rest, liver and heart are primary consumers of blood lactate, while skeletal muscle, adipose tissue and "other tissues" produce lactate. Lactate production from "other tissues" includes the contribution from inactive upper body muscles and red blood cells. Pyruvate exchange occurs primarily between skeletal muscle

(uptake) and “other tissues” (release) due to its small arterial concentration; elsewhere, its effect is negligible.

During exercise in skeletal muscle, lactate release keeps increasing, while the pyruvate flux changes from net uptake to net release (Henderson et al., 2004). Increased lactate release from skeletal muscle affects lactate uptake by liver leading to increased glucose production via gluconeogenesis.

Alanine: Even though the contribution of protein to energy metabolism is negligible compared to carbohydrates and lipids, amino acids are important gluconeogenic precursors in liver. In this model, alanine represents all the gluconeogenic amino acids. Only liver consumes alanine for gluconeogenesis, while inactive muscles in “other tissues” are the main sources in addition to skeletal muscle. Skeletal muscle produces more alanine during exercise, which then, is converted to glucose in liver.

Fatty acids and glycerol: Free fatty acids and glycerol are produced from lipolysis of triglycerides (TG) in adipose tissue. However, the whole body lipolysis rate is about 2 times greater than the whole body fatty acid oxidation rate, which means that ~50% of fatty acids are re-esterified to TG (Frayn et al., 1994;Klein and Wolfe, 1990). About 15% of re-esterification occurs in adipose tissue (Frayn et al., 1994) and liver takes up the extra fatty acids from the blood. Liver utilizes fatty acids as a main fuel. About half of the fatty acids taken up by liver are oxidized and half re-esterified to TG. Since adipose tissue lacks glycerol phosphorylase, glycerol produced from lipolysis cannot be directly utilized in adipose tissue for triglyceride synthesis (Reshef et al., 2003). Therefore, liver takes up all glycerol produced in adipose tissue, and utilizes it as a gluconeogenic precursor and a substrate for TG synthesis.

While whole body lipolysis rate is increased 2-3 fold during exercise, whole body fatty acid oxidation is increased 3-4 fold (Friedlander et al., 1999). Thus, the fraction of fatty acids being re-esterified into TG decreases.

2.2.3. Dynamic mass balances

The concentration dynamics of substrates in each tissue compartment (except "other tissues") are described by dynamic mass balances. The "other tissues" compartment is represented as a source or sink of substrates without any dynamics and metabolic reactions that satisfies the whole-body mass balance at rest. Assuming a perfectly mixed lumped tissue-capillary compartment, we can express the dynamic mass balance for *substrate i* in *tissue x* as (Cabrera et al., 1998;Salem et al., 2002):

$$V_{eff,x,i}\frac{dC_{x,i}}{dt} = P_{x,i} - U_{x,i} + Q_x(C_{a,i} - \sigma_{x,i}C_{x,i}) \qquad (2.1)$$

where $V_{eff,x,i}$ is the effective volume of *substrate i* in *tissue x*, $P_{x,i}$ is the production rate of *substrate i*, $U_{x,i}$ is the utilization rate of *substrate i*, Q_x is the blood flow to *tissue x*, $C_{a,i}$ is the arterial concentration of *substrate i*, $\sigma_{x,i}$ is the partition coefficient of *substrate i*, and $C_{x,i}$ is the concentration of *substrate i* in *tissue x*. The first two terms in Eq. (2.1) represent the net metabolic reaction rate of *substrate i* in *tissue x*. The third term, $Q_x(C_{a,i}-\sigma_{x,i}C_{x,i})$ represents the net uptake or release rate of *substrate i* in *tissue x*. We consider nine substrates to be transported between blood and tissue: glucose, pyruvate, lactate, glycerol, alanine, fatty acids, triglyceride, oxygen, and carbon dioxide.

For the substrates that exist only in tissue cells, right side of Eq. (2.1) contains just the net metabolic reaction term. Appendix I summarizes all the dynamic mass balance equations in *tissue x*.

Since each tissue is considered as a lumped tissue-capillary compartment, the actual distribution volume ($V_{eff,x,i}$) of *substrate i* differs from the physical tissue volume (V_x).(Cabrera et al., 1998) For *substrate i* which exists both in blood and in tissue, $V_{eff,x,i} = 0.93V_x + \sigma_{x,i}(0.07V_x)$; for *substrate i* which exists only in tissue, $V_{eff,x,i} = 0.8V_x$.

The venous blood from each tissue has a distinct composition of substrates. Based on the perfect mixing assumption, the venous concentration from *tissue x* equals $\sigma_{x,i}C_{x,i}$. Except for oxygen and carbon dioxide which are assumed constant, the arterial substrate concentrations are computed from the mixed-venous concentration of all tissues:

$$C_{mv,i} = \frac{\sum_x Q_x \sigma_{x,i} C_{x,i}}{\sum_x Q_x} \tag{2.2}$$

where $C_{mv,i}$ is the mixed venous concentration of *substrate i*.

The net rate of reaction is expressed in terms of $\phi_{x,k\to i}$, the reaction flux from *substrate k* to *substrate i*:

$$R_{x,i} = P_{x,i} - U_{x,i} = \sum_{k=1}^{m} \beta_{k\to i}\phi_{x,k\to i} - \sum_{k=1}^{n} \beta_{i\to k}\phi_{x,i\to k} \tag{2.3}$$

where $\beta_{k\to i}$ is the corresponding stoichiometric coefficient, *m* is the number of reaction fluxes forming *substrate i*, and *n* is the number of reaction fluxes consuming *substrate i.*

2.2.4. Metabolic reaction rates

Each substrate is metabolized by various biochemical reactions producing ATP to fuel cellular processes. To define the metabolic reaction fluxes in tissue, it is assumed that each reaction flux is expressed with a general irreversible bi-bi substrate to product enzymatic reaction coupled with controller energy metabolite pairs:

$$X + Y \xrightarrow{E_1 \quad E_2} V + W$$

where E_1 and E_2 are ATP and ADP or vice-versa, and/or NADH and NAD^+ or vice versa. The corresponding reaction flux equation in *tissue x* can be expressed as (Salem et al., 2002;Zhou et al., 2005):

$$\phi_{x,X\text{-}Y\rightarrow V\text{-}W} = V_{x,X\text{-}Y\rightarrow V\text{-}W}\left(\frac{\frac{C_X}{K_X}\cdot\frac{C_Y}{K_Y}}{1+\frac{C_X}{K_X}+\frac{C_Y}{K_Y}+\frac{C_X}{K_X}\cdot\frac{C_Y}{K_Y}}\right)\left(\frac{PS^{\pm}}{\mu^{\pm}+PS^{\pm}}\right)\left(\frac{RS^{\pm}}{\nu^{\pm}+RS^{\pm}}\right) \qquad (2.4)$$

where $V_{x,X\text{-}Y\rightarrow V\text{-}W}$, K_X and K_Y are Michaelis-Menten parameters specific to the reaction process, C_X and C_Y are concentrations of *substrate X* and *Y* in *tissue x*. In this expression, phosphorylation state, $PS^+ = C_{ATP}/C_{ADP}$, and redox state, $RS^+ = C_{NADH}/C_{NAD+}$. For some reactions, the effect of these controllers can be in the opposite direction. In this case, $PS^- = 1/PS^+$ and $RS^- = 1/RS^+$. In addition, $\mu^{\pm}$ and $\nu^{\pm}$ are parameters for the metabolic controllers. However, AMP is one of the main allosteric regulators of glycogen phosphorylase (for glycogenolysis) and phosphofructokinase-1 (PFK-1, for glycolysis II). Since AMP is not included in this model, AMP/ATP is approximated by $[ADP/ATP]^2$ (Appendix II).

2.2.5. Neural activation of metabolic fluxes during exercise

In skeletal muscle and heart, neural stimulation induces an increase in intracellular calcium concentration, which promotes the muscle contraction. Calcium is the one of the main activators for metabolic reaction fluxes such as glycolysis, glycogenolysis, tricarboxylic acid (TCA) cycle, and oxidative phosphorylation. However, calcium changes much faster (<100ms) than hormonal or allosteric activators (>1min)

and produces an instantaneous change in the metabolic flux rate. Therefore, we assume that glycogenolysis, glycolysis II and III (glucose-6-phosphate to pyruvate), pyruvate oxidation, TCA cycle, oxidative phosphorylation, and ATP hydrolysis flux rates undergo an instantaneous change at the onset of exercise. The degree of activation depends on work rate (WR) applied during exercise. This is simulated by modifying reaction rate coefficient for the *metabolic flux i (X-Y⟶V-W)* in *tissue x*:

$$V_{x,X-Y\to V-W} = V^{0}_{x,X-Y\to V-W} \cdot \frac{\phi_{x,ATP\to ADP}(exercise)}{\phi_{x,ATP\to ADP}(rest)} \tag{2.5}$$

2.2.6. Hormonal modulation of metabolic reaction fluxes during exercise

Tissues connected by blood circulation can communicate through hormonal signals such as insulin and glucagon, which are secreted by the pancreas. In this model, the interaction via hormonal signals provides a significant feedback mechanism that facilitates glucose homeostasis during exercise. The effect of signaling is characterized by the ratio of glucagon to insulin, which strongly correlates with the change in hepatic glucose production during exercise (Wasserman and Vranic, 1986). Therefore, we assume that the glucagon-insulin ratio affects glycogenolysis and all gluconeogenesis steps in liver. For these reactions, the *metabolic flux i* in *tissue x* have maximum rate coefficients modulated by the glucagon-insulin ratio:

$$V_{x,i} = V^{0}_{x,i} \cdot \left(1.0 + \lambda^{G}_{x,i} \frac{(GIR(t) - GIR(0))^{2.0}}{\alpha^{G}_{x,i} + (GIR(t) - GIR(0))^{2.0}} \right) \tag{2.6}$$

where *GIR* is the ratio of arterial glucagon (C_G) and insulin (C_I) concentrations ($GIR=C_G/C_I$), and $\lambda^{G}_{x,i}$ and $\alpha^{G}_{x,i}$ are parameters for GIR related effect.

In contrast, heart and skeletal muscles have no receptor for glucagon, but they can respond to an epinephrine signal during exercise. Therefore, we assume that for *metabolic flux i* (viz., glycogenolysis, glucose phosphorylation by hexokinase, lipolysis, and fatty acid oxidation) in *tissue x* (heart or skeletal muscle), the reaction rate coefficients are modulated as:

$$V_{x,i} = V_{x,i}^{0} \cdot \left(1.0 + \lambda_{x,i}^{E} \frac{(C_E(t) - C_E(0))^{2.0}}{\alpha_{x,i}^{E} + (C_E(t) - C_E(0))^{2.0}} \right) \tag{2.7}$$

where C_E is the arterial epinephrine concentration, and $\lambda_{x,i}^{E}$ and $\alpha_{x,i}^{E}$ are parameters for epinephrine related effect.

Lipolysis in adipose and GI tissues is modulated by both epinephrine and insulin levels. Thus, the combination of GIR and epinephrine factors is used to control the flux rate:

$$V_{x,i} = V_{x,i}^{0} \cdot \left(1.0 + \lambda_{x,i}^{G} \frac{(GIR(t) - GIR(0))^{2.0}}{\alpha_{x,i}^{G} + (GIR(t) - GIR(0))^{2.0}} + \lambda_{x,i}^{E} \frac{(C_E(t) - C_E(0))^{2.0}}{\alpha_{x,i}^{E} + (C_E(t) - C_E(0))^{2.0}} \right) \tag{2.8}$$

2.2.7. Glucagon/Insulin controller

The secretion of glucagon and insulin from the pancreas is affected by blood glucose levels, but during moderate and short duration exercise, a direct neural stimulation and blood epinephrine levels are more significant because the arterial glucose concentration is almost constant. In this work, we postulate that work rate affects circulating epinephrine levels, which then modulates glucagon and insulin secretion by the pancreas. To implement this concept, we adapt an integral rein controller corresponding to what Saunders et al. (Saunders et al., 2000;Saunders et al., 1998)

developed to maintain the blood glucose level. This controller produces a zero steady-state error upon disturbance by making the equilibrium of blood glucose concentration depend on a balance of glucagon and insulin. In our model, an integral rein controller incorporates epinephrine to affect secretion dynamics of insulin assuming an exercise-induced change in the glucagon-insulin ratio.

The blood epinephrine level changes with a step increase in work rate according to an empirical relation:

$$C_E(t) = C_E(0) + \omega(WR) \cdot \left(1.0 - \exp\left(t / \tau_E\right)\right) \tag{2.9}$$

where $\omega(WR)$ is a steady state gain to a step change in work rate applied during exercise, and τ_E is a time constant for the epinephrine dynamics. Incorporating an integral rein control following Saunders et al. (Saunders et al., 2000;Saunders et al., 1998), the glucagon dynamics are described by:

$$\frac{dC_G}{dt} = C_G(\theta(C_{a,Glc})(h - k_1(C_G(t) - C_G(0)) - k_2(C_I(t) - C_I(0))) - D) \tag{2.10}$$

and the insulin dynamics by:

$$\begin{aligned}\frac{dC_I}{dt} = {} & C_I(\psi(C_{a,Glc})(h - k_3(C_G(t) - C_G(0)) - k_4(C_I(t) - C_I(0))) - D) \\ & - \frac{k_5(C_E(t) - C_E(0))}{k_6 + (C_E(t) - C_E(0))}\end{aligned} \tag{2.11}$$

where $\theta(C_{a,Glc})$ is a decreasing function of $C_{a,Glc}$, $\psi(C_{a,Glc})$ is an increasing function of $C_{a,Glc}$, and h, D, k_1, k_2, k_3, k_4, k_5, and k_6 are controller parameters. $\theta(C_{a,Glc})$ and $\psi(C_{a,Glc})$ are formulated to give an arterial glucose concentration of 5 mM at steady state (Saunders et al., 1998).

$$\theta(C_{a,Glc}) = \begin{cases} 1 & C_{a,Glc} \le 2.5 \\ 1-(C_{a,Glc}-2.5)^2/25 & 2.5 \le C_{a,Glc} \le 7.5 \\ 0 & 7.5 \le C_{a,Glc} \end{cases} \quad (2.12)$$

$$\psi(C_{a,Glc}) = \begin{cases} 0 & C_{a,Glc} \le 2.5 \\ 1-(C_{a,Glc}-7.5)^2/25 & 2.5 \le C_{a,Glc} \le 7.5 \\ 1 & 7.5 \le C_{a,Glc} \end{cases} \quad (2.13)$$

2.2.8. Regional blood flows

In response to a step increase in work rate, blood flows in heart (H) and skeletal muscle (SM) increase, while blood flows in the gastrointestinal (GI) and liver (LI) tissues decrease. The blood flow for *tissue x* (= H, SM, GI, LI) changes according to:

$$Q_x(t) = Q_x(0) + \delta_x(1-\exp(-t/\tau_Q)) \quad (2.14)$$

where δ_x is a steady state gain for the blood flow change in *tissue x*, and τ_Q is a time constant. Blood flows to non-specified tissues are assumed to be constant during exercise.

2.2.9. ATP hydrolysis related to work rate

The input to the whole body model during exercise is a step change of ATP hydrolysis rate ($\phi_{x,ATP\to ADP}$) in heart and skeletal muscle due to increased muscular work. For skeletal muscle, ATP hydrolysis rate depends on a work rate (WR) according to Cabrera et al. (Cabrera et al., 1999):

$$\phi_{m,ATP\to ADP}(WR) = \phi_{m,ATP\to ADP}(rest) + \gamma_m \cdot WR \quad (2.15)$$

where γ_m is a conversion factor in skeletal muscle (Cabrera et al., 1999).

2.2.10. Parameter Estimation for Model Simulation

Some parameter values needed to simulate metabolism of a normal human under resting steady-state conditions after an overnight fast are available from the literature: physiological parameters in tissue/organ compartments of the whole body (Table 2.1); arterial blood concentrations for key chemical species involved in transport and metabolism (Table 2.2); steady-state uptake/release rates ($Q_x(C_{a,i}-\sigma_{x,i}C_{x,i})$) for specific tissue/organs (Table 2.3). For the "other tissues" compartment, steady-state uptake/release rates are set to maintain a zero net balance in the whole-body except for glucose (Table 2.3). Steady-state substrate concentrations in each tissue are obtained from *in vivo* human and animal studies or approximated based on concentrations in a similar tissue (Table 2.4).

Flux balance analysis (Zhou et al., 2005) is applied to each tissue compartment to determine intracellular metabolic fluxes at rest, $\phi_{X\to Y}$ as given in Table 2.5. This analysis is implemented using steady-state mass balances of all metabolites and fluxes from the literature. Steady-state fluxes and concentrations are derived from the dynamic mass balance equation (Eq. 2.1) with the time derivative set to zero. Since the human body is an open system that is constantly changing, no steady state exists for all metabolite concentrations in tissues. Glycogen in liver and TG in adipose tissue are considered to continuously decrease even at resting condition. Starting with the known flux and uptake/release rates, the unknown flux rates are determined. For example, from liver studies (Shulman et al., 1985;Miyoshi et al., 1988), net glucose production rate is obtained from uptake-release data; the futile cycle rate is used to calculate individual flux rates between glucose and glucose-6-phosphate (G6P).

For the metabolic fluxes, the Michaelis-Menten parameters K_M are set to the initial tissue concentration of the corresponding substrate unless reported in the literature (Table 2.6). The maximum metabolic rate coefficient at rest, $V^0_{x,i}$ (Table 2.5) is calculated from the resting flux, tissue concentration, and K_M. The partition coefficients $\sigma_{t,i}$ (Table 2.7) are computed from the net uptake/release rate, blood flow rate, and arterial and tissue concentrations. Parameters that modulate $V_{x,X\text{-}Y\rightarrow V\text{-}W}$ during exercise by hormonal and neural activation are evaluated by determining values for which simulated model outputs correspond closely with experimental data from human exercise studies. These include whole-body glucose appearance and disappearance rates (Hirsch et al., 1991) and arterial substrate concentrations (Hirsch et al., 1991;Wahren et al., 1975). The parameter values are adjusted as needed to make model predictions correspond to quantitative and qualitative physiological responses. Parameter values for hormonal action ($\lambda^G_{x,i}$, $\lambda^E_{x,i}$, $\alpha^G_{x,i}$ and $\alpha^E_{x,i}$) are listed in Table 2.8.

In response to a step change in work rate, blood flow in *tissue x* (= H, SM, GI, LI) changes according to Eq. 2.14, whose parameters are the steady-state gain δ_x and time constant τ_Q (Table 2.9). For skeletal muscle, ATP hydrolysis rate depends on a work rate (Eq. 2.15) with conversion factor, γ_m (Table 2.9) (Cabrera et al., 1999). On the other hand, at maximal intensity exercise, the oxygen consumption in the heart, $\phi_{H,\mathrm{O2}\rightarrow\mathrm{H2O}}$ increases up to 4 times its resting level. During moderate intensity exercise, the increase in $\phi_{H,\mathrm{O2}\rightarrow\mathrm{H2O}}$ is much smaller (<3%) than that of skeletal muscle ($\phi_{SM,\mathrm{O2}\rightarrow\mathrm{H2O}}$). Thus, the contribution of the heart to whole body oxygen consumption becomes negligible. Since the oxygen consumption rate is closely related to ATP production rate, we assume that

ATP hydrolysis in heart increases 3 times from the rest. In contrast, ATP hydrolysis rates for other tissues are kept constant.

Most parameters related to the dynamic responses of epinephrine, glucagon and insulin to a step change in work rate are estimated by optimal least-squares fitting of the model predicted concentrations to concentration data from a 60-min exercise test (Hirsch et al., 1991). The optimal parameter estimates are obtained using '*lsqcurvefit*' (MATLAB), a nonlinear optimization algorithm. The differential equations of the model are solved using '*ode15s*' (MATLAB), an implicit integration algorithm for stiff systems. Following Saunders et al. (Saunders et al., 2000;Saunders et al., 1998), the controller parameter D is set to 0.1 and h was calculated from the resting condition with blood glucose of 5mM. Table 2.9 gives the parameter values for the epinephrine, glucagon and insulin dynamics.

Given all input functions and model parameters, the differential equations of the whole body model are solved numerically with an efficient, robust integrator (DLSODE) designed for stiff systems (CASC; http://www.llnl.gov/CASC/odepack/software/dlsode.f).

2.3. SIMULATION RESULTS

The whole-body model is applied to simulate metabolic responses during moderate intensity exercise, viz., a cycle ergometer test with a work rate of 150 W (60% VO_{2max}) maintained for 60 min. A step change in a work rate generated 5-fold increase in epinephrine concentration (data not shown), which via the glucagon-insulin controller, induced a 45% decrease in the arterial insulin concentration and an 18% increase in the arterial glucagon concentration over 60 min of exercise (Figure 2.4A). Consequently,

glucagon-insulin ratio increased 114% mainly due to declining insulin levels during exercise (Figure 2.4B). The exercise induced hormonal change modulated fluxes in affected tissues, and consequently, the whole-body glucose production increased about 3 fold (from 0.73 to 2.06 mmol/min) at the end of 60 min exercise with almost zero glucose balance (total sum of glucose uptake and release rates in all tissues) (Figure 2.5). During exercise, skeletal muscle used most of the increase in whole body glucose production and the arterial glucose concentration declined by only ~10%. Off-setting changes in whole-body glucose production by liver and utilization by skeletal muscle maintained glucose homeostasis during exercise (Figure 2.6A).

Arterial fatty acids concentration decreased to 0.59 mM (its minimum value) at 20 min, and then increased to 0.94 mM by 60 min (Figure 2.6B). Pyruvate concentration increased to 0.2 mM at 10 min, and then slowly decreased to 0.16 mM (data not shown). However, lactate concentration increased quickly and monotonically from 0.7 to 1.7 mM over 60 min (Figure 2.6C). Glycerol increased linearly by 4 fold from 0.07 to 0.29 mM (Figure 2.6D). As shown in Figures 2.4-2.6, these simulations showed good agreement with experimental data obtained in humans during moderate intensity exercise (Bergman and Brooks, 1999;Hirsch et al., 1991;Wahren et al., 1975), except for lactate concentration dynamics.

The increased glucagon-insulin ratio during exercise changed glucose production in liver. Net hepatic glycogen breakdown increased from 0.38 to 1.54 mmol/min, while net gluconeogenesis rate increased from 0.35 to 0.52 mmol/min (Figure 2.7A). The relative contribution of gluconeogenesis continuously decreased to 25% of total glucose production at 60 min starting from 48% at rest (Figure 2.7B).

Based on the ATP hydrolysis rate applied in each tissue, skeletal muscle consumed more than 85% of total ATP production during exercise. Indeed at exercise onset the ATP turnover rate in skeletal muscle increased by about 40-fold. Figure 2.8A shows the dynamic contribution to ATP production from the fuel sources in skeletal muscle during exercise. The contribution of PCR was confined to the first 5 min of exercise with less than 20 % of ATP production during this period. Carbohydrates provided 75~95% of ATP production throughout exercise, but their contribution kept decreasing with time. In contrast, the contribution of lipids kept increasing with time, starting from 4% of ATP production during the first two minutes of exercise. Since glycogen is more readily available for utilization than fatty acids, the contribution from carbohydrates went up to 95% at 5 min from ~30% at rest. Thus, up to the first 10 min of exercise, carbohydrates contributed more than 90% for the energy production, but gradually decreased to ~74% at the end of exercise (Figure 2.8B).

Sources for both carbohydrates and lipids in skeletal muscle come from internal stores (glycogen, TG) and from blood (glucose, fatty acids). Figures 2.9A and 2.9B show the relative contribution of sources to carbohydrates and lipids utilization. Total fatty acid utilization in muscle increased 12 fold during exercise (Figure 2.9A). While net TG breakdown provided 20% of total fatty-acid utilization at rest, its contribution increased to ~50% over the first 30 min of exercise and approached 35% at 60 min. At the onset of exercise, glycogen supplied ~97% of glucose and kept decreasing up to 80% at 60 min (Figure 2.9B). Even though the contribution of blood glucose was small, it increased 10 fold after 60 min.

2.4. DISCUSSION

In this study, we developed and validated a multi-scale model of fuel homeostasis which 1) differentiates tissues with distinct metabolic pathways, 2) includes transport and biochemical reactions of major fuel sources, 3) incorporates the effect of hormonal control by insulin, glucagon, and epinephrine to regulate the metabolic processes in each tissue, and 4) consequently, relates cellular metabolic processes and their regulation to whole body responses.

2.4.1. Control of glucose homeostasis during exercise

Fuel metabolism during exercise is controlled by the neuroendocrine system (Sigal et al., 2004). Exercise induces an increase in glucagon and a decrease in insulin via α- and/or β-adrenergic stimulation in pancreas (Samols and Weir, 1979;Harvey et al., 1974;Luyckx and Lefebvre, 1974). For prolonged exercise, the fall in blood glucose has a further effect on the secretion of glucagon (Galbo et al., 1977). Consequently, these changes in neural and hormonal signals modulate the metabolic rates in affected tissues. Since whole-body glucose utilization may rise by 3 fold during moderate intensity exercise, the endogenous glucose production by liver should match this increase to prevent hypoglycemia. If liver failed to respond to the exercise-induced signals, blood glucose concentration would decrease at a rate of 0.08 mM/min (Wasserman and Cherrington, 1991). Thus, the coupling between glucose utilization in muscle and glucose production in liver is very important for maintaining glucose homeostasis during exercise.

We postulated that exercise-induced change in epinephrine affects the pancreatic hormonal secretion, which then modulates the metabolic flux rates in tissues to achieve

glucose homeostasis during exercise. Indeed, simulations with our model show glucose homeostasis during moderate intensity exercise (Figure 2.5). Exercise increased the epinephrine signal via a feed-forward mechanism (sympathetic stimulation), which was then used to decrease the secretion of insulin in the glucagon-insulin controller (Figure 2.4). Since insulin inhibits the secretion of glucagon, the decreased insulin signal failed to suppress glucagon secretion making its level increased. The increased glucagon-insulin ratio modulated the metabolic reaction rates in liver, GI and adipose tissue to make them release more glucose and fatty acids into blood. In contrast, skeletal muscle and heart responded to exercise by direct neural activation and epinephrine signal. In skeletal muscle, direct neural activation increased by about 40 fold the rates of glycolysis II, III (G6P to pyruvate), glycogenolysis, pyruvate oxidation, TCA cycle, oxidative phosphorylation, and ATP hydrolysis. Epinephrine affected the rates of glycogenolysis, glucose phosphorylation by hexokinase, fatty acid oxidation and lipolysis by hormone-sensitive lipase. The coordinated changes of these reactions in liver and skeletal muscle led to the close coupling between glucose utilization and production in whole body. In accord with the 'Glucose shunt concept' introduced by Bergman et al. (Bergman et al., 1999b), most glucose is shunted to the active skeletal muscle. Indeed, model simulations show that glucose uptake by skeletal muscle is about 20% of the whole body glucose utilization at rest, but increases to 70% during exercise. Therefore, it is evident from this study that the interaction between liver and skeletal muscle is essential for blood glucose homeostasis during exercise.

In Figure 2.5, whole body glucose production rate showed a sigmoidal increase during exercise. This implies that glucose uptake in skeletal muscle needs to have a

similar dynamic change. A direct neural activation exhibiting a fast increase at the onset of exercise is not consistent with this response. Instead, an activation mechanism must provide a slow initial response, which may be associated with the epinephrine signal. This hypothesis has an experimental basis: It has been shown that exercise activates glucose transport in skeletal muscle by stimulating translocation of glucose transporters (GLUT-4) possibly via AMP kinase (Kemp et al., 1999;Musi and Goodyear, 2003;Lund et al., 1995) or calcium signaling (Richter et al., 2003). The modulation of glucose transporter activity may allow control of the glucose transport rate, but this mechanism cannot be directly incorporated because this model cannot represent facilitated glucose transport. Alternatively, Wasserman et al. (Wasserman and Halseth, 1998) showed that glucose phosphorylation is the primary rate limiting step of glucose utilization in skeletal muscle during exercise. Furthermore, it was hypothesized that exercise increases glucose phosphorylation by making hexokinase (HK) enzyme bind to mitochondria where HK has an abundant access to ATP and becomes less sensitive to product inhibition by glucose-6-phosphate (Chen and Gollnick, 1994;Wasserman and Ayala, 2005). Assuming that exercise influences the increase of hexokinase fraction associated with mitochondria, the corresponding increase of glucose phosphorylation rate could be represented by the epinephrine signal. With this activation scheme, the glucose uptake by skeletal muscle follows the experimental time course that shows a sigmoidal increase with little change over the first 10-min period of exercise.

2.4.2. Hepatic glycogenolysis and gluconeogenesis

Liver is responsible for endogenous glucose production forming glucose through glycogenolysis and gluconeogenesis. Experimental methods have been developed to measure hepatic glycogenolysis and gluconeogenesis rates *in vivo* using various carbon tracers (Bergman et al., 2000), di-deuterated water (Landau et al., 1995) or NMR spectroscopy (Hundal et al., 2000). However, no "gold standard" exists for measuring gluconeogenesis rate *in vivo* (Trimmer et al., 2002). For instance, the carbon tracer method using precursor-to-product ratio has the uncertainty associated with the dilution of precursor carbon label in the citric acid cycle (Krebs et al., 1966). NMR spectroscopy provides only net breakdown of glycogen, but not absolute rates. Furthermore, the application of NMR spectroscopy during exercise is limited.

Since measuring the dynamic changes of glycogenolysis and gluconeogenesis *in vivo* during exercise is currently not feasible, we use model simulations to predict the dynamic changes of hepatic glycogenolysis and gluconeogenesis during exercise. The validity of these simulations relies on the ability of the mathematical model to simulate experimental data related to dynamic changes of whole body glucose production rate and the arterial concentrations of major gluconeogenic precursors. As shown by the simulation results, good agreement exists with the experimental data for whole body glucose production rate (Figure 2.5). Trimmer et al. (Trimmer et al., 2002) measured gluconeogenesis rate for two different exercise intensities (45% and 65% VO2max) using mass isotopomer distribution analysis; the relative contribution of gluconeogenesis was 20~25% of total hepatic glucose production over a 30~90 min period of exercise with lower contribution at higher exercise intensity. As shown in Figure 2.7, the model

predicted the relative contribution of gluconeogenesis as 25% after 30 min. Accounting for differences in exercise intensities (60% VO2max in this study vs. 65% VO2max in Timmer et al. (Trimmer et al., 2002)), the predicted contribution of gluconeogenesis is just a little higher than the measurement by Trimmer et al. (Trimmer et al., 2002) Furthermore, the model can predict the dynamic changes over the entire exercise period instead of being confined to only later stages of exercise because of experimental limitations. This is an example of how our mechanistic mathematical model can be used as a complement to experimental studies. Model simulations that can predict dynamic metabolic responses provide a means to investigate control mechanisms and quantify their effects. Without a mechanistic model and computer simulations, such analysis would not be possible.

2.4.3. Fuel oxidation in skeletal muscle

At rest, skeletal muscle consumes fatty acids as a major fuel source. Since exercise modifies the internal milieu (via altered enzyme activity in muscle and change in the muscle fiber recruitment) and external milieu (via fuel delivery to muscle), it affects the fuel oxidation pattern in skeletal muscle. The relative importance of carbohydrates and lipids to the whole-body fuel oxidation can be measured with indirect calorimetry and tracer studies (Martin, III et al., 1993;Friedlander et al., 1997). Even though the whole body fuel oxidation can be used as a surrogate representation for skeletal muscle during exercise, the contribution from other tissue/organ systems is difficult to assess and should be taken into account. Model simulation, however, can provide a quantitative evaluation of the interaction between skeletal muscle and other tissue/organ systems that

allows an analysis of the influence of the latter on fuel availability in skeletal muscle during exercise.

In our model, tissues were grouped based on their metabolically distinctive characteristics. Even skeletal muscle was divided into active (leg muscle) and inactive (upper body) muscle to differentiate the effect of exercise on the specific part of tissues. In this way, the fuel oxidation characteristic of active skeletal muscle during exercise could be examined. Measurements of whole-body fuel oxidation and the relative contribution of fuel sources show that the contribution of carbohydrate in overnight fasted men can increase to 60~80% during 60% VO_{2max} exercise (Martin, III et al., 1993;Bergman and Brooks, 1999). Model simulations suggest that the actual contribution of carbohydrates in active skeletal muscle (i.e. legs) is about 70~90%. This is higher than reported from whole-body measurements because other rates of fatty acid oxidation, i.e., those by other tissue/organ systems (liver, adipose tissue, other tissues) are included in these measurements. Table 2.10 shows the model predicted values for the whole-body RQ during exercise. Whole-body RQ increased to 0.94 at 7 min of exercise, and then slowly decreased to 0.9 at the end of exercise. Model predictions were compared with experimental data (Bergman and Brooks, 1999), and were in close agreement except for 15 min. The predicted RQ in the skeletal muscle compartment increased to 0.96 and slowly decreased to 0.92. The higher RQ indicates a greater role of carbohydrate metabolism in the active skeletal muscle. Bergman et al. (Bergman et al., 1999a) and Odland et al. (Odland et al., 1998) measured leg RQ using arteriovenous balance technique, and reported leg RQ values around 0.97~1.0, which are significantly larger than our model predictions. This difference occurs because their subjects consumed

meals less than 4 hr before the exercise test and our model assumes overnight fasting (~12hr).

In accord with the 'Crossover Concept' of Brooks and Mercier (Brooks and Mercier, 1994), carbohydrate utilization increases with exercise intensity. While fatty acid utilization is increased for the mild and moderate intensity exercise, it is down-regulated at higher intensity (over 65% VO_{2max}). Since the model-simulated responses correspond to exercise at 60% VO_{2max} only, the crossover concept cannot be explored thoroughly. However, during the prolonged exercise, skeletal muscle glycogen depletion induces a gradual up-regulation of fatty acid oxidation (Brooks and Mercier, 1994). At the onset of exercise (Figure 2.8B), carbohydrate metabolism in skeletal muscle (mostly from glycogen breakdown) increased quickly by ~95% and then decreased gradually to 75% of total energy production. Thus, our model describes the shift of the crossover point due to glycogen depletion.

Over the first 10~20 min of exercise, the model simulation showed that the internal stores of glycogen and TG provided almost 90% of energy production in skeletal muscle, but then decreased to 70% at 60 min (Figure 2.8). This implies that the interaction between tissue/organ systems (external milieu) becomes more important in prolonged exercise in order to increase the external fuel availability in skeletal muscle. The increases in glucose production in liver and lipolysis in adipose tissue are main contributors for glucose and fatty acid availability. As simulated in this model, skeletal muscle released more than 90% of lactate into blood during exercise, which was recycled to produce glucose in liver (i.e., 'Cori cycle'). Also, the glycerol release from lipolysis in adipose tissue increased, and arterial alanine concentration increased (Figure 2.6D) due to

its release from skeletal muscle. All these processes provide additional gluconeogenic precursors for liver to produce a sufficient amount of glucose for the increased glucose utilization in skeletal muscle. Thus, the model simulations can be used to quantify coordinated modulation of metabolic processes among tissue/organ systems.

2.4.4. Model advantages, limitations and future developments

To our knowledge, this is the first mechanistic model of glucose homeostasis that links cellular metabolism to whole-body responses and incorporates effects of hormonal control on fuel metabolism of various tissues/organs. Bergman et al. (Bergman et al., 1979) and others (Vicini et al., 1999;Krudys et al., 2005) have developed "minimal models" to quantify the degree of insulin resistance from a glucose tolerance test. While these models are simple in nature, they show good clinical applicability to be tailored to the individual subject, which is not possible with our current model due to its large-scale nature and the numerous parameters incorporated in its formulation. However, "minimal models" only include the effects of insulin as well as insulin-independent/dependent tissue compartments. Thus, these models are not general enough to be applied to other kinds of physiological conditions (e.g., exercise) or pharmacological interventions. On the other hand, the real advantage of our model is to assist testing hypotheses about mechanisms of metabolic control and to make dynamic predictions of metabolite concentrations and flux rates in various tissues, which are in most cases difficult to assess with current technology.

Since blood glucose is regulated by two hormones that act in opposite directions to inhibit the secretion of each other, the balance between them is more important than

individual absolute levels (Saunders et al., 1998). Thus, it is very significant to include both glucagon and insulin to describe glucose homeostasis. Saunders et al. (Saunders et al., 1998) applied the concept of integral rein control with two hormones in a mathematical model of glucose regulation. The model, however, was not validated with experimental data. In contrast, our mathematical model of whole body glucose homeostasis includes all important fuel sources (glucose, glycogen, fatty acids, TG, lactate, etc.) and distinguishes tissue/organs with different metabolic characteristics. Furthermore, it accounts for insulin and glucagon effects on cellular metabolic processes, their regulation via interaction among tissues, and the consequent whole-body response.

Although our model simulations compare well with most experimental data, one obvious limitation is that the dynamics of arterial lactate concentration do not correspond to experimental data (Figure 2.6C). Instead of an overshoot at the onset of exercise (Bergman et al., 1999c), it showed a first-order exponential increase. A possible source of this discrepancy is the assumption of homogeneity in the tissue-cells compartment of skeletal muscle. Recently, Zhou et al. (Zhou et al., 2005) showed that distinguishing cytosol and mitochondria in this compartment leads to different dynamics of cytosolic and mitochondrial $NADH/NAD^+$ ratios and to more physiological lactate concentration time profiles. Since lactate is produced in the cytosol by lactate dehydrogenase, it is expected that the cytosolic $NADH/NAD^+$ ratio may regulate lactate production during exercise. Also, lactate is transported via carrier-mediated facilitated diffusion, which requires distinguishing blood from tissue. Therefore, future modifications to the model should incorporate distinct blood and extravascular tissue compartments and distinguish cytosol from mitochondria in the tissue-cells compartment.

An alternative way to investigate lactate metabolism during exercise in a minimally invasive manner is to evaluate the dynamic changes in the arterial lactate to pyruvate concentration ratio, [L/P]. When analyzing the [L/P] ratio in femoral venous blood, our model simulations showed that L/P ratio values were around 10 (data not shown), at rest and during exercise, as previously reported (Henderson et al., 2004). However, model simulations were not able to reproduce the [L/P] values in arterial blood, which experimentally have been shown to rise an order of magnitude during exercise (Henderson et al., 2004). A likely cause of this discrepancy is that arterial pyruvate concentration predicted by our model increased slightly instead of decreasing during exercise. This may be the result of not having a source of lactate release and pyruvate uptake between the femoral effluent and the arterial side, which is still uncertain. Our model also does not have any additional tissue/organ compartment between these sites, but only a gas exchanger and a pump. As a consequence, the arterial L/P ratio predicted by our model cannot rise up by an order of magnitude.

Another limitation in this model is the assumption of lumped irreversible enzymatic reactions. Several biochemical reactions are combined such that each reaction step includes at least one irreversible reaction whose reverse flux is several orders of magnitude smaller than the forward flux. Although this approximation is appropriate under some conditions, a more general model would describe biochemical reactions as reversible for consistency with thermodynamic equilibrium.

2.5. CONCLUSION

Our model of whole-body fuel metabolism that distinguishes tissue/organ systems and incorporates hormonal control can simulate the coordinated responses of various metabolic pathways within distinct tissues/organs subsystems leading to glucose homeostasis during moderate intensity exercise. This model not only simulates the dynamic changes of hormonal signals, but also predicts the metabolic responses in each tissue during exercise. The importance of hepatic glycogenolysis as a major pathway for glucose production in liver is evident from model simulations. Furthermore, model simulations could be a valuable complement to experimental studies and provide quantitative, dynamic information on the relative importance of carbohydrate and lipids for fuel oxidation in skeletal muscle.

TABLE 2.1. Characteristic parameters and steady state values of O_2 consumption and CO_2 production

Tissue/Organ	Blood Flow ($L\ min^{-1}$)	Tissue Weight (Kg)	VO_2 ($ml\ min^{-1}$)	VCO_2 ($ml\ min^{-1}$)
Brain	0.75	1.49	51.07	51.07
Heart	0.25	0.25	26.80	20.61
Liver	1.5	1.5	62.72	43.72
GI	1.1	2.0	10.21	10.21
Muscle	0.9	20.0	41.04	32.01
Adipose	0.36	11.0†	10.08	7.17
Others	1.74	33.76	48.08	35.21
Whole body	5.5	70.0	250	200

Assume a normal overnight fasted human at rest with 0.8 RQ (respiratory quotient=VCO_2/VO_2). VO_2 and VCO_2 are oxygen consumption and carbon dioxide production rates. Values in "others" are set to balance the whole body values. Data are taken from the reference (Kim et al., 2007).

† Based on 16% body fat content.

TABLE 2.2. Arterial substrate concentrations

Substrate	Arterial Concentration (mM) *
GLC	5.0
PYR	0.068
LAC	0.7
ALA	0.192
FFA	0.66
GLR	0.07
O2	8.0
CO2	21.7
TG	0.99

*Steady state values for a normal overnight fasted human at rest. Data are taken from the reference (Kim et al., 2007).

TABLE 2.3. Uptake and release rates (mmol min^{-1}) in each tissue/organ system

	GLC	PYR	LAC	ALA	FFA	GLR	TG
Brain	0.380	0	0	0	0	0	0
Heart	0.040	0	0.040	0	0.035	0	0
Liver	-0.731	0	0.270	0.320	0.210	0.140	-0.029
GI Track	0.076	0	0	0	-0.120	-0.040	0.006
Muscle	0.165	0.005	-0.112	-0.040	0.046	-0.003	0.003
Adipose	0.038	0	-0.056	0	-0.211	-0.097	0.02
Others*	0.062	-0.005	-0.142	-0.280	0.040	0	0
Sum	-0.03	0	0	0	0	0	0

Steady state values for a normal overnight fasted human at rest. Tissue with positive value takes up the corresponding substrate while one with negative value releases it.
*Values in "others" are set for zero balance. Data are taken from the reference (Kim et al., 2007).

TABLE 2.4. Substrate concentrations (mM) in each tissue

Substrate	Brain	Heart	Muscle	GI	Liver	Adipose
GLC	1.12	1.0	0.48	1.0	8.0	2.54
PYR	0.15	0.2	0.048	0.2	0.37	0.37
LAC	1.45	3.88	1.44	3.88	0.82	0.82
ALA	0	0	1.3	0	0.23	0
GLR	0	0.015	0.064	0.015	0.07	0.22
FFA	0	0.021	0.53	0.021	0.57	0.57
TG	0	3.12	14.8	450	2.93	990
O2	0.027	0.96	0.49	0.49	0.027	0.027
CO2	15.43	20.0	15.43	15.43	15.43	15.43
G6P	0.16	0.17	0.24	0.17	0.2	0.2
GLY	2.0	33.0	95.0	33.0	417	0
GAP	0.15	0.01	0.08	0.01	0.11	0.11
GRP	0	0.29	0.15	0.29	0.24	0.24
ACoA	0.068	0.0012	0.0022	0.0012	0.035	0.035
CoA	0.06	0.012	0.018	0.012	0.14	0.14
NAD+	0.064	0.40	0.45	0.4	0.45	0.45
NADH	0.026	0.045	0.05	0.045	0.05	0.05
ATP	2.45	3.4	6.15	3.4	2.74	2.74
ADP	0.54	0.02	0.02	0.02	1.22	1.22
Pi	2.4	1.66	2.70	1.66	4.6	4.6
PCR	4.6	8.3	20.1	8.3	0	0
CR	5.6	3.5	10.45	3.5	0	0

Steady state values for a normal overnight fasted human at rest. Data are taken from the reference (Kim et al., 2007).

TABLE 2.5. Metabolic flux, $\phi_{X\to Y}$ (mmol min^{-1}) and maximum rate coefficient, $V^0_{X\to Y}$ (mmol min^{-1}) in each tissue

Fluxes	Brain		Heart		Muscle		GI		Liver		Adipose	
	$\phi_{X\to Y}$	$V^0_{X\to Y}$	$\phi_{X\to Y}$	$V^0_{X\to Y}$	$\phi_{X\to Y}$	$V^0_{X\to Y}$	$\phi_{X\to Y}$	$V^0_{X\to Y}$	$\phi_{X\to Y}$	$V^0_{X\to Y}$	$\phi_{X\to Y}$	$V^0_{X\to Y}$
$\phi_{GLC\to G6P}$	0.38	0.79	0.04	0.088	0.165	0.398	0.076	0.167	0.17	0.765	0.038	0.079
$\phi_{G6P\to GAP}$	0.38	1.52	0.04	0.16	0.165	0.66	0.076	0.304	0.17	0.68	0.038	0.152
$\phi_{GAP\to PYR}$	0.76	12.16	0.08	1.28	0.33	5.280	0.152	2.432	0.34	5.44	0.056	0.896
$\phi_{PYR\to GAP}$	0	0	0	0	0	0	0	0	0.93	7.44	0	0
$\phi_{GAP\to G6P}$	0	0	0	0	0	0	0	0	1.04	2.08	0	0
$\phi_{G6P\to GLC}$	0	0	0	0	0	0	0	0	0.9	1.8	0	0
$\phi_{G6P\to GLY}$	0.003	0.012	0.04	0.16	0.125	0.5	0	0	0.1	0.4	0	0
$\phi_{GLY\to G6P}$	0.003	0.024	0.04	0.32	0.125	1.0	0	0	0.48	3.84	0	0
$\phi_{PYR\to LAC}$	0.7	2.8	0.088	0.352	1.0	14.85	0.2	0.8	0.21	0.84	0.036	0.144
$\phi_{LAC\to PYR}$	0.7	2.8	0.128	0.512	0.888	12.51	0.2	0.8	0.48	1.92	0.01	0.04
$\phi_{GLR\to GRP}$	0	0	0.004	0.016	0.127	0.508	0	0	0.144	0.576	0	0
$\phi_{GAP\to GRP}$	0	0	0	0	0	0	0	0	0	0	0.02	0.080
$\phi_{GRP\to GAP}$	0	0	0	0	0	0	0	0	0.111	0.444	0	0
$\phi_{PYR\to ALA}$	0	0	0	0	0.04	0.08	0	0	0	0	0	0
$\phi_{ALA\to PYR}$	0	0	0	0	0	0	0	0	0.32	0.64	0	0
$\phi_{PYR\to ACoA}$	0.76	6.08	0.12	0.96	0.183	2.745	0.152	1.216	0	0	0.03	0.24
$\phi_{FFA\to ACoA}$	0	0	0.035	0.28	0.055	0.701	0	0	0.136	1.088	0.01	0.16
$\phi_{ACoA\to FFA}$	0	0	0	0	0	0	0	0	0.112	0.896	0	0
$\phi_{TGL\to FFA}$	0	0	0.004	0.008	0.13	0.26	0.04	0.08	0.004	0.008	0.097	0.19
$\phi_{FFA\to TGL}$	0	0	0.012	0.096	0.381	3.048	0	0	0.1	0.8	0.06	0.48
$\phi_{ACoA\to CO2}$	0.76	12.16	0.4	6.4	0.623	9.968	0.152	2.432	0.976	15.62	0.08	1.28
$\phi_{O2\to H2O}$	2.28	18.71	1.165	9.327	1.832	14.68	0.456	3.653	2.702	22.18	0.25	2.05
$\phi_{PCR\to CR}$	1.86	7.44	2.0	8.0	20.0	80.0	2.0	8.0	0	0	0	0
$\phi_{CR\to PCR}$	1.86	7.44	2.0	8.0	20.0	80.0	2.0	8.0	0	0	0	0
$\phi_{ATP\to ADP}$	15.20	30.4	7.33	14.66	10.82	21.64	3.04	6.08	13.92	27.84	2.74	5.47

Steady state values for a normal overnight fasted human at rest.

TABLE 2.6. Distinctive metabolic parameter values

Flux	K_M	Brain	Heart	Muscle	GI	Liver	Adipose
$\phi_{GLC \rightarrow G6P}$	K_{GLC}	0.05	0.1	0.1	0.1	10.0	0.1
$\phi_{O2 \rightarrow H2O}$	K_{O2}	0.7	0.7	0.7	0.7	0.7	0.7
$\phi_{PYR \rightarrow LAC}$ †	K_{PYR}			0.6			
$\phi_{LAC \rightarrow PYR}$	K_{LAC}			17.0			
$\phi_{PYR \rightarrow ACoA}$	K_{PYR}			0.065			

Values are in mM except for K_{O2} which is in μM. References are given in parenthesis.
† For this flux, ν+ = 0.011 mM. Data are taken from the reference (Kim et al., 2007).

TABLE 2.7. Partition coefficient $\sigma_{x,i}$ (dimensionless) values associated with blood-tissue transport

Substrate	Brain	Heart	Muscle	GI	Liver	Adipose
GLC	4.012	4.84	9.931	4.931	0.680	1.927
PYR	0.442	0.34	1.301	0.34	0.184	0.184
LAC	0.483	0.139	0.572	0.18	0.634	0.942
ALA			0.226		0.162	
GLR		4.667	1.146	7.091	0.0481	1.543
FFA		24.76	1.149	36.62	1.053	2.235
TG		0.317	0.067	0.002	0.343	0.001
O2	183.7	3.468	12.17	15.48	218.3	270.58
CO2	1.603	1.269	1.509	1.433	1.510	1.441

Blank means no uptake or release of the corresponding substrate.

TABLE 2.8. Hormonal control parameters: λ_i (dimensionless) and α_i (pM)

A. GIR regulated flux

Flux	Parameter	GI	Liver	Adipose
$\phi_{PYR\rightarrow GAP}$	$\lambda_{PYR\rightarrow GAP}$		0.5	
	$\alpha_{PYR\rightarrow GAP}$		0.07	
$\phi_{GAP\rightarrow G6P}$	$\lambda_{GAP\rightarrow G6P}$		0.5	
	$\alpha_{GAP\rightarrow G6P}$		0.07	
$\phi_{G6P\rightarrow GLC}$	$\lambda_{G6P\rightarrow GLC}$		1.0	
	$\alpha_{G6P\rightarrow GLC}$		0.07	
$\phi_{GLY\rightarrow G6P}$	$\lambda_{GLY\rightarrow G6P}$		3.0	
	$\alpha_{GLY\rightarrow G6P}$		0.07	
$\phi_{ALA\rightarrow PYR}$	$\lambda_{ALA\rightarrow PYR}$		1.0	
	$\alpha_{ALA\rightarrow PYR}$		0.07	
$\phi_{TGL\rightarrow FFA\text{-}GLR}$	$\lambda_{TG\rightarrow FFAGLR}$	1.5		1.5
	$\alpha_{TG\rightarrow FFA\text{-}GLR}$	0.07		0.07

B. Epinephrine regulated flux

Flux	Parameter	Heart	Muscle	GI	Adipose
$\phi_{GLC\rightarrow G6P}$	$\lambda_{GLC\rightarrow G6P}$	3.0	18.0		
	$\alpha_{GLC\rightarrow G6P}$	1000	1000		
$\phi_{GLY\rightarrow G6P}$	$\lambda_{GLY\rightarrow G6P}$		0.3		
	$\alpha_{GLY\rightarrow G6P}$		10		
$\phi_{FFA\rightarrow ACoA}$	$\lambda_{FFA\rightarrow ACoA}$	2.0	9.0		
	$\alpha_{FFA\rightarrow ACoA}$	447.2	447.2		
$\phi_{PYR\rightarrow ALA}$	$\lambda_{PYR\rightarrow ALA}$		2		
	$\alpha_{PYR\rightarrow ALA}$		1000		
$\phi_{TGL\rightarrow FFA\text{-}GLR}$	$\lambda_{TG\rightarrow FFA\text{-}GLR}$	0.5	2.5	2.0	2.0
	$\alpha_{TG\rightarrow FFA\text{-}GLR}$	1000	1000	1000	1000

TABLE 2.9. Estimated parameters for model simulations

Parameter	Value	Unit
δ_{heart}	0.375	L min^{-1}
δ_{muscle}	8.1	L min^{-1}
δ_{GI}	-0.4	L min^{-1}
τ_Q	0.1	min
$C_E(0)$	250	pM
$\omega(WR)$	1100	pM
τ_E	30	min
γ_m	2.68	mmol min^{-1} W^{-1}
$C_G(0)$	25.48	pM
$C_I(0)$	47.72	pM
k1	0.1979	pM^{-1} min^{-1}
k2	0.0430	pM^{-1} min^{-1}
k3	0.1861	pM^{-1} min^{-1}
k4	0.0432	pM^{-1} min^{-1}
k5	0.869	pM min^{-1}
k6	0.1157	pM
h	0.133	min^{-1}
D	0.1	min^{-1}

TABLE 2.10. Whole body RQ during exercise

Time	15 min	30 min	45 min	60 min
Model Simulation	0.93	0.92	0.91	0.90
Experiment[†]	0.96±0.02	0.92±0.02	0.91±0.02	0.90±0.01

[†] Taken from the reference (Bergman and Brooks, 1999) using data for the untrained fasted group exercising at 59% VO2max

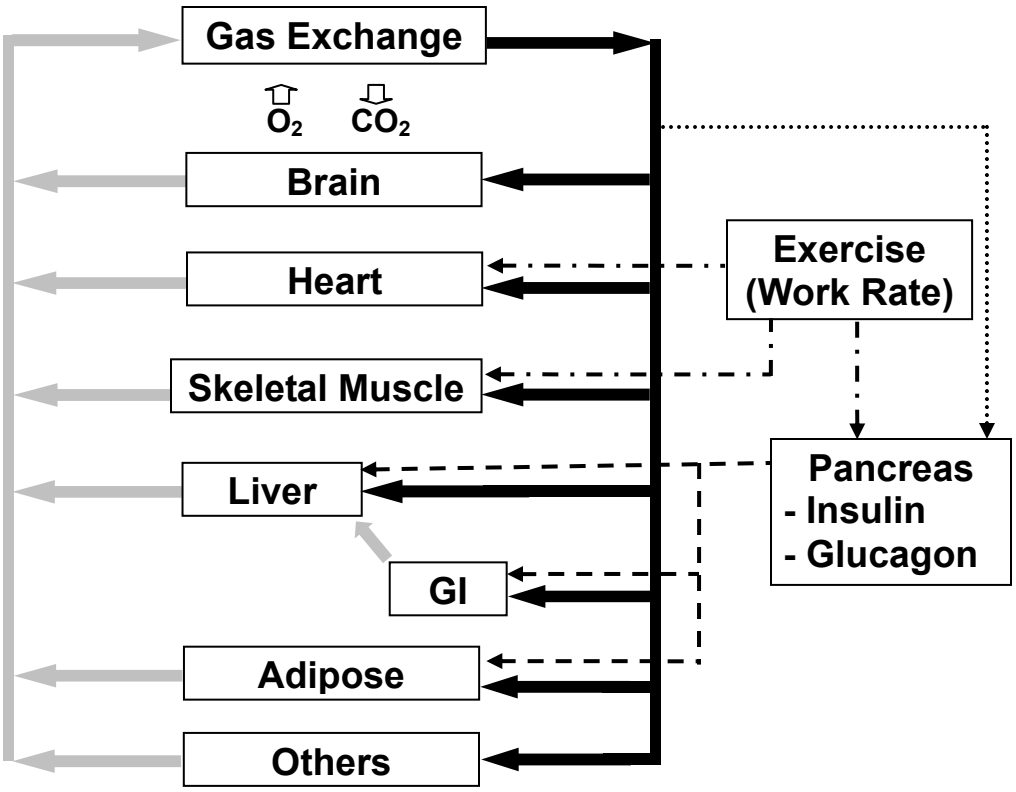

FIGURE 2.1. Whole body system diagram

Each tissue is connected via the blood supply that carries substrates to organs/tissues in arterial blood (black solid arrows). Venous blood (gray solid arrows) leaving these tissues/organs takes away byproducts and becomes arterial blood to re-start the circulation after releasing carbon dioxide and taking up oxygen in lungs (gas exchange). Exercise sends neuroendocrine signals (dash-dot arrows) to heart, skeletal muscle and pancreas. In addition, feedback signal (dotted arrow) from the arterial glucose concentration can be sent to pancreas. Finally, glucagon-insulin ratio signal (dash arrow) from pancreas is sent to liver, GI (gastrointestinal) tract and adipose tissue.

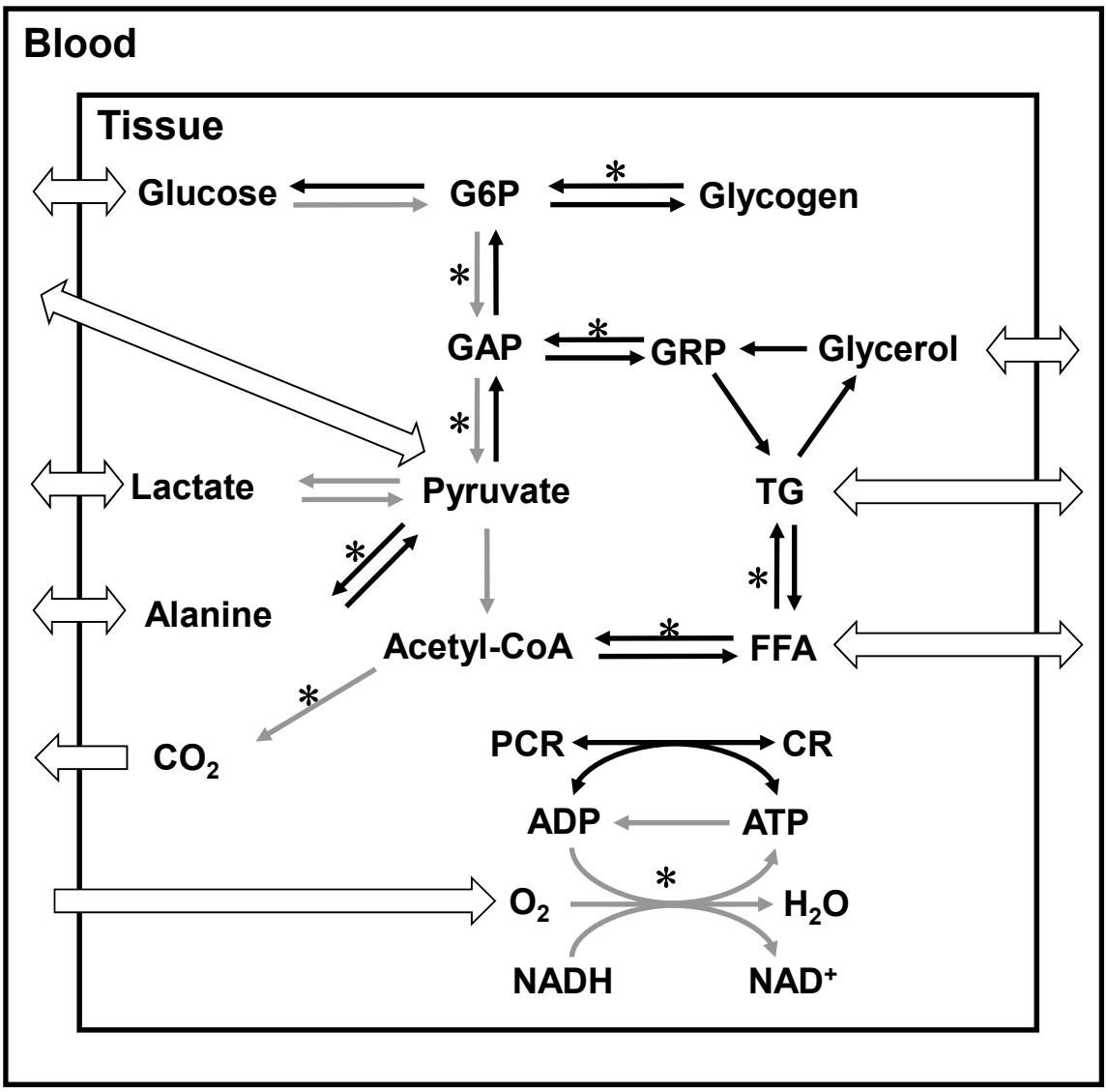

FIGURE 2.2. General metabolic pathways in whole body model

Nine substrates connected with open arrows are transported between tissue and blood. While gray arrows are common pathways in all tissues, black arrows are tissue specific pathways. The pathways marked with asterisk (*) are composed of several reaction steps but lumped into one step in this model. G6P: glucose-6-phosphate; GAP: glyceraldehyde-3-phosphate; GRP: glycerol-3-phosphate; TG: triglycerides; FFA: free fatty acid; ACoA: Acetyl CoA; PCR: phosphocreatine; CR: creatine.

Pathways	Brain	Heart	Muscle	GI	Liver	Adipose
Gluconeogenesis I, II, III (PYR→GAP,GAP→G6P,G6P→GLC)					■	
Glycogen synthesis (G6P→GLY)	■	■	■		■	
Glycogenolysis (GLY→G6P)	■	■	■		■	
Fatty acid synthesis (ACoA→FFA)					■	
Fatty acid oxidation (FFA→ACoA)		■	■		■	■
Lipolysis (TG→FFA+GLR)		■	■	■	■	■
TG synthesis (FFA+GRP→TG)		■	■	■	■	■
Glycerol Phosphorylation (GLR→GRP)		■	■		■	
GAP reduction (GAP→GRP)						■
GRP oxidation (GRP→GAP)					■	
Alanine breakdown (ALA→PYR)					■	
Alanine synthesis (PYR→ALA)			■			
PCR breakdown (PCR→CR)	■	■	■	■		
PCR synthesis (CR→PCR)	■	■	■	■		

FIGURE 2.3. Map for tissue specific metabolic pathways

In addition to the common pathways shown in Figure 2.2, each tissue has different kinds of metabolic pathways. Blank filled with gray color means the existence of the corresponding pathway. GLC: glucose; PYR: pyruvate; GLY: glycogen; GLR: glycerol; ALA: alanine.

A

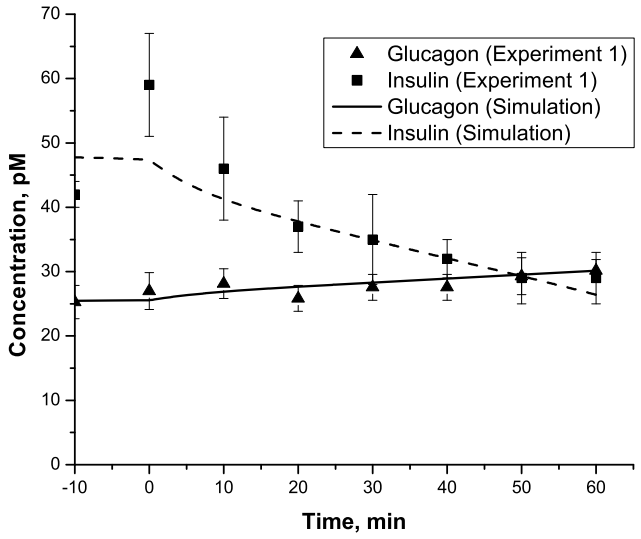

B

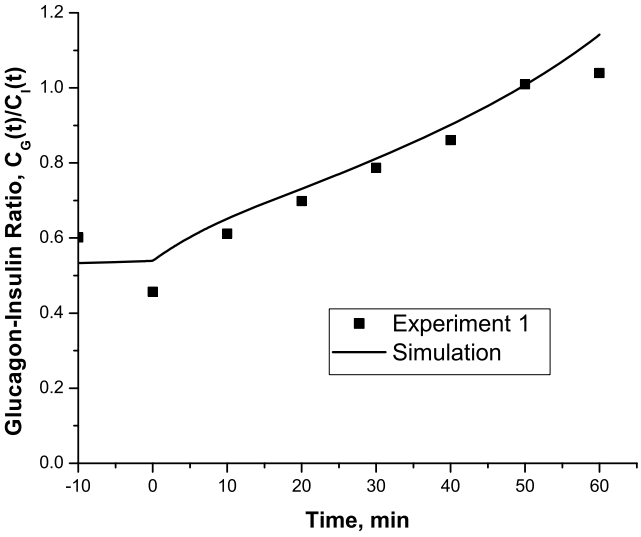

FIGURE 2.4. Dynamic responses of arterial glucagon and insulin concentrations (A) and glucagon-insulin ratio (B) to a step increase in work rate (150W) from resting state at 0 min

Scattered data points are taken from *in vivo* exercise studies of humans (Hirsch et al., 1991). Lines represent model simulations. Simulations from -10 to 0 min represent the steady state responses.

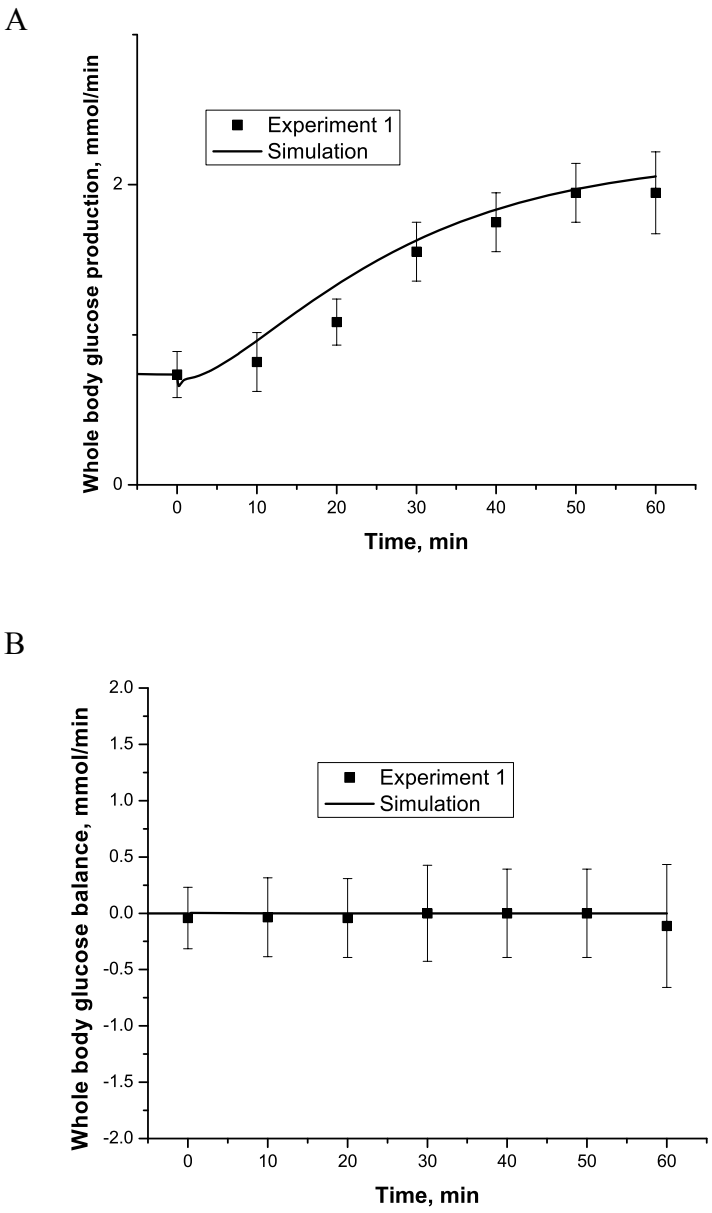

FIGURE 2.5. Dyanmic changes in whole body glucose production (A) and whole body glucose balance (B) during 60 min exercise

Whole body glucose balance = whole body glucose production – whole body glucose utilization. Scattered data points are taken from *in vivo* exercise studies of humans (Hirsch et al., 1991). Lines represent model simulations.

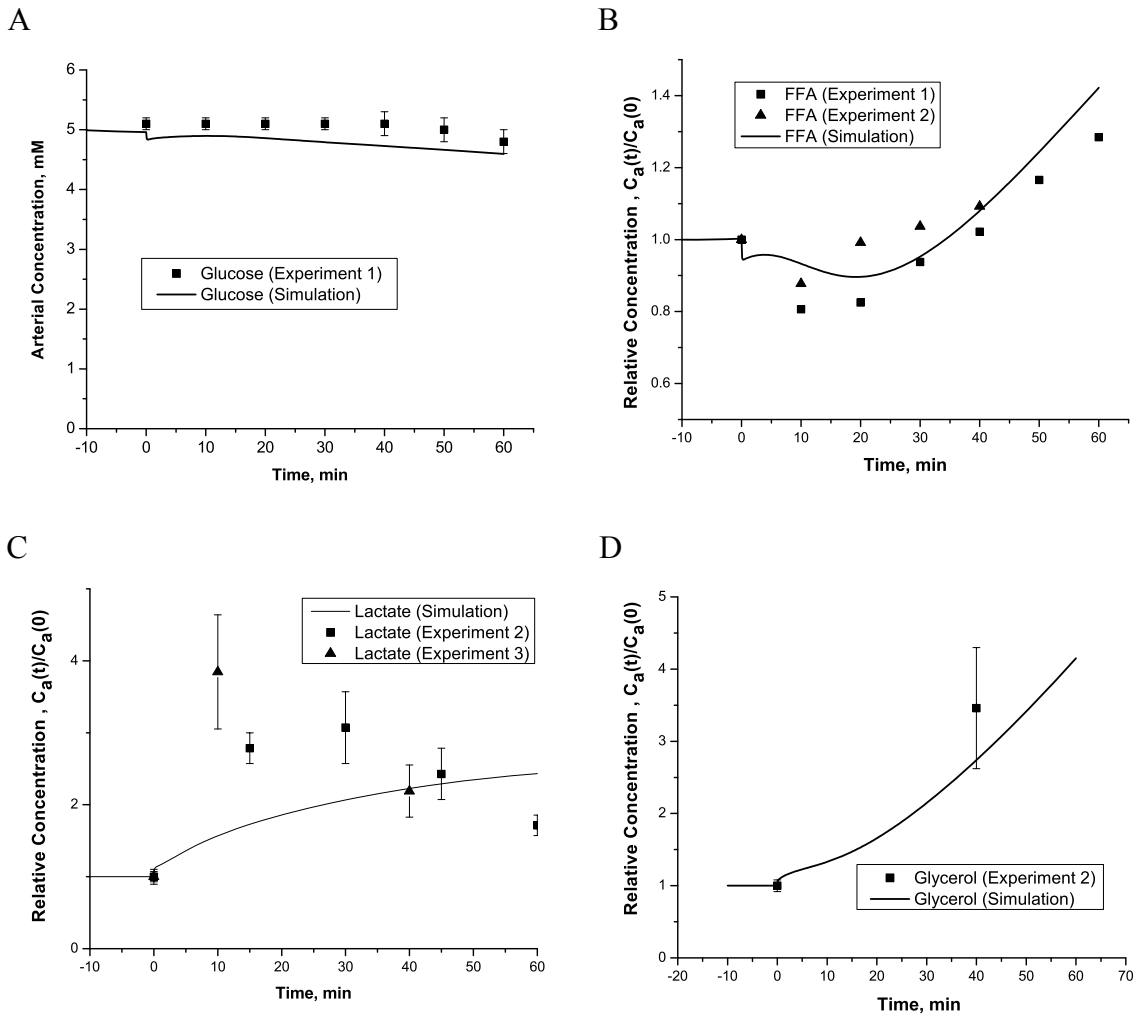

FIGURE 2.6. Dynamic responses of arterial substrate concentrations to a step increase in work rate (150W) from resting state at 0 min

A: glucose concentration, B: relative concentration of free fatty acids (FFA), C: pyruvate and lactate concentrations, D: glycerol concentration. Relative concentration of FFA is defined as the ratio between concentrations at time t and 0. Scattered data points are taken from *in vivo* exercise studies of humans ((Bergman and Brooks, 1999;Wahren et al., 1975) where only control group results were taken). Lines represent model simulations.

A

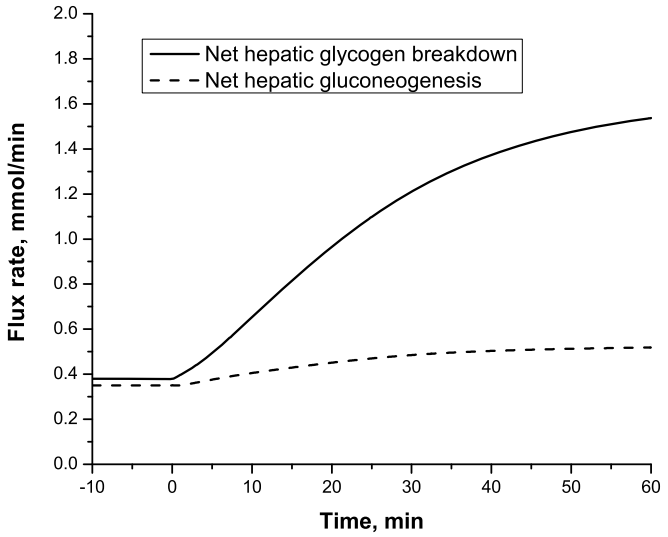

B

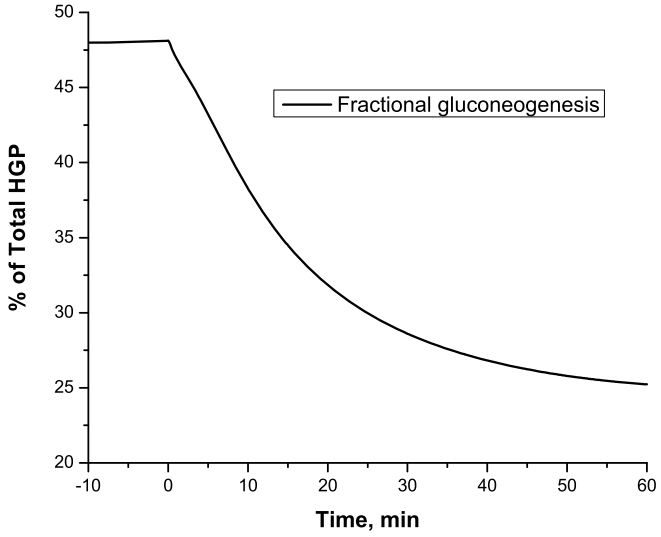

FIGURE 2.7. Dynamic responses of hepatic glycogenolysis and gluconeogenesis (A) and fractional hepatic glucneogenesis (B) to a step increase in work rate (150W) from resting state at 0 min

Fractional gluconeogenesis means the percent contribution of gluconeogenesis for hepatic glucose production (HGP). Lines represent model simulations.

A

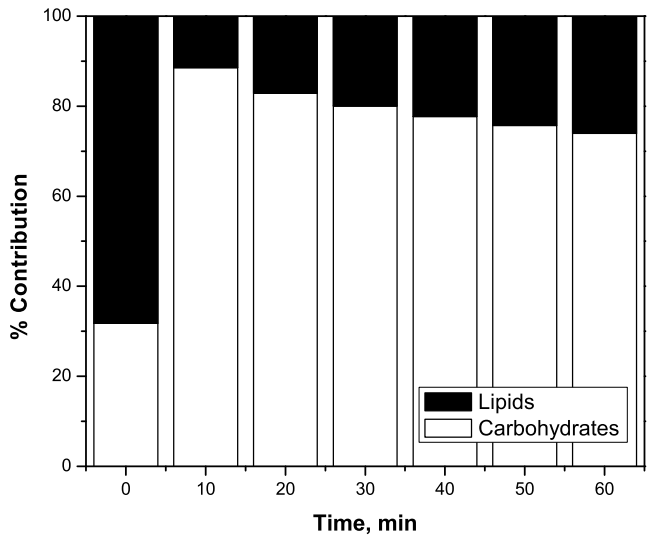

B

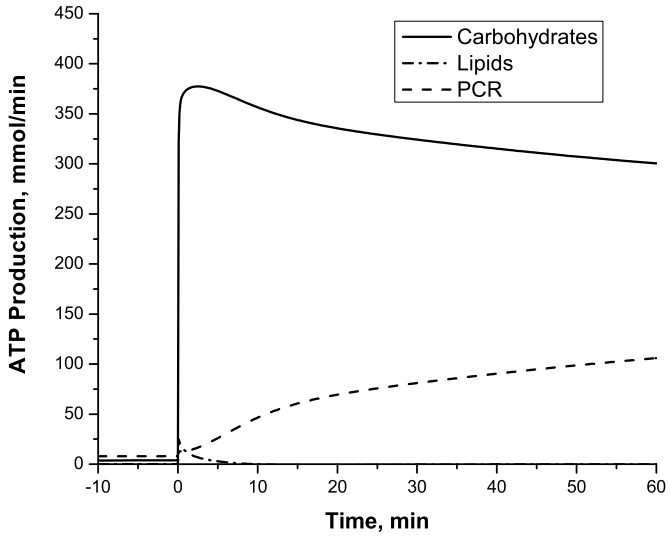

FIGURE 2.8. Contribution of fuel sources for ATP production in skeletal muscle during 60 min exercise

A: contribution of carbohydrates, lipids, and PCR; B: relative contribution of carbohydrates and lipids;

A

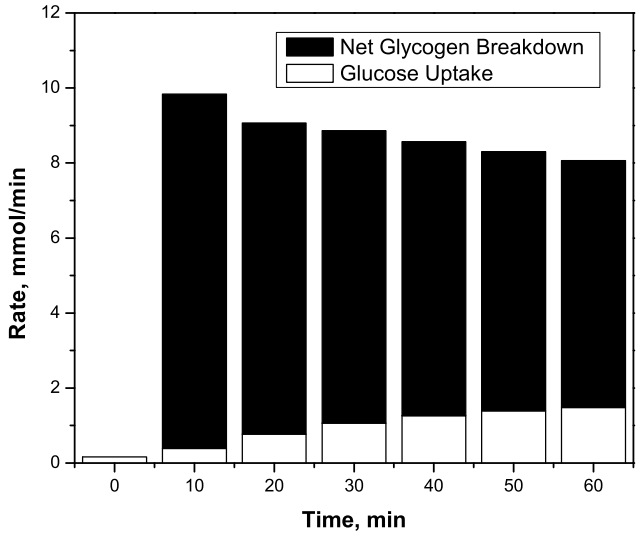

B

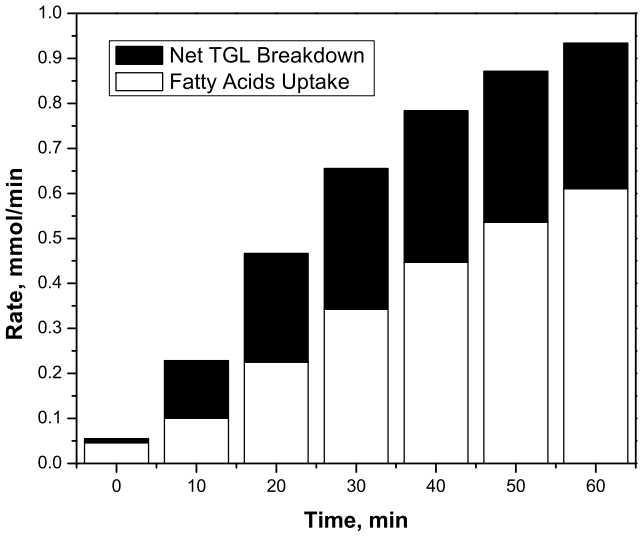

FIGURE 2.9. Dynamic changes of carbohydrates (intramuscular glycogen, blood glucose) (A) and lipids (intramuscular TG, blood fatty acids) (B) utilization rates during 60 min exercise

CHAPTER 3.

A COMPUTATIONAL MODEL OF ADIPOSE TISSUE METABOLISM *IN VIVO* DURING INTRAVENOUS EPINEPHRINE INFUSION

3.1. INTRODUCTION

Adipose tissue is no longer considered a metabolically quiescent storage depot of lipids, but an active organ that regulates plasma fatty acid (FA) levels (Frayn, 2002;Frayn et al., 2003) and secretes various cytokines and hormones such as leptin, adiponectin, resistin, tumor necrosis factor (TNF)-α and visfatin (Trayhurn and Beattie, 2001;Frayn et al., 2003). The understanding of adipose tissue metabolism and its regulation is underscored by the demonstration of its role in the development of insulin resistance, regulation of satiety, and other metabolic functions (Kahn et al., 2006;Frayn, 2001).

Since adipose tissue does not have a unique artery (inflow) and vein (outflow), reliable *in vivo* data across this tissue are limited. In fact, the only location available for arteriovenous difference measurement in human is the subcutaneous fat bed in the abdominal wall (Samra et al., 1996;Frayn et al., 1994;Coppack et al., 1990). Based on data from this single depot, generalizations cannot be made about all metabolically heterogeneous depots (subcutaneous vs. visceral) of adipose tissue (Jensen, 2002). As an alternative, *in vivo* microdialysis has been applied to study adipose tissue metabolism in humans, but it provides only qualitative data of several metabolites in the interstitium. *In vitro* studies of tissue explants or isolated cells do not provide comparable physiological data with respect to *in vivo* conditions (Frayn et al., 2003). Mathematical models and simulations of adipose tissue metabolism *in vivo* offer a method for quantitative analysis

of control mechanisms for lipid mobilization and for prediction of physiological responses.

Adipose tissue comprises about 20% of body weight but its rate of utilizing oxygen in the basal state is less than 2% of whole body rate of oxygen consumption (Frayn et al., 1995). Despite its negligible contribution to energetics, it actively participates in the whole body fuel homeostasis by modulating lipid metabolism. Regulation of breakdown (lipolysis) and synthesis (esterification) of triglycerides (TG) in adipose tissue controls lipid flux into circulation. Since adipose tissue via lipolysis releases more FA into circulation than required for oxidation, a significant part of the released FA are re-esterified in adipose tissue and in other organs. This triglyceride- fatty acid (TG-FA) cycle, is composed of an intra-adipose tissue cycle and an extra-adipose tissue cycle. FA released into plasma are taken up by the liver, re-esterified, and secreted as very large density lipoprotein (VLDL)-TG, which are then transported to the periphery to be reincorporated into adipose tissue TG (Newsholme and Crabtree, 1976;Klein and Wolfe, 1990;Frayn et al., 1994). As proposed by Newsholme et al. (Newsholme and Crabtree, 1976), the existence of TG-FA cycle provides for increased sensitivity and flexibility in controlling lipid mobilization.

Hormone sensitive lipase (HSL) was considered the only rate limiting enzyme for lipolysis of TG in adipose tissue (Large et al., 1998). However, recently, it has been shown that HSL deficient mice retain the basal lipolysis rate and respond to the beta-adrenergic stimulation, although the response was quantitatively less than in normal controls (Okazaki et al., 2002;Zechner et al., 2005;Haemmerle et al., 2002). The accumulation of diglycerides (DG) in the adipose tissue of HSL knockout mice suggests that HSL is the rate limiting enzyme for the hydrolysis of DG and not TG (Haemmerle et

al., 2002). Adipose TG lipase (ATGL) has been suggested to be the key enzyme involved in TG hydrolysis in the adipose tissue (Schweiger et al., 2006;Haemmerle et al., 2006;Zimmermann et al., 2004). TG lipolysis was shown to be severely impaired in ATGL-deficient mice accumulating large amount of fat in major organs and leading to premature death (Haemmerle et al., 2006). The integrated response of these lipase reactions is essential to understand the metabolic regulation of lipolysis in the adipose tissue.

Re-esterification of fatty acids requires a source of glycerol-3-phosphate (G3P). Since the activity of glycerol kinase is very low in the adipose tissue (Edens et al., 1990b), it cannot form G3P from glycerol in significant quantities. Instead, glucose and/or pyruvate are utilized to produce G3P. The use of pyruvate to form G3P has been termed glyceroneogenesis (Reshef et al., 2003). Quantitative estimation of glyceroneogenesis has not been performed in humans *in vivo*. Animal studies using isotopic tracers have shown that glyceroneogenesis is the dominant pathway in different physiological and nutritional conditions (Tordjman et al., 2003;Brito et al., 2006) (C. K. Nye, R. W. Hanson, and S. C. Kalhan, unpublished data). These data underscore the need to examine the metabolism of the precursors for G3P by the adipose tissue.

In the present study, we have developed a mathematical model of adipose tissue metabolism *in vivo* in humans in the fasting state and investigated the integrated response to increased lipolysis induced by epinephrine. The intravenous epinephrine infusion study in human inguinal fat bed was used to validate the model simulations (Samra et al., 1996). We assessed the capability of the model to reproduce and predict the physiological responses to enzymatic modulation in steady state by altering the expression levels of ATGL and HSL. We hypothesized that a metabolic subdomain exists in the adipose

tissue due to the large volume fraction of lipid droplets and most of the metabolic reactions occur in a small region of adipose tissue. In addition, we postulated that the individual lipase reactions are differentially activated during epinephrine infusion resulting in the distinctive dynamics of lipolytic intermediates (i.e., DG, MG). Finally, we used this model to predict the source of G3P. We hypothesized that the increase in FA levels during epinephrine infusion inhibits pyruvate oxidation and increases glyceroneogenesis.

3.2. METHODS

A mathematical model of adipose tissue metabolism was developed that incorporates essential transport and reaction processes. The model is composed of spatially lumped cellular and blood compartments. Exchange of substrates occurs between the two compartments via simple diffusion or carrier-mediated transport. For a minimal representation of the consequences of glucose and fatty acid metabolism, individual metabolic pathways are lumped to include at least one irreversible reaction step favoring the formation of product (Figure 3.1). The reversible reactions catalyzed by lactate dehydrogenase (LDH) and G3P dehydrogenase have forward and reverse rate coefficients that are related by the thermodynamic constraint (Appendix III). Pathways associated with TG breakdown and synthesis include various lipolytic intermediates (i.e., DG, MG) and regulatory enzymes, i.e., ATGL, HSL, MGL (monoglyceride lipase) as shown in Figure 3.1.

3.2.1. Chemical species

The major metabolic species related to glucose and fatty acid metabolism were

incorporated into the model. Glycolytic species included glucose (GLC), glucose-6-phosphate (G6P), glycerol-3-phosphate (G3P), glyceraldehydes-3-phosphate (GAP), pyruvate (PYR), and lactate (LAC). Chemical species for lipid metabolism included FA, TG, DG, MG, fatty acyl-CoA (FAC), free CoA, and glycerol (GLR). Palmitate with 16 carbons was considered to represent all FAs. TG, DG, and MG were considered esterified products of G3P and palmitate. Acetyl-CoA (ACoA) and oxygen were included for substrate oxidation. ATP, ADP, inorganic phosphate (Pi), NADH, and NAD^+ were incorporated into the reaction steps where they were required as co-substrates. Finally, alanine (ALA) was used as the representative amino acid.

3.2.2. Model Specifications and Assumptions

The basal condition for model simulations was the overnight fasted human at rest. Data from arteriovenous balance studies of the subcutaneous adipose tissue bed (Frayn et al., 1991;Frayn et al., 1995;Frayn et al., 1994;Coppack et al., 1990) and biochemical data of enzyme activity (Zechner et al., 2005;Shen et al., 1998;Large et al., 1998), were utilized to develop the framework of metabolic fluxes. Various assumptions were required in the absence of experimental data.

Carbohydrate and energy metabolism: Glucose and FA are the major fuels for adipose tissue. Approximately 50% of the glucose taken up by the adipose tissue is used for oxidative metabolism and about 40% is released as lactate (Frayn et al., 1995;Coppack et al., 1990). FA oxidation accounted for the remaining oxygen consumption. The relative contribution of glucose and FA to oxidative metabolism is consistent with reported respiratory quotient (RQ) of 0.91 (Coppack et al., 1990). Synthesis and breakdown of glycogen were considered to be negligible (Jurczak et al.,

2007). We assumed that less than 10% of glucose uptake was converted to G3P, which can also be formed from pyruvate via glyceroneogenesis (Reshef et al., 2003). Uptake of glucose and release of lactate by the adipose tissue of humans indicates a significant glycolytic contribution to G3P (Coppack et al., 1990). In contrast, animal studies using isotopic tracers have shown glyceroneogenesis to be the major pathway for G3P synthesis under different physiological and nutritional conditions (Tordjman et al., 2003;Brito et al., 2006). Therefore, we assumed equal contribution of glycolysis and glyceroneogenesis in the basal state. However, we investigated the effects of different weightings of the two pathways during epinephrine infusion.

Lipid metabolism: The contribution of lipolysis in the blood compartment by lipoprotein lipase (LPL) was determined from the arteriovenous difference (AVD) of TG in adipose tissue bed (Samra et al., 1996). The intracellular rates of lipolysis by ATGL, HSL, and MGL were estimated from the difference between AVDs of glycerol and TG such that ~15% of the produced FA are re-utilized inside adipose tissue (Frayn et al., 1994;Coppack et al., 1990). Finally, fluxes through individual lipase reaction were estimated based on the 10-fold higher activity that HSL has for DG than for TG and MG (Shen et al., 1998;Haemmerle et al., 2002). Thus, the flux rate for DG breakdown by HSL was calculated first and then those for TG and MG breakdown by HSL. The maximum rate coefficient of HSL ($V_{max,k}$) for TG and MG breakdown were 10-times lower than that for DG breakdown.

Although FA can be transported by both simple diffusion and carrier-mediated transport (Bradbury, 2006), the simple diffusion of FA was assumed in this model.

Amino acid metabolism: A net release of amino acids into plasma from adipose tissue occurs in the fasting state (Patterson et al., 2002). Alanine and glutamine are

released in significant quantities and there is a net uptake of glutamate by the adipose tissue (Frayn et al., 1991). The net release of amino acids by the adipose tissue and the rate of proteolysis in the adipose tissue were used to calculate the mass transport and the rates of appearance of amino acids as represented by alanine (Patterson et al., 2002;Coppack et al., 1996).

Reaction Kinetics: Kinetic expressions based on *in vitro* data for each elementary enzymatic reaction were not feasible for this *in vivo* study. Instead, we used a phenomenological Michaelis-Menten (M-M) equation constrained by the physiological conditions. We assumed that all metabolic reactions are expressed by a general bi-bi M-M form. The kinetic parameters such as the phenomenological M-M constants (i.e., $K_{m,k}$, $K_{i,k}$, $K_{f,k}$ and $K_{b,k}$) were set to the initial tissue concentrations of the corresponding substrates. Since we used a top-down approach to relate the responses of different scales (i.e., cellular and tissue levels), several reaction steps are lumped. Palmitate and alanine represent the entire family of fatty acids and amino acids. The efficacy of this approach has been demonstrated in other studies (Kim et al., 2007;Zhou et al., 2005). Since the maximum rate coefficients are determined from *in vivo* flux data and the phenomenological M-M constants, the metabolic fluxes described by this method can be bounded within physiological limits.

Intracellular compartmentation: Due to the large volume fraction of lipid droplets in the adipocyte, we postulated that most of the metabolites are localized in a small sub-cellular domain. The effect of cellular localization of chemical species was examined by modulating the volume fraction of adipose cellular compartment (v_{cf}). The cellular volume fraction assuming localization was optimally estimated using data from the literature. For comparison, simulation without localization assumed the physical volume

fraction of adipose tissue cells (v_{cf} = 0.8). TG, DG, and MG, whose concentrations are high compared with other substrates, were not assumed localized in the subdomain.

Activation of lipolytic reactions: HSL can break down all lipolytic intermediates (i.e., TG, DG and MG), while ATGL is responsible for hydrolyzing TG only (Large et al., 2004;Langin and Arner, 2006;Zechner et al., 2005). The breakdown of MG is not subject to beta-adrenergic stimulation (Large et al., 2004;Zechner et al., 2005). We assumed that the following three lipolytic reactions are subject to beta-adrenergic stimulation: 1) TG breakdown to DG by ATGL, 2) TG breakdown to DG by HSL, and 3) DG breakdown to MG by HSL. We compared two different schemes for activating lipolytic reactions. We tested the hypothesis that individual lipolytic reactions were differentially activated during epinephrine infusion as quantified by different degrees of activation (λ_k). Thus, the rates of TG and DG breakdown could be increased to different extents. Simulations of differential activation for lipase reactions were compared with simulations of uniform activation (λ_k) values so that TG and DG breakdown have the same stimulation.

Beta-adrenergic stimulation: Cyclic-AMP (cAMP) dependent protein kinase A (PKA) phosphorylates HSL and other proteins including perilipin upon beta-adrenergic stimulation (Brasaemle et al., 2000). The time scale of increase in cAMP levels and activation of PKA is reported to be less than 1 min (Honnor et al., 1985). In contrast, the response to the intravenous epinephrine infusion showed that the peak concentration of venous epinephrine was reached after ~30min (Samra et al., 1996). The time scales of fatty acids and glycerol releases were more comparable to that of venous epinephrine levels (Samra et al., 1996). Consequently, the effect of instantaneous changes in cAMP levels on the simulated responses would be negligible in the time frame of our model simulation (~60min). Therefore, we have lumped all the cascade controls of the

molecular level regulatory mechanisms into the action of epinephrine by introducing a phenomenological equation relating the activation of lipolytic reactions to the venous epinephrine levels. With this algorithm, the modulation of maximum rate constants (V_{max}) by epinephrine represents not only the activation of lipase, but also concomitant activation of other proteins including perilipin.

3.2.3. Dynamic mass balance equations

The dynamic mass balance equations describe changes in substrate concentration in blood and adipose cells in tissue. The blood compartment represents plasma in equilibrium with interstitial fluid. The concentration of substrate i in the blood compartment is determined by:

$$V_b \cdot \frac{dC_{b,i}}{dt} = Q \cdot (C_{a,i} - C_{b,i}) + R_{b,i} - J_{b\leftrightarrow c,i} \tag{3.1}$$

where $C_{a,i}$ is the arterial concentration; $C_{b,i}$ is the capillary blood concentration (equal to the adipose venous concentration $C_{v,i}$); Q is the blood flow in adipose tissue; $J_{b\leftrightarrow c,i}$ is the net mass transport flux across the blood-cell exchange barrier; $R_{b,i}$ is the net metabolic reaction rate of substrate i in the blood compartment; V_b is the volume of blood compartment, which is equal to the physical volume of capillary blood and interstitial fluid comprising 20% of total tissue volume (V_{tissue}). Since oxygen and carbon dioxide are transported as free and bound forms in the blood, the effective volume of the blood compartment is different from the physical volume as shown in Appendix IV.

In the adipose cellular compartment, the dynamic mass equation of substrate i is

$$V_c \cdot \frac{dC_{c,i}}{dt} = R_{c,i} + J_{b\leftrightarrow c} \tag{3.2}$$

where $C_{c,i}$ is the cellular concentration; $R_{c,i}$ is the net metabolic reaction rate of substrate

i; V_c is the volume of the cellular compartment.

For convenience in simulation, the compartment volumes in Eq. (3.1) and (3.2) were replaced with the volume fractions ($v_{bf} = V_b/V_{tissue}$ or $v_{cf} = V_c/V_{tissue}$). Consequently, blood flow and rate coefficients in this model are specified per unit volume of tissue. For comparison to experimental data, the blood flow, AVD, and metabolic reaction rates from the model equations were converted from a tissue volume basis to a tissue wet weight basis by division with mass density.

3.2.4. Mass transport flux between blood and tissue

The substrates involved in blood-tissue transport are glucose, lactate, pyruvate, alanine, glycerol, FA, carbon dioxide, and oxygen. They are transported via either simple diffusion or carrier-mediated (facilitated) transport. The mass transport flux of glycerol, FA, oxygen and carbon dioxide between blood and cell ($J_{b\leftrightarrow c,i}$) occurs by passive diffusion:

$$J_{b\leftrightarrow c,i} = \gamma_i \cdot (C_{b,i} - C_{c,i}) \tag{3.3a}$$

where γ_i is the mass transport coefficient of *substrate i*. The mass transport flux of glucose, pyruvate, lactate and alanine occurs by facilitated transport:

$$J_{b\leftrightarrow c,i} = T_{\max,i}\left(\frac{C_{b,i}}{M_{m,i} + C_{b,i}} - \frac{C_{c,i}}{M_{m,i} + C_{c,i}}\right) \tag{3.3b}$$

where $T_{max,i}$ is the maximum mass transport coefficient of *substrate i* and $M_{m,i}$ is the M-M constant of *substrate i*.

3.2.5. Metabolic flux

The metabolic reaction rates ($R_{x,i}$, x = b or c) are the net result of metabolic

reactions producing and utilizing the corresponding substrate:

$$R_{x,i} = \sum_k \alpha_{i,k}\phi_{x,k} \ , \quad x = b \text{ or } c \tag{3.4}$$

where $\phi_{x,k}$ is the flux rate of the metabolic reaction k including *substrate i*; $\alpha_{i,k}$ is the corresponding stoichiometric coefficient, which is either positive (product) or negative (reactant). The net reaction rate for each substrate is shown in Table 3.1.

Metabolic fluxes are expressed with a general irreversible bi-bi substrate to product enzymatic reaction coupled with controller energy metabolite pairs (Kim et al., 2007).

$$X + Y \xrightarrow{E_1 \quad E_2} V + W$$

where E_1 and E_2 are ATP and ADP or vice-versa, and/or NADH and NAD^+ or vice-versa. The corresponding reaction flux equation for flux k can be expressed as:

$$\phi_k = V_{\max,k}\left(\frac{PS^{\pm}}{\mu^{\pm} + PS^{\pm}}\right)\left(\frac{RS^{\pm}}{\nu^{\pm} + RS^{\pm}}\right)\left(\frac{C_X \cdot C_Y}{K_{m,k} + C_V \cdot C_W \cdot K_{m,k}/K_{i,k} + C_X \cdot C_Y}\right) \tag{3.5}$$

where C_X, C_Y, C_V, and C_W are reactant and product concentrations; $V_{max,k}$ is the maximum rate coefficient in flux k; $K_{m,k}$ is the phenomenological M-M constant for the reactants; $K_{i,k}$ is the constant for the product inhibition. Product inhibition occurs only in reactions specified in Appendix I. PS^+ (= C_{ATP}/C_{ADP}) and RS^+ (= C_{NADH}/C_{NAD+}) indicate cellular phosphorylation and redox states. For some reactions, the effect of these controllers can be in the opposite direction. In this case, $PS^- = 1/PS^+$ and $RS^- = 1/RS^+$. In addition, $\mu^{\pm}$ and $\nu^{\pm}$ are parameters for the metabolic controllers.

Fluxes of lactate dehydrogenase and G3P dehydrogenase reactions, which can be close to thermodynamic equilibrium, are described as reversible reactions:

$$\phi_{\mathrm{k}} = \left(\frac{V_{\mathrm{f,k}} \frac{C_{\mathrm{X}} \cdot C_{\mathrm{Y}}}{K_{\mathrm{f,k}}} - V_{\mathrm{b,k}} \frac{C_{\mathrm{V}} \cdot C_{\mathrm{W}}}{K_{\mathrm{b,k}}}}{1 + \frac{C_{\mathrm{X}} \cdot C_{\mathrm{Y}}}{K_{\mathrm{f,k}}} + \frac{C_{\mathrm{V}} \cdot C_{\mathrm{W}}}{K_{\mathrm{b,k}}}} \right) \tag{3.6}$$

where $V_{f,k}$ and $V_{b,k}$ are the forward and reverse rate coefficients; $K_{f,k}$ and $K_{b,k}$ are the phenomenological M-M constants for reactants and products; K_{eq} is the equilibrium constant calculated from the Gibbs free energy of reaction. The reaction rate coefficients are related by a thermodynamic constraint (or Haldane relationship):

$$V_{\mathrm{f,k}} = V_{\mathrm{b,k}} \frac{K_{eq} \cdot K_{\mathrm{f,k}}}{K_{\mathrm{b,k}}} \tag{3.7}$$

In the blood compartment, the breakdown of TG to FAs and glycerol is the only reaction that is catalyzed by LPL. Since some LPL is carried by blood (Karpe et al., 1998), the activity of LPL reaction depends on adipose blood flow:

$$\phi_{\mathrm{TG}\rightarrow\mathrm{GLR,LPL}} = V_{\mathrm{max,\,LPL}} \left(\frac{C_{\mathrm{b,TG}}}{K_{\mathrm{m,LPL}} + C_{\mathrm{b,TG}}} \right) \left(\frac{Q}{K_{\mathrm{m,Q}} + Q} \right) \tag{3.8}$$

where $K_{m,LPL}$ and $K_{m,Q}$ are phenomenological M-M constants for the LPL reaction.

In addition to the metabolic control by the cellular phosphorylation and redox state, epinephrine provides further regulation by stimulating lipolysis reactions governed by ATGL and HSL. The maximum rate coefficients for these three reactions undergo further modulation by epinephrine according to an empirical relation (Kim et al., 2007):

$$V_{\mathrm{max},k} = V^{0}_{\mathrm{max},k} \cdot \left(1.0 + \lambda_k \frac{(C_E(t) - C_E(0))^2}{\alpha + (C_E(t) - C_E(0))^2} \right) \tag{3.9}$$

where $C_E(t)$ is the epinephrine concentration in adipose venous at time t; $V^{0}_{\mathrm{max},k}$ is the basal state maximum rate coefficient; λ_k and α are parameters. Here, λ_k indicates the degree of activation for a corresponding lipolytic reaction.

3.2.6. Parameter determination at basal state

Starting with the mass transport fluxes (Table 3.2), the unknown flux rates were determined with appropriate assumptions on fuel metabolism as described above. Once all the metabolic fluxes were estimated (Table 3.3 and 3.4), then parameter values at basal state were determined together with the metabolite concentrations in blood and tissue (Table 3.5 and 3.6). Since 60~85% of adipose tissue is lipids with 90~99% being TG (Albright and Stern, 1998), the concentrations of non-lipid substrates in total tissue volume are difficult to quantify. However, their levels in the intracellular water of the adipocyte have been shown to be comparable to those in other tissues (Denton et al., 1966). When data of adipose tissue were not available, we used the concentrations in skeletal muscle (Table 3.6). The phenomenological M-M parameters, $K_{m,k}$, $K_{i,k}$, $K_{f,k}$ and $K_{b,k}$ were set to the initial tissue concentrations of the corresponding substrates. The maximum metabolic rate coefficients for irreversible reactions, $V_{max,k}$ were calculated from basal flux, tissue concentration, and $K_{m,k}$ (Table 3.3). The equilibrium constant was also utilized to calculate the forward and reverse rate coefficients ($V_{f,k}$ and $V_{b,k}$) for reversible reactions (Table 3.4). Mass transport coefficients ($T_{max,i}$ and γ_i) were computed from arteriovenous differences, blood flow rate, and concentrations in arterial blood and tissue. The parameter λ_k must be optimally estimated using data from *in vivo* epinephrine infusion studies in humans. Other model parameters are listed in Table 3.7.

3.2.7. Model simulation for epinephrine infusion

Corresponding to *in vivo* studies (Samra et al., 1996), the epinephrine infusion was simulated with a constant rate infusion for 60min (Samra et al., 1996). Since the tissue responds to the epinephrine levels in the interstitial fluid, the epinephrine levels in

adipose venous outflow were used to stimulate the cellular metabolic reactions. The epinephrine levels in the adipose tissue vein and in the adipose tissue were assumed to be in equilibrium. However, epinephrine infusion modulated the blood flow to adipose tissue as well as the arterial glycerol and FA concentrations, while the arterial levels of other metabolites were kept constant (Samra et al., 1996). Thus, venous epinephrine concentration ($C_{v,Epi}$), adipose tissue blood flow (Q), and arterial substrate concentrations for glycerol and FA ($C_{a,GLR}$, $C_{a,FA}$) were the only input functions for model simulation (Figure 3.2). These empirical relations are shown in Table 3.8.

3.2.8. Simulation strategies

The effect of intracellular compartmentation of chemical species was examined by modulating the cellular volume fraction (v_{cf}). As a comparative reference, simulations were conducted of 'localized' (i.e., optimally estimated v_{cf}) and of 'non-localized' responses (i.e., v_{cf}=0.8). Also, the effects of activation with different values of λ_k (i.e., differential activation) and with equal values of λ_k (i.e., uniform activation) were compared. The effects of different ratios of glycolysis and glyceroneogenesis on the synthesis of G3P were simulated during epinephrine infusion. An equal ratio (1:1) of these processes was assumed for the basal state.

3.2.9. Parameter estimation and numerical solution

Values of the volume fraction of cellular compartment (v_{cf}), hormonal control (λ_k) and parameters of the model input functions were estimated by minimizing the sum of squared errors between the experimental data and the corresponding simulated outputs in response to epinephrine infusion. The experimental data from studies in humans,

included AVDs of glycerol, FA and TG across the inguinal fat bed *in vivo* and the concentration dynamics of glycerol and FA in the venous blood draining the inguinal fat bed (Samra et al., 1996). The model equations were numerically solved using a stiff ordinary differential equation solver, 'ode15s' (MATLAB®, The MathWorks Inc.). Optimal estimates of the model and input parameters were obtained using 'lsqcurvefit' (MATLAB®, The MathWorks Inc.) with 'ode15s'.

3.2.10. Sensitivity Analysis

The sensitivity of the model parameters was quantified by the change in the sum of squared differences between simulated model outputs with different parameter values. Since a thorough statistical analysis of all the model parameters is not feasible, parameter sensitivity directly related to the lipid mobilization was investigated by perturbing the parameters individually. A sensitivity index for i th parameter, θ_i can be computed as done previously (Beard, 2005):

$$S_i = \max\left(\frac{\left|E(\theta_i^* + 0.1\theta_i^*) - E(\theta_i^*)\right|}{0.1E(\theta_i^*)}\right) \tag{3.11}$$

where S_i is a sensitivity index; E is the sum of squared residuals for a model output; θ_i^* is the ith parameter at its optimum. This equation represents the changes in the model output in response to 10% change in a specific parameter from its optimum.

3.3. RESULTS

3.3.1. Basal state analysis

The metabolic flux rates during basal state were estimated using the dynamic mass balance equations at steady state (Table 3.3 and 3.4). Approximately 45% (0.8

μmol·min^{-1}·kg^{-1}) of glucose taken up by adipose tissue was released as lactate and pyruvate (($J_{PYR,b\leftrightarrow c}$+$J_{LAC,b\leftrightarrow c}$, Table 3.2), ~5% was utilized to synthesize G3P for re-esterfication of fatty acids ($\phi_{\mathrm{GAP}\leftrightarrow\mathrm{G3P}}$, Table 3.4), and ~50% was oxidized ($\phi_{\mathrm{PYR}\leftrightarrow\mathrm{ACoA}}$, Table 3.3). When the activities of HSL for TG and MG breakdown were based on that of DG breakdown, it showed that ~84% of TG breakdown was catalyzed by ATGL ($\phi_{\mathrm{TG}\rightarrow\mathrm{DG,ATGL}}/(\phi_{\mathrm{TG}\rightarrow\mathrm{DG,ATGL}}+\phi_{\mathrm{TG}\rightarrow\mathrm{DG,HSL}})$) and ~89% of MG breakdown was catalyzed by MGL ($\phi_{\mathrm{MG}\rightarrow\mathrm{GLR,MGL}}/(\phi_{\mathrm{MG}\rightarrow\mathrm{GLR,HSL}}+\phi_{\mathrm{MG}\rightarrow\mathrm{GLR,MGL}})$) with an insignificant contribution by HSL (Table 3.3). VLDL-TG breakdown by LPL in the blood compartment comprised 13% of total TG breakdown in adipose tissue bed ($\phi_{\mathrm{TG}\rightarrow\mathrm{GLR,LPL}}/(\phi_{\mathrm{TG}\rightarrow\mathrm{DG,ATGL}}+\phi_{\mathrm{TG}\rightarrow\mathrm{DG,HSL}}+\phi_{\mathrm{TG}\rightarrow\mathrm{GLR,LPL}})$, Table 3.3). The total production of FA by lipolysis in the tissue was 10.3 μmol·min^{-1}·kg^{-1} ($\phi_{\mathrm{TG}\rightarrow\mathrm{DG,ATGL}}+\phi_{\mathrm{TG}\rightarrow\mathrm{DG,HSL}}+\phi_{\mathrm{DG}\rightarrow\mathrm{MG,HSL}}$, Table 3.3): ~84% of FA were released into the circulation ($J_{FA,b\leftrightarrow c}$, Table 3.2), ~12% was re-esterified ($\phi_{\mathrm{G3P\text{-}FAC}\rightarrow\mathrm{DG}}+\phi_{\mathrm{DG\text{-}FAC}\rightarrow\mathrm{TG}}$) and ~4% was oxidized ($\phi_{\mathrm{FAC}\rightarrow\mathrm{ACoA}}$) (Table 3.3). In contrast, ~99.7% of glycerol produced was released into the circulation ($J_{FA,b\leftrightarrow c}$, Table 3.2) with insignificant re-utilization within the tissue ($\phi_{\mathrm{GLR}\rightarrow\mathrm{G3P}}$, Table 3.3).

3.3.2. Effect of change in lipase activity

Beginning with the basal model parameters, the basal maximum rate constants (V_{max}) for HSL and ATGL were modulated to simulate the effect of change in lipase activity. V_{max} for HSL reactions ($V_{max,HSL,TG\rightarrow DG}$, $V_{max,HSL,DG\rightarrow MG}$, $V_{max,HSL,MG\rightarrow GLR}$) were modulated in order to examine the effect of over- and under-expression of the enzyme. Multiplying the V_{max} with a factor smaller than one, represents knockdown of the expression of the corresponding enzyme, while multiplying with a factor larger than one

represents over-expression. The new steady-state flux rates were determined after the model parameters were perturbed. Similarly, the steady-state fluxes for the reaction catalyzed by ATGL ($V_{max,ATGL,TG\rightarrow DG}$) were determined.

Figure 3.3A shows rates of release of FA and glycerol at the steady state in relation to the change in activities of HSL and ATGL relative to control value (=1). A decrease in the activity of ATGL to zero lowered the rate of release of FA by 88%, while a decrease in the activity of HSL caused a 68% reduction in the release rate of FA. The rate of release of glycerol decreased by 76% associated with HSL and 66% associated with ATGL. As shown in Figure 3.3B, the model simulations showed a 6-fold increase in concentration of DG (relative to control) with decreasing HSL activity. In contrast, DG concentration decreased by ~85% with decreasing ATGL activity because of the lower production of DG from TG hydrolysis by ATGL. There was no significant difference in the tissue concentration of MG as a result of varying enzyme activities.

Over-expressing ATGL increased the rates of release of both FA and glycerol more than those with the over-expression of HSL (~150% in ATGL vs. ~50% in HSL). The magnitude of increase was higher for FA (150% increase) than for glycerol (120% increase). The higher production of DG as a result of TG hydrolysis by ATGL resulted in the accumulation of DG. In contrast, the over-expression of HSL resulted in a higher rate of breakdown of DG relative to TG hydrolysis and, consequently, lower tissue levels of DG. The levels of MG were increased by higher activities of both ATGL and HSL.

3.3.3. Model validation and intracellular compartmentation

Model simulations showed that epinephrine infusion increased glycerol (~3 fold) and FA (~4 fold) release rates (i.e., AVD) from adipose tissue into the circulation (Figure

3.4A, 3.4B). Simulated AVD responses are in agreement with the experimental data assuming localized metabolism (v_{cf}=0.031) and differential activation of lipases (i.e., λ_k) with parameter values in Table 3.9 The effect of v_{cf} on glycerol AVD was much less than that on FA AVD. When the lipase reactions were not localized (v_{cf}=0.8), the initial increase in FA release rate was slower and 30~50% smaller than that found experimentally (Figure 3.4A, 3.4B). Model simulation showed that the breakdown of plasma TG by LPL, as indicated by AVD, gradually increased by a factor of 5 (Figure 3.4C). Both glycerol and FA concentrations in the venous blood reached maximal values around ~25min with 20% and 70% increases, but returned to basal values at the end of epinephrine infusion (Figure 3.5). The localization of lipase reactions had minimal effect on the response of glycerol in the venous blood (Figure 3.5A). However, the initial dynamics of FA (up to 30min) were much slower without localization (v_f=0.8) resulting in 10~20% lower venous levels (Figure 3.5B).

3.3.4. Regulation of lipase activities

The parameter values for which the model simulations produced the best fit to experimental data are listed in Table 3.9 for differential and uniform activation (λ_k). In the former, the optimal estimates for λ_k indicate that the activation of lipolytic reactions catalyzed by HSL and ATGL increased by 1.7~7.2 fold. The activation required to convert DG to MG by HSL (λ_k = 6.2) was approximately 4 times larger (λ_k = 0.7~0.9) than for other reactions. With uniform activation (λ_k = 3.18), all lipase reactions were increased by the 4.18 fold. Figure 3.3 and 3.4 show the effect of different lipase regulations in response to epinephrine infusion. When the metabolic reactions were localized (v_f=0.031), the AVD and the venous concentration dynamics of FA were in good

agreement with experimental data with both activation schemes. In contrast, the AVD of glycerol during the first 30 min was 15~20% lower with uniform activation than with differential activation. This produced lower glycerol concentration in the venous outflow (Figure 3.4A and 3.5A).

3.3.5. MG and DG dynamics

Due to the intracellular TG-FA cycle, the simulated ratio of FA to glycerol released from adipose tissue cells into the blood circulation at basal state, $J_{FA,b\leftrightarrow c}/J_{GLR,b\leftrightarrow c}$ ~2.5 (Figure 3.6A) was lower than the theoretical maximum ratio of 3. However, this ratio increased above the theoretical maximum of 5.6 at 8min and then gradually decreased to 2.8 at 60min. A ratio above 3 indicates an accumulation of the glycerol moiety in adipose tissue as DG and/or MG. Therefore, the model can be used to predict the major contributors to the accumulation of glycerol by simulating the tissue dynamics of lipolytic intermediates (DG and MG). Model simulations showed that MG continuously accumulated in tissue during epinephrine infusion (0.2mM to 0.93mM), while DG levels decreased from 2mM to 1.1mM (Figure 3.6B).

3.3.6. Re-esterification dynamics

Increased FA availability as a result of TG breakdown in the adipose tissue resulted in a higher intracellular re-esterification rate (Figure 3.7A). Model simulations showed that the re-esterification rate reached its maximum (1.45 μmol/kg/min) at 10min and gradually decreased toward the basal value. An increased re-esterification rate was associated with an increased rate of G3P synthesis. The relative contribution of glyceroneogenesis to G3P synthesis increased 3~14% during epinephrine infusion

regardless of its fractional contribution at the basal state (Figure 3.7B).

3.3.7. Sensitivity Analysis

The sensitivity of the model parameters was quantified by the change in the sum of squared differences between simulated model outputs with different parameter values. In addition to the parameters (V_c, $\lambda_{ATGL,TG\rightarrow DG}$, $\lambda_{HSL,TG\rightarrow DG}$, and $\lambda_{HSL,DG\rightarrow MG}$) optimally estimated from the experimental data, V_{max} and K_m for the reactions involved in lipolysis and transacylation were investigated as well. The sensitivity indices of the various model parameters are listed in Table 3.10. The high sensitivity indices of the parameters involved in breakdown of DG by HSL and MG by MGL (e.g., $\lambda_{HSL,DG\rightarrow MG}$, $V_{max,HSL,DG\rightarrow MG}$ and $V_{max,MGL,MG\rightarrow GLR}$) suggest that the model output is more responsive to the changes in these parameters. In contrast, the low sensitivity indices of the parameters involved in breakdown of TG by HSL and ATGL (e.g., $\lambda_{HSL,TG\rightarrow DG}$, $V_{max,HSL,TG\rightarrow DG}$, $K_{m,ATGL,TG\rightarrow DG}$ *and* $K_{m,HSL,TG\rightarrow DG}$) suggest a minimal effect of these parameters on the model output.

3.4. DISCUSSION

Even though adipose tissue plays a significant role in regulating whole body fuel metabolism, it has been difficult to get reliable quantitative data (e.g., exchange of substrates) due to the heterogeneity of fat depots. Furthermore, data from various kinds of experimental studies must be integrated to get a coherent understanding of adipose tissue metabolism. Therefore, we developed a physiologically based mechanistic model of adipose tissue metabolism that includes key metabolites and regulatory enzymes in the metabolic pathways. With this model, we integrated available information on mass transport mechanisms for the tissue-blood substrate exchange, cellular metabolic

pathways and their control mechanisms, as well as specific physiological characteristics of adipose tissue. Estimated parameters and dynamic responses by the model simulations were similar to those in the literature and provided insight into those that cannot be estimated *in vivo*.

3.4.1. Effect of altered expression levels of lipases

LPL catalyzes hydrolysis of VLDL-TG in the capillary bed of the adipose tissue. Until recently, HSL was considered the only lipase responsible for hydrolyzing intracellular TG stores. However, the existence of another intracellular lipase was proposed since it was reported that HSL deficient mice retain the basal lipolytic rate (Okazaki et al., 2002;Zechner et al., 2005;Haemmerle et al., 2002). The critical roles of this new lipase, ATGL have been shown in various studies with transgenic mice (Haemmerle et al., 2006). Due to the experimental difficulties, however, the comprehensive analysis on physiological responses in these transgenic mice could not be done, and *in vitro* studies had to be resorted for the indirect measurement. Therefore, we used the model to reproduce and predict the physiological responses arising from the genetic modulation.

As shown in Figure 3.3A, the simulations confirm the important role of ATGL in regulating the basal lipolytic rate. The greater decrease of FA release by knocking down ATGL expression than that of HSL is consistent with experimental observations with transgenic mice, where ATGL-deficient mice have substantially lower levels of plasma FA (60% lower than the control) in association with massive accumulation of lipid (Haemmerle et al., 2006). In contrast, HSL- deficient mice have moderate reduction (10~20%) in the plasma FA levels without significant decrease in the basal lipolytic rate

(Wang et al., 2001). As expected from the fact that DG can be hydrolyzed only by HSL, it was shown that DG accumulated in the adipose tissue of HSL-deficient mice (Haemmerle et al., 2002).

The model simulations, which were in good agreement with experimental observations, provided additional information on the lipolytic intermediate levels in other alterations. However, the reduction in the rate of release of FA with decreasing HSL activity seems to be higher in the model simulation because the basal lipolytic rate was unaltered in HSL-deficient mice. This discrepancy could be associated with a concomitant increase in ATGL expression of HSL- deficient mice to compensate for the decreased lipolytic rate due to the reduction in HSL activity. Indeed, when the expression of HSL was knocked out, the model was able to simulate a 3-fold increase in ATGL activity that maintained the rate of release of FA from the adipose tissue (data not shown).

3.4.2. Intracellular compartmentation

The localized metabolism in a subdomain volume of adipose tissue cells had significant impact on simulated responses. A smaller subdomain volume produced faster dynamic responses for the substrate exchange and adipose venous concentration of glycerol and FA (Figure 3.4 and 3.5). Furthermore, the higher concentrations increased the blood-tissue concentration gradient to produce the required mass transport rate for sufficient metabolism. This effect was magnified by the initial acceleration in the rate of lipolysis in the tissue that increased intracellular concentrations of glycerol and FA. The localized metabolic subdomain is consistent with a small cytosolic volume due to large lipid droplet in adipocyte (Moore et al., 2005;Denton et al., 1966). Furthermore, the volume fraction of this metabolic subdomain estimated by the model corresponds to the

volume fraction of intracellular water space (1~4% of total tissue volume) measured from *in vitro* studies of adipose fat pad (Denton et al., 1966;Crofford and Renold, 1965)

Recent *in vitro* studies of adipocyte lipid mobilization showed that major lipolytic enzymes and proteins are co-localized in a subcellular domain during beta-adrenergic stimulation (Granneman et al., 2007;Moore et al., 2005;Clifford et al., 2000). The localization of enzyme complexes reduces the transit time of metabolites which allows faster cellular dynamics (Welch and Easterby, 1994). To simulate cellular dynamic responses observed experimentally, cellular metabolites and enzymes should be localized to a metabolic subdomain of ~3% of total adipose tissue volume. Under this condition, model simulations can relate the intracellular mechanisms to the physiological response of the adipose tissue bed.

3.4.3. Differential regulation of lipases

Regulation of lipase reaction during beta-adrenergic stimulation involves complex cellular mechanisms (Langin and Arner, 2006;Large et al., 2004). While HSL is highly regulated via reversible phosphorylation by protein kinase A (PKA), the breakdown of TG by HSL requires co-activation of another protein called perilipin, which coats lipid droplets and prevents HSL and ATGL from hydrolyzing TG (Clifford et al., 2000). Consequently, the lipolysis of TG is an integrated process involving differential regulation of major lipases and other proteins. Only with differential activation for regulating lipase reactions did model simulations compare well with experimental data.

After 30 min of epinephrine infusion, glycerol AVD reached ~60% and FA AVD reached ~80% of their steady-state values. The faster dynamic response and higher FA production from adipose tissue (Figure 3.4) is required to generate the sufficient

concentration gradient for blood-tissue transport. The estimated parameter values (Table 3.9) show that DG breakdown by HSL required four times higher activation during beta-adrenergic stimulation than TG breakdown by ATGL and HSL. To simulate experimental data, the first and the second steps in lipid mobilization were stimulated to different extents. These data are consistent with the suggested role of perilipin in TG hydrolysis (Sztalryd et al., 2003;Londos et al., 1995)

The model was formulated using the biochemical data that MG breakdown by HSL and MGL are not subject to the activity change via phosphorylation with constant maximum rate coefficients (Large et al., 2004;Zechner et al., 2005). As a consequence, while MG levels in adipose tissue increased, DG levels in adipose tissue decreased over time due to the greater increase in HSL activity for DG breakdown. The accumulation of either MG or DG can be expected from a ratio of glycerol to FA release rate higher than 3. However, model simulations predicted that accumulation of MG and not DG occurs (Figure 3.6B). *In vitro* study of human adipose tissue showed 46~53% reduction in the DG levels during the increased lipolysis (Edens et al., 1990a), which is close to our model simulations (45% reduction). Measurement of dynamic changes of lipolytic intermediates (e.g., DG, MG) during epinephrine infusion *in vivo* will be required to confirm the model predictions of differential activation of lipase reactions.

3.4.4. Source of G3P for re-esterification

Glyceroneogenesis, an abbreviated version of gluconeogenesis, involves the formation of G3P from precursors other than glucose or glycerol (Reshef et al., 2003). Since the adipose tissue lacks glycerol kinase, it cannot directly utilize glycerol for TG synthesis (Reshef et al., 2003). Therefore, G3P for the intracellular re-esterification of FA

is formed from either glucose or pyruvate. We used the model to predict the relative contribution of glucose and pyruvate to G3P synthesis during the intravenous epinephrine infusion. In the absence of available *in vivo* human data, we assumed that glucose via glycolysis and pyruvate via glyceroneogenesis contribute equally in the basal state. Model simulations showed the effect of varying these contributions. Intracellular re-esterification increased by up to 13% during epinephrine infusion (Figure 3.7A). In the absence of changes in other hormone levels during epinephrine infusion (Samra et al., 1996), the re-esterification rate was primarily regulated by the availability of substrates. Model simulation showed that the increased rate of G3P synthesis occurred with a greater contribution of glyceroneogenesis regardless of its relative contribution at the basal state. FAC levels increased ~80% (data not shown), which increased re-esterification during epinephrine infusion. Increase in FAC levels due to lipolysis resulted in an increased ratio of acetyl CoA to free CoA (~20%, data not shown), which inhibited the oxidation of pyruvate by decreasing the activity of pyruvate dehydrogenase (PDH). Indeed, Figure 3.7A showed that ACoA synthesis from pyruvate decreased 12%, while that from FAC increased 13%. These responses suggest that the increased flux of glyceroneogenesis comes from reduction in pyruvate oxidation. Noting that the experimental epinephrine infusion rate did not alter the arterial glucose and insulin levels (Samra et al., 1996), an increase in the glucose uptake during epinephrine infusion is unlikely. Correspondingly, model simulation predicted a relatively small contribution of glycolysis. Overall, our model provided quantitative understanding of the change in *in vivo* metabolic flux rate induced by a physiological perturbation.

3.4.5. Sensitivity Analysis

There are four parameters (e.g., $\lambda_{HSL,TG\rightarrow DG}$, $V_{max,HSL,TG\rightarrow DG}$, $K_{m,ATGL,TG\rightarrow DG}$ *and* $K_{m,HSL,TG\rightarrow DG}$) whose sensitivity indices are smaller than 0.1 indicating that these parameters were poorly estimated. Since two enzymes (ATGL and HSL) can hydrolyze TG, the one with the dominant contribution to the TG breakdown in the basal state (i.e., ATGL reaction) will have the higher sensitivity unless additional intracellular data are added to examine the differential effect of the individual enzymes. Thus, the model parameters related to TG breakdown by HSL have low sensitivity indices. For these parameters to be estimated precisely, changes in activities of these enzymes must be measured.

The low sensitivity of Km parameters, whose values were taken from the literature, may have resulted from the very high TG concentration in the adipose tissue. With a smaller Km value than the substrate level, the reactions breaking down TG are of zero order (i.e., independent of concentration). Therefore, the sensitivity indices for these Km values were computed as zero. Note that there are three parameters whose sensitivity indices are greater than one. Two parameters relate to DG breakdown by HSL and one relates to MG breakdown by MGL. Therefore, reactions involving DG and MG breakdown have a more significant effect on the model simulations in response to the intravenous epinephrine infusion.

3.4.6. Model limitations

This model was developed from the experimental data obtained from a local subcutaneous adipose tissue bed (Coppack et al., 1990;Frayn et al., 1994;Frayn et al., 1991;Frayn et al., 1989;Samra et al., 1996). Therefore, it may not simulate the whole-

body kinetic responses as measured by isotopic tracer studies. In addition, we did not incorporate the heterogeneity of various adipose depots in the body. To investigate the role of adipose tissue in relation to metabolic disorders, a model that incorporates different types of adipose depots will be required to predict the integrated response of adipose tissue in the whole body.

The effect of beta-adrenergic stimulation on the rates of lipolytic reactions was simulated by changing the maximum rate coefficient (V_{max}) of Michaelis-Menten metabolic flux equations. With these equations, activation of enzymatic reactions can also be achieved with lower K_m values that lead to increased substrate affinity. Although some K_m values were available from the literature, we had to assume others equal to the tissue levels of corresponding substrates. Because of the uncertainty of many K_m values, we did not simulate how variations of these would affect lipolytic reactions rates. An alternative strategy for future studies would be to incorporate detailed enzyme kinetics related to various lipase reactions, but this would introduce even more unknown parameters. To make such an analysis worthwhile, many more experiments must be performed to obtain appropriate data.

Due to the lack of experimental data for adipose tissue, we had to use intracellular concentration data for GAP, NADH, NAD+, Pi, O_2 and CO_2 from those in the skeletal muscle. It could introduce some miscomputations. However, this is unlikely to cause significant problems since the concentrations of these metabolites do not change significantly during experimental perturbations.

3.5. CONCLUSIONS

A physiologically based mathematical model of adipose tissue metabolism was developed to simulate dynamic responses to intravenous infusion of epinephrine. The model not only simulated the exchange of substrates across the tissue bed and the concentration dynamics in the venous blood for FA and glycerol, but also provided quantitative predictions on the metabolic regulation in the adipose tissue. A key finding in our study is the recognition of a metabolic subdomain in adipose tissue where most of the enzymes and metabolic substrates were localized. By incorporating the mechanisms for regulating various lipase reactions to mobilize TG, the model showed that these lipase reactions were differentially activated during epinephrine infusion resulting in the distinctive dynamic responses of lipolytic intermediates. Critical experiments are needed to test model predictions of metabolic regulation in adipose tissue.

TABLE 3.1. Net reaction rate ($R_{b,i}$ or $R_{c,i}$) for each substrate in blood and cellular compartments

Substrate	Net Reaction Rate, $R_{b,i}$ or $R_{c,i}$
Blood	
GLR	$\phi_{TG\rightarrow GLR,LPL}$
FA	$3\phi_{TG\rightarrow GLR,LPL}$
TG	$-\phi_{TG\rightarrow GLR,LPL}$
Cells	
GLC	$-\phi_{GLC\rightarrow G6P}$
PYR	$\phi_{GAP\rightarrow PYR}+\phi_{ALA\rightarrow PYR}-\phi_{PYR\leftrightarrow LAC}-\phi_{PYR\rightarrow G3P}-\phi_{PYR\rightarrow ACoA}$
LAC	$\phi_{PYR\leftrightarrow LAC}$
ALA	$-\phi_{ALA\rightarrow PYR}+\phi_{Proteolysis}$
GLR	$\phi_{MG\rightarrow GLR,MGL}+\phi_{MG\rightarrow GLR,HSL}+0.5\phi_{MG\text{-}MG\rightarrow DG}+\phi_{MG\text{-}DG\rightarrow TG}-\phi_{GLR\rightarrow G3P}$
FA	$\phi_{TG\rightarrow DG,ATGL}+\phi_{TG\rightarrow DG,HSL}+\phi_{DG\rightarrow MG,HSL}+\phi_{MG\rightarrow GLR,HSL}+\phi_{MG\rightarrow GLR,MGL}-\phi_{FA\rightarrow FAC}$
TG	$\phi_{DG\rightarrow FAC}+0.5\phi_{DG\text{-}DG\rightarrow TG}+\phi_{DG\text{-}MG\rightarrow TG}-\phi_{TG\rightarrow DG,ATGL}-\phi_{TG\rightarrow DG,HSL}$
O2	$-\phi_{O2\rightarrow H2O}$
CO2	$\phi_{PYR\rightarrow ACoA}+2\phi_{ACoA\rightarrow CO2}$
G6P	$\phi_{GLC\rightarrow G6P}-\phi_{G6P\rightarrow GAP}$
GAP	$2\phi_{G6P\rightarrow GAP}-\phi_{GAP\rightarrow PYR}-\phi_{GAP\leftrightarrow G3P}$
G3P	$\phi_{GAP\leftrightarrow G3P}+\phi_{PYR\rightarrow G3P}+\phi_{GLR\rightarrow G3P}-\phi_{G3P\text{-}FAC\rightarrow DG}$
ACoA	$\phi_{PYR\rightarrow ACoA}+8\phi_{FAC\rightarrow ACoA}-\phi_{ACoA\rightarrow CO2}$
FAC	$\phi_{FA\rightarrow FAC}-8\phi_{FAC\rightarrow ACoA}-2\phi_{G3P\rightarrow DG}-\phi_{DG\rightarrow TG}$
CoA	$2\phi_{G3P\rightarrow DG}+\phi_{DG\rightarrow TG}+\phi_{ACoA\rightarrow CO2}-\phi_{PYR\rightarrow ACoA}-\phi_{FA\rightarrow FAC}-7\phi_{FAC\rightarrow ACoA}$
DG	$\phi_{TG\rightarrow DG,ATGL}+\phi_{TG\rightarrow DG,HSL}+\phi_{G3P\rightarrow DG}+0.5\phi_{MG\text{-}MG\rightarrow DG}$ $-\phi_{DG\rightarrow MG,HSL}-\phi_{DG\rightarrow TG}-\phi_{MG\text{-}DG\rightarrow TG}-\phi_{DG\text{-}DG\rightarrow TG}$
MG	$\phi_{DG\rightarrow MG,HSL}+0.5\phi_{DG\text{-}DG\rightarrow TG}-\phi_{MG\rightarrow GLR,HSL}-\phi_{MG\rightarrow GLR,MGL}-\phi_{MG\text{-}DG\rightarrow TG}-\phi_{MG\text{-}MG\rightarrow DG}$
ATP	$2\phi_{GAP\rightarrow PYR}+\phi_{ACoA\rightarrow CO2}+6\phi_{O2\rightarrow H2O}-\phi_{GLC\rightarrow G6P}-\phi_{G6P\rightarrow GAP}$ $-3\phi_{PYR\rightarrow G3P}-2\phi_{FA\rightarrow FAC}-\phi_{GLR\rightarrow G3P}-\phi_{ATP\rightarrow ADP}$
ADP	$-R_{c,ATP}$
Pi	$2\phi_{PYR\rightarrow G3P}+2\phi_{FA\rightarrow FAC}+\phi_{G3P\rightarrow DG}+\phi_{ATP\rightarrow ADP}-\phi_{GAP\rightarrow PYR}-\phi_{ACoA\rightarrow CO2}-6\phi_{O2\rightarrow H2O}$
NAD+	$\phi_{PYR\leftrightarrow LAC}+\phi_{GAP\leftrightarrow G3P}+2\phi_{PYR\rightarrow G3P}+2\phi_{O2\rightarrow H2O}-\phi_{GAP\rightarrow PYR}-\phi_{PYR\rightarrow ACoA}-14\phi_{FAC\rightarrow ACoA}-4\phi_{ACoA\rightarrow CO2}$
NADH	$-R_{c,NAD+}$

GLC, glucose; PYR, pyruvate; LAC, lactate; ALA, alanine; GLR, glycerol; FA, fatty acids; G6P, glucose-6-phosphate; GAP, glyceraldehyde-3-phasphate; G3P, glycerol-3-phosphate; ACoA, acetyl CoA; FAC, fatty acyl CoA; CoA, free CoA; Pi, inorganic phosphate. $\phi_{A\rightarrow B}$ is the flux rate of the metabolic reaction

TABLE 3.2. Basal mass transfer flux rates between blood and cells, and associated parameters

Substrate	$J_{b\leftrightarrow c,i}$ *	$T_{max,i}$ †	$M_{m,i}$ ‡	γ_i §
GLC	1.88	11.73	4939	
PYR	-0.13	0.48	72	
LAC	-1.55	9.84	750	
ALA	-0.57**	1.73	268	
GLR	-3.42			0.171
FA	-8.59			0.030
O2	19.82			0.615
CO2	-18.03			0.072

* $J_{b\leftrightarrow c,i}$, net mass transport flux across the blood-cell exchange barrier (μmol·min^{-1}·kg wet tissue^{-1}). Negative values mean the release of corresponding substrate from tissue and vice versa. Data are from *in vivo* human studies (Coppack et al., 1990;Frayn et al., 1994) except for the marked with **, which is from the references (Coppack et al., 1996;Patterson et al., 2002).

† $T_{max,i}$, maximum mass transport coefficient of *substrate i* (μmol·min^{-1}·kg wet tissue^{-1}).

‡ $M_{m,i}$, Michaelis-Menten (M-M) constant of *substrate i* (μM).

§ γ_i , mass transport coefficient of *substrate i* (l·min^{-1}·kg wet tissue^{-1}).

TABLE 3.3. Basal reaction flux rates and associated parameters for irreversible reaction fluxes

Fluxes	Flux Rate*	$V_{X\rightarrow Y}$*	K_m†	K_i†	$\mu^{\pm}$§	$\nu^{\pm}$§
$\phi_{GLC\rightarrow G6P}$	1.88	4.06	460000‡	570		
$\phi_{G6P\rightarrow GAP}$	1.88	7.53	570		0.72 (−)	
$\phi_{GAP\rightarrow PYR}$	3.56	28.44	216000‡		0.72 (−)	9 (−)
$\phi_{PYR\rightarrow G3P}$	0.21	1.66	250		1.39 (+)	0.11 (+)
$\phi_{GLR\rightarrow G3P}$	0.01	0.02	1012000‡			
$\phi_{ALA\rightarrow PYR}$	2.08	4.16	1300			
$\phi_{Proteolysis}$	2.65**	2.65				
$\phi_{PYR\rightarrow ACoA}$	3.74	22.46	50000‡	25		9 (−)
$\phi_{FA\rightarrow FAC}$	1.70	6.82	200000‡		1.39 (+)	
$\phi_{FAC\rightarrow ACoA}$	0.42	2.55	16000‡	25		9 (−)
$\phi_{TG\rightarrow DG,ATGL}$	3.35	3.38	10			
$\phi_{TG\rightarrow DG,HSL}$	0.65	0.66	10			
$\phi_{DG\rightarrow MG,HSL}$	3.29	6.58	2000			
$\phi_{MG\rightarrow GLR,HSL}$	0.33	0.66	200			
$\phi_{MG\rightarrow GLR,MGL}$	2.67	29.37	2000			
$\phi_{G3P\text{-}FAC\rightarrow DG}$	0.43	0.85	104000‡			
$\phi_{DG\text{-}FAC\rightarrow TG}$	0.43	0.85	160000‡			
$\phi_{DG\text{-}DG\rightarrow TG}$	0.60	1.20	2000			
$\phi_{MG\text{-}MG\rightarrow DG}$	0.32	0.64	200			
$\phi_{MG\text{-}DG\rightarrow TG}$	0.27	0.54	400000‡			
$\phi_{ACoA\rightarrow CO2}$	7.14	57.15	67500‡		0.72 (−)	9 (−)
$\phi_{O2\rightarrow H2O}$	19.82	79.32	27‡		0.72 (−)	0.11 (+)
$\phi_{ATP\rightarrow ADP}$	125.40	376.19	4600	15180000‡		
$\phi_{TG\rightarrow GLR,LPL}$	0.61	0.62	10			

* Values are in μmol·min^{-1}·kg wet tissue^{-1}. $V_{max,k}$, maximum rate coefficient.

** Data is from the references (Coppack et al., 1996;Patterson et al., 2002).

† Values are in μmol·kg wet tissue^{-1} except for the marked (‡), which are in (μmol·kg wet tissue^{-1})^2. $K_{m,k}$, phenomenological M-M constant for the reactants; $K_{i,k}$, phenomenological M-M constant for the product inhibition

§ Values are dimensionless. (+) represents μ^+ or ν^+ while (−) represents μ^- or ν^-. $\mu^{\pm}$ and $\nu^{\pm}$, parameters for the metabolic controllers.

TABLE 3.4. Basal reaction flux rates and associated parameters for reversible reaction fluxes

Fluxes	Flux Rate*	$V_{f,\,X\leftrightarrow V}$†	$V_{b,\,X\leftrightarrow V}$†	$K_{f,\,X\leftrightarrow V}$‡	$K_{b,\,X\leftrightarrow V}$‡	$K_{eq,\,X\leftrightarrow V}$§
$\phi_{\mathrm{PYR}\leftrightarrow\mathrm{LAC}}$	1.55**	4.67	0.023	12500	648000	1.06×10^{4}
$\phi_{\mathrm{GAP}\leftrightarrow\mathrm{G3P}}$	0.21	0.62	3.3×10^{-7}	4000	585000	2.77×10^{8}

* Values are in μmol·min^{-1}·kg wet tissue^{-1}. Data marked with ** is from the reference (Coppack et al., 1990).
† $V_{f,k}$ and $V_{b,k}$, forward and reverse rate coefficients (μmol·min^{-1}·kg wet tissue^{-1}).
‡ $K_{f,k}$ and $K_{b,k}$, phenomenological M-M constants for reactants and products (μmol·kg wet tissue^{-1})^{2}.
§ K_{eq}, equilibrium constant calculated from the Gibbs free energy of reaction (dimensionless), which is from the reference (Alberty, 2003).

TABLE 3.5. Arterial and venous substrate concentrations

Substrate	Arterial Concentration*†	Venous Concentration*§
GLC	5000	4939
PYR	68	72
LAC	700	750
ALA	192	282
GLR	70	200
FA	660	719
TG	990	970
O2 (Total)	8000	7360
O2 (Free)	84‡	66‡
CO2 (Total)	21700	22218
CO2 (Free)	1124‡	1151‡

* Values are in μM.
† Data are from the reference (Kim et al., 2007).
‡ Free concentrations of O2 and CO2 are calculated from the equations given in Appendix IV.
§ Venous concentrations are calculated from the corresponding arteriovenous difference and arterial concentration data.

TABLE 3.6. Substrate concentration in the cellular compartment

Substrate	Concentration*	Reference
GLC	2540	(Tiessen et al., 2002)
PYR	250	(Denton et al., 1966)
LAC	1440	(Jansson et al., 1994)
ALA	1300‡	(Kim et al., 2007)
GLR	220	(Jansson et al., 1994;Stumvoll et al., 2000)
FA	1000	
TG	990000†	(Albright and Stern, 1998)
O2	34‡	(Dash and Bassingthwaighte, 2006a;Popel, 1989)
CO2 (Total)	15427‡	(Dash and Bassingthwaighte, 2006a;Geers and Gros, 2000)
CO2 (Free)	1403‡	(Dash and Bassingthwaighte, 2006a;Geers and Gros, 2000)
G6P	570	(Denton et al., 1966)
GAP	80‡	(Kim et al., 2007)
G3P	1300	(Denton et al., 1966)
ACoA	25	(Denton and Halperin, 1968)
FAC	80	(Denton and Halperin, 1968)
CoA	200	(Denton and Halperin, 1968)
DG	2000†	(Arner and Ostman, 1974)
MG	200†	(Arner and Ostman, 1974)
ATP	4600	(Denton et al., 1966)
ADP	3300	(Denton et al., 1966)
Pi	2700‡	(Kim et al., 2007)
NAD+	450‡	(Kim et al., 2007)
NADH	50‡	(Kim et al., 2007)

*Values are in μM and based on the volume of intracellular water except for those marked with † which are based on the total cellular volume. Values marked with ‡ are from skeletal muscle studies.

TABLE 3.7. Miscellaneous model parameters and the input functions

	Values	Units
$K_{m,Q}$	31	$ml \cdot min^{-1} \cdot kg^{-1}$
α	0.04	nM^2
Q_0	0.031†	$ml \cdot min^{-1} \cdot kg^{-1}$
$C_{v,Epi,0}$	0.1†	nM

$K_{m,Q}$, phenomenological M-M constants for LPL reaction; α, parameter for epinephrine action; Q_0, adipose tissue blood flow at basal state; $C_{v,Epi,0}$, epinephrine concentration in adipose tissue vein at basal state. Data marked with † are from the references (Samra et al., 1996;Jansson et al., 1994).

TABLE 3.8. Model input functions

Time (min)	Input Functions
$t \le 15$	$Q = Q_0$, $C_{v,Epi} = C_{v,Epi,0}$, $C_{a,GLR} = C_{a,GLR,0}$, $C_{a,FFA} = C_{a,FFA,0}$
$t > 15$	$Q = Q_0 \cdot \left(1 + 7.32 \cdot (1 - e^{-(t-15)/62.317)})\right)$ $C_{v,Epi} = C_{v,Epi,0} + 6.837 \times 10^{-2} \cdot (t-15) - 1.903 \times 10^{-3} \cdot (t-15)^2 + 1.453 \times 10^{-5} \cdot (t-15)^3$ $C_{a,GLR} = C_{a,GLR,0} + 7.979 \cdot (t-15) - 0.256 \cdot (t-15)^2 + 0.002 \cdot (t-15)^3$ $C_{a,FA} = C_{a,FA,0} + 84.486 \cdot (t-15) - 2.544 \cdot (t-15)^2 + 0.02 \cdot (t-15)^3$

Parameters for the input functions were optimally estimated based on the data from the human *in vivo* study (Samra et al., 1996). Q: Blood flow to the adipose tissue; $C_{v,Epi}$: Epinephrine concentration in the vein; $C_{a,GLR}$, $C_{a,FA}$: Arterial glycerol and FA concentrations. Time courses of these input functions are shown in Figure 3.2.

TABLE 3.9. Estimated model parameters

Parameters	Differential Activation	Uniform Activation
$\lambda_{TG \rightarrow DG,ATGL}$	0.72	3.18
$\lambda_{TG \rightarrow DG,HSL}$	0.91	3.18
$\lambda_{DG \rightarrow MG,HSL}$	6.19	3.18

Values are dimensionless.

TABLE 3.10. Sensitivity indices of the model parameters related to the lipid mobilization

Parameters	Sensitivity Index (S_i)*
v_{cf}	0.298
$\lambda_{ATGL,TG\rightarrow DG}$	0.202
$\lambda_{HSL,TG\rightarrow DG}$	0.045
$\lambda_{HSL,DG\rightarrow MG}$	1.925
$V_{max,ATGL,TG\rightarrow DG}$	0.386
$V_{max,HSL,TG\rightarrow DG}$	0.054
$V_{max,HSL,DG\rightarrow MG}$	2.310
$V_{max,HSL,MG\rightarrow GLR}$	0.102
$V_{max,MGL,MG\rightarrow GLR}$	2.473
$K_{m,ATGL,TG\rightarrow DG}$	0
$K_{m,HSL,TG\rightarrow DG}$	0
$K_{m,HSL,DG\rightarrow MG}$	0.098
$K_{m,MGL,MG\rightarrow GLR}$	0.251
$K_{m,HSL,MG\rightarrow GLR}$	0.281
$K_{m,FAC\text{-}G3P\rightarrow DG}$	0.282
$K_{m,DG\rightarrow TG}$	0.281
$K_{m,DG\text{-}DG\rightarrow TG\text{-}MG}$	0.280
$K_{m,MG\text{-}MG\rightarrow DG\text{-}GLR}$	0.288
$K_{m,MG\text{-}DG\rightarrow TG\text{-}GLR}$	0.298

* Values are dimensionless.

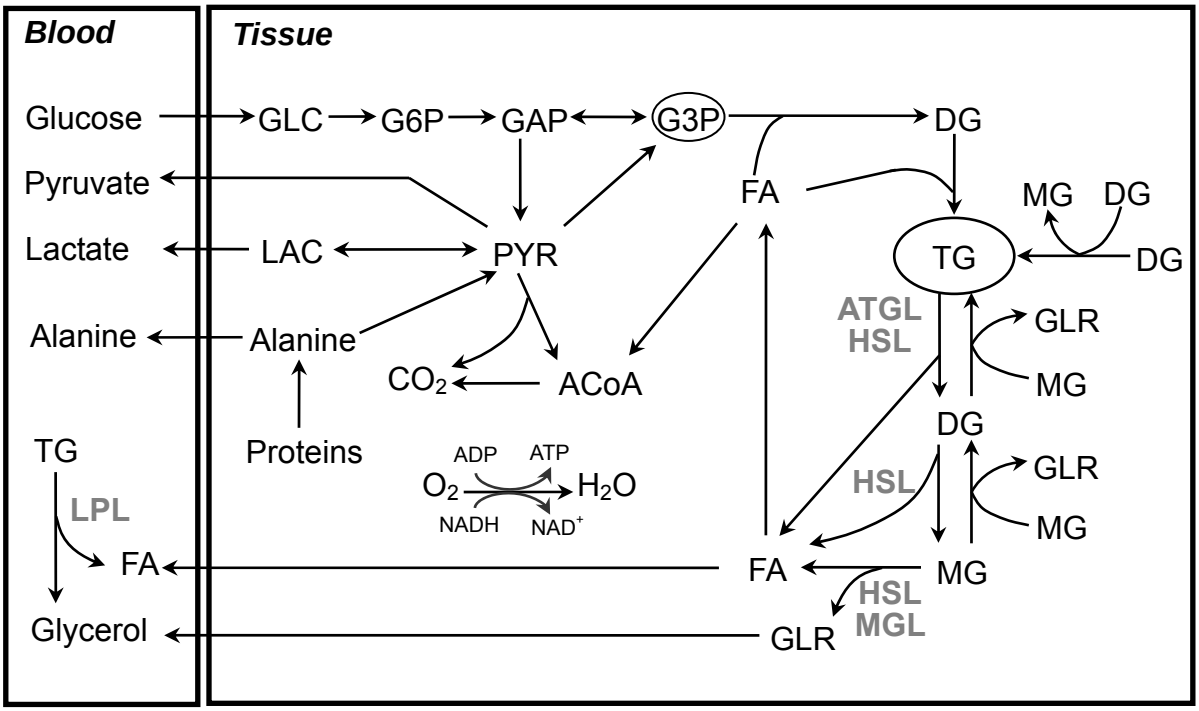

FIGURE 3.1. Metabolic pathways involved in triglycerides synthesis and breakdown in the adipose tissue

As shown, glucose is taken up from, and pyruvate, lactate, free fatty acids, glycerol, and alanine are released, into the blood compartment. Alanine is considered to represent all amino acids released by protein breakdown. Glycerol-3-phosphate, used for the esterification of fatty acids, is formed either from glucose via glycolysis or from pyruvate via glyceroneogenesis. The various steps in the esterification and hydrolysis of triglycerides are shown. ATP-ADP and/or NADH-NAD^+ are used as co-substrates in the model, but are not shown except for the oxidative phosphorylation. The arrow with both ends indicates a reversible reaction step. GLC, glucose; PYR, pyruvate; LAC, lactate; ALA, alanine; GLR, glycerol; FA, fatty acids; G6P, glucose-6-phosphate; GAP, glyceraldehyde-3-phasphate; G3P, glycerol-3-phosphate; ACoA, acetyl CoA; FAC, fatty acyl CoA; TG, triglycerides; DG, diglycerides; MG, monoglycerides; LPL, Lipoprotein Lipase; ATGL, Adipose Triglyceride Lipase; HSL, Hormone Sensitive Lipase; MGL, Monoglyceride Lipase.

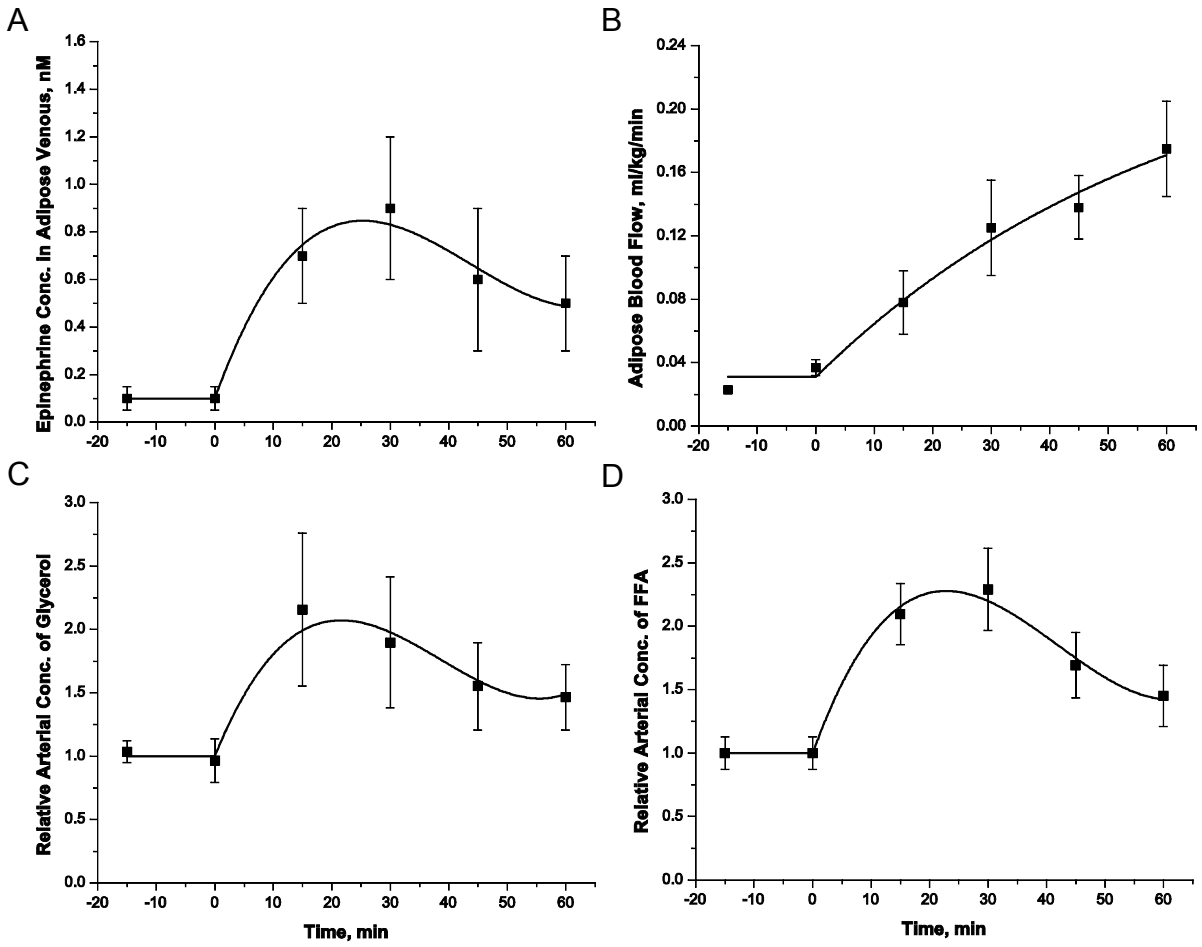

FIGURE 3.2. Dynamic changes in epinephrine concentration in adipose tissue vein (A), adipose tissue blood flow (B), and relative arterial concentrations of glycerol and FA (C, D) following the intravenous infusion of epinephrine at time=0

Relative arterial concentration is the ratio of arterial concentrations at any time $t>0$ to $t=0$. Squares represent the experimental data (mean±SEM) of Samra et al. (Samra et al., 1996). Solid lines are the model simulations.

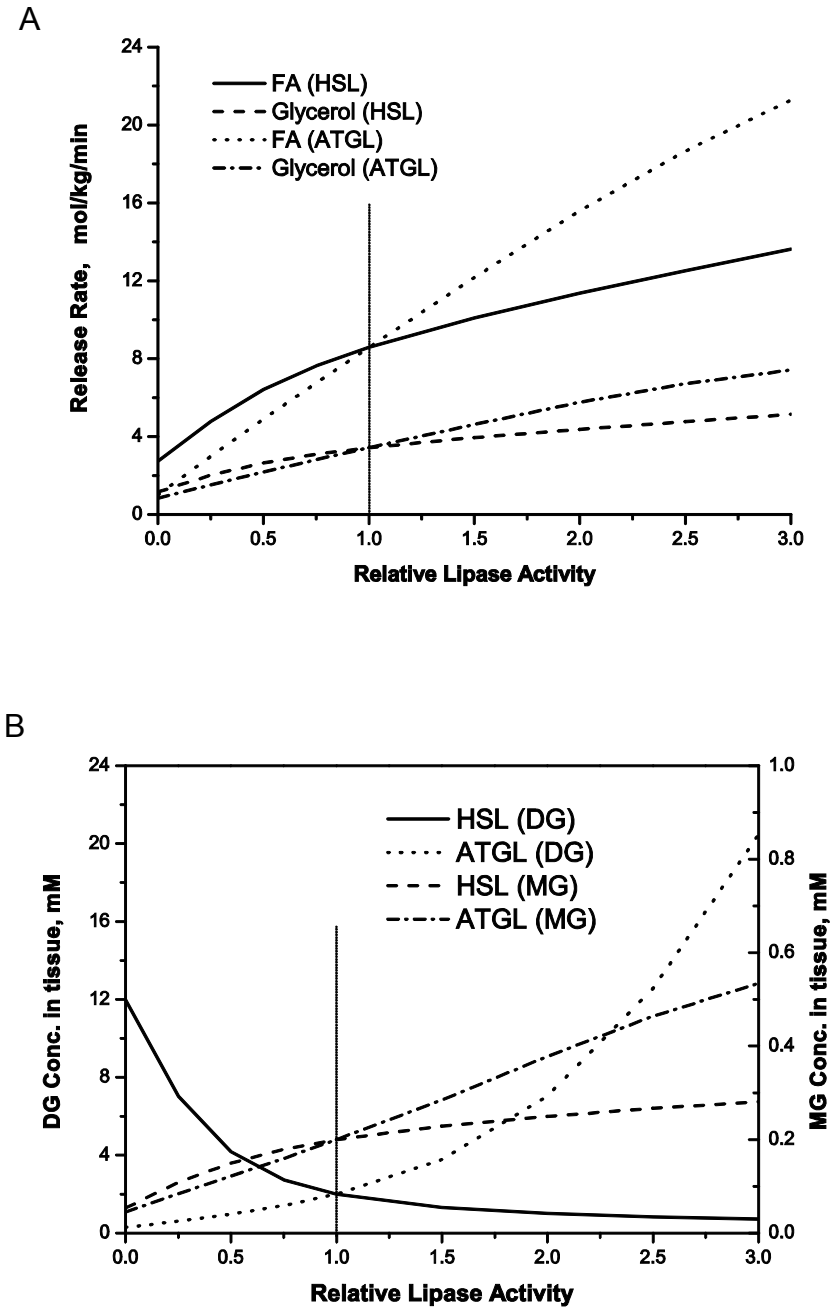

FIGURE 3.3. Effect of varying levels of lipase expression in the basal state

(A) the rates of releases of FA (Solid: HSL, Dash double dotted: ATGL) and glycerol (Dashed: HSL, Dash dotted: ATGL) and (B) the tissue concentrations of DG (Solid: HSL, Dash double dotted: ATGL) and MG (Dashed: HSL, Dash dotted: ATGL). Relative lipase activity is the enzyme activity of ATGL or HSL relative to the control value.

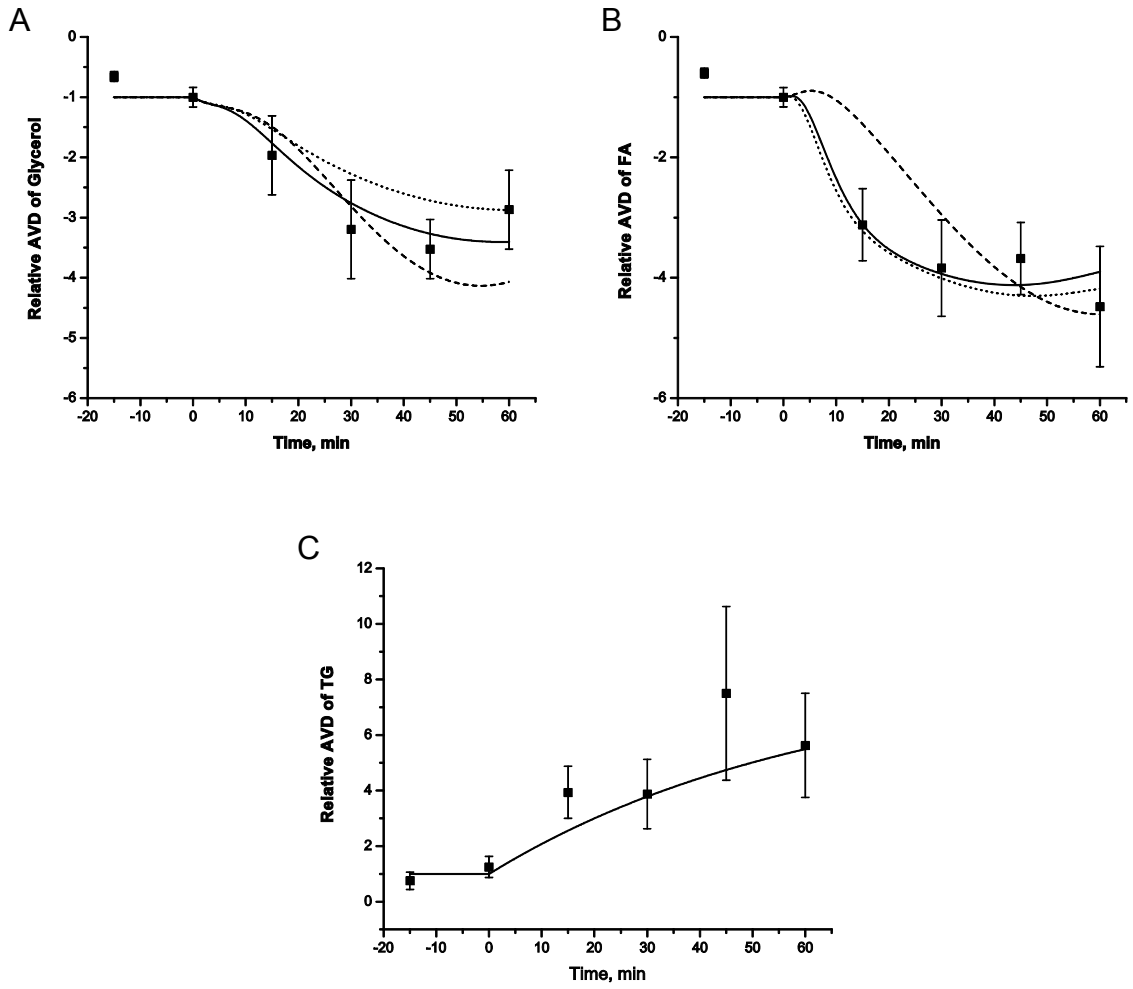

FIGURE 3.4. Dynamic exchanges of glycerol (A), FA (B) and TG (C) across adipose tissue bed in response to the intravenous infusion of epinephrine

Relative AVD = AVD(t)/AVD(0), is the ratio of arteriovenous differences (AVD) at any time $t>0$ to $t=0$. Squares represent the experimental data (mean±SEM) of Samra et al. (Samra et al., 1996). Solid (localized, differential), dotted (localized, uniform) and dashed (unlocalized, differential) lines in (A) and (B) are the model simulations according to the localized (V_{cf}=0.031) or unlocalized (V_{cf}=0.8) metabolic subdomain and the uniform (same λ_k) or differential (different λ_k) activation of intracellular lipases. Solid line in (C) is the model simulation.

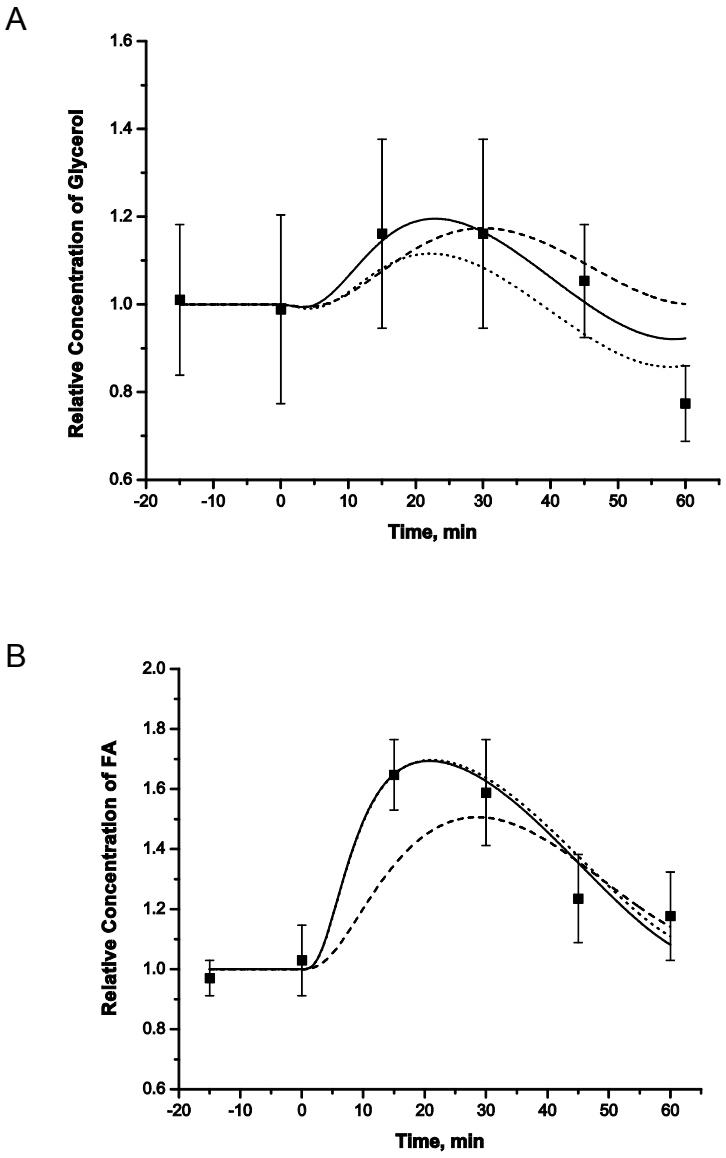

FIGURE 3.5. Dynamic changes in the relative concentrations of glycerol (A) and FA (B) in adipose venous blood during the intravenous infusion of epinephrine

Relative concentration is the ratio of concentrations at any time $t>0$ to $t=0$. Squares represent the experimental data (mean±SEM) of Samra et al. (Samra et al., 1996). Solid (localized, differential), dotted (localized, uniform) and dashed (unlocalized, differential) lines are the model simulations according to the localized (V_{cf}=0.031) or unlocalized (V_{cf}=0.8) metabolic subdomain and the uniform (same λ_k) or differential (different λ_k) activation of intracellular lipases.

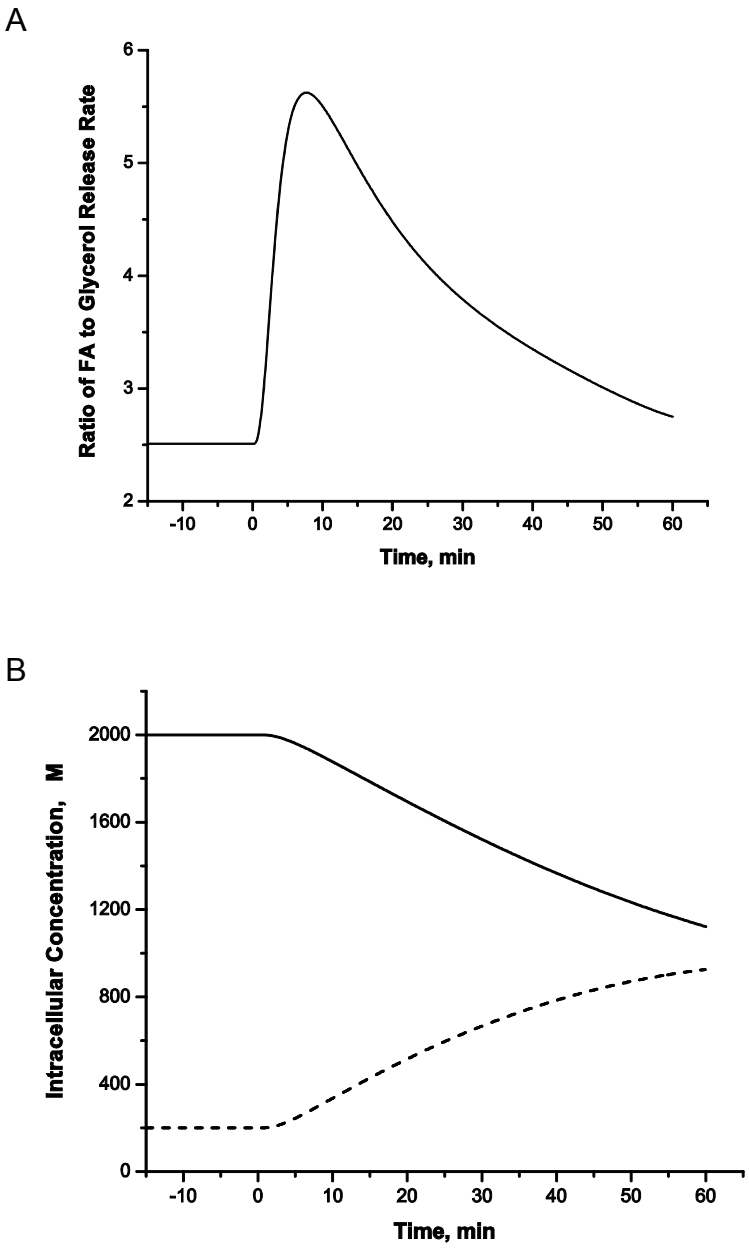

FIGURE 3.6. Model-simulated ratio of FA to glycerol released by the adipose cellular compartment (i.e., $J_{FA,b\leftrightarrow c}/J_{GLR,b\leftrightarrow c}$) (A) and changes in intracellular lipolytic intermediates (i.e., DG: solid line, MG: dashed line) (B) in response to the intravenous infusion of epinephrine

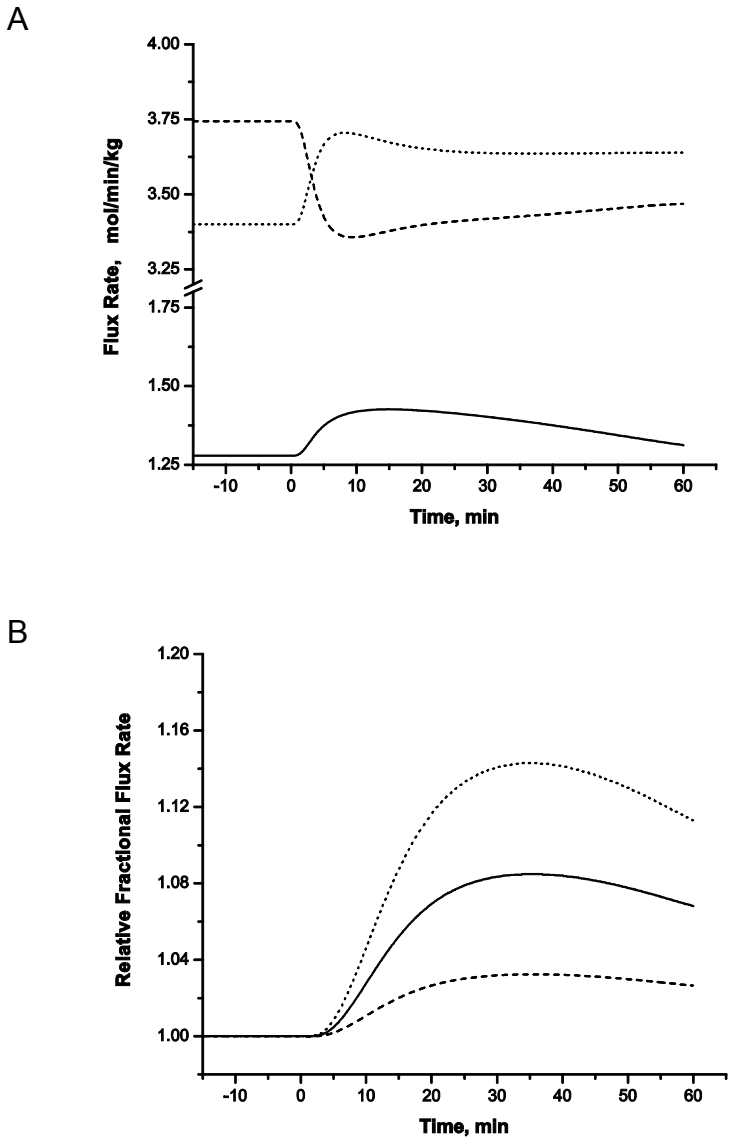

FIGURE 3.7. (A) Model-simulated dynamic responses of FAC dependent re-esterification rate (solid line), ACoA synthesis from pyruvate (dashed line) and FAC (dotted line). (B) Relative fractional glyceroneogenesis with different contributions at the basal state

The fractional glyceroneogenesis, $F_{GRNG}(t) = \phi_{\mathrm{PYR}\rightarrow\mathrm{G3P}} / (\phi_{\mathrm{GAP}\leftrightarrow\mathrm{G3P}} + \phi_{\mathrm{PYR}\rightarrow\mathrm{G3P}})$ and the relative F_{GRNG} is the ratio of $F_{GRNG}(t)$ at any time $t>0$ to $t=0$. The solid line represents the equal contribution of glycolysis and glyceroneogenesis ($F_{GRNG}(0)=0.5$) while the dashed and dotted lines represent higher ($F_{GRNG}(0)=0.8$) and lower ($F_{GRNG}(0)=0.2$) contribution of glyceroneogenesis.

CHAPTER 4.

REGULATION OF ADIPOSE TISSUE METABOLISM IN HUMANS: ANALYSIS OF RESPONSES TO THE HYPERINSULINEMIC-EUGLYCEMIC CLAMP EXPERIMENT

4.1. INTRODUCTION

As one of the most potent antilipolytic hormones, insulin suppresses the breakdown of triglycerides (TG) stores in the adipose tissue. Since the stimulation of TG breakdown is regulated via a complex mechanism involving various lipases and other proteins (Schweiger et al., 2006;Londos et al., 1999), its suppression by insulin would require the modulation of associated regulatory pathways. Studies in transgenic animals suggest that hormone sensitive lipase (HSL), adipose triglyceride lipase (ATGL) and perilipin A are the major regulators of intracellular lipolysis (Sztalryd et al., 2003;Haemmerle et al., 2002;Haemmerle et al., 2006). Insulin can suppress lipolysis by modulating the activities of these proteins. It transcriptionally down-regulates the activity of ATGL (Kershaw et al., 2006). In addition, it acutely affects the activities of HSL and perilipin A by promoting their dephosphorylation via two different mechanisms (Stralfors and Honnor, 1989;Carmen and Victor, 2006). It reduces the levels of cyclic AMP (cAMP) by activating phosphodiesterase (PDB). In addition, protein phosphatase 1 (PP1) is activated by insulin dephosphorylating HSL and perilipin directly. Even though the activity of ATGL can only be regulated transcriptionally, the TG breakdown by ATGL can be affected indirectly via dephosphorylation of perilipin. Our previous computational model of adipose tissue metabolism (Kim et al., 2008) suggested differential activation of

lipolytic reactions by epinephrine. While insulin can suppress the breakdown of TG and diglycerides (DG) involving different cellular mechanisms, it is not certain whether the lipolytic reactions catalyzed by different lipases are equally suppressed by the action of insulin. However, the quantitative analysis of the regulation of lipolysis by insulin has not been examined *in vivo*.

The synthesis of TG in adipose tissue requires a source of glycerol-3-phospahte (G3P) other than glycerol because it has low activity of glycerol kinase. Either glucose or pyruvate (and even lactate) can be used for the synthesis of G3P. Glyceroneogenesis is the pathway for the synthesis of G3P using pyruvate (or lactate) as a precursor (Reshef et al., 2003). In humans, adipose tissue releases lactate as a result of glucose utilization suggesting the glucose as a major precursor. In contrast, studies in rats suggest that glyceroneogenesis is the dominant pathway to synthesize G3P in the adipose tissue even when the rate of glucose uptake is high (Nye et al., 2008). The re-utilization of pyruvate or lactate for the synthesis of G3P via different pools of triose phosphates in the adipose tissue could reconcile these apparently contradictory data. Our previous model of adipose tissue metabolism described the intracellular re-utilization of pyruvate by incorporating two separate pathways to synthesize G3P without considering the two separate pools of triose phosphates. The consideration of two separate domains (i.e., heterogeneity) of triose phosphates will be able to enhance our understanding on the regulation of glyceroneogenesis and therefore, TG synthesis in response to physiological perturbations.

Phosphoenolpyruvate carboxykinase (PEPCK) is a key regulatory enzyme of glyceroneogenesis. Increased activity of PEPCK is associated with obesity (Chang et al., 2008). Indeed, PEPCK is one of the primary targets for anti-diabetic drugs, thiazolidinediones (TZDs) due to its critical role in the regulation of re-esterification of

free fatty acid (FFA) (Tordjman et al., 2003). As shown in transgenic mice studies, the overexpression of PEPCK in the adipose tissue results in obesity in these mice without insulin resistance (Franckhauser et al., 2002). The increased rate of re-esterification of FFA resulted in a decreased rate of FFA release into circulation and lowering of the plasma levels of FFA in these animals. In addition to changes in PEPCK activity, the availability of substrates can also regulate the flux through glyceroneogenesis. Indeed, the fact that obese people have higher interstitial levels of lactate than lean people might suggest the importance of substrate availability for the synthesis of G3P, and therefore, TG (Qvisth et al., 2007). Even though the activity of PEPCK is suppressed by insulin, the rate of glyceroneogenesis increases in response to glucose infusion (Nye et al., 2008). Despite the importance of glyceroneogenesis in the regulation of TG synthesis, definitive in vivo studies have not been performed. Thus, the regulatory mechanism for increased glyceroneogenesis in response to insulin remains uncertain.

In the present study, we modified the computational model of adipose tissue metabolism (Kim et al., 2008) to 1) examine the suppression of various lipolytic reactions by insulin; 2) investigate the mechanism that regulates the flux through glyceroneogenesis in response to insulin/glucose infusion; and 3) examine the effects of increasing the arterial levels of lactate and of changes in PEPCK activity on glyceroneogenesis and re-esterification of FFA. We hypothesized that the breakdown of TG and DG by ATGL and HSL are differentially suppressed by the action of insulin. It is expected that the distinctive changes in the levels of lipolytic intermediates (i.e., DG and monoglycerides, MG) will result from the differential suppression of lipolytic reactions by insulin. We also hypothesized that glyceroneogenesis increases in response to insulin due to the increased availability of pyruvate as well as the favorable cellular redox (i.e.,

NADH/NAD^+) and phosphorylation (i.e., ATP/ADP) states. With respect to the effect of increased substrate availability, we postulated that the increased levels of lactate as in obese patients facilitate the accretion of fat into the adipose tissue. Finally, if the higher PEPCK activity is not sufficient to increase the rate of FFA re-esterification, then the induction of additional enzymes may be required. Consequently, we examined the effect of increasing the activity of acyl CoA synthetase (ACS) on the rate of FFA re-esterification due to its importance on the synthesis of fatty acyl CoA (FAC), a co-substrate for TG synthesis.

4.2. METHODS

Hyperinsulinemic-euglycemic clamp experiment in humans is an effective method for investigating the regulation of TG breakdown and synthesis by insulin. This technique has been widely used as a gold standard for quantifying insulin resistance *in vivo*. It quantifies the amount of glucose required to be infused intravenously as a result of elevating plasma insulin concentration in order to maintain plasma glucose concentrations at a given setpoint. Following a constant rate infusion of insulin, the level of plasma glucose is maintained by varying the rate of glucose infusion. The rate of glucose infusion in the steady state is a determinant of the person's insulin sensitivity. To simulate the responses associated with such a physiological perturbation, an earlier model of adipose tissue metabolism *in vivo* (Kim et al., 2008) in a fasting state was enhanced by incorporating additional metabolites and metabolic pathways that are significant in the fed state.

4.2.1. Metabolites, Pathways, and Cellular Distribution

Insulin stimulates glucose uptake by increasing the translocation of glucose

transporter 4 (GLUT4) to the plasma membrane. In addition, insulin increases rates of fluxes through several intracellular metabolic pathways including glycogen synthesis and glycolysis. Stimulation of fatty acid synthesis from glucose (i.e., *de novo* lipogenesis) requires a source of NADPH. The primary source of NADPH is the pentose phosphate pathway where NADPH is generated when glucose-6-phosphate is oxidized to ribulos-5-phospahte (R5P). R5P can re-enter the glycolytic pathway at the level of fructose-6-phosphate (F6P) and glyceraldehyde-3-phosphate (GAP). By incorporating F6P, glycogen (GLY), R5P, NADP+ and NADPH, this enhanced model can describe the glycogen cycle, pentose phosphate pathway and de novo lipogenesis (Figure. 4.1).

Data from studies in humans show that there is a net uptake of glucose across the adipose tissue in fasting and fed states (Coppack et al., 1990;Jansson et al., 1994). These data have been used to suggest the direct utilization of glucose for the synthesis of glycerol-3-phosphate (G3P). However, studies in rats suggest that pyruvate (via glyceroneogenesis) is the dominant carbon source of G3P (Nye et al., 2008). The only way to reconcile these data would be the re-utilization of pyruvate or lactate for the synthesis of G3P via separate pools of triose phosphates within adipose tissue (i.e., heterogeneity). In this model, the heterogeneity associated with the triose phosphates are considered to be localized in distinct cellular subdomains: either glycolytic (GAP1 and G3P1) or glyceroneogenic (GAP2 and G3P2).

4.2.2. Dynamics Mass Balances of Substrates

Substrate transport and metabolic reaction dynamics in blood and in cellular compartments are represented by mass balance equations. In the blood compartment of volume V_b, the concentration $C_{b,i}$ of the substrate i changes with time:

$$V_b \frac{dC_{b,i}}{dt} = Q(t)[C_{a,i}(t) - C_{b,i}] + R_{b,i} - J_{b\leftrightarrow c,i} \quad (4.1)$$

where $J_{b\leftrightarrow c,i}$ is the net mass transport rates from blood to cells, and $R_{b,i}$ is the net reaction rate. The arterial concentration, $C_{a,i}$(t) and the blood flow, Q(t) are given as input functions as specified from experiments. The concentration, $C_{c,i}$ substrate i in the cellular compartment changes with time:

$$V_{c,i} \frac{dC_{c,i}}{dt} = R_{c,i} \quad + \quad J_{b\leftrightarrow c,i} \quad (4.2)$$

where $R_{c,i}$ is the net reaction rate in the cellular compartment and $V_{c,i}$ is the volume of the cellular compartment occupied by substrate i .

4.2.3. Transport and Metabolic Fluxes

The passive simple diffusion of glycerol, FA, O_2 and CO_2 between blood and cellular domains is:

$$J_{b\leftrightarrow c,i} = \gamma_i \left[C_{b,i} - C_{c,i} \right] \quad (4.3)$$

where γ_i is the mass transport coefficient of substrate i. The carrier-mediated facilitated transport of glucose, pyruvate, lactate, and alanine is:

$$J_{b\leftrightarrow c,i} = T_{\max,i} \left(\frac{C_{b,i}}{M_{m,i} + C_{b,i}} - \frac{C_{c,i}}{M_{m,i} + C_{c,i}} \right) \quad (4.4)$$

where $T_{max,i}$ is the maximum mass transport coefficient of substrate i and $M_{m,i}$ is the Michaelis-Menten (M-M) constant of substrate i.

The net reaction rates ($R_{x,i}$) involve one or more metabolic reaction fluxes (ϕ_k), which are complex nonlinear functions of substrate concentrations (Appendix III). For those reactions that are far from thermodynamic equlibrium, the reaction flux, ϕ_k is

represented by a general irreversible bi-bi substrate-to-product enzymatic reaction coupled with controller energy metabolite pairs:

$$\phi_{\mathrm{k}} = V_{\max,\,\mathrm{k}} \left(\frac{PS^{\pm}}{\mu^{\pm} + PS^{\pm}} \right) \left(\frac{RS_1^{\pm}}{\nu^{\pm} + RS_1^{\pm}} \right) \left(\frac{RS_2^{\pm}}{\eta^{\pm} + RS_2^{\pm}} \right) \left(\frac{C_{\mathrm{X}} \cdot C_{\mathrm{Y}}}{K_{\mathrm{m,k}} + C_{\mathrm{V}} \cdot C_{\mathrm{W}} \cdot K_{\mathrm{m,k}} / K_{\mathrm{i,k}} + C_{\mathrm{X}} \cdot C_{\mathrm{Y}}} \right) \quad (4.5)$$

where C_X, C_Y, C_V, and C_W are reactant and product concentrations; $V_{max,k}$ is the maximum rate coefficient and $K_{m,k}$ is a phenomenological M-M constant; PS^+ (= C_{ATP}/C_{ADP}), RS_1^+ (= C_{NADH}/C_{NAD+}) and RS_2^+ (= C_{NADPH}/C_{NADP+}) indicate the cellular phosphorylation and redox states. For some reactions, the effect of these controllers can be in the opposite direction (viz., $PS^- = 1/PS^+$, $RS_1^- = 1/RS_1^+$ and $RS_2^- = 1/RS_2^+$). In addition, $\mu^{\pm}$, $\nu^{\pm}$ and $\eta^{\pm}$ are parameters for the metabolic controllers.

The reactions that are close to thermodynamic equilibrium and reversible are represented by the flux relationship:

$$\phi_{\mathrm{k}} = \left(\frac{V_{\mathrm{f,k}} \frac{C_{\mathrm{X}} \cdot C_{\mathrm{Y}}}{K_{\mathrm{f,k}}} - V_{\mathrm{b,k}} \frac{C_{\mathrm{V}} \cdot C_{\mathrm{W}}}{K_{\mathrm{b,k}}}}{1 + \frac{C_{\mathrm{X}} \cdot C_{\mathrm{Y}}}{K_{\mathrm{f,k}}} + \frac{C_{\mathrm{V}} \cdot C_{\mathrm{W}}}{K_{\mathrm{b,k}}}} \right) \quad (4.6)$$

where $V_{f,k}$ and $V_{b,k}$ are the forward and reverse rate coefficients; $K_{f,k}$ and $K_{b,k}$ are the phenomenological M-M constants for reactants and products. The forward and reverse rate coefficients are related by Haldane relationship. The reversible reactions are those catalyzed by lactate dehydrogenase, G3P dehydrogenase, and glucose-6-phosphate (G6P) isomerase.

4.2.4. Insulin Modulation of Fluxes

The translocation of glucose transporter and several metabolic fluxes were modulated by the action of insulin. Even though changes in the levels of plasma insulin

are instantaneous in response to intravenous infusion of insulin, the resultant increase in the rate of glucose uptake is significantly delayed. The delay in the action of insulin is related to the transport of insulin from the plasma to the interstitium across vascular endothelium (Yang et al., 1989). Additional delay in insulin action is related to the translocation of GLUT4 to the plasma membrane (Muretta et al., 2008). Activation of the intermediary proteins in the insulin signaling cascade is considered to be instantaneous (Grimmsmann et al., 2002). Thus, the interstitial level of insulin, C_I(t) that modulates the cellular processes changes with time according to

$$C_I(t) = C_I(0) + [C_I(\infty) - C_I(0)][1 - \exp(-t/\tau)] \tag{4.7}$$

where τ is the time constant and $C_I(\infty)$ is the steady-state value. The interstitial concentration of insulin was set equal to 21% of its plasma level (Bodenlenz et al., 2005).

The maximum glucose transport coefficient, $T_{max,GLC}$ dynamically changes depending on interstitial insulin concentration:

$$\frac{dT_{\max,GLC}}{dt} = 1 + \theta C_I(t) - \left[1 + \theta C_I(0)\right]\frac{T_{\max,GLC}(t)}{T_{\max,GLC}(0)} \tag{4.8}$$

where θ is the parameter indicating the degree of activation by insulin and initially, $T_{\max,GLC}(0)$. When C_I reaches a steady state, then $T_{\max,GLC}(t)$ will reach a constant value.

Changes in the rate coefficients of other metabolic fluxes are assumed to be relatively fast and related to C_I(t). For the metabolic reactions that are activated by insulin, glycolysis ($\phi_{\mathrm{GLC}\to\mathrm{G6P}}$, $\phi_{\mathrm{F6P}\to\mathrm{GAP}}$, $\phi_{\mathrm{GAP}\to\mathrm{PYR}}$), glycogen synthesis ($\phi_{\mathrm{G6P}\to\mathrm{GLY}}$) and pyruvate oxidation ($\phi_{\mathrm{PYR}\to\mathrm{ACoA}}$), the reaction rate coefficients increase with insulin concentration:

$$V^{+}_{\max,k} = V^{0}_{\max,k}\left(1 + \lambda_k \frac{[C_I(t) - C_I(0)]^2}{C_I(0)^2 + [C_I(t) - C_I(0)]^2}\right) \tag{4.9}$$

$V^0_{\max,k}$ is the basal state maximum rate coefficient and λ_k indicates the degree of activation for a corresponding reaction by insulin. For reactions that are suppressed, viz., glycogenolysis ($\phi_{\text{GLY}\rightarrow\text{G6P}}$), proteolysis ($\phi_{\text{PRT}\rightarrow\text{ALA}}$) and lipolysis ($\phi_{\text{TG}\rightarrow\text{DG,ATGL}}$, $\phi_{\text{TG}\rightarrow\text{DG,HSL}}$, $\phi_{\text{DG}\rightarrow\text{MG,HSL}}$), the reaction rate coefficients decrease with insulin concentration:

$$V^-_{\max,k} = V^0_{\max,k}\left(\frac{\alpha_k}{\alpha_k + C_I(t)^2}\right) \tag{4.10}$$

where α_k indicates the degree of suppression.

4.2.5. Parameter estimates and simulation strategy

Values of substrate concentrations, transport and metabolic fluxes and associated model parameters in the basal state (Table 4.1-4.3) were based on previous analysis (Kim et al., 2008). The fluxes and parameters related to the mass transport between blood and cellular compartments are the same. Some of intracellular metabolic fluxes and model parameters were modified because of additional pathways and metabolic intermediates.

The parameters related to suppression of the lipolytic reactions (i.e., α_k) were determined first by simulating steady-state insulin dose-response data from *in vivo* human studies (Stumvoll et al., 2000). These reactions are independent of the parameters that modulate glucose metabolism. Simulated steady-state responses to different levels of plasma insulin [35pM, 113pM and 383pM] were examined. For steady-state simulation, arterial glycerol and FFA concentrations were additional inputs to the model. Simulated concentrations of glycerol in the venous effluent blood were compared with the published experimental data.

After successful evaluation of the model parameters (i.e., α_k), the simulated

responses during hyperinsulinemic-euglycemic clamp in humans were examined. Corresponding to *in vivo* studies (Coppack et al., 1989b;Coppack et al., 1989a), the responses to a constant rate infusion of insulin [35mU/m^2/min] administered intravenously for 120min, were examined. Based on *in vivo* data (Yang et al., 1989), a time constant of 10min was assumed so that the interstitial levels of insulin reached a steady state around 30min in response to a step increase in the plasma insulin levels from 40pM to 350pM (Figure 4.2). Adipose blood flow Q(t) and arterial concentration dynamics $C_{a,i}$(t) of glucose, lactate, glycerol, FFA, and TG were given as input functions (Figure 4.3).

A hyperinsulinemic-euglycemic clamp experiment requires a variable rate of infusion of exogenous glucose to maintain the arterial levels of glucose, which is represented in the model by the input function for arterial glucose concentrations. All the input functions are listed in Table 4.4. Optimal estimates of the model parameters (Table 4.5) related to insulin action (i.e., λ_k) were obtained by comparison with data from *in vivo* human studies (Coppack et al., 1989a;Coppack et al., 1989b). Parameters related to suppression of the lipolytic reactions (i.e., α_k) were set to the square of interstitial insulin concentration in the basal state (i.e., $C_I(0)^2$=70.6 pM^2) for TG and DG breakdowns by ATGL and HSL ($\phi_{TG\rightarrow DG,ATGL}$, $\phi_{TG\rightarrow DG,HSL}$, $\phi_{DG\rightarrow MG,HSL}$).

Model simulations were obtained to investigate the effects of different physiological and/or metabolic conditions. The model equations were solved numerically using an integrator for stiff, ordinary differential equations, 'ode15s' (MATLAB®, MathWorks Inc.). Optimal estimates of the model and input parameters were obtained using 'lsqcurvefit' (MATLAB®) with 'ode15s'.

4.3. RESULTS

4.3.1. Steady-state analysis of the insulin dose response

The steady-state response to increasing insulin dose was examined by simulating (1) changes in the levels of glycerol in the venous blood, (2) FFA release rate from TG breakdown, and (3) FFA re-esterification rate. The venous blood levels of glycerol decreased exponentially from 203μM to 55μM with increasing levels of insulin from 35pM to 383pM (Figure 4.4A). Model simulations correspond well with experimental data until the plasma insulin level reaches 113pM. At the highest insulin level [383pM], the simulated venous glycerol was about 35% higher than the experimental data. However, when the plasma TG breakdown was suppressed by setting the maximum rate coefficient for LPL reaction to zero, Model simulations was in good agreement with experimental data (Figure 4.4A).

With a higher insulin level, the rate of intracellular lipolysis (i.e., FFA release from the breakdown of TG, DG and MG) decreased from 11.6 to 0.9 μmol/kg/min (Figure 4.4B). The rate of total lipolysis (i.e., intracellular lipolysis and plasma TG hydrolysis by LPL) showed a similar response. The relative contribution from LPL action to total lipolysis was higher at high insulin concentration (~5% at 35pM to ~40% at 383pM). There was no significant change in the intracellular re-esterification of FFA. As a consequence, the fractional rate of intracellular re-esterification of FFA released from TG breakdown increased from ~11% to ~112%. Total fractional re-esterification including FFA produced by LPL, changed from ~10% to ~75%.

4.3.2. Simulation of hyperinsulinemic-euglycemic clamp

Model input functions: The model input functions (Table 4.4) were fitted to *in*

vivo data. At constant insulin infusion rate (35mU/m^2/min), the plasma level of insulin showed a step increase (Figure 4.2) reaching a steady state value of 350pM by 15min corresponding to data in literature (Coppack et al., 1989b). The simulated interstitial levels of insulin increased from 8.4pM to 73.5pM (Figure 4.2). During the hyperinsulinemic clamp experiment, the plasma glucose concentration varied by ~10% (Figure 4.3A), which was tracked by the model simulation. The arterial lactate showed a sigmoidal increase (~40%) reaching a steady state at 30min (Figure 4.3B). The levels of arterial glycerol and FFA decreased exponentially by ~60% and ~90% respectively (Figure 4.3C and 4.3D). Also, the arterial levels of TG decreased linearly by ~20% (Figure 4.3E). The infusion of glucose and insulin resulted in the temporal increase in the adipose blood flow reaching its maximum (2.5 fold increase) at ~30min and slowly returning to the basal value (Figure 4.3F).

Venous concentration dynamics: By varying the levels of arterial substrates and adipose blood flow, we simulated the concentration dynamics of metabolic substrates in the venous blood. The parameter values related to insulin action (i.e., λ_k) were optimally estimated (Table 4.5) by comparison of simulations to data. After the onset of insulin infusion, the venous glucose levels decreased by 10~20% reaching a steady state at 30min, whereas the venous lactate levels showed a sharp sigmoidal increase (~40%) for 30min and then a slow increase (Figure 4.5A and 4.5B). The suppression of lipolysis by insulin resulted in the exponential decreases in both FFA and glycerol in the venous effluent that reached steady-state levels after 30min. While the glycerol concentration decreased to ~28% of the basal state, the FFA concentrations in the venous blood decreased to ~12% (Figure 4.5C and 4.5D). Also, the venous TG levels decreased linearly by ~20% at 120min (Figure 4.5E). The simulated venous concentration dynamics of

various substrates were in good agreement with data from *in vivo* studies.

4.3.3. Regulation of lipolysis

Insulin suppresses the lipolytic reactions catalyzed by ATGL and HSL by different cellular mechanisms (viz., TG breakdown by ATGL vs. TG and DG breakdown by HSL). Differential suppression of lipolytic reactions was simulated using larger α_k values [635 pM^2] for the ATGL reaction than the α_k values [70.6 pM^2] for the HSL reactions. For uniform suppression of lipolysis by insulin, the same α_k values [70.6 pM^2] were applied for all lipolytic reactions. With uniform suppression, ATGL and HSL reactions decreased ~97% from their basal rates (Figure 4.6A). With differential suppression, the degree of suppressing ATGL reaction was reduced by ~10% compared with that of uniform suppression. These simulations were compared with those where TG breakdown by ATGL is not suppressed. Changes in α_k for the ATGL reaction affected the venous FFA concentration when ATGL was not suppressed by insulin (Figure 4.6B). The intracellular DG and MG showed distinctive responses depending on the relative suppression of ATGL and HSL reactions (Figure 4.6C). With uniform suppression of ATGL and HSL, the concentrations of DG decreased linearly by ~50 μM in 120 min. With differential suppression of the ATGL reaction, DG changed only after 60min. Without suppression of the ATGL reaction, DG increased linearly ~20% after 120min. With or without suppression of the ATGL reaction, MG decreased exponentially decreased from 200 μM to 30 μM (simulation not shown).

4.3.4. Sources of G3P and regulation of glyceroneogenesis

Model simulations predict the contributions of glycolysis and glyceroneogenesis

to the synthesis of G3P required for the re-esterification of FFA during the hyperinsulinemic-euglycemic clamp experiment. For these experiments, the rates of G3P synthesis via glycolysis and via glyceroneogenesis were normalized to their rates in the basal state. The relative increase (~70%) via glyceroneogenesis was larger than the relative increase (~50%) via glycolysis (Figure 4.7A). Driving forces for the increased flux rates are the increased cellular phosphorylation state indicated by ~40% higher C_{ATP}/C_{ADP} and the decreased (i.e., reduced) cellular redox state indicated by ~40% lower C_{NAD+}/C_{NADH} (Figure 4.7B). When arterial lactate concentrations increased from 0.7mM to 1.5mM, the rate of glyceroneogenesis increased ~15% from 0.38μmol/kg/min and the rate of re-esterification increased ~10% from 1.27 μmol/kg/min (Figure 4.8).

4.3.5. Effect of reduced insulin action

Model simulations (Figure 4.9) show the effects of reduced insulin action on glucose transport ($\lambda_{Tmax,GLC}$ in $J_{b\leftrightarrow c,GLC}$), glycolysis ($\lambda_{Glycolysis}$ in $\phi_{\mathrm{GLC}\rightarrow\mathrm{G6P}}$, $\phi_{\mathrm{F6P}\rightarrow\mathrm{GAP}}$ and $\phi_{\mathrm{GAP}\rightarrow\mathrm{PYR}}$), glycogen synthesis ($\lambda_{Glycogen\ Synthesis}$ in $\phi_{\mathrm{G6P}\rightarrow\mathrm{GLY}}$) and pyruvate oxidation (λ_{PDH} in $\phi_{\mathrm{PYR}\rightarrow\mathrm{ACoA}}$). These λ_k parameters of the model that are related to the stimulatory insulin action were decreased to 20% of the reference values. The rate of glucose uptake by the adipose tissue decreased (from 9.8 μmol/kg/min) by ~30% from lower $\lambda_{Tmax,GLC}$, by ~60% from lower $\lambda_{Glycolysis}$, by ~15% from lower $\lambda_{Glycogen\ Synthesis}$, and by ~1% from lower λ_{PDH}.

Simulations also showed the effect of reduced insulin action on the lactate release rate (negative) from adipose tissue (Figure 4.10). Decreasing the λ parameters by 40% had distinctly different effects. The lactate release rate was reduced by 21% with

decreased $\lambda_{Tmax,GLC}$ and by 62% with decreased $\lambda_{Glycolysis}$. In contrast, it was increased by 31% with decreased $\lambda_{Glycogen\ Synthesis}$ and increased by 7% with decreased λ_{PDH} increased.

4.3.6. Altered enzyme expressions

In silico transgenic experiments by model simulations predict responses to altered enzyme expressions. The activity of PEPCK (i.e., $V_{max,PYR\rightarrow GAP2}$) was modulated in the basal state to determine its effects on the rates of glyceroneogenesis and FFA release from adipose tissue into the circulation (Figure 4.11). A 3-fold increase in PEPCK activity (i.e., $3\cdot V_{max,PYR\rightarrow GAP2}$) increased flux through glyceroneogenesis by ~70% (from 0.38 to 0.65 μmol/kg/min), but did not increase the FFA release rate. However, when the activity of acyl CoA synthetase (ACS) was increased two fold (i.e., $2\cdot V_{max,FFA\rightarrow FAC}$) together with PEPCK, there was ~12% decrease in the FFA release rate (8.6μmol/kg/min) and the glyceroneogenesis rate increased more than doubled.

4.4. DISCUSSION

Comparison of model simulations with available experimental data provides confidence in the validity of this mechanistic model of adipose tissue metabolism. Consequently, the model is expected to be able to simulate a variety of responses under conditions for which no experimental data is currently available. This study focuses on the regulation of lipolysis and re-esterification by insulin. Simulations indicate the significance of regulating LPL reactions with the suppressed intracellular lipolysis. Differential suppression of lipolytic reactions is not evident based on the dynamic changes in the venous concentrations of FFA and glycerol, but the changes in DG level may suggest the differential regulation by insulin. In accord with experimental data,

simulations show glyceroneogenesis to be the dominant pathway for G3P synthesis even when the glucose uptake by the adipose tissue increases. Elevation of blood lactate levels enhances flux through the glyceroneogenesis pathway, which increases the re-esterification rate of FFA. Simulations demonstrate possible metabolic responses to altered expressions of PEPCK and ACS. Finally, the sensitivity analysis of model parameters indicates that insulin-stimulated glucose uptake could be severely affected by the impairment of the GLUT4 translocation and glycolysis. Furthermore, reduced insulin action in these steps blunted the production of lactate by insulin.

4.4.1. Steady-state analysis

Model simulations of the dependence of venous glycerol and rates of lipolysis and re-esterification of FFA on insulin level correspond well to experimental data (Figure 4.4). At the highest insulin level, the simulated glycerol level was ~35% higher than found experimentally. However, when the hydrolysis of plasma TG (i.e., VLDL-TG) by LPL was completely suppressed, simulated outputs and experimental data were in good agreement, which may suggest that the additional production of glycerol (i.e., the possible source of error) may come from the breakdown of plasma TG by LPL rather than from the intracellular TG breakdown. Therefore, it can be pointed out that our model can simulate the lipolytic responses from intracellular lipolysis but has some limitations associated with the breakdown of plasma TG by LPL. In fact, plasma TG hydrolysis by LPL in the basal state accounts for only ~13% of the total TG breakdown in the adipose tissue from *in vivo* (Coppack et al., 1990;Frayn et al., 1994) and *in silico* studies (Kim et al., 2008). Consequently, the effect of simulating LPL reaction was not evident in the basal state. However, the simulations in this study suggest that when the rate of lipolysis

decreases more than 90% of the basal state, the breakdown of plasma TG by LPL makes a significant contribution to the total rate of TG breakdown in the adipose tissue, Therefore, simulating TG breakdown by LPL becomes critical when the intracellular lipolysis is suppressed by insulin.

4.4.2. Regulation of lipolysis

Since the breakdown of TG and DG are catalyzed by different enzymes, viz., ATGL, HSL (Schweiger et al., 2006) and the first step in TG hydrolysis involves other regulatory proteins, such as perilipin A and adipophilin (Miyoshi et al., 2007;Sztalryd et al., 2003), we hypothesized that TG and DG breakdowns are differentially suppressed by insulin. Therefore, the model parameters for these reactions were varied to simulate different insulin effects: differential suppression or no suppression of the ATGL reaction and uniform suppression of ATGL and HSL reactions. Although insulin can transcriptionally down-regulate the activity of ATGL (Kershaw et al., 2006), it is negligible over the time scale of interest (~2hr). Instead, we assumed that insulin can suppress the breakdown of TG by ATGL indirectly by perilipin A since the inactivation of perilipin A limits the access of both ATGL and HSL to the TG stores, i.e., lipid droplets (Miyoshi et al., 2007). Model simulations predict the integrated responses that affect different regulation mechanisms.

The degree of suppression of ATGL did not affect the venous dynamics of glycerol since the production of glycerol depends on the hydrolysis of MG by HSL and MGL, which are not subject to the insulin mediated suppression. Simulations without suppressing ATGL reaction by insulin produced consistently higher levels of FFA in the venous blood (Figure 4.6B). Suppression by more than 50% did not further change

venous FFA concentration dynamics, which limited the analysis of differential suppression of these intracellular lipolytic reactions based on blood measurements. Differential activation of lipolytic reactions during epinephrine infusion could generate distinctive changes in lipolytic intermediates (Kim et al., 2008). Thus, simulations were used to predict insulin responses of intracellular DG and MG concentrations. Whereas MG levels did not change, changes in DG could be distinguished. With uniform suppression of lipolytic reactions, DG continuously decreased with insulin; whereas with differential suppression of ATGL reaction, DG increased. If ATGL is not suppressed by insulin, then DG increases more than 20%. Although corresponding *in vivo* experiments are not available, *in vitro* studies showed that insulin increases DG (Edens et al., 1990a). These studies used palmitate in the incubation medium. Therefore, the rate of DG synthesis was not limited by the availability of fatty acids. Without the infusion of fatty acids or the ingestion of mixed meal, the availability of fatty acids can limit the synthesis of DG and TG. Therefore, the accumulation of DG during hyperinsulinemic clamp experiment might be lower than that from *in vitro* studies. Model simulations, however, indicate that DG levels may provide a clue to the mechanism by which insulin suppresses lipolytic reactions.

4.4.3. Glyceroneogenesis and PEPCK over-expression

The metabolic importance of glyceroneogenesis in adipose tissue was examined by simulating responses to the increased rate of TG-FFA cycle during epinephrine infusion (Kim et al., 2008). However, there was no change in the rate of glucose uptake during intravenous epinephrine infusion. Therefore, in the previous model, we could not determine the adipose tissue response to increased rate of glucose uptake. In the present

study, the effect of increasing glucose uptake on the relative contributions of glycolysis and glyceroneogenesis to the synthesis of glycerol-3-phosphate was analyzed. Model simulations showed that glycolytic and glyceroneogenic fluxes for G3P synthesis increased with stimulated glucose uptake. This may seem counter-intuitive because PEPCK, a regulatory enzyme for glyceroneogenesis, is down-regulated by insulin (Beale and Tishler, 1992). However, the transcriptional regulation of PEPCK by insulin requires a longer time to act than related to the time scale of acute infusion experiments. Furthermore, the activity of PEPCK in adipose tissue is high enough to meet the metabolic requirements (Reshef and Hanson, 1972;Reshef et al., 1969). Consequently, in acute response to insulin infusion the availability of substrates regulates the metabolic flux through glyceroneogenesis rather than the activity of PEPCK *per se*.

In response to insulin and glucose infusion, changes in cellular redox and phosphorylation states can also modulate the rate of metabolic reactions associated with the synthesis of G3P. Simulations showed that an increased rate of glycolytic flux rate by insulin decreased the redox state (C_{NAD+}/C_{NADH}) and increased the phosphorylation state (C_{ATP}/C_{ADP}) and supplies of GAP and pyruvate. These state increases the driving force of flux through glyceroneogenesis.

Glyceroneogenesis plays a significant role in regulating the synthesis of G3P (and therefore TG). Thus, pyruvate and lactate are important as precursors. Indeed, insulin resistant obese patient have higher levels of plasma and interstitial levels of lactate in the adipose tissue (Jansson et al., 1994;Qvisth et al., 2007). The effect of elevated plasma lactate on re-esterification of FFA and glyceroneogenesis was analyzed from *in silico* experiments with elevated levels of arterial lactate. Model simulations showed that FFA re-esterification and flux through glyceroneogenesis increased 10~15%. Higher levels of

lactate in plasma were associated with higher lactate levels in tissue. Since the cellular lactate levels affect the redox potential and pyruvate levels, the elevated lactate levels can promote the synthesis of G3P that increases intracellular FFA re-esterification.

Simulated responses from the altered PEPCK expression were obtained by changing the maximum reaction rate coefficient for the reaction catalyzed by PEPCK. Even though the activity of PEPCK increased the flux through glyceroneogenesis, the FFA release rate into circulation did not decrease. Simulations indicated that synthesis of FAC from FFA by ACS should increase together with PEPCK activity to increase the rate of FFA re-esterification as measured in the transgenic animals (Franckhauser et al., 2002). Decreased FFA release rate from adipose tissue was also observed by the treatment of diabetic subjects with TZDs (Tordjman et al., 2003). Since TZDs are PPARγ agonists, they can affect several metabolic pathways involved in glucose and fatty acids homeostasis. *In vivo* studies showed that the PPARγ treatment upregulated the genes for PEPCK and ACS in the adipose tissue (Way et al., 2001;Martin et al., 1997). Simulations were consistent with these observations as indicated by increases in enzyme activities and flux rates. These simulations indicate that the upregulation of PEPCK *per se* is not sufficient to increase the rate of FFA re-esterification and are expected to be accompanied by the induction of other enzymes, specifically, ACS.

4.4.5. Effect of impaired insulin action

Insulin resistance is a state of tissue or whole body requiring higher levels of insulin to elicit a normal response (Summers, 2006). The decreased rate of insulin stimulated glucose uptake is one of the major defects resulted from insulin resistance. This effect was simulated by decreasing the model parameter values related to

stimulatory insulin action. Impairments in GLUT4 translocation and glycolysis including phosphorylation of glucose had more significant effect on the rate of glucose uptake by the adipose tissue than changes in rates of glycogen synthesis and pyruvate oxidation. This indicates that glucose transport and subsequent phosphorylation are the principal sites of defective insulin action in the adipose tissue. Indeed, various *in vivo* studies in skeletal muscle showed that the stimulation of GLUT4 translocation and phosphorylation of glucose were the primary impairments in type 2 diabetes (Rothman et al., 1992;Shulman and Rothman, 1996). Even though the rate of glycogen synthesis was impaired in these patients, it was secondary to the defects in glucose transport and phosphorylation.

In vivo studies in humans showed that the insulin resistant obese subjects in the basal state had an elevated lactate release, which did not increase in response to insulin infusion (Qvisth et al., 2007). In contrast, the normal lean subjects showed an increase of lactate release rate during the hyperinsulinemic-euglycemic clamp experiment (Qvisth et al., 2007). By decreasing model parameters associated with GLUT4 translocation and glycolysis, the rate of lactate release decreased. When the parameter decreases are sufficiently large, the lactate release rate returned to the basal state as reported from *in vivo* studies in obese subjects. The opposite response occurred with the impaired glycogen synthesis and pyruvate oxidation. One explanation is that glycogen synthesis and pyruvate oxidation are not the predominant mechanisms of consumption of glucose taken up by the adipose tissue. More than 70% of glucose taken up by the skeletal muscle is converted to glycogen during hyperinsulinemic-euglycemic clamp (Serlie et al., 2005;DeFronzo et al., 1981). In contrast, in the adipose tissue, model simulations showed that only ~30% of glucose uptake was used for this purpose. More is used to produce

lactate than occurs in skeletal muscle. This indicates the relative importance of lactate production for insulin-stimulated glucose disposal in the adipose tissue. Consistent with experimental data, model simulations show that the pathways for defective insulin action play an important role in the adipose tissue and that insulin resistance is associated with the decreased translocation of glucose transporters and glycolysis in adipose tissue.

4.4.6. Model limitation

One limitation of the enhanced model of adipose tissue metabolism is incomplete suppression of plasma TG breakdown in response to insulin, which depends on the breakdown of TG by LPL in the blood compartment. *In vivo* human studies (Coppack et al., 1989a) find that plasma levels of TG slowly decreased by ~20% in response to insulin. Since the reaction flux of TG hydrolysis by LPL in the enhanced model depends on the total plasma level of TG, the plasma TG breakdown rate cannot be decreased to a negligible level as indicated by the *in vivo* studies (Coppack et al., 1989a). LPL may have different affinity toward various lipoproteins (e.g., VLDL, chylomicrons, LDL etc.). Indeed, chylomicrons have more than 50 fold higher affinities toward LPL (Xiang et al., 1999). Furthermore, the size distribution of plasma VLDL shifted toward a smaller size during a hyperinsulinemic clamp experiment (Lewis et al., 1993). Therefore, LPL might have lower specific affinity toward TG-depleted small VLDL. Future studies should consider varying activities of LPL for different lipoproteins to describe the regulation of plasma TG breakdown.

4.5. CONCLUSIONS

An enhanced model of adipose tissue metabolism *in vivo* simulated steady-state responses to insulin as well as dynamic changes in venous concentrations of metabolites during the hyperinsulinemic-euglycemic clamp experiment. Our simulations studies indicate that the regulation of LPL becomes important when intracellular lipolysis is suppressed by insulin. Different activities of LPL toward various lipoproteins should be considered to investigate the regulation of lipolysis in the adipose tissue. Differential suppression of lipolytic reactions by insulin is required to increase the levels of DG as measured in *in vitro* studies. Model simulations indicate that glyceroneogenesis is the dominant pathway for G3P synthesis even when the rate of glucose uptake is increased by elevated C_{NADH}/C_{NAD+} and C_{ATP}/C_{ADP}. Simulations of the effect of altered enzyme expression indicated that the increased rate of re-esterification requires the upregulation of both PEPCK and ACS activities. Simulations suggested that impaired GLUT4 translocation and glycolysis (i.e., phosphorylation) in adipose tissue blunted the response of insulin-stimulated lactate production.

TABLE 4.1. Substrate concentration in the blood and the cellular compartment

Substrate	Blood*	Cell*
GLC	5000	2540
PYR	68	200
LAC	700	1440
ALA	192	1300
GLR	70	220
FA	660	1000
TG	990	990000
O2	8000	34
O2 (Free)	84	
CO2 (Total)	21700	15427
CO2 (Free)	1124	1403
GLY		13000 (Rigden et al., 1990)
G6P		210 (Saggerson and Greenbaum, 1970)
F6P		60 (Saggerson and Greenbaum, 1970)
GAP1, GAP2		10
G3P1, G3P2		150 (Saggerson and Greenbaum, 1970)
R5P		4 (Casazza and Veech, 1986)
ACoA		25
FAC		70 (Saggerson and Greenbaum, 1970)
CoA		200
DG		2000
MG		200
ATP		3840 (Saggerson and Greenbaum, 1970)
ADP		1270 (Saggerson and Greenbaum, 1970)
Pi		2700
NAD+		450 (Saggerson and Greenbaum, 1970)
NADH		0.14 (Saggerson and Greenbaum, 1970)
NADP+		0.93 (McLean et al., 1967;PASTAN et al., 1963)
NADPH		7.1 (McLean et al., 1967;PASTAN et al., 1963)

*Values are in μM. Data are taken from Kim et al. (Kim et al., 2008) or the references, which are listed with parentheses.

TABLE 4.2. Basal reaction flux rates and associated parameters

Fluxes	Flux Rate*	$V_{X\rightarrow Y}$*	K_m†	K_i†	$\mu^{\pm}$§	$\nu^{\pm}$ or $\eta^{\pm}$§
$\phi_{GLC\rightarrow G6P}$	1.88	4.06	384000‡	210		
$\phi_{F6P\rightarrow GAP1}$	1.96	7.83	60		0.33 (−)	
$\phi_{GAP1\rightarrow PYR}$	3.90	31.20	27000‡		0.33 (−)	3214 (−)
$\phi_{G6P\rightarrow GLY}$	0.21**	0.84	210		3.02 (+)	
$\phi_{GLY\rightarrow G6P}$	0.31**	1.24	35100000‡		0.33 (−)	
$\phi_{G6P\rightarrow R5P}$	0.07**	0.28	210			3214 (−)
$\phi_{R5P\rightarrow F6P-GAP1}$	0.07**	0.14	4			0.13 (−)§§
$\phi_{PYR\rightarrow GAP2}$	0.38	3.01	200		3.02 (+)	0.0003 (+)
$\phi_{GLR\rightarrow G3P2}$	0.01	0.04	220		3.02 (+)	
$\phi_{ALA\rightarrow PYR}$	3.08	6.16	1300			
$\phi_{PYR\rightarrow ALA}$	1.00	2.00	200			
$\phi_{Proteolysis}$	2.65	2.65				
$\phi_{PYR\rightarrow ACoA}$	3.92	23.52	100000‡	25		3214 (−)
$\phi_{FA\rightarrow FAC}$	1.71	6.86	15000‡		3.02 (+)	
$\phi_{FAC\rightarrow ACoA}$	0.44	2.61	14000‡	25		3214 (−)
$\phi_{ACoA\rightarrow FA}$	0.08**	0.64	25‡			7.63 (+)§§
$\phi_{TG\rightarrow DG,ATGL}$	3.35	3.35				
$\phi_{TG\rightarrow DG,HSL}$	0.65	0.65				
$\phi_{DG\rightarrow MG,HSL}$	3.29	6.58	2000			
$\phi_{MG\rightarrow GLR,HSL}$	0.33	0.66	200			
$\phi_{MG\rightarrow GLR,MGL}$	2.67	29.37	2000			
$\phi_{G3P1-FAC\rightarrow DG}$	0.04	0.08	10500‡			
$\phi_{G3P2-FAC\rightarrow DG}$	0.39	0.77	10500‡			
$\phi_{DG-FAC\rightarrow TG}$	0.43	0.85	140000‡			
$\phi_{DG-DG\rightarrow TG}$	0.60	1.20	2000			
$\phi_{MG-MG\rightarrow DG}$	0.32	0.64	200			
$\phi_{MG-DG\rightarrow TG}$	0.27	0.54	400000‡			
$\phi_{ACoA\rightarrow CO2}$	7.32	58.57	67500‡		0.33 (−)	3214 (−)
$\phi_{O2\rightarrow H2O}$	20.43	81.73	27‡		0.33 (−)	0.0003 (+)
$\phi_{ATP\rightarrow ADP}$	129.0	258.0	3840			
$\phi_{TG\rightarrow GLR,LPL}$	0.61	1.22	990000			

* Values are in μmol·min^{-1}·kg wet tissue^{-1}. $V_{max,k}$, maximum rate coefficient. Data are from the reference (Kim et al., 2008) except for those marked with **, which are from the references, (Rigden et al., 1990) and (Strawford et al., 2004).

† Values are in μmol·kg wet tissue^{-1} except for the marked (‡), which are in (μmol·kg wet tissue^{-1})^2. $K_{m,k}$, $K_{i,k}$, phenomenological M-M constant for reactant and product.

§ Values are dimensionless. $\mu^{\pm}$, $\nu^{\pm}$ and $\eta^{\pm}$, parameters for the metabolic controllers. Those marked with §§, represent $\eta^{\pm}$. (+) represents μ^{+}, ν^{+} or η^{+} while (−) represents μ^{-}, ν^{-} or η^{-}.

TABLE 4.3. Basal reaction flux rates and associated parameters for reversible reaction fluxes

Fluxes	Flux Rate	$V_{f,\,X\leftrightarrow V}$ †	$V_{b,\,X\leftrightarrow V}$ †	$K_{f,\,X\leftrightarrow V}$ ‡	$K_{b,\,X\leftrightarrow V}$ ‡	$K_{eq,\,X\leftrightarrow V}$ §
$\phi_{G6P\leftrightarrow F6P}$	1.91	42.7	37.0	210	60	0.33**
$\phi_{PYR\leftrightarrow LAC}$	1.55	19.7	15.1	80	648000	1.06×10^{4}
$\phi_{GAP1\leftrightarrow G3P1}$	0.04	0.12	7.3×10^{-6}	4	67500	2.77×10^{8}
$\phi_{GAP2\leftrightarrow G3P2}$	0.38	1.13	6.9×10^{-5}	4	67500	2.77×10^{8}

Data are from Kim et al. (Kim et al., 2008) except for those marked with ** which is from the reference (Staples and Suarez, 1997).

† $V_{f,k}$ and $V_{b,k}$, forward and reverse rate coefficients (μmol·min^{-1}·kg wet tissue^{-1}).

‡ $K_{f,k}$ and $K_{b,k}$, phenomenological M-M constants for reactants and products (μmol·kg wet tissue^{-1})^2.

§ K_{eq}, equilibrium constant (dimensionless).

TABLE 4.4. Model input functions

Time (min)	Input Functions*
$t \le 15$	$Q = Q_0$, $C_I = C_{I,0}$, $C_{a,GLC} = C_{a,GLC,0}$, $C_{a,LAC} = C_{a,LAC,0}$ $C_{a,GLR} = C_{a,GLR,0}$, $C_{a,FFA} = C_{a,FFA,0}$, $C_{a,TG} = C_{a,TG,0}$
$t > 15$	$Q = Q_0 \cdot \left(1 + 7.76 \cdot (1 - e^{-(t-15)/20.54}) - 7.68 \cdot (1 - e^{-(t-15)/36.48})\right)$ $C_I = C_{I,0} + 65.1 \cdot \left(1 - e^{-(t-15)/10}\right)$ $C_{a,GLC} = C_{a,GLC,0} \cdot \left(1 - 0.177 \cdot (t-15)^{5.26} / (22.82^{5.26} + (t-15)^{5.26}) + 0.421 \cdot (1 - e^{-(t-15)/350.3})\right)$ $C_{a,LAC} = C_{a,LAC,0} \cdot \left(1 + 0.389 \cdot (t-15)^{7.05} / (18.88^{7.05} + (t-15)^{7.05})\right)$ $C_{a,GLR} = C_{a,GLR,0} \cdot \left(0.41 + 0.59 e^{-(t-15)/10.38}\right)$ $C_{a,FA} = C_{a,FA,0} \cdot \left(0.11 + 0.89 e^{-(t-15)/17.22}\right)$ $C_{a,TG} = C_{a,TG,0} \cdot \left(1 - 0.0015 \cdot (t-15)\right)$

*Parameters for the input functions were optimally estimated based on the data from the human *in vivo* study (Coppack et al., 1989b;Coppack et al., 1989a;Karpe et al., 2002). Q: Blood flow to the adipose tissue; C_I: Insulin concentration in the interstitial fluid; $C_{a,GLC}$, $C_{a,LAC}$, $C_{a,GLR}$, $C_{a,FA}$, $C_{a,TG}$: Arterial concentrations of glucose, lactate, glycerol, FA and TG; $C_{a,i,0}$: Initial arterial concentration of chemical species i as shown in Table 4.1. Time courses of these input functions are shown in Figure 4.2.

TABLE 4.5. Estimated and miscellaneous model parameters

	Values	Units
Parameters for Stimulative Insulin Actions		
$\lambda_{Tmax,GLC}$	0.02	
$\lambda_{Glycolysis}$	5.01	
$\lambda_{Glycogen\ Synthesis}$	14.67	
λ_{PDH}	3.00	
Parameters for Inhibitory Insulin Actions		
$\alpha_{TG\rightarrow DG,ATGL}$	70.6, 635‡	pM^2
$\alpha_{TG\rightarrow DG,HSL}$	70.6	pM^2
$\alpha_{DG\rightarrow MG,HSL}$	70.6	pM^2
$\alpha_{GLY\rightarrow G6P}$	70.6	pM^2
$\alpha_{PRT\rightarrow ALA}$	70.6	pM^2
Miscellaneous parameters		
Q_0	0.031†	$ml \cdot min^{-1} \cdot kg^{-1}$
$C_{I,0}$	8.4†	pM
$V_{c,i}$		
TG,DG,MG	0.8†	
GAP1,GAP2,G3P1,G3P2	0.016	
Others	0.032†	

λ_k and α_k, parameters for insulin action; Q_0, adipose tissue blood flow at basal state; $C_{I,0}$, insulin concentration in the interstitial fluid at basal state. Data marked with † are taken from the reference (Kim et al., 2008).

‡ Two different values of $\alpha_{TG\rightarrow DG,ATGL}$ were used to simulate the different degree of suppression of ATGL reaction by insulin.

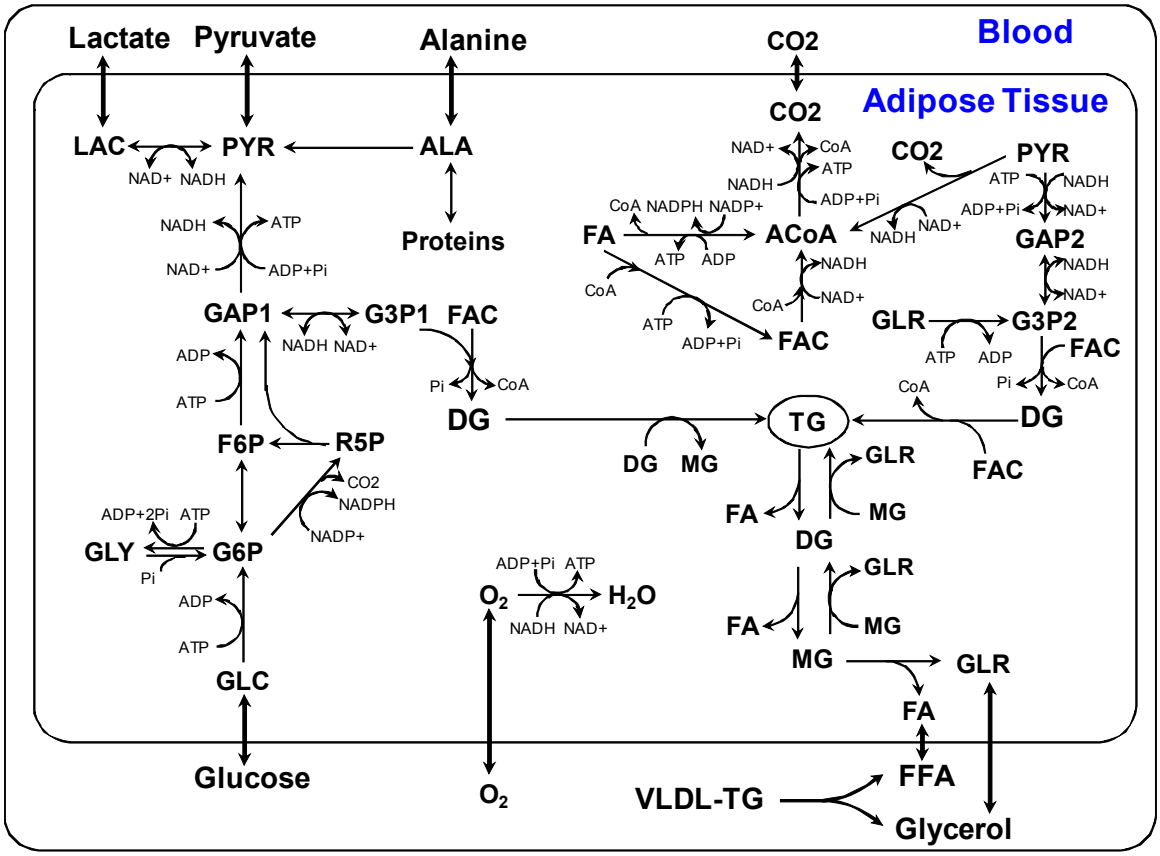

FIGURE 4.1. Metabolic pathways in the adipose tissue.

The model incorporates various metabolic pathways including glycolysis, glycogen cycle, pentose phosphate shunt, pyruvate oxidation, beta-oxidation, tricarboxylic acid cycle, oxidative phosphorylation, proteolysis and the esterification and hydrolysis of triglycerides. Glycerol-3-phosphate (G3P), used for the esterification of fatty acids, is formed either from glucose via glycolysis or from pyruvate via glyceroneogenesis. Triose phosphates (GAP, G3P) are heterogeneously distributed in the cellular compartment. GAP1 and G3P1 represent the triose phosphate pool from glycolysis, whereas GAP2 and G3P2 represent the pool from glyceroneogenesis. The arrow with both ends indicates a reversible reaction step. GLC, glucose; PYR, pyruvate; LAC, lactate; ALA, alanine; GLR, glycerol; FA, fatty acids; GLY, glycogen; G6P, glucose-6-phosphate; F6P, fructose-6-phosphate; R5P, ribulose-5-phosphate; GAP, glyceraldehyde-3-phasphate; G3P, glycerol-3-phosphate; ACoA, acetyl CoA; FAC, fatty acyl CoA; TG, triglycerides; DG, diglycerides; MG, monoglycerides;

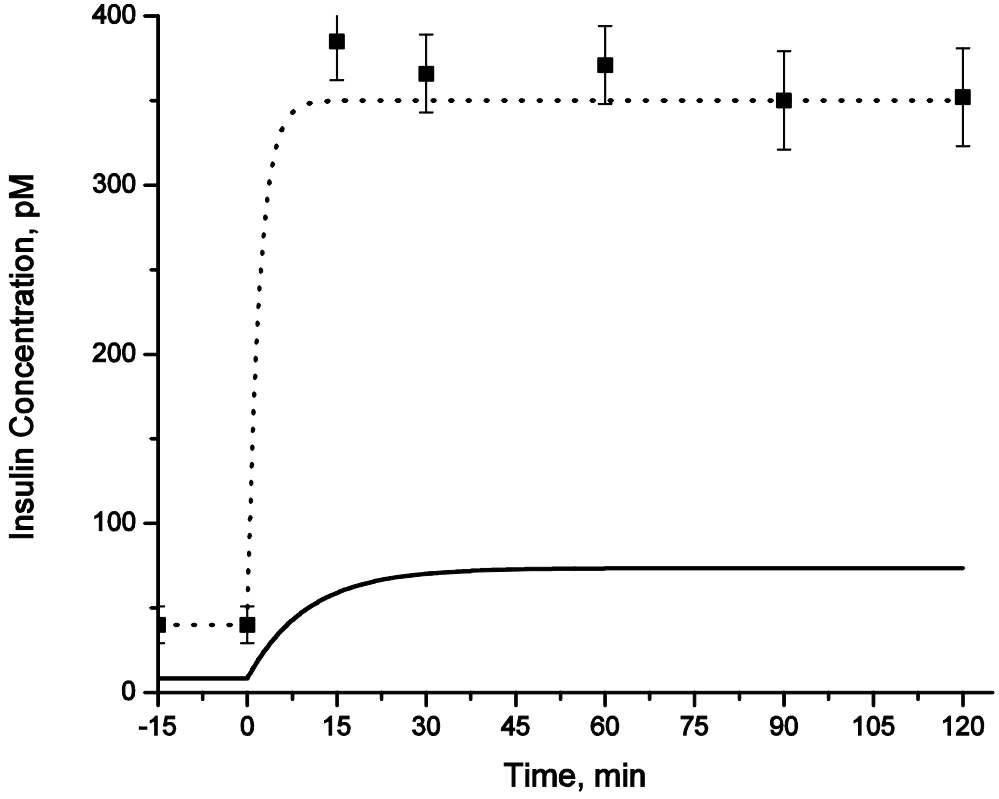

FIGURE 4.2. Dynamic changes in the plasma and interstitial concentrations of insulin following a constant rate intravenous infusion of insulin at 0min

Assuming a step increase in the plasma levels of insulin (dotted line), the corresponding levels of insulin in the interstitial fluid (solid line) was simulated assuming a time constant of 10min. Square symbol represents the plasma levels of insulin from the experimental studies in human (Coppack et al., 1989b).

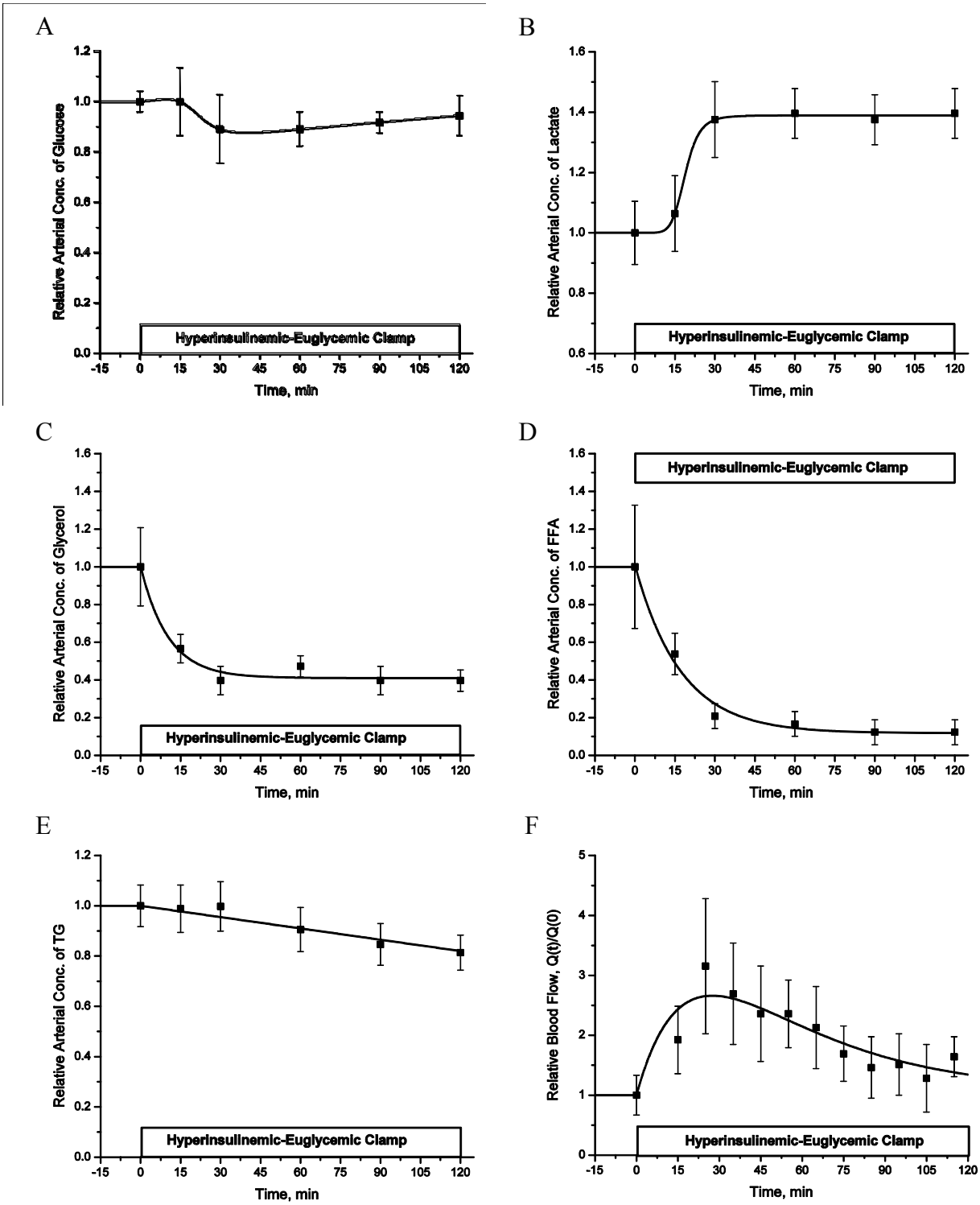

FIGURE 4.3. Dynamic changes in the arterial concentrations of glucose (A), lactate (B), glycerol (C), FFA (D) and TG (E), and the adipose blood flow (F) during hyperinsulinemic-euglycemic clamp.

Relative concentration/blood flow is the ratio of concentration/blood flow at any time t>0 to t=0. Squares represent the experimental data (mean±S.E.M.) from the references (Coppack et al., 1989b;Coppack et al., 1989a;Karpe et al., 2002). Solid lines are model simulations.

A

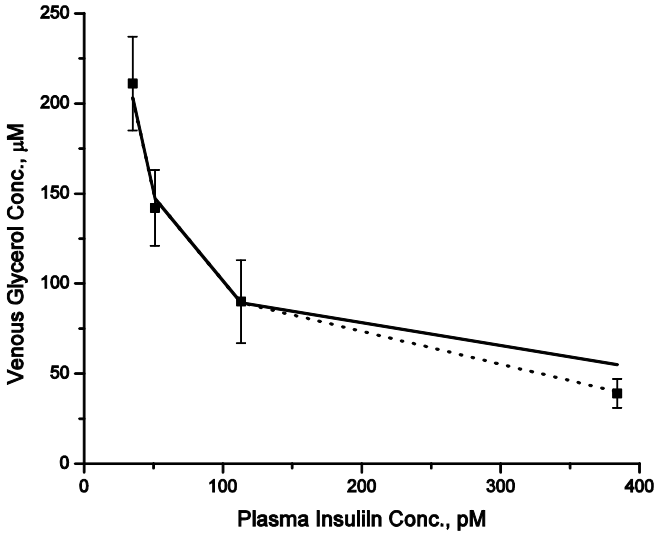

B

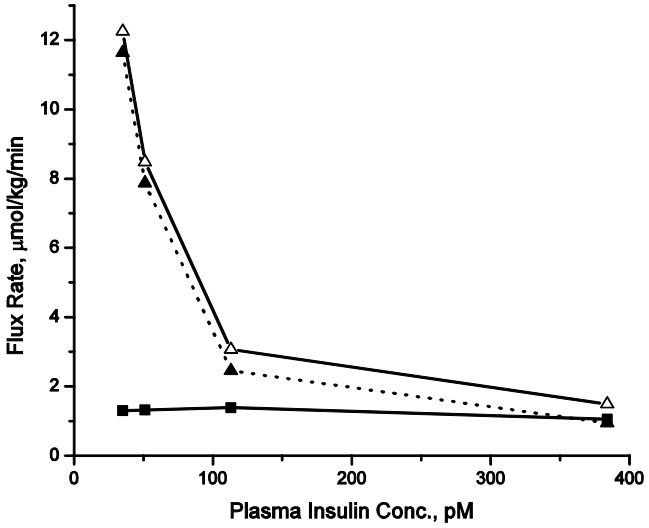

FIGURE 4.4. Steady state insulin dose-responses for the venous glycerol concentrations and the rates of lipolysis and re-esterification

(A): Filled square symbol represents the experimental data from the reference (Stumvoll et al., 2000). Solid and dotted line represent the model simulations with (dotted line) or without (solid line) the complete suppression of plasma TG breakdown by LPL at the plasma insulin concentration of 383pM.
(B): While open triangle with solid line represents the rate of total lipolysis in the blood and cellular compartments, filled triangle with dotted line represents the rate of intracellular lipolysis. Filled square with solid line represents the rate of re-esterification of FFA.

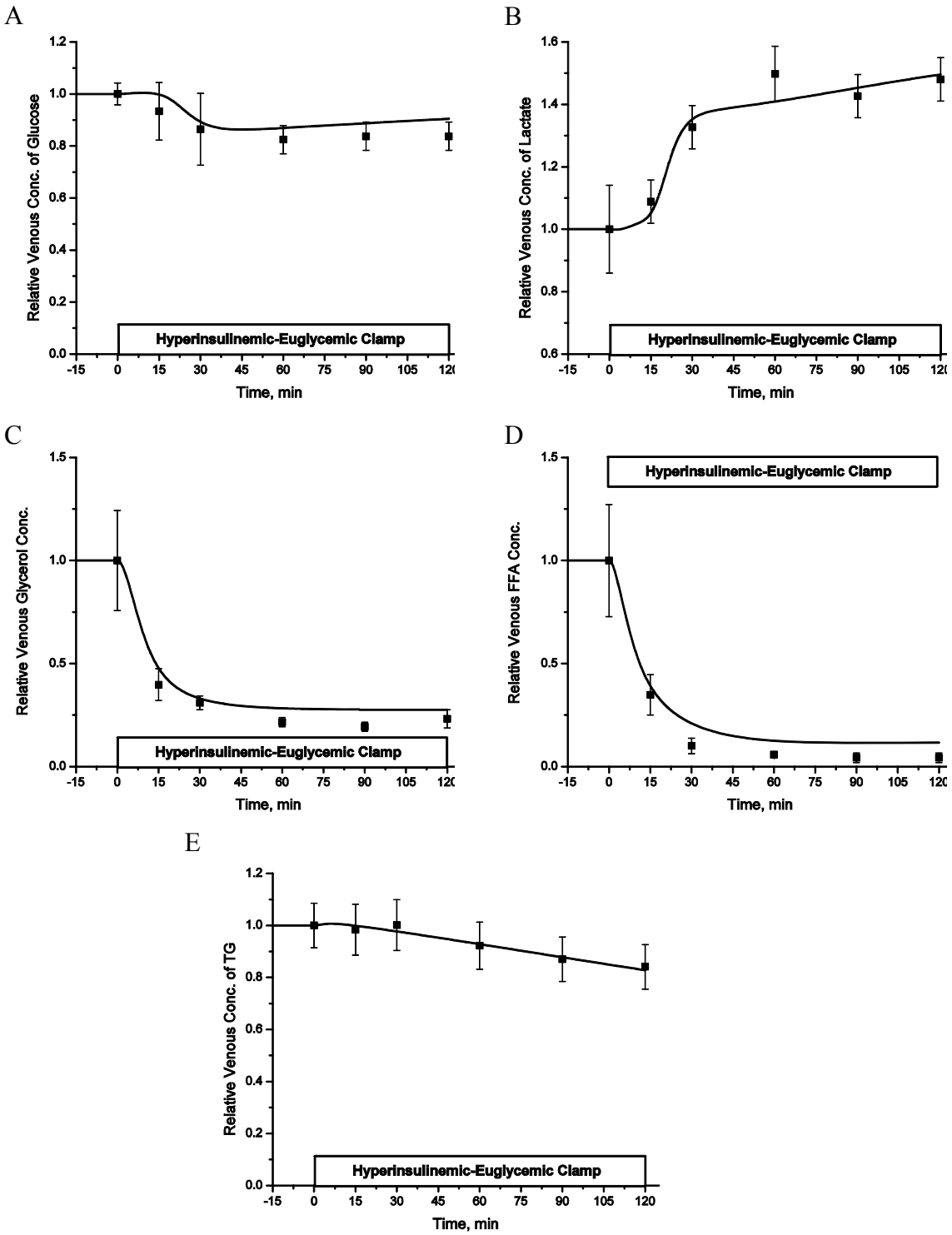

FIGURE 4.5. Dynamic changes in the venous concentrations of glucose (A), lactate (B), glycerol (C), FFA (D) and TG (E) in the adipose tissue during hyperinsulinemic-euglycemic clamp.

Relative concentration is the ratio of concentration at any time $t>0$ to $t=0$. Squares represent the experimental data (mean±S.E.M.) from the references (Coppack et al., 1989b;Coppack et al., 1989a). Solid lines are model simulations.

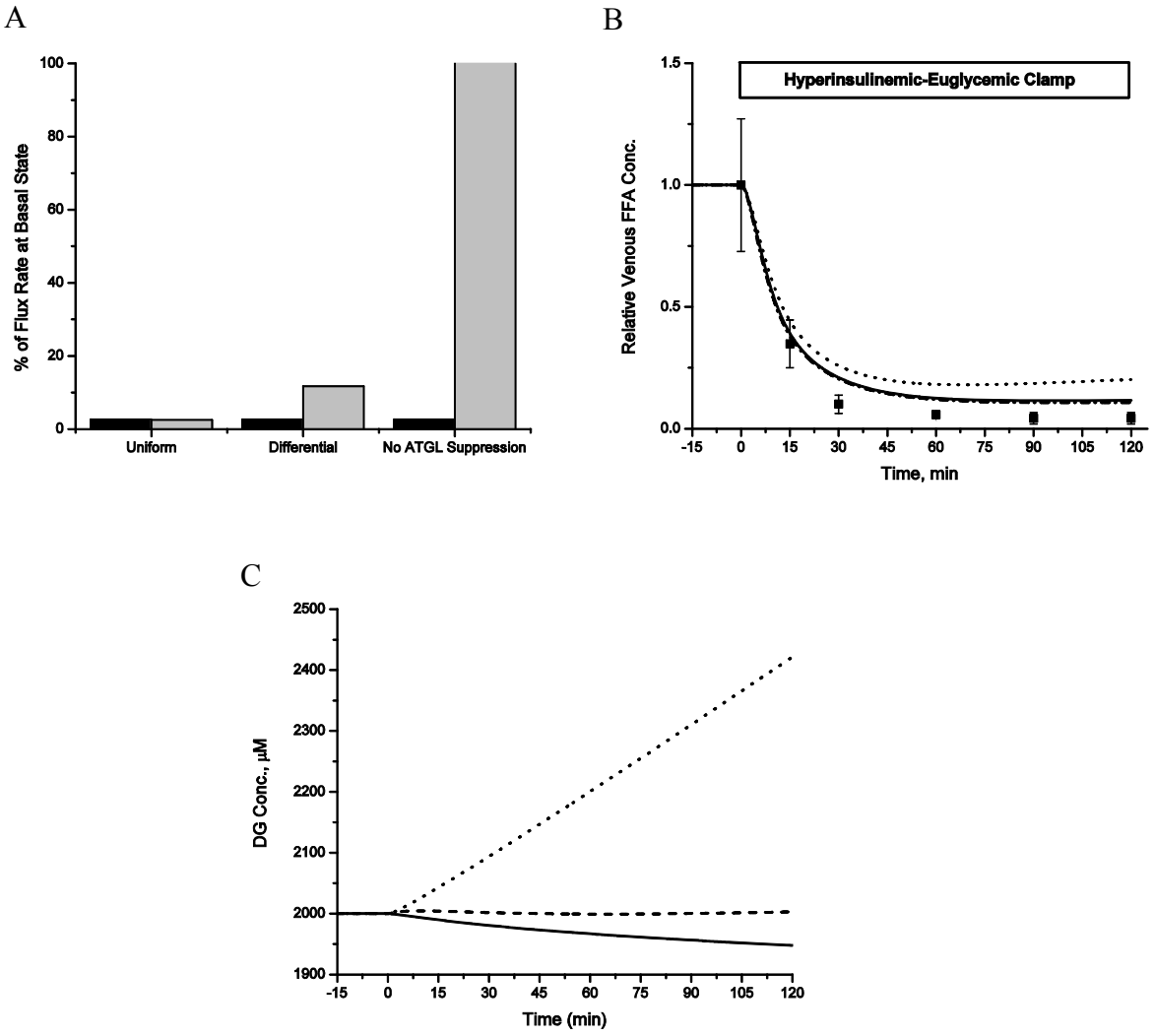

FIGURE 4.6. Effect of differential suppression of lipolytic reactions on the venous concentration dynamics of FFA and the changes in the levels of DG

(A): Relative changes in the flux rate of TG breakdown by ATGL (light gray bar, ▭) and TG and DG breakdowns by HSL (black bar, ▬) as a result of modulating the model parameter, $\alpha_{TG\rightarrow DG,ATGL}$. The different values of $\alpha_{TG\rightarrow DG,ATGL}$ were used for "Uniform ($\alpha_{TG\rightarrow DG,ATGL}$=70.6pM^2)" and "Differential ($\alpha_{TG\rightarrow DG,ATGL}$=70.6pM^2)". $V_{max,\ TG\rightarrow DG,ATGL}$ was not modulated by insulin in case of "No ATGL suppression". (B),(C): Dynamic changes in the relative venous concentrations of FFA (B) and the intracellaur concentrations of DG (C). Relative venous concentration is the ratio of venous concentration at any time t>0 to t=0. Squares represent the experimental data (mean±S.E.M.) from the references (Coppack et al., 1989b). Model simulations (solid line: "Uniform", dashed line: "Differential" and dotted line: "No ATGL suppression) were based on the different values of $\alpha_{TG\rightarrow DG,ATGL}$ as mentioned in (A).

A

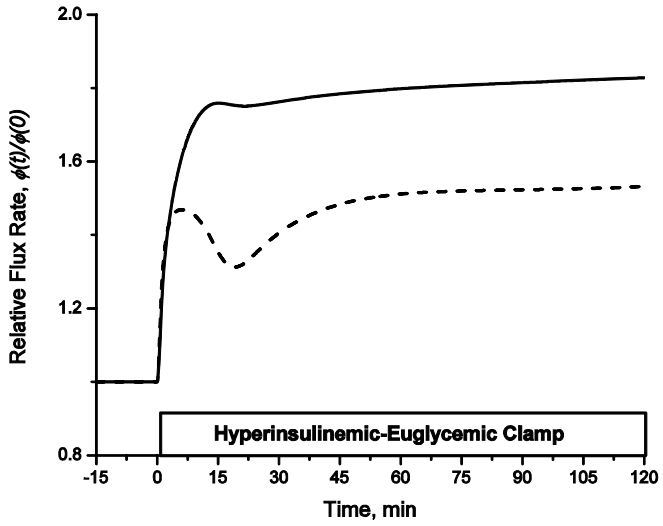

B

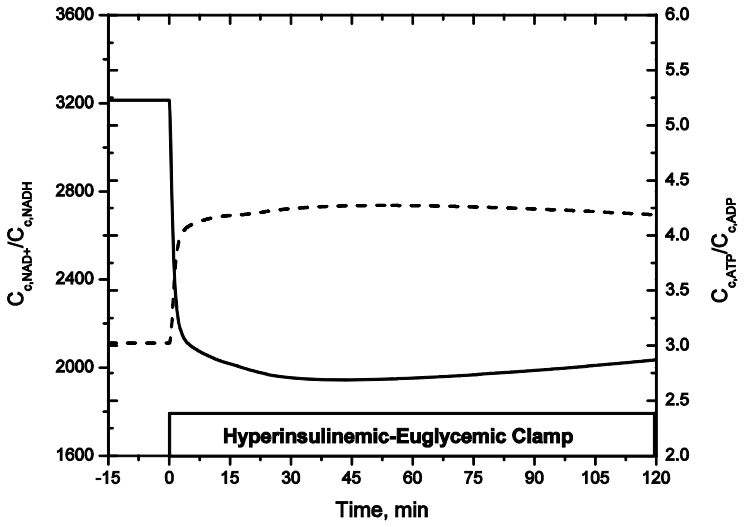

FIGURE 4.7. Relative changes in the rate of G3P synthesis via direct glycolysis and glyceroneogenesis (A) and the dynamic changes in the cellular phosphorylation and redox states (B)

(A): Solid and dashed line are the model simulations representing the relative changes in the rate of G3P synthesis via glyceroneogenesis (solid line) and via direct glycolysis (dashed line). Relative flux rate is the ratio of flux rate at any time $t>0$ to $t=0$.

(B): Solid and dashed line are the model simulations representing the changes in the cellular redox (solid line, $C_{c,NAD+}/C_{c,NADH}$) and phosphorylation (dashed line, $C_{c,ATP}/C_{c,ADP}$) states.

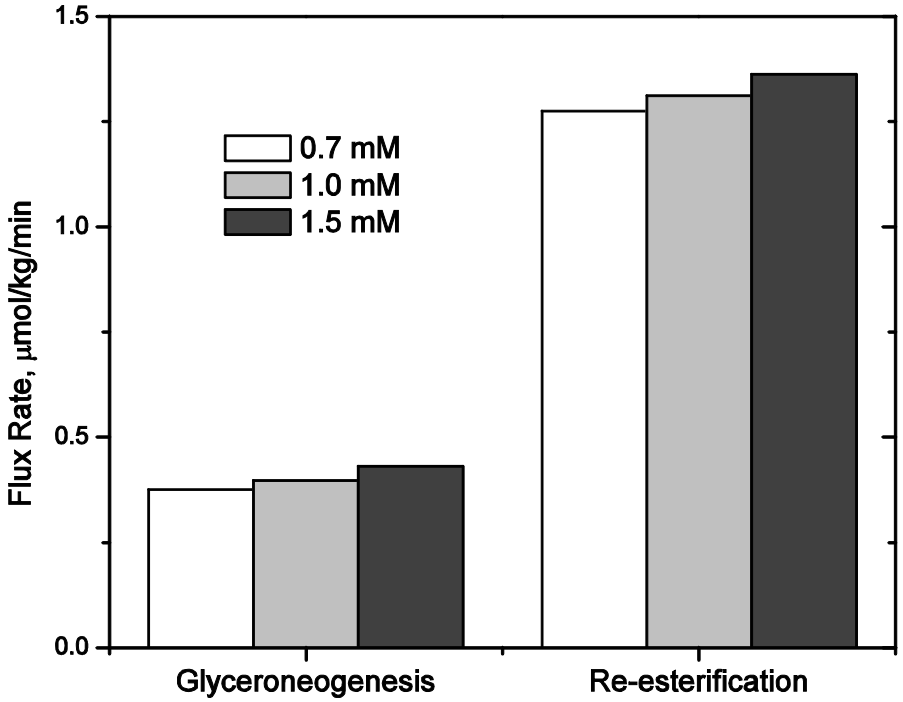

FIGURE 4.8. Effect of arterial lactate concentrations on the rates of glyceroneogenesis and re-esterification of FFA

The model simulated the changes in flux rates (glyceroneogenesis and re-esterification of FFA) at the steady state as a result of varying the arterial levels of lactate. The concentrations of arterial lactate used for the simulations are 0.7mM (open bar,), 1.0mM (light gray bar,) and 1.5mM (dark gray bar,).

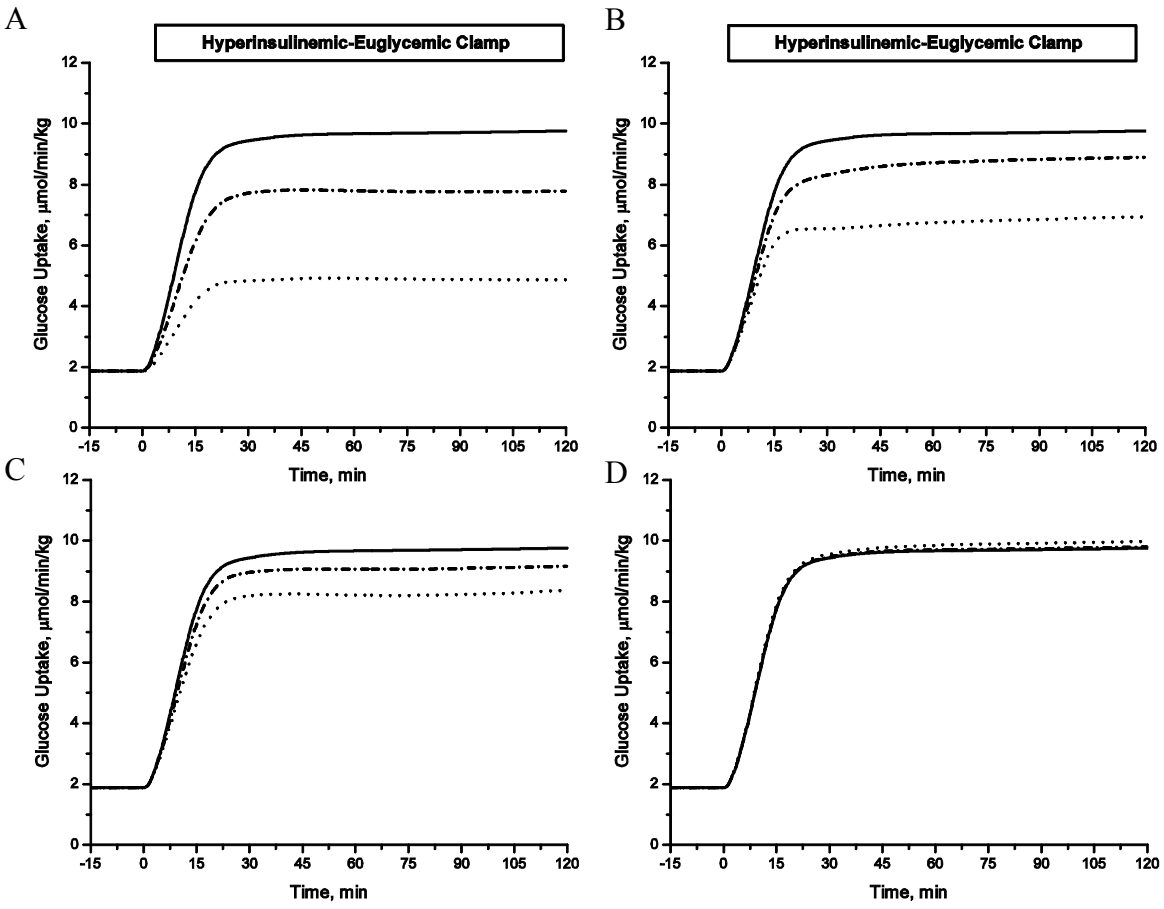

FIGURE 4.9. Effect of defective insulin action on the rate of glucose uptake

The model predicted the changes in the rate of glucose uptake during hyperinsulinemic-euglycemic clamp as a result of varying the model parameters related to the stimulative insulin action; (A)$\lambda_{Glycolysis}$, (B)$\lambda_{Tmax,GLC}$, (C) $\lambda_{Glycogen\ Synthesis}$ and (D) λ_{PDH}. The parameters are decreased up to 20% of their estimated values in Table 4.5; Solid line (100% of estimated value, no change), dash-dotted line (60% of estimated value) and dotted line (20% of estimated value).

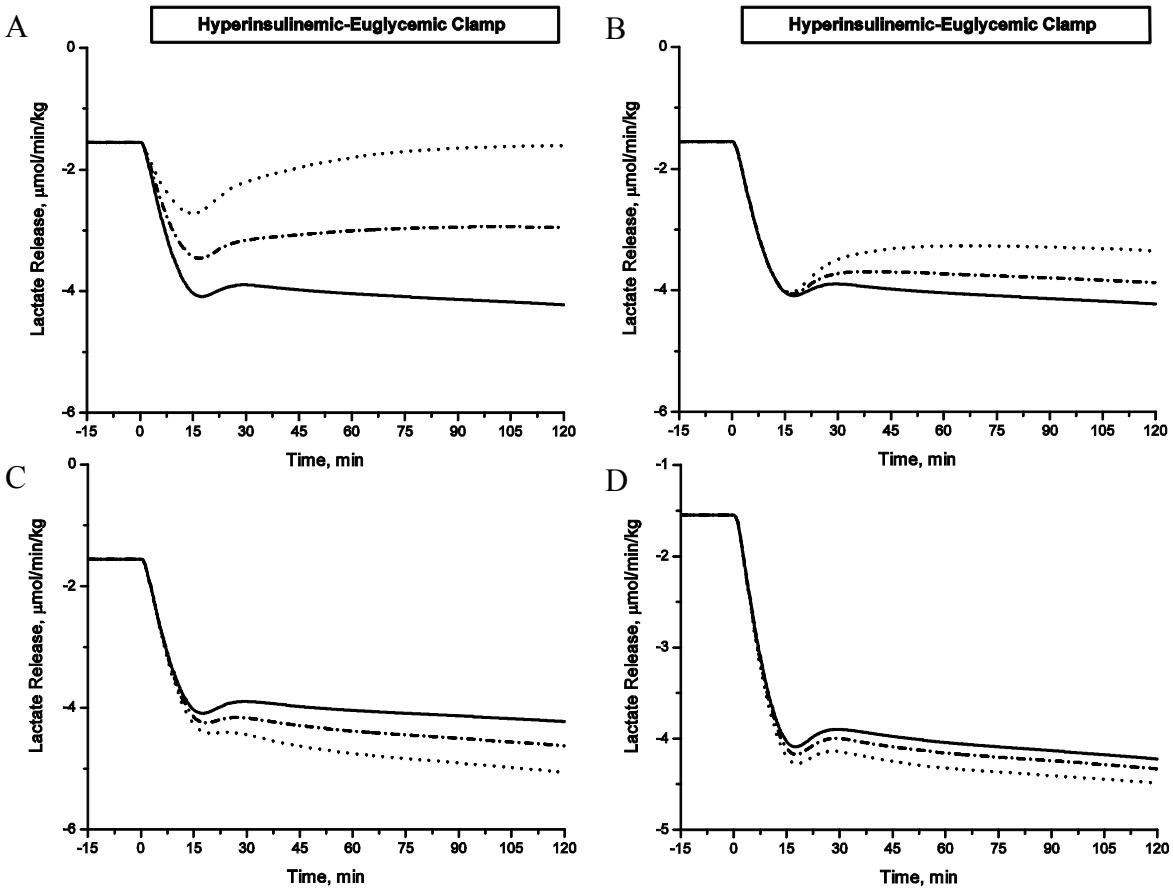

FIGURE 4.10. Effect of defective insulin action on the rate of lactate release

The model predicted the changes in the rate of lactate release during hyperinsulinemic-euglycemic clamp as a result of varying the model parameters related to the stimulative insulin action; (A)$\lambda_{Glycolysis}$, (B)$\lambda_{Tmax,GLC}$, (C) $\lambda_{Glycogen\ Synthesis}$ and (D) λ_{PDH}. The parameters are decreased up to 60% of their estimated values in Table 4.5; Solid line (100% of estimated value, no change), dash-dotted line (80% of estimated value) and dotted line (60% of estimated value).

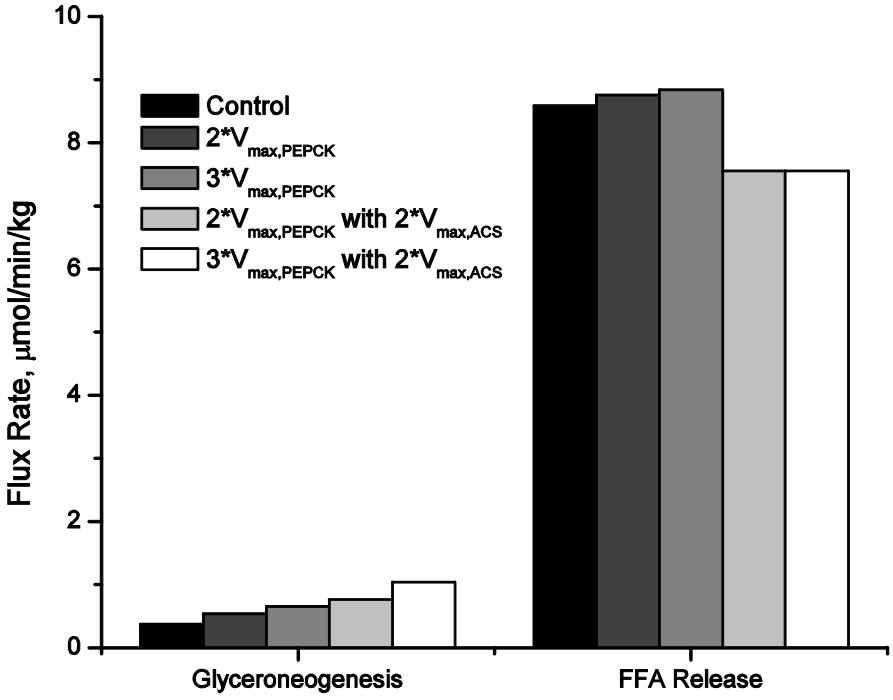

FIGURE 4.11. Effect of altered enzyme activity on the rates of glyceroneogenesis and FFA release

Control (■) is the model simulations with the maximum rate coefficients for PEPCK and ACS in the basal state ($V_{max,PEPCK}$ and $V_{max,ACS}$). For other simulations, $V_{max,PEPCK}$ increased two to three fold with or without two fold increase in $V_{max,ACS}$; Dark gray (■): $2*V_{max,PEPCK}$ and $V_{max,ACS}$; Gray (■): $3*V_{max,PEPCK}$ and $V_{max,ACS}$; Light gray (■):$2*V_{max,PEPCK}$ and $2*V_{max,ACS}$; Open bar (□):$3*V_{max,PEPCK}$ and $2*V_{max,ACS}$.

CHAPTER 5.

SUMMARY AND FUTURE DIRECTIONS

5.1. SUMMARY

The overall goal of this study was to quantitatively analyze *in vivo* regulatory mechanisms of fuel metabolism in adipose tissue and the whole body. Mechanistic computational models are developed to address hypotheses with respect to the hormonal regulation of metabolic pathways, intracellular compartmentation and altered enzyme expression. Model simulations of metabolic responses to various physiological perturbations are compared with experimental data in humans for validation. Simulations also predict responses that have not been measured and can be the basis for designing critical experiments.

5.1.1. Whole body fuel homeostasis during exercise

A multi-scale computational model of whole-body metabolism was developed to predict fuel homeostasis during exercise. The model includes the necessary tissue/organ subsystems and hormonal signals that regulate the metabolic reactions. Model simulations show that a change in the glucagon-to-insulin ratio can modulate the metabolic flux rates of different tissues in a coordinated way not only to provide oxidative substrates, but also to prevent hypoglycemia. This supports the hypothesis that exercise-induced change in epinephrine affects the pancreatic secretion of glucagon and insulin. Furthermore, simulations show the importance of hepatic glycogenolysis as a major pathway for glucose production in liver. The model provides dynamic information on the relative contribution of carbohydrates and lipids for oxidative metabolism in the

skeletal muscle during exercise. Simulations indicate that external fuel supplies from other tissue/organ systems to skeletal muscle become important during prolonged exercise.

5.1.2. Adipose tissue metabolism

(a) In response to epinephrine

A computational model of adipose tissue metabolism is developed to investigate the regulation of TG breakdown and synthesis. Model simulations of physiological responses in human during intravenous epinephrine infusion provided the impetus to quantify an active intracellular metabolic subdomain (~3% of total tissue volume) in the adipose tissue, where most of cellular metabolites and enzymes are localized. Simulations support the hypothesis that lipolytic reactions catalyzed by HSL and ATGL are differentially stimulated in response to epinephrine infusion. Indeed, the model simulations are in good agreement with data only when DG breakdown by HSL is preferentially activated. Furthermore, differential stimulation of lipolytic reactions produces distinctive changes in the intracellular levels of lipolytic intermediates (i.e., DG and MG). Increased levels of FAC associated with stimulated lipolysis increase the ratio of acetyl CoA to free CoA, which inhibits pyruvate oxidation and provides more pyruvate for glyceroneogenesis. These model simulations show that glyceroneogenesis is the dominant pathways for G3P synthesis when the TG-FFA cycle rate increases in response to epinephrine.

(b) In response to insulin

To analyze metabolic responses during a hyperinsulinemic-euglycemic clamp

experiment, an enhanced model of adipose tissue metabolism is needed that incorporates additional pathways and metabolic intermediates, and distinguishes heterogeneous pools of triose phosphate. Model simulations show that different affinities of LPL toward various lipoproteins are needed to quantitatively characterize lipolysis regulation in the adipose tissue. Differential suppression of lipolytic reactions by insulin does not affect venous concentration dynamics, but produces distinctive dynamic changes in DG levels of adipose tissue. Model simulations support the hypothesis that glyceroneogenesis is the dominant pathway to synthesize G3P even when insulin increases the glucose uptake rate by adipose tissue. Also, simulations indicate that elevated levels of NADH/NAD+ and ATP/ADP are primary driving forces for increasing flux through glyceroneogenesis.

(c) Altered enzyme activity

Model simulations of metabolic responses from altering the activities of HSL and ATGL correspond well with data from studies of transgenic knockout mice. These simulations show that knockout of ATGL severely impairs breakdown of TG stores, which underscores that importance of ATGL for the basal state lipolysis. In HSL-deficient mice, FFA release rate does not change because of compensatory increases in ATGL activity. The importance of PEPCK activity in the regulation of glyceroneogenesis and re-esterification is examined by simulations corresponding to data from mice with overexpressed PEPCK in adipose tissue. These simulations indicate that the upregulation of PEPCK *per se* is not sufficient to increase the re-esterification rate, but requires upregulation of ACS activity.

5.2. FUTURE DIRECTIONS

The heterogeneity of different adipose tissue depots (i.e., subcutaneous vs. visceral) have been studied extensively, but not the heterogeneity within a single adipose depot. Heterogeneous pools of triose phosphates incorporated into the current model of adipose tissue metabolism are needed to reconcile the seemingly contradictory results from the experimental studies in humans and rats. Since the adipose tissue takes up glucose and releases lactate, glucose would appear to be the major precursor for G3P synthesis, but other studies show that glyceroneogenesis is the dominant pathway G3P synthesis. A mechanism to accommodate these data could be re-utilization of pyruvate or lactate for G3P synthesis via separate pools of triose phosphates. Assuming two separate pools of triose phosphates, the current model describes intracellular re-utilization of pyruvate for G3P synthesis with only one cellular compartment.

In addition to re-utilizing pyruvate, lactate may be re-utilized. In fact, intercellular transport of lactate within the same tissue has been proposed based on studies of the lactate shuttle in skeletal muscle and brain, where the glycolytic tissue releases lactate and the oxidative tissue with mitochondria takes up lactate (Brooks, 2007;Pellerin et al., 1998). Following these studies, lactate could be produced in one cell, and then re-utilized in another separated by interstitial fluid. This mechanism with a net movement of lactate via interstitium in the adipose tissue is shown in a metabolic pathway diagram (Figure 5.1). The glycolytic cells (compartment) produce lactate, which is utilized by the glyceroneogenic cells.The transport of lactate has a favorable feature for the synthesis of G3P since the conversion of lactate to pyruvate in the glyceroneogenic cells can generate NADH, a co-substrate for glyceroneogenesis. As a consequence, the intercellular transport of lactate can transfer the redox potential as well as the carbon source. For the

development of this two-cell model, experimental data are needed that characterize the metabolism of different cell types.

The utilization of lactate in the adipose tissue was first postulated by Simonsen et al. (1994) after comparing the levels of several metabolites in the venous plasma and the interstitium. They showed that lactate had a substantially higher concentration difference between the venous plasma and the interstitial fluid than other metabolic substrates. It was postulated that different types of cells in the adipose tissue take up lactate before it reaches the blood circulation. Indeed, many studies showed the different metabolic characteristics of cells in adipose tissue. *In vitro* studies showed that the larger adipocytes have the higher relative conversion of glucose to lactate (DiGirolamo et al., 1992). This is consistent with the data in humans that show the obese patients have larger average adipocyte size and higher interstitial levels of lactate than the lean control subjects (Jansson et al., 1994). Other cells in adipose tissue include preadipocytes, macrophages, stromal-vascular cells, etc. In fact, obesity is associated with the increased macrophages levels in the adipose tissue (Kanda et al., 2006). In addition, the anti-diabetic drugs, TZDs affect the amount of preadipocytes in the adipose tissue as well as the size of adipocytes (Okuno et al., 1998). These different types of cells with distinctive metabolic characteristics can contribute to the heterogeneity in the adipose tissue. Metabolic characterization of these different cell types in adipose tissue is important for quantitative analysis of proposed mechanism of lactate re-utilization. Further studies on the heterogeneity in adipose tissue is essential for understanding the regulation of glyceroneogenesis and TG synthesis, which can lead to identifying targets for therapeutic interventions of metabolic disorders.

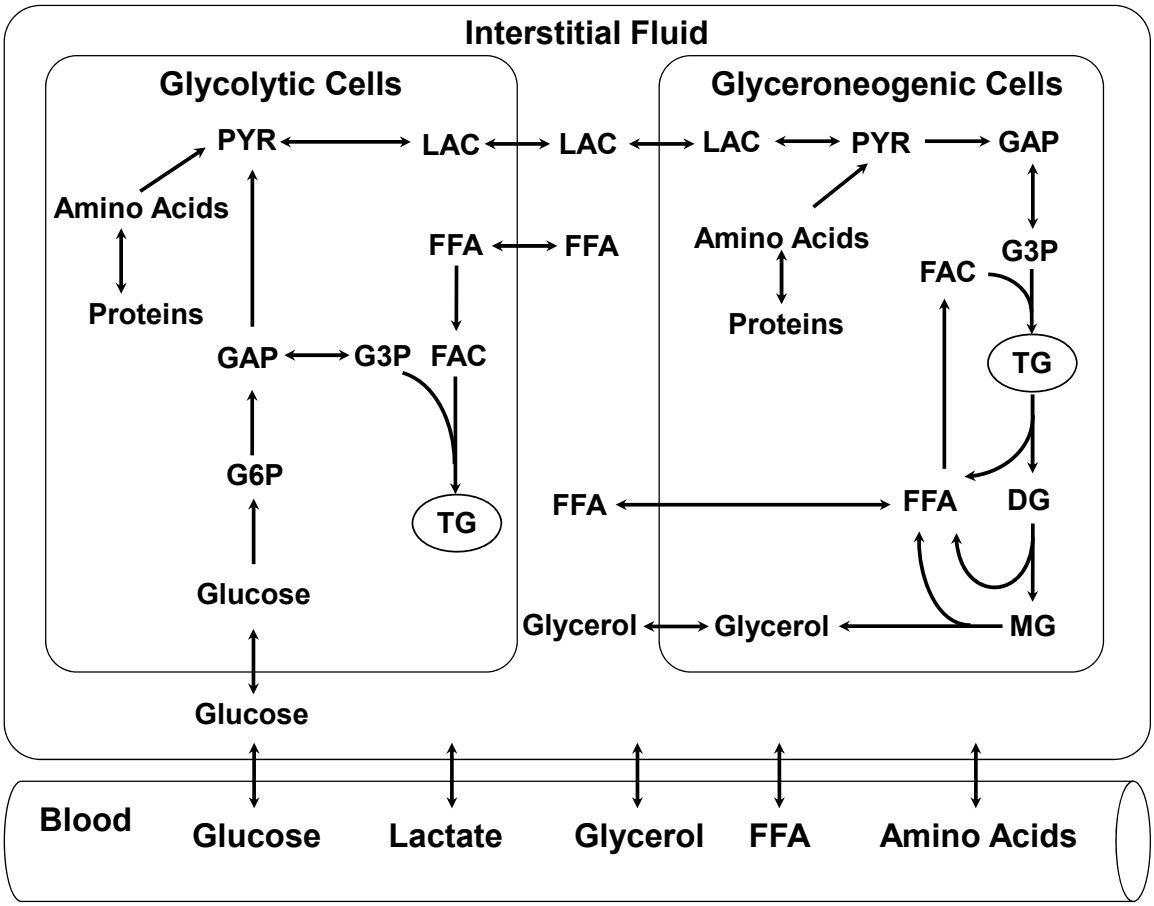

FIGURE 5.1. Metabolic pathway diagram for two cell type hypothesis

Two cell type hypothesis assumes that the adipose tissue is composed of two heterogeneous cells (or compartments), which are in equilibrium with interstitial fluid. Diffusible metabolites are transported between blood and interstitial fluid, and taken up or released by the cellular compartments. The glycolytic cells take up glucose, some of which can be used to synthesize glycerol-3-phosphate (G3P). Most of them are released as lactate into the interstitial fluid. On the other hand, the glyceroneogenic cells take up lactate and use it for the synthesis of G3P. Amino acids can also contribute as an additional source of pyruvate/lactate.

APPENDIX I. KINETIC EQUATIONS FOR THE METABOLIC REACTIONS USED IN THE WHOLE BODY MODEL

1. Glycolysis I $\mathrm{GLC} + \mathrm{ATP} \rightarrow \mathrm{G6P} + \mathrm{ADP}$

$$\phi_{x,\mathrm{GLC}\rightarrow\mathrm{G6P}} = V_{x,\mathrm{GLC}\rightarrow\mathrm{G6P}} \left(\frac{PS_x^+}{\mu_x^+ + PS_x^+} \right) \left(\frac{\frac{C_{x,\mathrm{GLC}}}{K_{x,\mathrm{GLC}}}}{1+\frac{C_{x,\mathrm{GLC}}}{K_{x,\mathrm{GLC}}}} \right)$$

2. Glycolysis II $\mathrm{G6P} + \mathrm{ATP} \rightarrow 2\ \mathrm{GA3P} + \mathrm{ADP}$

$$\phi_{x,\mathrm{G6P}\rightarrow\mathrm{GAP}} = V_{x,\mathrm{G6P}\rightarrow\mathrm{GA3P}} \left(\frac{\left(PS_x^-\right)^2}{(\mu_x^-)^2 + \left(PS_x^-\right)^2} \right) \left(\frac{\frac{C_{x,\mathrm{G6P}}}{K_{x,\mathrm{G6P}}}}{1+\frac{C_{x,\mathrm{G6P}}}{K_{x,\mathrm{G6P}}}} \right)$$

3. Glycolysis III $\mathrm{GAP} + \mathrm{Pi} + \mathrm{NAD}^+ + 2\mathrm{ADP} \rightarrow \mathrm{PYR} + \mathrm{NADH} + 2\mathrm{ATP}$

$$\phi_{x,\mathrm{GAP}\rightarrow\mathrm{PYR}} = V_{x,\mathrm{GAP}\rightarrow\mathrm{PYR}} \left(\frac{RS_x^-}{\nu_x^- + RS_x^-} \right) \left(\frac{PS_x^-}{\mu_x^- + PS_x^-} \right) \left(\frac{\frac{C_{x,\mathrm{GAP}}}{K_{x,\mathrm{GAP}}} \cdot \frac{C_{x,\mathrm{Pi}}}{K_{x,\mathrm{Pi}}}}{1+\frac{C_{x,\mathrm{GAP}}}{K_{x,\mathrm{GAP}}}+\frac{C_{x,\mathrm{Pi}}}{K_{x,\mathrm{Pi}}}+\frac{C_{x,\mathrm{GAP}}}{K_{x,\mathrm{GAP}}} \cdot \frac{C_{x,\mathrm{Pi}}}{K_{x,\mathrm{Pi}}}} \right)$$

4. Gluconeogenesis I $\mathrm{PYR} + 3\mathrm{ATP} + \mathrm{NADH} \rightarrow \mathrm{GAP} + 3\mathrm{ADP} + \mathrm{NAD}^+ + 2\mathrm{P_i}$

$$\phi_{x,\mathrm{PYR}\rightarrow\mathrm{GAP}} = V_{x,\mathrm{PYR}\rightarrow\mathrm{GAP}} \left(\frac{RS_x^+}{\nu_x^+ + RS_x^+} \right) \left(\frac{PS_x^+}{\mu_x^+ + PS_x^+} \right) \left(\frac{\frac{C_{x,\mathrm{PYR}}}{K_{x,\mathrm{PYR}}}}{1+\frac{C_{x,\mathrm{PYR}}}{K_{x,\mathrm{PYR}}}} \right)$$

5. Gluconeogenesis II $2\mathrm{GAP} \rightarrow \mathrm{G6P} + \mathrm{P_i}$

$$\phi_{x,\mathrm{GAP}\rightarrow\mathrm{G6P}} = V_{x,\mathrm{GAP}\rightarrow\mathrm{G6P}} \left(\frac{\frac{C_{x,\mathrm{GAP}}}{K_{x,\mathrm{GAP}}}}{1+\frac{C_{x,\mathrm{GAP}}}{K_{x,\mathrm{GAP}}}} \right)$$

6. Gluconeogenesis III $\mathrm{G6P} \rightarrow \mathrm{GLC} + \mathrm{P_i}$

$$\phi_{x,\mathrm{G6P}\rightarrow\mathrm{GLC}} = V_{x,\mathrm{G6P}\rightarrow\mathrm{GLC}} \left(\frac{\frac{C_{x,\mathrm{G6P}}}{K_{x,\mathrm{G6P}}}}{1+\frac{C_{x,\mathrm{G6P}}}{K_{x,\mathrm{G6P}}}} \right)$$

7. Glycogenesis $\mathrm{G6P} + \mathrm{ATP} \rightarrow \mathrm{GLY} + \mathrm{ADP} + 2\ \mathrm{Pi}$

$$\phi_{x,\mathrm{G6P}\rightarrow\mathrm{GLY}} = V_{x,\mathrm{G6P}\rightarrow\mathrm{GLY}} \left(\frac{PS_x^+}{\mu_x^+ + PS_x^+} \right) \left(\frac{\frac{C_{x,\mathrm{G6P}}}{K_{x,\mathrm{G6P}}}}{1+\frac{C_{x,\mathrm{G6P}}}{K_{x,\mathrm{G6P}}}} \right)$$

8. Glycogenolysis $\mathrm{GLY} + \mathrm{Pi} \rightarrow \mathrm{G6P}$

$$\phi_{x,\mathrm{GLY}\rightarrow\mathrm{G6P}} = V_{x,\mathrm{GLY}\rightarrow\mathrm{G6P}} \left(\frac{\left(PS_x^-\right)^2}{(\mu_x^-)^2 + \left(PS_x^-\right)^2} \right) \left(\frac{\frac{C_{x,\mathrm{GLY}}}{K_{x,\mathrm{GLY}}} \cdot \frac{C_{x,\mathrm{Pi}}}{K_{x,\mathrm{Pi}}}}{1+\frac{C_{x,\mathrm{GLY}}}{K_{x,\mathrm{GLY}}}+\frac{C_{x,\mathrm{Pi}}}{K_{x,\mathrm{Pi}}}+\frac{C_{x,\mathrm{GLY}}}{K_{x,\mathrm{GLY}}} \cdot \frac{C_{x,\mathrm{Pi}}}{K_{x,\mathrm{Pi}}}} \right)$$

9. Pyruvate Reduction $\mathrm{PYR} + \mathrm{NADH} \rightarrow \mathrm{LAC} + \mathrm{NAD^+}$

$$\phi_{x,\mathrm{PYR}\rightarrow\mathrm{LAC}} = V_{x,\mathrm{PYR}\rightarrow\mathrm{LAC}} \left(\frac{RS_x^+}{\nu_x^+ + RS_x^+} \right) \left(\frac{\frac{C_{x,\mathrm{PYR}}}{K_{x,\mathrm{PYR}}}}{1+\frac{C_{x,\mathrm{PYR}}}{K_{x,\mathrm{PYR}}}} \right)$$

10. Lactate Oxidation $\mathrm{LAC} + \mathrm{NAD^+} \rightarrow \mathrm{PYR} + \mathrm{NADH}$

$$\phi_{x,\mathrm{LAC}\rightarrow\mathrm{PYR}} = V_{x,\mathrm{LAC}\rightarrow\mathrm{PYR}} \left(\frac{RS_x^-}{\nu_x^- + RS_x^-} \right) \left(\frac{\frac{C_{x,\mathrm{LAC}}}{K_{x,\mathrm{LAC}}}}{1+\frac{C_{x,\mathrm{LAC}}}{K_{x,\mathrm{LAC}}}} \right)$$

11. Glycerol Phosphorylation $\mathrm{GLR} + \mathrm{ATP} \rightarrow \mathrm{GRP} + \mathrm{ADP}$

$$\phi_{x,\mathrm{GLR}\rightarrow\mathrm{GRP}} = V_{x,\mathrm{GLR}\rightarrow\mathrm{GRP}} \left(\frac{PS_x^+}{\mu_x^+ + PS_x^+} \right) \left(\frac{\frac{C_{x,\mathrm{GLR}}}{K_{x,\mathrm{GLR}}}}{1+\frac{C_{x,\mathrm{GLR}}}{K_{x,\mathrm{GLR}}}} \right)$$

12. GAP Reduction $\mathrm{GAP + NADH \rightarrow GRP + NAD^+}$

$$\phi_{x,\mathrm{GAP}\rightarrow\mathrm{GRP}} = V_{x,\mathrm{GAP}\rightarrow\mathrm{GRP}} \left(\frac{RS_x^+}{\nu_x^+ + RS_x^+} \right) \left(\frac{\frac{C_{x,\mathrm{GAP}}}{K_{x,\mathrm{GAP}}}}{1 + \frac{C_{x,\mathrm{GAP}}}{K_{x,\mathrm{GAP}}}} \right)$$

13. Glycerol 3-P Oxidation $\mathrm{GRP + NAD^+ \rightarrow GAP + NADH}$

$$\phi_{x,\mathrm{GRP}\rightarrow\mathrm{GAP}} = V_{x,\mathrm{GRP}\rightarrow\mathrm{GAP}} \left(\frac{RS_x^-}{\nu_x^- + RS_x^-} \right) \left(\frac{\frac{C_{x,\mathrm{GRP}}}{K_{x,\mathrm{GRP}}}}{1 + \frac{C_{x,\mathrm{GRP}}}{K_{x,\mathrm{GRP}}}} \right)$$

14. Alanine Formation $\mathrm{PYR \rightarrow ALA}$

$$\phi_{x,\mathrm{PYR}\rightarrow\mathrm{ALA}} = V_{x,\mathrm{PYR}\rightarrow\mathrm{ALA}} \left(\frac{\frac{C_{x,\mathrm{PYR}}}{K_{x,\mathrm{PYR}}}}{1 + \frac{C_{x,\mathrm{PYR}}}{K_{x,\mathrm{PYR}}}} \right)$$

15. Alanine Utilization $\mathrm{ALA \rightarrow PYR}$

$$\phi_{x,\mathrm{ALA}\rightarrow\mathrm{PYR}} = V_{x,\mathrm{ALA}\rightarrow\mathrm{PYR}} \left(\frac{\frac{C_{x,\mathrm{ALA}}}{K_{x,\mathrm{ALA}}}}{1 + \frac{C_{x,\mathrm{ALA}}}{K_{x,\mathrm{ALA}}}} \right)$$

16. Pyruvate Oxidation $\mathrm{PYR + CoA + NAD^+ \rightarrow ACoA + NADH + CO_2}$

$$\phi_{x,\mathrm{PYR}\rightarrow\mathrm{ACoA}} = V_{x,\mathrm{PYR}\rightarrow\mathrm{ACoA}} \left(\frac{RS_x^-}{\nu_x^- + RS_x^-} \right) \left(\frac{\frac{C_{x,\mathrm{PYR}}}{K_{\mathrm{vPYR}}} \cdot \frac{C_{x,\mathrm{CoA}}}{K_{x,\mathrm{CoA}}}}{1 + \frac{C_{x,\mathrm{PYR}}}{K_{x,\mathrm{PYR}}} + \frac{C_{x,\mathrm{CoA}}}{K_{x,\mathrm{CoA}}} + \frac{C_{x,\mathrm{PYR}}}{K_{x,\mathrm{PYR}}} \cdot \frac{C_{x,\mathrm{CoA}}}{K_{x,\mathrm{CoA}}}} \right)$$

17.Fatty Acid Oxidation $\mathrm{FA + 8CoA + 2ATP + 14NAD^+ \rightarrow 8ACoA + 2\ ADP + 2\ Pi + 14NADH}$

$$\phi_{x,\mathrm{FFA}\rightarrow\mathrm{ACoA}} = V_{x,\mathrm{FFA}\rightarrow\mathrm{ACoA}} \left(\frac{RS_x^-}{\nu_x^- + RS_x^-} \right) \left(\frac{\frac{C_{x,\mathrm{FFA}}}{K_{x,\mathrm{FFA}}} \cdot \frac{C_{x,\mathrm{CoA}}}{K_{x,\mathrm{CoA}}}}{1 + \frac{C_{x,\mathrm{FFA}}}{K_{x,\mathrm{FFA}}} + \frac{C_{x,\mathrm{CoA}}}{K_{x,\mathrm{CoA}}} + \frac{C_{x,\mathrm{FFA}}}{K_{x,\mathrm{FFA}}} \cdot \frac{C_{x,\mathrm{CoA}}}{K_{x,\mathrm{CoA}}}} \right)$$

18.Fatty Acid Synthesis

$$8A\text{CoA} + 7\text{ATP} + 14\text{NADH} \rightarrow \text{FA} + 8\text{CoA} + 7\text{ADP} + 7\text{Pi} + 14\text{NAD}^+$$

$$\phi_{x,\text{ACoA}\rightarrow\text{FA}} = V_{x,\text{ACoA}\rightarrow\text{FA}} \left(\frac{RS_x^+}{\nu_x^+ + RS_x^+} \right) \left(\frac{PS_x^+}{\mu_x^+ + PS_x^+} \right) \left(\frac{\frac{C_{x,\text{ACoA}}}{K_{x,\text{ACoA}}}}{1 + \frac{C_{x,\text{ACoA}}}{K_{x,\text{ACoA}}}} \right)$$

19. Lipolysis

$$\text{TG} \rightarrow \text{GLR} + 3\text{FA}$$

$$\phi_{x,\text{TG}\rightarrow\text{FFA-GLR}} = V_{x,\text{TG}\rightarrow\text{FFA-GLR}} \left(\frac{\frac{C_{x,\text{TG}}}{K_{x,\text{TG}}}}{1 + \frac{C_{x,\text{TG}}}{K_{x,\text{TG}}}} \right)$$

20. Triglyceride Synthesis

$$\text{GRP} + 3\text{ FA} + 6\text{ATP} \rightarrow \text{TG} + 6\text{ADP} + 7\text{Pi}$$

$$\phi_{x,\text{FFA-GRP}\rightarrow\text{TG}} = V_{x,\text{FFA-GRP}\rightarrow\text{TG}} \left(\frac{PS_x^+}{\mu_x^+ + PS_x^+} \right) \left(\frac{\frac{C_{x,\text{FFA}}}{K_{x,\text{FFA}}} \cdot \frac{C_{x,\text{GRP}}}{K_{x,\text{GRP}}}}{1 + \frac{C_{x,\text{FFA}}}{K_{x,\text{FFA}}} + \frac{C_{x,\text{GRP}}}{K_{x,\text{GRP}}} + \frac{C_{x,\text{FFA}}}{K_{x,\text{FFA}}} \cdot \frac{C_{x,\text{GRP}}}{K_{x,\text{GRP}}}} \right)$$

21.TCA Cycle

$$A\text{CoA} + \text{ADP} + \text{Pi} + 4\text{NAD}^+ \rightarrow 2\text{CO}_2 + \text{CoA} + \text{ATP} + 4\text{NADH}$$

$$\phi_{x,\text{ACoA}\rightarrow\text{CO}_2} = V_{x,\text{ACoA}\rightarrow\text{CO}_2} \left(\frac{RS_x^-}{\nu_x^- + RS_x^-} \right) \left(\frac{PS_x^-}{\mu_x^- + PS_x^-} \right) \left(\frac{\frac{C_{x,\text{ACoA}}}{K_{x,\text{ACoA}}} \cdot \frac{C_{x,\text{Pi}}}{K_{x,\text{Pi}}}}{1 + \frac{C_{x,\text{ACoA}}}{K_{x,\text{ACoA}}} + \frac{C_{x,\text{Pi}}}{K_{x,\text{Pi}}} + \frac{C_{x,\text{ACoA}}}{K_{x,\text{ACoA}}} \cdot \frac{C_{x,\text{Pi}}}{K_{x,\text{Pi}}}} \right)$$

22. Oxidative Phosphorylation

$$\text{O}_2 + 6\text{ADP} + 6\text{Pi} + 2\text{NADH} \rightarrow 2\text{H}_2\text{O} + 6\text{ATP} + 2\text{NAD}^+$$

$$\phi_{x,\text{O2}\rightarrow\text{H2O}} = V_{x,\text{O2}\rightarrow\text{H2O}} \left(\frac{PS_x^-}{\mu_x^- + PS_x^-} \right) \left(\frac{RS_x^+}{\nu_x^+ + RS_x^+} \right) \left(\frac{\frac{C_{x,\text{O2}}}{K_{x,\text{O2}}} \cdot \frac{C_{x,\text{Pi}}}{K_{x,\text{Pi}}}}{1 + \frac{C_{x,\text{O2}}}{K_{x,\text{O2}}} + \frac{C_{x,\text{Pi}}}{K_{x,\text{Pi}}} + \frac{C_{x,\text{O2}}}{K_{x,\text{O2}}} \cdot \frac{C_{x,\text{Pi}}}{K_{x,\text{Pi}}}} \right)$$

23. Phosphocreatine Breakdown

$$\text{PCR} + \text{ADP} \rightarrow \text{CR} + \text{ATP}$$

$$\phi_{x,\text{PCR}\rightarrow\text{CR}} = V_{x,\text{PCR}\rightarrow\text{CR}} \left(\frac{PS_x^-}{\mu_x^- + PS_x^-} \right) \left(\frac{\frac{C_{x,\text{PCR}}}{K_{x,\text{PCR}}}}{1 + \frac{C_{x,\text{PCR}}}{K_{x,\text{PCR}}}} \right)$$

24. Phosphocreatine Synthesis	$\mathrm{CR} + \mathrm{ATP} \rightarrow \mathrm{PCR} + \mathrm{ADP}$

$$\phi_{x,\mathrm{CR}\rightarrow PCR} = V_{x,\mathrm{CR}\rightarrow\mathrm{PCR}} \left(\frac{PS_x^+}{\mu_x^+ + PS_x^+} \right) \left(\frac{\frac{C_{x,\mathrm{CR}}}{K_{x,\mathrm{CR}}}}{1+\frac{C_{x,\mathrm{CR}}}{K_{x,\mathrm{CR}}}} \right)$$

25. ATP Hydrolysis	$\mathrm{ATP} \rightarrow \mathrm{ADP} + \mathrm{Pi}$

$$\phi_{x,\mathrm{ATP}\rightarrow\mathrm{ADP}} = V_{x,\mathrm{ATP}\rightarrow\mathrm{ADP}} \left(\frac{C_{x,\mathrm{ATP}}}{K_{\mathrm{ATP}} + C_{x,\mathrm{ATP}}} \right)$$

APPENDIX II. DYNAMIC MASS BALANCE EQUATIONS USED IN THE WHOLE BODY MODEL

1. GLC: $$V_{eff,x,\mathrm{GLC}}\frac{dC_{x,\mathrm{GLC}}}{dt}=\phi_{x,\mathrm{G6P}\rightarrow\mathrm{GLC}}-\phi_{x,\mathrm{GLC}\rightarrow\mathrm{G6P}}+Q_x(C_{a,\mathrm{GLC}}-\sigma_{x,\mathrm{GLC}}C_{x,\mathrm{GLC}})$$

2. PYR: $$V_{eff,x,\mathrm{PYR}}\frac{dC_{x,\mathrm{PYR}}}{dt}=\phi_{x,\mathrm{GAP}\rightarrow\mathrm{PYR}}+\phi_{x,\mathrm{LAC}\rightarrow\mathrm{PYR}}+\phi_{x,\mathrm{ALA}\rightarrow\mathrm{PYR}}-\phi_{x,\mathrm{PYR}\rightarrow\mathrm{GAP}}-\phi_{x,\mathrm{PYR}\rightarrow\mathrm{LAC}}-\phi_{x,\mathrm{PYR}\rightarrow\mathrm{ALA}}+Q_x(C_{a,\mathrm{PYR}}-\sigma_{x,\mathrm{PYR}}C_{x,\mathrm{PYR}})$$

3. LAC: $$V_{eff,x,\mathrm{LAC}}\frac{dC_{x,\mathrm{LAC}}}{dt}=\phi_{x,\mathrm{PYR}\rightarrow\mathrm{ALA}}-\phi_{x,\mathrm{LAC}\rightarrow\mathrm{PYR}}+Q_x(C_{a,\mathrm{LAC}}-\sigma_{x,\mathrm{LAC}}C_{x,\mathrm{LAC}})$$

4. ALA: $$V_{eff,x,\mathrm{ALA}}\frac{dC_{x,\mathrm{ALA}}}{dt}=\phi_{x,\mathrm{PYR}\rightarrow\mathrm{ALA}}-\phi_{x,\mathrm{ALA}\rightarrow\mathrm{PYR}}+Q_x(C_{a,\mathrm{ALA}}-\sigma_{x,\mathrm{ALA}}C_{x,\mathrm{ALA}})$$

5. GLR: $$V_{eff,x,\mathrm{GLR}}\frac{dC_{x,\mathrm{GLR}}}{dt}=\phi_{x,\mathrm{TG}\rightarrow\mathrm{FFA\text{-}GLR}}-\phi_{x,\mathrm{GLR}\rightarrow\mathrm{GRP}}+Q_x(C_{a,\mathrm{GLR}}-\sigma_{x,\mathrm{GLR}}C_{x,\mathrm{GLR}})$$

6. FFA: $$V_{eff,x,\mathrm{FFA}}\frac{dC_{x,\mathrm{FFA}}}{dt}=3\phi_{x,\mathrm{TG}\rightarrow\mathrm{FFA\text{-}GLR}}+\frac{\phi_{x,\mathrm{ACoA}\rightarrow\mathrm{FFA}}}{8}-\phi_{x,\mathrm{FFA\text{-}GRP}\rightarrow\mathrm{TG}}-\phi_{x,\mathrm{FFA}\rightarrow\mathrm{ACoA}}+Q_x(C_{a,\mathrm{FFA}}-\sigma_{x,\mathrm{FFA}}C_{x,\mathrm{FFA}})$$

7. TG: $$V_{eff,x,\mathrm{TG}}\frac{dC_{x,\mathrm{TG}}}{dt}=\frac{\phi_{x,\mathrm{FFA\text{-}GRP}\rightarrow\mathrm{TG}}}{3}-\phi_{x,\mathrm{TG}\rightarrow\mathrm{FFA\text{-}GLR}}+Q_x(C_{a,\mathrm{TG}}-\sigma_{x,\mathrm{TG}}C_{x,\mathrm{TG}})$$

8. O2: $$V_{eff,x,\mathrm{O2}}\frac{dC_{x,\mathrm{O2}}}{dt}=-\phi_{x,\mathrm{O2}\rightarrow\mathrm{H2O}}+Q_x(C_{a,\mathrm{O2}}-\sigma_{x,\mathrm{O2}}C_{x,\mathrm{O2}})$$

9. CO2: $$V_{eff,x,\mathrm{CO2}}\frac{dC_{x,\mathrm{CO2}}}{dt}=\phi_{x,\mathrm{PYR}\rightarrow\mathrm{ACoA}}+\phi_{x,\mathrm{ACoA}\rightarrow\mathrm{CO2}}+Q_x(C_{a,\mathrm{CO2}}-\sigma_{x,\mathrm{CO2}}C_{x,\mathrm{CO2}})$$

10. G6P: $$V_{eff,x,\mathrm{G6P}}\frac{dC_{x,\mathrm{G6P}}}{dt}=\phi_{x,\mathrm{GLC}\rightarrow\mathrm{G6P}}+\phi_{x,\mathrm{GLY}\rightarrow\mathrm{G6P}}+\frac{\phi_{x,\mathrm{GAP}\rightarrow\mathrm{G6P}}}{2}-\phi_{x,\mathrm{G6P}\rightarrow\mathrm{GLC}}-\phi_{x,\mathrm{G6P}\rightarrow\mathrm{GLY}}-\phi_{x,\mathrm{G6P}\rightarrow\mathrm{GAP}}$$

11. GLY: $$V_{eff,x,\mathrm{GLY}}\frac{dC_{x,\mathrm{GLY}}}{dt}=\phi_{x,\mathrm{G6P}\rightarrow\mathrm{GLY}}-\phi_{x,\mathrm{GLY}\rightarrow\mathrm{G6P}}$$

12. GAP: $$V_{eff,x,\mathrm{GAP}}\frac{dC_{x,\mathrm{GAP}}}{dt}=2\phi_{x,\mathrm{G6P}\to\mathrm{GAP}}+\phi_{x,\mathrm{PYR}\to\mathrm{GAP}}+\phi_{x,\mathrm{GRP}\to\mathrm{GAP}}-\phi_{x,\mathrm{GAP}\to\mathrm{G6P}}-\phi_{x,\mathrm{GAP}\to\mathrm{PYR}}-\phi_{x,\mathrm{GAP}\to\mathrm{GRP}}$$

13. GRP: $$V_{eff,x,\mathrm{GRP}}\frac{dC_{x,\mathrm{GRP}}}{dt}=2\phi_{x,\mathrm{GAP}\to\mathrm{GRP}}+\phi_{x,\mathrm{GRL}\to\mathrm{GRP}}-\phi_{x,\mathrm{GRP}\to\mathrm{GAP}}-\frac{\phi_{x,\mathrm{FFA\text{-}GRP}\to\mathrm{TG}}}{3}$$

14. ACoA: $$V_{eff,x,\mathrm{ACoA}}\frac{dC_{x,\mathrm{ACoA}}}{dt}=\phi_{x,\mathrm{PYR}\to\mathrm{ACoA}}+8\phi_{x,\mathrm{FFA}\to\mathrm{ACoA}}-\phi_{x,\mathrm{ACoA}\to\mathrm{CO2}}-\phi_{x,\mathrm{ACoA}\to\mathrm{FFA}}$$

15. CoA: $$V_{eff,x,\mathrm{CoA}}\frac{dC_{x,\mathrm{CoA}}}{dt}=\phi_{x,\mathrm{ACoA}\to\mathrm{CO2}}+\phi_{x,\mathrm{ACoA}\to\mathrm{FFA}}-\phi_{x,\mathrm{PYR}\to\mathrm{ACoA}}-8\phi_{x,\mathrm{FFA}\to\mathrm{ACoA}}$$

16. NAD+:

$$V_{eff,x,\mathrm{NAD+}}\frac{dC_{x,\mathrm{NAD+}}}{dt}=\phi_{x,\mathrm{PYR}\to\mathrm{GAP}}+\phi_{x,\mathrm{PYR}\to\mathrm{LAC}}+\phi_{x,\mathrm{GAP}\to\mathrm{GRP}}+2\phi_{x,\mathrm{O2}\to\mathrm{H2O}}+\frac{14\phi_{x,\mathrm{ACoA}\to\mathrm{FFA}}}{8}$$
$$-\phi_{x,\mathrm{GAP}\to\mathrm{PYR}}-\phi_{x,\mathrm{LAC}\to\mathrm{PYR}}-\phi_{x,\mathrm{GRP}\to\mathrm{GAP}}-\phi_{x,\mathrm{PYR}\to\mathrm{ACoA}}-4\phi_{x,\mathrm{ACoA}\to\mathrm{CO2}}-14\phi_{x,\mathrm{FFA}\to\mathrm{ACoA}}$$

17. NADH:

$$V_{eff,x,\mathrm{NAD+}}\frac{dC_{x,\mathrm{NAD+}}}{dt}=\phi_{x,\mathrm{GAP}\to\mathrm{PYR}}+\phi_{x,\mathrm{LAC}\to\mathrm{PYR}}+\phi_{x,\mathrm{GRP}\to\mathrm{GAP}}+\phi_{x,\mathrm{PYR}\to\mathrm{ACoA}}+4\phi_{x,\mathrm{ACoA}\to\mathrm{CO2}}$$
$$+14\phi_{x,\mathrm{FFA}\to\mathrm{ACoA}}-\phi_{x,\mathrm{PYR}\to\mathrm{GAP}}-\phi_{x,\mathrm{PYR}\to\mathrm{LAC}}-\phi_{x,\mathrm{GAP}\to\mathrm{GRP}}-2\phi_{x,\mathrm{O2}\to\mathrm{H2O}}-\frac{14\phi_{x,\mathrm{ACoA}\to\mathrm{FFA}}}{8}$$

18. ATP:

$$V_{eff,x,\mathrm{ATP}}\frac{dC_{x,\mathrm{ATP}}}{dt}=2\phi_{x,\mathrm{GAP}\to\mathrm{PYR}}+\phi_{x,\mathrm{ACoA}\to\mathrm{CO2}}+6\phi_{x,\mathrm{O2}\to\mathrm{H2O}}+\phi_{x,\mathrm{PCR}\to\mathrm{CR}}-\phi_{x,\mathrm{GLC}\to\mathrm{G6P}}$$
$$-\phi_{x,\mathrm{G6P}\to\mathrm{GAP}}-3\phi_{x,\mathrm{PYR}\to\mathrm{GAP}}-\phi_{x,\mathrm{G6P}\to\mathrm{GLY}}-\phi_{x,\mathrm{GLR}\to\mathrm{GRP}}-2\phi_{x,\mathrm{FFA}\to\mathrm{ACoA}}-\frac{7\phi_{x,\mathrm{ACoA}\to\mathrm{FFA}}}{8}$$
$$-2\phi_{x,\mathrm{FFA\text{-}GRP}\to\mathrm{TG}}-\phi_{x,\mathrm{CR}\to\mathrm{PCR}}-\phi_{x,\mathrm{ATP}\to\mathrm{ADP}}$$

19. ADP:

$$V_{eff,x,\mathrm{ADP}}\frac{dC_{x,\mathrm{ADP}}}{dt}=\phi_{x,\mathrm{GLC}\to\mathrm{G6P}}+\phi_{x,\mathrm{G6P}\to\mathrm{GAP}}+3\phi_{x,\mathrm{PYR}\to\mathrm{GAP}}+\phi_{x,\mathrm{G6P}\to\mathrm{GLY}}+\phi_{x,\mathrm{GLR}\to\mathrm{GRP}}$$
$$+2\phi_{x,\mathrm{FFA}\to\mathrm{ACoA}}+\frac{7\phi_{x,\mathrm{ACoA}\to\mathrm{FFA}}}{8}+2\phi_{x,\mathrm{FFA\text{-}GRP}\to\mathrm{TG}}+\phi_{x,\mathrm{CR}\to\mathrm{PCR}}+\phi_{x,\mathrm{ATP}\to\mathrm{ADP}}$$
$$-2\phi_{x,\mathrm{GAP}\to\mathrm{PYR}}-\phi_{x,\mathrm{ACoA}\to\mathrm{CO2}}-6\phi_{x,\mathrm{O2}\to\mathrm{H2O}}-\phi_{x,\mathrm{PCR}\to\mathrm{CR}}$$

20. Pi:
$$V_{eff,x,\mathrm{Pi}}\frac{dC_{x,\mathrm{Pi}}}{dt}=2\phi_{x,\mathrm{PYR}\rightarrow\mathrm{GAP}}+\frac{\phi_{x,\mathrm{GAP}\rightarrow\mathrm{G6P}}}{2}+\phi_{x,\mathrm{G6P}\rightarrow\mathrm{GLC}}+2\phi_{x,\mathrm{G6P}\rightarrow\mathrm{GLY}}+2\phi_{x,\mathrm{FFA}\rightarrow\mathrm{ACoA}}$$
$$+\frac{7\phi_{x,\mathrm{ACoA}\rightarrow\mathrm{FFA}}}{8}+\frac{7\phi_{x,\mathrm{FFA\text{-}GRP}\rightarrow\mathrm{TG}}}{3}+\phi_{x,\mathrm{ATP}\rightarrow\mathrm{ADP}}-\phi_{x,\mathrm{GAP}\rightarrow\mathrm{PYR}}-\phi_{x,\mathrm{GLY}\rightarrow\mathrm{G6P}}$$
$$-\phi_{x,\mathrm{ACoA}\rightarrow\mathrm{CO2}}-6\phi_{x,\mathrm{O2}\rightarrow\mathrm{H2O}}$$

21. PCR:
$$V_{eff,x,\mathrm{PCR}}\frac{dC_{x,\mathrm{PCR}}}{dt}=\phi_{x,\mathrm{CR}\rightarrow\mathrm{PCR}}-\phi_{x,\mathrm{PCR}\rightarrow\mathrm{CR}}$$

22. CR:
$$V_{eff,x,\mathrm{CR}}\frac{dC_{x,\mathrm{CR}}}{dt}=\phi_{x,\mathrm{PCR}\rightarrow\mathrm{CR}}-\phi_{x,\mathrm{CR}\rightarrow\mathrm{PCR}}$$

APPENDIX III. KINETIC EQUATIONS FOR THE METABOLIC REACTIONS USED IN THE ADIPOSE TISSUE MODEL

1. Glycolysis I $\mathrm{GLC} + \mathrm{ATP} \rightarrow \mathrm{G6P} + \mathrm{ADP}$

$$\phi_{\mathrm{GLC}\rightarrow\mathrm{G6P}} = V_{\mathrm{GLC}\rightarrow\mathrm{G6P}} \left[\frac{K_{\mathrm{i,GLC}\rightarrow\mathrm{G6P}}}{K_{\mathrm{i,GLC}\rightarrow\mathrm{G6P}} + C_{\mathrm{G6P}}} \right] \left[\frac{\dfrac{C_{\mathrm{GLC}} C_{\mathrm{ATP}}}{K_{\mathrm{m,GLC}\rightarrow\mathrm{G6P}}}}{1 + \dfrac{C_{\mathrm{G6P}}}{K_{\mathrm{i,GLC}\rightarrow\mathrm{G6P}}} + \dfrac{C_{\mathrm{GLC}} C_{\mathrm{ATP}}}{K_{\mathrm{m,GLC}\rightarrow\mathrm{G6P}}}} \right]$$

2. Glycolysis II $\mathrm{G6P} \leftrightarrow \mathrm{F6P}$

$$\phi_{\mathrm{G6P}\leftrightarrow\mathrm{F6P}} = \left[\frac{V_{\mathrm{f,G6P}\leftrightarrow\mathrm{F6P}} \dfrac{C_{\mathrm{G6P}}}{K_{\mathrm{G6P}}} - V_{\mathrm{b,G6P}\leftrightarrow\mathrm{F6P}} \dfrac{C_{\mathrm{F6P}}}{K_{\mathrm{F6P}}}}{1 + \dfrac{C_{\mathrm{G6P}}}{K_{\mathrm{G6P}}} + \dfrac{C_{\mathrm{F6P}}}{K_{\mathrm{F6P}}}} \right]$$

3. Glycolysis III $\mathrm{F6P} + \mathrm{ATP} \rightarrow 2\,\mathrm{GAP_{GC}} + \mathrm{ADP}$

$$\phi_{\mathrm{F6P}\rightarrow\mathrm{GAP_{GC}}} = V_{\mathrm{F6P}\rightarrow\mathrm{GAP_{GC}}} \left[\frac{\left[\dfrac{C_{\mathrm{ADP}}}{\mathrm{C_{ATP}}} \right]^2}{\left[\mu^{-}_{\mathrm{F6P}\rightarrow\mathrm{GAP_{GC}}} \right]^2 + \left[\dfrac{C_{\mathrm{ADP}}}{\mathrm{C_{ATP}}} \right]^2} \right] \left[\frac{\dfrac{C_{\mathrm{F6P}}}{K_{\mathrm{m,F6P}\rightarrow\mathrm{GAP_{GC}}}}}{1 + \dfrac{C_{\mathrm{F6P}}}{K_{\mathrm{m,F6P}\rightarrow\mathrm{GAP_{GC}}}}} \right]$$

4. Glycolysis IV $\mathrm{GAP_{GC}} + \mathrm{Pi} + \mathrm{NAD^+} + 2\mathrm{ADP} \rightarrow \mathrm{PYR} + \mathrm{NADH} + 2\mathrm{ATP}$

$$\phi_{\mathrm{GAP_{GC}}\rightarrow\mathrm{PYR}} = V_{\mathrm{GAP_{GC}}\rightarrow\mathrm{PYR}} \left[\frac{\left[\dfrac{C_{\mathrm{NAD}}}{\mathrm{C_{NADH}}} \right]}{\left[\nu^{-}_{\mathrm{GAP_{GC}}\rightarrow\mathrm{PYR}} \right] + \left[\dfrac{C_{\mathrm{NAD}}}{\mathrm{C_{NADH}}} \right]} \right] \left[\frac{\left[\dfrac{C_{\mathrm{ADP}}}{\mathrm{C_{ATP}}} \right]^2}{\left[\mu^{-}_{\mathrm{GAP_{GC}}\rightarrow\mathrm{PYR}} \right]^2 + \left[\dfrac{C_{\mathrm{ADP}}}{\mathrm{C_{ATP}}} \right]^2} \right] \left[\frac{\dfrac{C_{\mathrm{GAP_{GC}}} C_{\mathrm{Pi}}}{K_{\mathrm{m,GAP_{GC}}\rightarrow\mathrm{PYR}}}}{1 + \dfrac{C_{\mathrm{GAP_{GC}}} C_{\mathrm{Pi}}}{K_{\mathrm{m,GAP_{GC}}\rightarrow\mathrm{PYR}}}} \right]$$

5. Pyruvate Reduction $\mathrm{PYR} + \mathrm{NADH} \leftrightarrow \mathrm{LAC} + \mathrm{NAD^+}$

$$\phi_{\mathrm{PYR}\leftrightarrow\mathrm{LAC}} = \left[\frac{V_{\mathrm{f,PYR}\leftrightarrow\mathrm{LAC}} \dfrac{C_{\mathrm{PYR}} C_{\mathrm{NADH}}}{K_{\mathrm{f,PYR}\leftrightarrow\mathrm{LAC}}} - V_{\mathrm{b,PYR}\leftrightarrow\mathrm{LAC}} \dfrac{C_{\mathrm{LAC}} C_{\mathrm{NAD}}}{K_{\mathrm{b,PYR}\leftrightarrow\mathrm{LAC}}}}{1 + \dfrac{C_{\mathrm{PYR}} C_{\mathrm{NADH}}}{K_{\mathrm{f,PYR}\leftrightarrow\mathrm{LAC}}} + \dfrac{C_{\mathrm{LAC}} C_{\mathrm{NAD}}}{K_{\mathrm{b,PYR}\leftrightarrow\mathrm{LAC}}}} \right]$$

6. Glycogen Synthesis $\mathrm{G6P} + \mathrm{ATP} \rightarrow \mathrm{GLY} + \mathrm{ADP} + 2\mathrm{P_i}$

$$\phi_{\mathrm{G6P}\rightarrow\mathrm{GLY}} = V_{\mathrm{G6P}\rightarrow\mathrm{GLY}} \left[\frac{\left[\dfrac{C_{\mathrm{ATP}}}{\mathrm{C_{ADP}}} \right]}{\left[\mu^{+}_{\mathrm{G6P}\rightarrow\mathrm{GLY}} \right] + \left[\dfrac{C_{\mathrm{ATP}}}{\mathrm{C_{ADP}}} \right]} \right] \left[\frac{\dfrac{C_{\mathrm{G6P}}}{K_{\mathrm{m,G6P}\rightarrow\mathrm{GLY}}}}{1 + \dfrac{C_{\mathrm{G6P}}}{K_{\mathrm{m,G6P}\rightarrow\mathrm{GLY}}}} \right]$$

7. Glycogen Phosphorylation $\mathrm{GLY + P_i \rightarrow G6P}$

$$\phi_{\mathrm{GLY\rightarrow G6P}} = V_{\mathrm{GLY\rightarrow G6P}} \left[\frac{\left[\frac{C_{\mathrm{ADP}}}{C_{\mathrm{ATP}}} \right]^2}{\left[\mu^{-}_{\mathrm{GLY\rightarrow G6P}} \right]^2 + \left[\frac{C_{\mathrm{ADP}}}{C_{\mathrm{ATP}}} \right]^2} \right] \left[\frac{\frac{C_{\mathrm{GLY}} C_{\mathrm{Pi}}}{K_{\mathrm{m,GLY\rightarrow G6P}}}}{1 + \frac{C_{\mathrm{GLY}} C_{\mathrm{Pi}}}{K_{\mathrm{m,GLY\rightarrow G6P}}}} \right]$$

8. ***Pentose Phosphate Shunt I*** $\mathrm{G6P + 2NADP+ \rightarrow R5P + 2NADPH + CO2}$

$$\phi_{\mathrm{G6P\rightarrow R5P}} = V_{\mathrm{G6P\rightarrow R5P}} \left[\frac{\left[\frac{C_{\mathrm{NADP+}}}{C_{\mathrm{NADPH}}} \right]}{\left[\eta^{-}_{\mathrm{G6P\rightarrow R5P}} \right] + \left[\frac{C_{\mathrm{NADP+}}}{C_{\mathrm{NADPH}}} \right]} \right] \left[\frac{\frac{C_{\mathrm{G6P}}}{K_{\mathrm{m,G6P\rightarrow R5P}}}}{1 + \frac{C_{\mathrm{G6P}}}{K_{\mathrm{m,G6P\rightarrow R5P}}}} \right]$$

9. ***Pentose Phosphate Shunt II*** $\mathrm{3R5P \rightarrow 2F6P + GAP_{GC}}$

$$\phi_{\mathrm{R5P\rightarrow F6P\text{-}GAP_{GC}}} = V_{\mathrm{R5P\rightarrow F6P\text{-}GAP_{GC}}} \left[\frac{\frac{C_{\mathrm{R5P}}}{K_{\mathrm{m,R5P\rightarrow F6P\text{-}GAP_{GC}}}}}{1 + \frac{C_{\mathrm{R5P}}}{K_{\mathrm{m,R5P\rightarrow F6P\text{-}GAP_{GC}}}}} \right]$$

10. GAP Reduction I $\mathrm{GAP_{GC} + NADH \leftrightarrow G3P_{GC} + NAD^+}$

$$\phi_{\mathrm{GAP_{GC}\leftrightarrow G3P_{GC}}} = \left[\frac{V_{\mathrm{f,GAP_{GC}\leftrightarrow G3P_{GC}}} \frac{C_{\mathrm{GAP_{GC}}} C_{\mathrm{NADH}}}{K_{\mathrm{f,GAP_{GC}\leftrightarrow G3PGC}}} - V_{\mathrm{b,GAP_{GC}\leftrightarrow G3P_{GC}}} \frac{C_{\mathrm{G3P_{GC}}} C_{\mathrm{NAD}}}{K_{\mathrm{b,GAP_{GC}\leftrightarrow G3P_{GC}}}}}{1 + \frac{C_{\mathrm{GAP_{GC}}} C_{\mathrm{NADH}}}{K_{\mathrm{f,GAP_{GC}\leftrightarrow G3P_{GC}}}} + \frac{C_{\mathrm{G3P_{GC}}} C_{\mathrm{NAD}}}{K_{\mathrm{b,GAP_{GC}\leftrightarrow G3P_{GC}}}}} \right]$$

11. Glyceroneogenesis $\mathrm{PYR + 3ATP + NADH \rightarrow GAP_{OC} + 3ADP + NAD^+ + 2P_i}$

$$\phi_{\mathrm{PYR\rightarrow GAP_{OC}}} = V_{\mathrm{PYR\rightarrow GAP_{OC}}} \left[\frac{\left[\frac{C_{\mathrm{NADH}}}{C_{\mathrm{NAD+}}} \right]}{\nu^{+}_{\mathrm{PYR\rightarrow GAP_{OC}}} + \left[\frac{C_{\mathrm{NADH}}}{C_{\mathrm{NAD+}}} \right]} \right] \left[\frac{\left[\frac{C_{\mathrm{ATP}}}{C_{\mathrm{ADP}}} \right]}{\left[\mu^{+}_{\mathrm{PYR\rightarrow GAP_{OC}}} \right] + \left[\frac{C_{\mathrm{ATP}}}{C_{\mathrm{ADP}}} \right]} \right] \left[\frac{\frac{C_{\mathrm{PYR}}}{K_{\mathrm{m,PYR\rightarrow GAP_{OC}}}}}{1 + \frac{C_{\mathrm{PYR}}}{K_{\mathrm{m,PYR\rightarrow GAP_{OC}}}}} \right]$$

12. GAP Reduction II $\mathrm{GAP_{OC} + NADH \leftrightarrow G3P_{OC} + NAD^+}$

$$\phi_{\mathrm{GAP_{OC}\leftrightarrow G3P_{OC}}} = \left[\frac{V_{\mathrm{f,GAP_{OC}\leftrightarrow G3P_{OC}}} \frac{C_{\mathrm{GAP_{OC}}} C_{\mathrm{NADH}}}{K_{\mathrm{f,GAP_{OC}\leftrightarrow G3P_{OC}}}} - V_{\mathrm{b,GAP_{OC}\leftrightarrow G3P_{OC}}} \frac{C_{\mathrm{G3P_{OC}}} C_{\mathrm{NAD}}}{K_{\mathrm{b,GAP_{OC}\leftrightarrow G3P_{OC}}}}}{1 + \frac{C_{\mathrm{GAP_{OC}}} C_{\mathrm{NADH}}}{K_{\mathrm{f,GAP_{OC}\leftrightarrow G3P_{OC}}}} + \frac{C_{\mathrm{G3P_{OC}}} C_{\mathrm{NAD}}}{K_{\mathrm{b,GAP_{OC}\leftrightarrow G3P_{OC}}}}} \right]$$

13. Glycerol Phosphorylation $\mathrm{GLR+ATP \rightarrow G3P_{OC}+ADP}$

$$\phi_{\mathrm{GLR\rightarrow G3P_{OC}}} = V_{\mathrm{GLR\rightarrow G3P_{OC}}} \left[\frac{\left[\frac{C_{\mathrm{ATP}}}{\mathrm{C_{ADP}}} \right]}{\left[\mu^{+}_{\mathrm{GLR\rightarrow G3P_{OC}}} \right] + \left[\frac{C_{\mathrm{ATP}}}{\mathrm{C_{ADP}}} \right]} \right] \left[\frac{\frac{C_{\mathrm{GLR_{OC}}}}{K_{\mathrm{m,GLR\rightarrow G3P_{OC}}}}}{1 + \frac{C_{\mathrm{GLR}}}{K_{\mathrm{m,GLR\rightarrow G3P_{OC}}}}} \right]$$

14. Alanine Utilization $\mathrm{ALA \rightarrow PYR}$

$$\phi_{\mathrm{ALA\rightarrow PYR}} = V_{\mathrm{ALA\rightarrow PYR}} \left[\frac{\frac{C_{\mathrm{ALA}}}{K_{\mathrm{m,ALA\rightarrow PYR}}}}{1 + \frac{C_{\mathrm{ALA}}}{K_{\mathrm{m,ALA\rightarrow PYR}}}} \right]$$

Alanine represents the amino acid pool.

15. Alanine Formation $\mathrm{PYR \rightarrow ALA}$

$$\phi_{\mathrm{PYR\rightarrow ALA}} = V_{\mathrm{PYR\rightarrow ALA}} \left[\frac{\frac{C_{\mathrm{PYR}}}{K_{\mathrm{m,PYR\rightarrow ALA}}}}{1 + \frac{C_{\mathrm{PYR}}}{K_{\mathrm{m,PYR\rightarrow ALA}}}} \right]$$

16. Proteolysis $\mathrm{Proteins \rightarrow ALA}$

$$\phi_{\mathrm{Proteolysis}} = V_{\mathrm{Proteolysis}}$$

17. Protein Synthesis $\mathrm{ALA \rightarrow Proteins}$

$$\phi_{\mathrm{Protein\ Synthesis}} = V_{\mathrm{Protein\ Synthesis}}$$

18. Pyruvate Oxidation $\mathrm{PYR + CoA + NAD^{+} \rightarrow ACoA + NADH + CO_2}$

$$\phi_{\mathrm{PYR\rightarrow ACoA}} = V_{\mathrm{PYR\rightarrow ACoA}} \left[\frac{\left[\frac{C_{\mathrm{NAD}}}{\mathrm{C_{NADH}}} \right]}{\left[\nu^{-}_{\mathrm{PYR\rightarrow ACoA}} \right] + \left[\frac{C_{\mathrm{NAD}}}{\mathrm{C_{NADH}}} \right]} \right] \left[\frac{\frac{C_{\mathrm{PYR}} C_{\mathrm{CoA}}}{K_{\mathrm{m,PYR\rightarrow ACoA}}}}{1 + \frac{C_{\mathrm{ACoA}}}{K_{\mathrm{i,PYR\rightarrow ACoA}}} + \frac{C_{\mathrm{PYR}} C_{\mathrm{CoA}}}{K_{\mathrm{m,PYR\rightarrow ACoA}}}} \right]$$

19.Fatty Acyl CoA Synthesis $\mathrm{FFA + CoA + 2ATP \rightarrow FAC + 2\ ADP + 2\ Pi}$

$$\phi_{\mathrm{FFA\rightarrow FAC}} = V_{\mathrm{FFA\rightarrow FAC}} \left[\frac{\left[\frac{C_{\mathrm{ATP}}}{\mathrm{C_{ADP}}} \right]}{\left[\mu^{+}_{\mathrm{FFA\rightarrow FAC}} \right] + \left[\frac{C_{\mathrm{ATP}}}{\mathrm{C_{ADP}}} \right]} \right] \left[\frac{\frac{C_{\mathrm{FFA}} C_{\mathrm{CoA}}}{K_{\mathrm{m,FFA\rightarrow FAC}}}}{1 + \frac{C_{\mathrm{FFA}} C_{\mathrm{CoA}}}{K_{\mathrm{m,FFA\rightarrow FAC}}}} \right]$$

20. ***Fatty Acid Oxidation*** $\mathrm{FAC} + 7\mathrm{CoA} + 14\mathrm{NAD}^{+} \rightarrow 8\mathrm{ACoA} + 14\mathrm{NADH}$

$$\phi_{\mathrm{FAC}\rightarrow\mathrm{ACoA}} = V_{\mathrm{FAC}\rightarrow\mathrm{ACoA}} \left[\frac{\left[\frac{C_{\mathrm{NAD+}}}{\mathrm{C}_{\mathrm{NADH}}} \right]}{\left[\nu^{-}_{\mathrm{FAC}\rightarrow\mathrm{ACoA}} \right] + \left[\frac{C_{\mathrm{NAD+}}}{\mathrm{C}_{\mathrm{NADH}}} \right]} \right] \left[\frac{\frac{C_{\mathrm{FAC}} C_{\mathrm{CoA}}}{K_{\mathrm{m,FAC}\rightarrow\mathrm{ACoA}}}}{1 + \frac{C_{\mathrm{ACoA}}}{K_{\mathrm{i,FAC}\rightarrow\mathrm{ACoA}}} + \frac{C_{\mathrm{FAC}} C_{\mathrm{CoA}}}{K_{\mathrm{m,FAC}\rightarrow\mathrm{ACoA}}}} \right]$$

21. TG Breakdown by ATGL $\mathrm{TG} \rightarrow \mathrm{DG} + \mathrm{FFA}$

$$\phi_{\mathrm{TG}\rightarrow\mathrm{DG}} = V_{\mathrm{TG}\rightarrow\mathrm{DG,ATGL}}$$

22. TG Breakdown by HSL $\mathrm{TG} \rightarrow \mathrm{DG} + \mathrm{FFA}$

$$\phi_{\mathrm{TG}\rightarrow\mathrm{DG}} = V_{\mathrm{TG}\rightarrow\mathrm{DG,HSL}}$$

23. DG Breakdown by HSL $\mathrm{DG} \rightarrow \mathrm{MG} + \mathrm{FFA}$

$$\phi_{\mathrm{DG}\rightarrow\mathrm{MG}} = V_{\mathrm{DG}\rightarrow\mathrm{MG,HSL}} \left[\frac{\frac{C_{\mathrm{DG}}}{K_{\mathrm{m,DG}\rightarrow\mathrm{MG}}}}{1 + \frac{C_{\mathrm{DG}}}{K_{\mathrm{m,DG}\rightarrow\mathrm{MG}}}} \right]$$

24. MG Breakdown by HSL $\mathrm{MG} \rightarrow \mathrm{GLR} + \mathrm{FFA}$

$$\phi_{\mathrm{MG}\rightarrow\mathrm{GLR}} = V_{\mathrm{MG}\rightarrow\mathrm{GLR,HSL}} \left[\frac{\frac{C_{\mathrm{MG}}}{K_{\mathrm{m,MG}\rightarrow\mathrm{GLR}}}}{1 + \frac{C_{\mathrm{MG}}}{K_{\mathrm{m,MG}\rightarrow\mathrm{GLR}}}} \right]$$

25. MG Breakdown by MGL $\mathrm{MG} \rightarrow \mathrm{GLR} + \mathrm{FFA}$

$$\phi_{\mathrm{MG}\rightarrow\mathrm{GLR}} = V_{\mathrm{MG}\rightarrow\mathrm{GLR,MGL}} \left[\frac{\frac{C_{\mathrm{MG}}}{K_{\mathrm{m,MG}\rightarrow\mathrm{GLR}}}}{1 + \frac{C_{\mathrm{MG}}}{K_{\mathrm{m,MG}\rightarrow\mathrm{GLR}}}} \right]$$

26. Lipogenesis $8\mathrm{ACoA} + 14\mathrm{NADPH} + 7\mathrm{ATP} \rightarrow \mathrm{FFA} + 8\mathrm{CoA} + 14\mathrm{NADP} + 7\mathrm{ADP} + 7\mathrm{P_i}$

$$\phi_{\mathrm{ACoA}\rightarrow\mathrm{FFA}} = V_{\mathrm{ACoA}\rightarrow\mathrm{FFA}} \left[\frac{\left[\frac{C_{\mathrm{ATP}}}{\mathrm{C}_{\mathrm{ADP}}} \right]}{\left[\mu^{+}_{\mathrm{ACoA}\rightarrow\mathrm{FFA}} \right] + \left[\frac{C_{\mathrm{ATP}}}{\mathrm{C}_{\mathrm{ADP}}} \right]} \right] \left[\frac{\left[\frac{C_{\mathrm{NADPH}}}{\mathrm{C}_{\mathrm{NADP+}}} \right]}{\left[\eta^{+}_{\mathrm{ACoA}\rightarrow\mathrm{FFA}} \right] + \left[\frac{C_{\mathrm{NADPH}}}{\mathrm{C}_{\mathrm{NADP+}}} \right]} \right] \left[\frac{\frac{C_{\mathrm{ACoA}}}{K_{\mathrm{m,ACoA}\rightarrow\mathrm{FFA}}}}{1 + \frac{C_{\mathrm{ACoA}}}{K_{\mathrm{m,ACoA}\rightarrow\mathrm{FFA}}}} \right]$$

27. DG Synthesis I $\mathrm{G3P_{GC}} + 2\mathrm{FAC} \rightarrow \mathrm{DG} + 2\mathrm{CoA} + \mathrm{Pi}$

$$\phi_{\mathrm{G3P_{GC}\text{-}FAC\rightarrow DG}} = V_{\mathrm{G3P_{GC}\text{-}FAC\rightarrow DG}} \left[\frac{\frac{C_{\mathrm{G3P_{GC}}} C_{\mathrm{FAC}}}{K_{\mathrm{m,G3P_{GC}\text{-}FAC\rightarrow DG}}}}{1 + \frac{C_{\mathrm{G3P_{GC}}} C_{\mathrm{FAC}}}{K_{\mathrm{m,G3P_{GC}\text{-}FAC\rightarrow DG}}}} \right]$$

28. DG Synthesis II $\mathrm{G3P_{OC}} + 2\mathrm{FAC} \rightarrow \mathrm{DG} + 2\mathrm{CoA} + \mathrm{Pi}$

$$\phi_{\mathrm{G3P_{OC}\text{-}FAC\rightarrow DG}} = V_{\mathrm{G3P_{OC}\text{-}FAC\rightarrow DG}} \left[\frac{\frac{C_{\mathrm{G3P_{OC}}} C_{\mathrm{FAC}}}{K_{\mathrm{m,G3P_{OC}\text{-}FAC\rightarrow DG}}}}{1 + \frac{C_{\mathrm{G3P_{OC}}} C_{\mathrm{FAC}}}{K_{\mathrm{m,G3P_{OC}\text{-}FAC\rightarrow DG}}}} \right]$$

29. TG Synthesis $\mathrm{DG} + \mathrm{FAC} \rightarrow \mathrm{TG} + \mathrm{CoA}$

$$\phi_{\mathrm{DG\text{-}FAC\rightarrow TG}} = V_{\mathrm{DG\text{-}FAC\rightarrow TG}} \left[\frac{\frac{C_{\mathrm{DG}} C_{\mathrm{FAC}}}{K_{\mathrm{m,DG\text{-}FAC\rightarrow TG}}}}{1 + \frac{C_{\mathrm{DG}} C_{\mathrm{FAC}}}{K_{\mathrm{m,DG\text{-}FAC\rightarrow TG}}}} \right]$$

30. Transacylation I $\mathrm{DG} + \mathrm{DG} \rightarrow \mathrm{TG} + \mathrm{MG}$

$$\phi_{\mathrm{DG\text{-}DG\rightarrow TG\text{-}MG}} = V_{\mathrm{DG\text{-}DG\rightarrow TG\text{-}MG}} \left[\frac{\frac{C_{\mathrm{DG}}}{K_{\mathrm{m,DG\text{-}DG\rightarrow TG\text{-}MG}}}}{1 + \frac{C_{\mathrm{DG}}}{K_{\mathrm{m,DG\text{-}DG\rightarrow TG\text{-}MG}}}} \right]$$

31. Transacylation II $\mathrm{MG} + \mathrm{MG} \rightarrow \mathrm{DG} + \mathrm{GLR}$

$$\phi_{\mathrm{MG\text{-}MG\rightarrow DG\text{-}GLR}} = V_{\mathrm{MG\text{-}MG\rightarrow DG\text{-}GLR}} \left[\frac{\frac{C_{\mathrm{MG}}}{K_{\mathrm{m,MG\text{-}MG\rightarrow DG\text{-}GLR}}}}{1 + \frac{C_{\mathrm{MG}}}{K_{\mathrm{m,MG\text{-}MG\rightarrow DG\text{-}GLR}}}} \right]$$

32. Transacylation III $\mathrm{MG} + \mathrm{DG} \rightarrow \mathrm{TG} + \mathrm{GLR}$

$$\phi_{\mathrm{MG\text{-}DG\rightarrow TG\text{-}GLR}} = V_{\mathrm{MG\text{-}DG\rightarrow TG\text{-}GLR}} \left[\frac{\frac{C_{\mathrm{MG}} C_{\mathrm{DG}}}{K_{\mathrm{m,MG\text{-}DG\rightarrow TG\text{-}GLR}}}}{1 + \frac{C_{\mathrm{MG}} C_{\mathrm{DG}}}{K_{\mathrm{m,MG\text{-}DG\rightarrow TG\text{-}GLR}}}} \right]$$

33. TCA Cycle $ACoA + ADP + Pi + 4NAD^+ \rightarrow 2CO_2 + CoA + ATP + 4NADH$

$$\phi_{ACoA\leftrightarrow CO2} = V_{ACoA\rightarrow CO2}\left[\frac{\left[\frac{C_{NAD+}}{C_{NADH}}\right]}{\left[\nu^{-}_{ACoA\rightarrow CO2}\right]+\left[\frac{C_{NAD+}}{C_{NADH}}\right]}\right]\left[\frac{\left[\frac{C_{ADP}}{C_{ATP}}\right]}{\left[\mu^{-}_{ACoA\rightarrow CO2}\right]+\left[\frac{C_{ADP}}{C_{ATP}}\right]}\right]\left[\frac{\frac{C_{ACoA}C_{Pi}}{K_{m,ACoA\rightarrow CO2}}}{1+\frac{C_{ACoA}C_{Pi}}{K_{m,ACoA\rightarrow CO2}}}\right]$$

34. Oxidative Phosphorylation $O_2 + 6ADP + 6Pi + 2NADH \rightarrow 2H_2O + 6ATP + 2NAD^+$

$$\phi_{O2\rightarrow H2O} = V_{O2\rightarrow H2O}\left[\frac{\left[\frac{C_{NADH}}{C_{NAD+}}\right]}{\left[\nu^{+}_{O2\rightarrow H2O}\right]+\left[\frac{C_{NAD+}}{C_{NADH}}\right]}\right]\left[\frac{\left[\frac{C_{ADP}}{C_{ATP}}\right]}{\left[\mu^{-}_{O2\rightarrow H2O}\right]+\left[\frac{C_{ADP}}{C_{ATP}}\right]}\right]\left[\frac{\frac{C_{O2}C_{Pi}}{K_{m,O2\rightarrow H2O}}}{1+\frac{C_{O2}C_{Pi}}{K_{m,O2\rightarrow H2O}}}\right]$$

35. ATP Hydrolysis $ATP \rightarrow ADP + Pi$

$$\phi_{ATP\rightarrow ADP} = V_{ATP\rightarrow ADP}\left[\frac{\frac{C_{ATP}}{K_{ATP\rightarrow ADP}}}{1+\frac{C_{Pi}C_{ADP}}{K_{i,ATP\rightarrow ADP}}+\frac{C_{ATP}}{K_{m,ATP\rightarrow ADP}}}\right]$$

36. TG Breakdown by LPL $TG \rightarrow GLR + 3FFA$

$$\phi_{TG\rightarrow FFA,LPL} = V_{TG\rightarrow FFA,LPL}\left[\frac{\frac{C_{TG}}{K_{m,TG\rightarrow FFA,LPL}}}{1+\frac{C_{TG}}{K_{m,TG\rightarrow FFA,LPL}}}\right]$$

This is the only reaction in the blood compartment which is governed by LPL.
Rate coefficient is activated by adipose blood flow.

APPENDIX IV. DYNAMIC MASS BALANCE EQUATIONS OF O2 AND CO2 USED IN THE ADIPOSE TISSUE MODEL

A-IV.1. O_2 TRANSPORT DYNAMICS

Assuming that adipose tissue has no myoglobin, the dynamic mass balance equation of oxygen in the cellular compartment describes only free dissolved O_2. On the contrary, since oxygen is transported via blood circulation as free dissolved O_2 and as bound oxy-hemoglobin (HbO_2), a special consideration is required to delineate the dynamics of oxygen in blood compartment. The assumptions of perfect mixing and rapid phase equilibrium among free O_2 in plasma (PL), red blood cells (RBC) and interstitial fluid (ISF) yield that free oxygen concentrations in each phase are same as:

$$C^F_{b,O2} = C^F_{PL,O2} = C^F_{RBC,O2} = C^F_{ISF,O2} \tag{A1}$$

where the superscript 'F' indicates concentration of free dissolved O_2.

The dynamic mass balance equation for O_2 in blood compartment can be expressed as:

$$V_{cp}\frac{dC^T_{b,O2}}{dt} + V_{ISF}\frac{dC^F_{ISF,O2}}{dt} = Q\left(C^T_{a,O2} - C^T_{b,O2}\right) - J_{b\leftrightarrow c,O2} \tag{A2}$$

where the superscript 'T' indicate total concentration; V_{cp} and V_{ISF} are the physical volumes of capillary blood and ISF, whose ratio is 7:13. Total concentration of O_2 in capillary blood is composed of free and bound ones as:

$$C^T_{x,O2} = C^F_{x,O2} + C_{x,HbO2} \tag{A3}$$

where x = (a,b); $C_{x,HbO2}$ is the oxygen concentration bound to hemoglobin.

The mass transport flux between blood and cells is given by

$$J_{b\leftrightarrow c,O2} = \gamma_{O2}\left(C^F_{b,O2} - C^F_{c,O2}\right) \tag{A4}$$

The concentrations of HbO_2 can be written in terms of their saturations as:

$$C_{x,HbO2} = 4.H_{RBC}.C_{RBC,Hb}.S_{x,HbO2} \tag{A5a}$$

$$S_{x,HbO2} = \frac{K_{HbO2}.\left(C^F_{x,O2}\right)^{n_H}}{1 + K_{HbO2}.\left(C^F_{x,O2}\right)^{n_H}} \tag{A5b}$$

where x = (a,b); H_{RBC} = 0.45 is hematocrit; $C_{RBC,Hb}$ = 5.2mM is the concentration of RBC; $S_{x,HbO2}$ is the saturation of HbO2; K_{HbO2} = 7800.7 $mM^{-2.7}$ is the Hill constant for HbO_2 saturation; n_H = 2.7 is the Hill coefficient for HbO_2 saturation.

Substituting Eq. (A5) in Eq. (A3), we have the expression for total O_2 concentrations as

$$C^T_{x,O2} = C^F_{x,O2} + \frac{4.H_{RBC}.C_{RBC,Hb}.K_{HbO2}.\left(C^F_{x,O2}\right)^{n_H}}{1 + K_{HbO2}.\left(C^F_{x,O2}\right)^{n_H}} \tag{A6}$$

Then, substituting Eq. (A1) and (A6) in Eq. (A2), the dynamic mass balance equation for O_2 is derived as:

$$V_{b,O2}\frac{dC^F_{b,O2}}{dt} = Q\left(C^T_{a,O2} - C^T_{b,O2}\right) - J_{b\leftrightarrow c,O2} \tag{A7}$$

where the effective volume of O_2 in blood compartment, $V_{b,O2}$ is expressed by

$$V_{b,O2} = V_{cp,O2} + V_{ISF,O2} = V_{cp}\left(1 + \frac{4.n_H.H_{RBC}.C_{RBC,Hb}.K_{HbO2}.\left(C^F_{b,O2}\right)^{n_H-1}}{\left[1 + K_{HbO2}.\left(C^F_{b,O2}\right)^{n_H}\right]^2}\right) + V_{ISF} \tag{A8}$$

A-IV.2. CO_2 TRANSPORT DYNAMICS

CO_2 is transported as free dissolved CO_2, as bound carbamino-hemoglobin ($HbCO_2$), and as bicarbonate (HCO_3^-) in capillary blood while it is transported as dissolved CO_2 and as HCO_3^- in ISF and cells. The dynamic mass balance equations for CO_2 must take into account different forms of CO_2 transport in RBC, plasma, ISF and cells. The assumptions of perfect mixing in each phase and rapid phase equilibrium among free CO_2 in plasma, RBC, and ISF yield that free oxygen concentrations in each phase are same as:

$$C^F_{b,CO2} = C^F_{PL,CO2} = C^F_{RBC,CO2} = C^F_{ISF,CO2} \tag{A9}$$

The dynamic mass balance equations for CO_2 can be expressed in blood compartment as:

$$V_{cp}\frac{dC^T_{b,CO2}}{dt} + V_{ISF}\frac{dC^T_{ISF,CO2}}{dt} = Q\left(C^T_{a,CO2} - C^T_{b,CO2}\right) - J_{b\leftrightarrow c,CO2} \tag{A10}$$

and in cellular compartment as:

$$V_c\frac{dC^T_{c,CO2}}{dt} = J_{b\leftrightarrow c,CO2} + R_{c,CO2} \tag{A11}$$

Total CO2 concentration in blood, ISF, and tissue cells are expressed as:

$$C^T_{x,CO2} = C^F_{x,CO2} + C_{x,HbCO2} + C_{x,HCO3\text{-}}, \quad x = (a,b) \tag{A11a}$$

$$C^T_{x,CO2} = C^F_{x,CO2} + C_{x,HCO3\text{-}}, \quad x = (ISF,c) \tag{A11b}$$

The mass transport flux is given by

$$J_{b\leftrightarrow c,CO2} = \gamma_{CO2}\left(C^F_{b,CO2} - C^F_{c,CO2}\right) \tag{A12}$$

The concentration of $HbCO_2$, $C_{x,HbCO2}$ ($x = a$ or b) can be written in terms of its saturation as:

$$C_{x,HbCO2} = 4.H_{RBC}.C_{RBC,Hb}.S_{x,HbCO2} \tag{A13a}$$

$$S_{x,HbCO2} = \frac{K_{HbCO2}.C^{F}_{x,CO2}}{1 + K_{HbCO2}.C^{F}_{x,CO2}} \tag{A13b}$$

where $S_{x,HbCO2}$ is the saturation of HbCO2; $K_{HbCO2} = 0.1237$ mM^{-1} is the Hill constant for $HbCO_2$ saturation. Applying the Henderson-Hasselbalch relation, the concentrations of HCO_3^- can be derived in terms of free CO2 and pH in capillary blood ($x = a$ or b) as:

$$C_{x,HCO3-} = \left[\frac{(1 - H_{RBC})}{C_{PL,H+}} + \frac{H_{RBC}}{C_{RBC,H+}}\right] K_{CO2hyd}.C^{F}_{x,CO2} \tag{A14a}$$

and in ISF and cells ($x = ISF$ or c) as:

$$C_{x,HCO3-} = \frac{K_{CO2hyd}.C^{F}_{x,CO2}}{C_{x,H+}} \tag{A14b}$$

where $K_{CO2hyd} = 7.95E\text{-}04$ mM is the equilibrium constant for CO_2 hydration reaction.

Substituting Eq. (A13) and (A14) into Eq. (A11), total CO_2 concentrations can be expressed as:

$$\begin{aligned} C^{T}_{x,CO2} = C^{F}_{x,CO2} &+ \frac{4.H_{RBC}.C_{RBC,Hb}.K_{HbCO2}.C^{F}_{x,CO2}}{1 + K_{HbCO2}.C^{F}_{x,CO2}} \\ &+ \left[\frac{(1 - H_{RBC})}{C_{PL,H+}} + \frac{H_{RBC}}{C_{RBC,H+}}\right] K_{CO2hyd}.C^{F}_{x,CO2}, \qquad x = (a,b) \end{aligned} \tag{A15a}$$

$$C^{T}_{x,CO2} = C^{F}_{x,CO2} + \frac{K_{CO2hyd}.C^{F}_{x,CO2}}{C_{x,H+}}, \quad x = (ISF, c) \tag{A15b}$$

$$C_{x,H+} = 10^{-pH_x+3} \tag{A15c}$$

where pH values in plasma, RBC, ISF and cells are assumed to be constant and set to 7.4, 7.24, 7.2 and 7.1, respectively (Dash and Bassingthwaighte, 2006b). Substituting Eq. (A15) in Eq. (A10) and (A11), the dynamic mass balance equations for CO_2 in blood and tissue compartments are derived as:

$$\left(V_{cp,CO2} + V_{ISF,CO2}\right)\frac{dC^F_{b,CO2}}{dt} = Q\left(C^T_{a,CO2} - C^T_{b,CO2}\right) - J_{b\leftrightarrow c,CO2} \tag{A16a}$$

$$V_{c,CO2}\frac{dC^F_{c,CO2}}{dt} = J_{b\leftrightarrow c,CO2} + R_{c,CO2} \tag{A16b}$$

where the effective volumes or volumes CO_2 in capillary blood, ISF, and tissue cells ($V_{cp,CO2}$, $V_{ISF,CO2}$ and $V_{c,CO2}$) are given by

$$V_{b,CO2} = V_{cp,CO2} + V_{ISF,CO2} \tag{A17a}$$

$$V_{cp,CO2} = V_{cp}\left(1 + \frac{4.H_{RBC}.C_{RBC,Hb}.K_{HbCO2}}{\left[1 + K_{HbCO2}.C^F_{b,CO2}\right]^2} + \left[\frac{(1-H_{RBC})}{C_{PL,H+}} + \frac{H_{RBC}}{C_{RBC,H+}}\right]K_{CO2hyd}\right) \tag{A17a}$$

$$V_{x,CO2} = V_x\left(1 + \frac{K_{CO2hyd}}{C_{x,H^+}}\right), \quad x = (ISF, c) \tag{A17c}$$

APPENDIX V. COMPUTER CODES FOR THE MODEL SIMULATIONS

A-V.1. WHOLE BODY MODEL FOR FUEL HOMEOSTASIS DURING EXERCISE

The following is the source code written in FORTRAN to simulate the dynamic responses during a moderate intensity exercise (150W) in a normal sedentary person with 70Kg body weight after an overnight (8~12hr) fasting. The simulation code utilizes a library, 'LSODES' in order to solve a set of ordinary differential equations.

```
!-----------------------------------------------------------------------
!
! Main simulation code for the whole body model during exercise
!
!-----------------------------------------------------------------------
    program wholebody
    external fex
    external jex
    double precision atol, rtol, rwork(500000), t, tout, tstep
    double precision y, y1, y2, y3, y4, y5, y6, fluxrate
    integer istate, itol, iopt, itask, neq
    integer iwork(300),i
    dimension y(134), y1(22), y2(22), y3(22), y4(22), y5(22), y6(22)
    double precision P, U, F, Q, UR, Ca, MR, V, GIR
    Common /tests/P(7,22),U(7,22),Q(7),UR(7,22),Ca(22),MR(7),Cp(22)
   1             ,V(7,22),GIR,tv,epi,RMR
    common/fx/ fluxrate(7,25)
    double precision tv, tend, t0, Cv(7,22), WR, RMR,glyg,gng
    data lrw/500000/, liw/300/

!OPEN OUTPUT FILE
    OPEN(11,FILE='brain.txt')
    OPEN(12,FILE='heart.txt')
    OPEN(13,FILE='muscle.txt')
    OPEN(14,FILE='GI.txt')
    OPEN(15,FILE='liver.txt')
    OPEN(16,FILE='adipose.txt')
    OPEN(17,FILE='mflux.txt')
    OPEN(7,FILE='up-rel.txt')
    OPEN(8,FILE='glu.txt')
    OPEN(9,FILE='art.txt')
    OPEN(10,FILE='fat.txt')
    OPEN(18,FILE='hormone.txt')
    OPEN(19,FILE='femoral.txt')
!NEQ = Number of Equations
    neq = 134

    t0 = 0.0d0
    tv = 0.0d0
    tend = 70.0
    tstep = 0.01d0
```

```
!   Set LSODES Parameter Values
      itol = 1
      rtol = 1.0d-8
      atol = 1.0d-8
      itask = 1
      istate = 1
      iopt = 0
      mf = 222

! Initial arterial concentrations of substrates

    Ca(1) = 5.0                                                    !GLC
    Ca(2) = 0.068                                                  !PYR
    Ca(3) = 0.7                                                    !LAC
    Ca(4) = 0.25                                                   !ALA
    Ca(5) = 0.07                                                   !GLR
    Ca(6) = 0.66                                                   !FA
    Ca(7) = 0.99                                                   !TGL
    Ca(8) = 8.0                                                    !O2
    Ca(9) = 21.7                                                   !CO2
    Ca(10) = 0.0
    Ca(11) = 0.0
    Ca(12) = 0.0
    Ca(13) = 0.0
    Ca(14) = 0.0
    Ca(15) = 0.0
    Ca(16) = 0.0
    Ca(17) = 0.0
    Ca(18) = 0.0
    Ca(19) = 0.0
    Ca(20) = 0.0
    Ca(21) = 0.0
    Ca(22) = 0.0

!SET INITIAL CONDITIONS
!
!This section sets the initial tissue concentrations for
!the substrates in mmol/kg wet weight.
!There is one set of initial conditions for each tissue
!compartment. The order of substrates are as follows:
!S1 = Glucose (GLC)
!S2 = Pyruvate (PYR)
!S3 = Lactate (LAC)
!S4 = Alanine (ALA)
!S5 = Glycerol (GLR)
!S6 = Free Fatty Acid (FA)
!S7 = Triglyceride (TGL)
!S8 = O2
!S9 = CO2
!S10 = Glucose-6-Phosphate (G6P)
!S11 = Glycogen (GLY)
!S12 = Glyceraldehyde 3-Phosphate (GAP)
!S13 = Glycerol-3oPhosphate (GRP)
!S14 = Acetyl CoA (ACoA)
!S15 = CoA
!S16 = NAD+
!S17 = NADH
```

```
!S18 = ATP
!S19 = ADP
!S20 = Pi
!S21 = Phospho Creatine(PCR)
!S22 = Creatine(CR)
!
!INITIAL CONDITIONS FOR THE BRAIN COMPARTMENT - y1(x)
    y1(1) = 1.12                                                !GLC
    y1(2) = 0.154                                               !PYR
    y1(3) = 1.45                                                !LAC
    y1(4) = 0.0                                                 !ALA
    y1(5) = 0.0                                                 !GLR
    y1(6) = 0.0                                                 !FA
    y1(7) = 0.0                                                 !TGL
    y1(8) = 0.027                                               !O2
    y1(9) = 15.43                                               !CO2
    y1(10) = 0.16                                               !G6P
    y1(11) = 2.0                                                !GLY
    y1(12) = 0.154                                              !GAP
    y1(13) = 0.0                                                !GRP
    y1(14) = 0.0068                                             !ACoA
    y1(15) = 0.0604                                             !CoA
    y1(16) = 0.064                                              !NAD+
    y1(17) = 0.026                                              !NADH
    y1(18) = 2.45                                               !ATP
    y1(19) = 0.536                                              !ADP
    y1(20) = 2.40                                               !Pi
    y1(21) = 4.60                                               !PCR
    y1(22) = 5.60                                               !CR
!
!INITIAL CONDITIONS FOR THE HEART COMPARTMENT - y2(x)
    y2(1) = 1.0                                                 !GLC
    y2(2) = 0.2                                                 !PYR
    y2(3) = 3.88                                                !LAC
    y2(4) = 0.0                                                 !ALA
    y2(5) = 0.015                                               !GLR
    y2(6) = 0.021                                               !FA
    y2(7) = 3.12                                                !TGL
    y2(8) = 0.963                                               !O2
    y2(9) = 20.0                                                !CO2
    y2(10) = 0.171                                              !G6P
    y2(11) = 33.0                                               !GLY
    y2(12) = 0.01                                               !GAP
    y2(13) = 0.29                                               !GRP
    y2(14) = 0.0012                                             !ACoA
    y2(15) = 0.012                                              !CoA
    y2(16) = 0.40                                               !NAD+
    y2(17) = 0.045                                              !NADH
    y2(18) = 3.4                                                !ATP
    y2(19) = 0.02                                               !ADP
    y2(20) = 1.66                                               !Pi
    y2(21) = 8.3                                                !PCR
    y2(22) = 3.5                                                !CR
!
!INITIAL CONDITIONS FOR THE SKELETAL MUSCLE COMPARTMENT - y3(x)
    y3(1) = 0.485                                               !GLC
    y3(2) = 0.0775                                              !PYR
    y3(3) = 1.44                                                !LAC
```

```
    y3(4) = 1.3                                                    !ALA
    y3(5) = 0.064                                                  !GLR
    y3(6) = 0.53                                                   !FA
    y3(7) = 14.8                                                   !TGL
    y3(8) = 0.49                                                   !O2
    y3(9) = 15.43                                                  !CO2
    y3(10) = 0.24                                                  !G6P
    y3(11) = 95.0                                                  !GLY
    y3(12) = 0.08                                                  !GAP
    y3(13) = 0.147                                                 !GRP
    y3(14) = 0.00223                                               !ACoA
    y3(15) = 0.0183                                                !CoA
    y3(16) = 0.45                                                  !NAD+
    y3(17) = 0.05                                                  !NADH
    y3(18) = 6.15                                                  !ATP
    y3(19) = 0.02                                                  !ADP
    y3(20) = 2.70                                                  !Pi
    y3(21) = 20.1                                                  !PCR
    y3(22) = 10.45                                                 !CR
!
!INITIAL CONDITIONS FOR THE GI COMPARTMENT - y4(x)
    y4(1) = 1.0                                                    !GLC
    y4(2) = 0.2                                                    !PYR
    y4(3) = 3.88                                                   !LAC
    y4(4) = 0.0                                                    !ALA
    y4(5) = 0.015                                                  !GLR
    y4(6) = 0.021                                                  !FA
    y4(7) = 990.0 !3.12                                            !TGL
    y4(8) = 0.49                                                   !O2
    y4(9) = 15.43                                                  !CO2
    y4(10) = 0.171                                                 !G6P
    y4(11) = 33.0                                                  !GLY
    y4(12) = 0.01                                                  !GAP
    y4(13) = 0.29                                                  !GRP
    y4(14) = 0.0012                                                !ACoA
    y4(15) = 0.012                                                 !CoA
    y4(16) = 0.40                                                  !NAD+
    y4(17) = 0.045                                                 !NADH
    y4(18) = 3.4                                                   !ATP
    y4(19) = 0.02                                                  !ADP
    y4(20) = 1.66                                                  !Pi
    y4(21) = 8.3                                                   !PCR
    y4(22) = 3.5                                                   !CR
!
!INITIAL CONDITIONS FOR THE LIVER COMPARTMENT - y5(x)
    y5(1) = 8.0                                                    !GLC
    y5(2) = 0.37                                                   !PYR
    y5(3) = 0.82                                                   !LAC
    y5(4) = 0.227                                                  !ALA
    y5(5) = 0.07                                                   !GLR
    y5(6) = 0.570                                                  !FA
    y5(7) = 2.93                                                   !TGL
    y5(8) = 0.027                                                  !O2
    y5(9) = 15.43                                                  !CO2
    y5(10) = 0.2                                                   !G6P
    y5(11) = 417                                                   !GLY
    y5(12) = 0.108                                                 !GAP
    y5(13) = 0.24                                                  !GRP
```

```
    y5(14) = 0.035                                                  !ACoA
    y5(15) = 0.14                                                   !CoA
    y5(16) = 0.45                                                   !NAD+
    y5(17) = 0.05                                                   !NADH
    y5(18) = 2.74                                                   !ATP
    y5(19) = 1.22                                                   !ADP
    y5(20) = 4.60                                                   !Pi
    y5(21) = 0.0                                                    !PCR
    y5(22) = 0.0                                                    !CR
!
!INITIAL CONDITIONS FOR THE ADIPOSE TISSUE COMPARTMENT - y6(x)
    y6(1) = 2.54                                                    !GLC
    y6(2) = 0.37                                                    !PYR
    y6(3) = 0.82                                                    !LAC
    y6(4) = 0.0                                                     !ALA
    y6(5) = 0.22                                                    !GLR
    y6(6) = 0.57                                                    !FA
    y6(7) = 990.0                                                   !TGL
    y6(8) = 0.027                                                   !O2
    y6(9) = 15.43                                                   !CO2
    y6(10) = 0.2                                                    !G6P
    y6(11) = 0.0                                                    !GLY
    y6(12) = 0.108                                                  !GAP
    y6(13) = 0.24                                                   !GRP
    y6(14) = 0.035                                                  !ACoA
    y6(15) = 0.14                                                   !CoA
    y6(16) = 0.45                                                   !NAD+
    y6(17) = 0.05                                                   !NADH
    y6(18) = 2.74                                                   !ATP
    y6(19) = 1.22                                                   !ADP
    y6(20) = 4.60                                                   !Pi
    y6(21) = 0.0                                                    !PCR
    y6(22) = 0.0                                                    !CR

    y(1:22)=y1(1:22)
    y(23:44)=y2(1:22)
    y(45:66)=y3(1:22)
    y(67:88)=y4(1:22)
    y(89:110)=y5(1:22)
    y(111:132)=y6(1:22)
    y(133)=25.48
    y(134)=47.75
    GIR=y(133)/y(134)-0.5336
!
!Write Initial Conditions to Output File
    write(7,60) t0, UR(1:7,1:9)
    write(8,60) t0,UR(3,1)+UR(2,1)+UR(1,1)+UR(4,1)+UR(6,1)+UR(7,1)
   1            ,-UR(5,1)
    write(9,60) t0, Ca(1:7), 0.38, 0.3505, 0.3505/0.7305,0.48,0.5205
    write(10,60) t0, UR(1:7,8)*22.4,SUM(UR(1:7,8)*22.4)
   1            ,UR(1:7,9)*22.4,SUM(UR(1:7,9)*22.4)
   1            ,-SUM(UR(1:7,9)*22.4)/SUM(UR(1:7,8)*22.4)
    write(11,60) t0, y1(:)
    write(12,60) t0, y2(:)
    write(13,60) t0, y3(:)
    write(14,60) t0, y4(:)
    write(15,60) t0, y5(:)
    write(16,60) t0, y6(:)
```

```
    write(17,60) t0, fluxrate(3,:)
    write(18,60) t0, y(133), y(134), y(133)/y(134)

    tout = t0 + tstep

    WR=125.0
! Do Loop to Control Code Flow
      DO 10 K=1,7000
        tv = t0
        if(tv.lt.10.0) then
            epi=0.0
            MR(1) = 15.197
            MR(2) = 7.332
            MR(3) = 10.821
            MR(4) = 3.04
            MR(5) = 13.924
            MR(6) = 2.736
            RMR=MR(3)/10.821
            Q(1)=0.75
            Q(2)=0.25
            Q(3)=0.9
            Q(4)=1.1
            Q(5)=0.4
            Q(6)=0.36
            Q(7)=1.74
        else if((tv.ge.10.0).and.(tv.le.70.0)) then
            epi=1100.0*(1.0-dexp(-(tv-10.0)/30.0))
            Q(2)=0.25*1.5*(1.0-dexp(-(tv-10.0)/0.1))+0.25
            Q(3)=0.9*9.0*(1.0-dexp(-(tv-10.0)/0.1))+0.9
            Q(4)=1.1-0.4*(1.0-dexp(-(tv-10.0)/0.1))
            MR(2)=7.332*3.0
            MR(3)=10.821+2.68*150.0
            RMR=MR(3)/10.821
        end if
!Call to lsodes for solutions of y(x)
 20  call dlsodes(fex, neq, y, tv, tout, itol, rtol, atol,
    1     itask, istate, iopt, rwork, lrw, iwork, liw, jex, mf)

!Check that integration was successful
    if (istate .eq. 2) then
        y1(1:22)=y(1:22)
        y2(1:22)=y(23:44)
        y3(1:22)=y(45:66)
        y4(1:22)=y(67:88)
        y5(1:22)=y(89:110)
        y6(1:22)=y(111:132)
        goto 71
    end if
    if (istate .eq. -1) then
       istate = 3
       tv = t0
       go to 20
      end if
!IF LSODES FAILS
    if (istate .lt. -1) then
        write(6,50)istate
        go to 40
```

```
    end if

! Reset Time Parameters and Other LSODES Parameters
   71   t0 = tout
        tout = t0 + tstep

!VENOUS CONCENTRATIONS leaving the brain
    Cv(1,1:22) = Ca(1:22) - UR(1,1:22)/Q(1)
!Venous Concentrations Leaving the Heart
    Cv(2,1:22) = Ca(1:22) - UR(2,1:22)/Q(2)
!Venous Concentrations Leaving the Skeletal Muscle
    Cv(3,1:22) = Ca(1:22) - UR(3,1:22)/Q(3)
!Venous Concentrations Leaving the Liver
    Cv(5,1:22) = Ca(1:22) - (UR(4,1:22)+UR(5,1:22))/(Q(4)+Q(5))
!Venous Concentrations Leaving the Adipose
    Cv(6,1:22) = Ca(1:22) - UR(6,1:22)/Q(6)
!Venous Concentrations Leaving the Other Tissues
    UR(7,1)=0.032
    UR(7,2)=-0.005
    UR(7,3)=-0.172
    UR(7,4)=-0.280
    UR(7,5)=0.0
    UR(7,6)=0.05
    UR(7,7)=0.0
    UR(7,8)=2.146
    UR(7,9)=-1.572
    Cv(7,1:9) = Ca(1:9) - UR(7,1:9)/Q(7)
    Cv(7,10:22) = Ca(10:22)

!Calculation of the new arterial blood concentration value
    I=7
    Ca(1:I) = (Cv(1,1:I)*Q(1) + Cv(2,1:I)*Q(2) + Cv(3,1:I)*Q(3)
   1        + Cv(5,1:I)*(Q(4)+Q(5)) + Cv(6,1:I)*Q(6) + Cv(7,1:I)*Q(7))
   2            /(Q(1) + Q(2) + Q(3) + Q(4) + Q(5) + Q(6) + Q(7))

      t = t0

!OUTPUT TO FILE
!   Writes the concentrations at every time:

    do i=1,132
        if(y(i).lt.0.0d0) then
            print *, 'negative conc. i=', i
        end if
    end do
    if(MOD(K,10).eq.0) then
    glyg=fluxrate(5,8)-fluxrate(5,7)
    gng=fluxrate(5,5)/2.0-fluxrate(5,2)
    write(7,60) t, UR(1:7,1:9)
    write(8,60) t,UR(3,1)+UR(2,1)+UR(1,1)+UR(4,1)+UR(6,1)+UR(7,1)
   1           ,-UR(5,1)
    write(9,60) t, Ca(1:7), glyg, gng, gng/(glyg+gng)
   1          ,fluxrate(5,8), fluxrate(5,5)/2.0
    write(10,60) t, UR(1:7,8)*22.4,SUM(UR(1:7,8)*22.4)
   1          ,UR(1:7,9)*22.4,SUM(UR(1:7,9)*22.4)
   1          ,-SUM(UR(1:7,9)*22.4)/SUM(UR(1:7,8)*22.4)
    write(11,60) t, y1(:)
```

```
    write(12,60) t, y2(:)
    write(13,60) t, y3(:)
    write(14,60) t, y4(:)
    write(15,60) t, y5(:)
    write(16,60) t, y6(:)
    write(17,60) t0, fluxrate(3,:)
    write(18,60) t0, y(133), y(134), y(133)/y(134)
    write(19,60) t, Cv(3,:)
    end if
 10    END DO

 40 stop
!ERROR CONDITIONS
 50 format(///22h error halt.. istate =,i3)

!OUTPUT TIME AND Y
 60    format(116F15.4)
!OUTPUT FLUXES
 70    format(111f8.4)
 80    format(2f8.2)
    end

    subroutine fex(n,t,y,ydot)
    double precision t, ydot, y, tv
    double precision y1(22), y2(22), y3(22), y4(22), y5(22), y6(22)
    double precision P, U, F, Q, UR, Ca, MR, V,GIR
    Common /tests/P(7,22),U(7,22),Q(7),UR(7,22),Ca(22),MR(7),Cp(22)
   1             ,V(7,22),GIR,tv
    Dimension y(134), ydot(134)
    Integer n,i

    y1(1:22)=y(1:22)
    y2(1:22)=y(23:44)
    y3(1:22)=y(45:66)
    y4(1:22)=y(67:88)
    y5(1:22)=y(89:110)
    y6(1:22)=y(111:132)

    GIR=y(133)/y(134)-0.5336

    if(Ca(1).lt.2.5) then
        phi=1.0
        psi=0.0
    else if((Ca(1).gt.2.5).and.(Ca(1).lt.7.5)) then
        phi=1.0-(Ca(1)-2.5)**2.0/25.0
        psi=1.0-(Ca(1)-7.5)**2.0/25.0
    else
        phi=0.0
        psi=1.0
    end if

    call brain(y1)
    call heart(y2)
    call muscle(y3)
    call gi(y4)
```

```
     Cp(1:3) = (Q(4)*(Ca(1:3) - UR(4,1:3)/Q(4))+Q(5)*Ca(1:3))
    1            /(Q(4)+Q(5))
     Cp(4) = Ca(4)
     Cp(5:7) = (Q(4)*(Ca(5:7) - UR(4,5:7)/Q(4))+Q(5)*Ca(5:7))
    1            /(Q(4)+Q(5))
     Cp(8:9) = (Q(4)*(Ca(8:9) - UR(4,8:9)/Q(4))+Q(5)*Ca(8:9))
    1            /(Q(4)+Q(5))
     Cp(10:22) = Ca(10:22)

     call liver(y5)
     call adipose(y6)

     do i=1,6
     ydot((1+22*(i-1)):(22*i)) = (P(i,1:22)-U(i,1:22)+UR(i,1:22))
    1                            /V(i,1:22)
     end do

     ydot(133)=y(133)*(phi*(0.1333-0.2707*(y(133)-25.48)
    1    -0.0535*(y(134)-47.75))-0.1)
     if(tv.ge.10.0) then
         ydot(134)=y(134)*(psi*(0.1333-0.1507*(y(133)-25.48)
    1    -0.0309*(y(134)-47.75))-0.1)-0.7002*1100*(1.0-dexp((t-10)/30))
    2     /(0.0762+1100*(1.0-dexp((t-10)/30)))
     else
         ydot(134)=y(134)*(psi*(0.1333-0.1507*(y(133)-25.48)
    1    -0.0309*(y(134)-47.75))-0.1)
     end if

     return
     end

!FUNCTION CALL 1 - BRAIN COMPARTMENT
     subroutine brain(y)
     double precision y(22), ptemp(22), utemp(22),tv
     double precision P, U, F, Q, UR, Ca, MR, V,GIR
     Common /tests/P(7,22),U(7,22),Q(7),UR(7,22),Ca(22),MR(7),Cp(22)
    1             ,V(7,22),GIR,tv
     Double Precision, Dimension(25) :: Vmax
     Double Precision, Dimension(22) :: s
     Double Precision, Dimension(26) :: Km

     Vmax(1) = 0.794
     Vmax(2) = 1.52
     Vmax(3) = 12.16
     Vmax(4) = 0.0
     Vmax(5) = 0.0
     Vmax(6) = 0.0
     Vmax(7) = 0.012
     Vmax(8) = 0.024
     Vmax(9) = 2.8
     Vmax(10) = 2.8
     Vmax(11) = 0.0
     Vmax(12) = 0.0
     Vmax(13) = 0.0
     Vmax(14) = 0.0
     Vmax(15) = 0.0
     Vmax(16) = 6.08
```

```
    Vmax(17) = 0.0
    Vmax(18) = 0.0
    Vmax(19) = 0.0
    Vmax(20) = 0.0
    Vmax(21) = 12.16
    Vmax(22) = 18.713
    Vmax(23) = 7.44
    Vmax(24) = 7.44
    Vmax(25) = MR(1)*2.0

!Km VALUES
    Km(1) = 0.05                                        !GLC
    Km(2) = 0.154                                       !PYR
    Km(3) = 1.45                                        !LAC
    Km(4) = 0.1                                         !ALA
    Km(5) = 0.1                                         !GLR
    Km(6) = 0.1                                         !FA
    Km(7) = 0.1                                         !TGL
    Km(8) = 7.0d-4                                      !O2
    Km(9) = 15.43                                       !CO2
    Km(10) = 0.16                                       !G6P
    Km(11) = 2.0                                        !GLY
    Km(12) = 0.154                                      !GAP
    Km(13) = 0.1                                        !GRP
    Km(14) = 0.0068                                     !ACoA
    Km(15) = 0.0604                                     !CoA
    Km(16) = 0.064                                      !NAD+
    Km(17) = 0.026                                      !NADH
    Km(18) = 2.45                                       !ATP
    Km(19) = 0.536                                      !ADP
    Km(20) = 2.40                                       !Pi
    Km(21) = 4.60                                       !PCR
    Km(22) = 5.60                                       !CR
    Km(23) = Km(16)/Km(17)                              !NAD/NADH
    Km(24) = Km(17)/Km(16)                              !NADH/NAD
    Km(25) = Km(18)/Km(19)                              !ATP/ADP
    Km(26) = Km(19)/Km(18)                              !ADP/ATP

    call flux(y,Vmax,Km,ptemp,utemp,1)
    P(1,1:22)=ptemp(1:22)
    U(1,1:22)=utemp(1:22)

! Partition coefficients
    s(1) = 4.0119                                           !GLC
    s(2) = 0.4416                                           !PYR
    s(3) = 0.4828                                           !LAC
    s(4) = 0.0                                              !ALA
    s(5) = 0.0                                              !GLR
    s(6) = 0.0                                              !FA
    s(7) = 0.0                                              !TGL
    s(8) = 183.704                                          !O2
    s(9) = 1.6034                                           !CO2
    s(10:22) = 0.0

! Effective Volumes
    V(1,1:9)=0.93*1.49 + s(1:9)*0.07*1.49
    V(1,10:22)=0.8*1.49
```

```
! Uptake/Release rates
    UR(1,1) = Q(1) * (Ca(1) - s(1)*y(1))
    UR(1,2) = Q(1) * (Ca(2) - s(2)*y(2))
    UR(1,3) = Q(1) * (Ca(3) - s(3)*y(3))
    UR(1,4:7) = 0.0
    UR(1,8) = Q(1) * (Ca(8) - s(8)*y(8))
    UR(1,9) = Q(1) * (Ca(9) - s(9)*y(9))
    UR(1,10:22) = 0.0

    return
    end

!FUNCTION CALL 2 - HEART COMPARTMENT
    subroutine heart(y)
    double precision y(22), ptemp(22), utemp(22), tv
    double precision P, U, F, Q, UR, Ca, MR, V,GIR,WR
    Common /tests/P(7,22),U(7,22),Q(7),UR(7,22),Ca(22),MR(7),Cp(22)
   1             ,V(7,22),GIR,tv,epi
    Double Precision, Dimension(25) :: Vmax
    Double Precision, Dimension(22) :: s
    Double Precision, Dimension(26) :: Km

    WR=1.0+3.0*epi**2.0/(1.0d6+epi**2.0)
    Vmax(1) = 0.088
    Vmax(2) = 0.16
    Vmax(3) = 1.28
    Vmax(4) = 0.0
    Vmax(5) = 0.0
    Vmax(6) = 0.0
    Vmax(7) = 0.16
    Vmax(8) = 0.16*2.0
    Vmax(9) = 0.352
    Vmax(10) = 0.512
    Vmax(11) = 0.016
    Vmax(12) = 0.0
    Vmax(13) = 0.0
    Vmax(14) = 0.0
    Vmax(15) = 0.0
    Vmax(16) = 0.96
    Vmax(17) = 0.28
    Vmax(18) = 0.0
    Vmax(19) = 0.008
    Vmax(20) = 0.096
    Vmax(21) = 6.4
    Vmax(22) = 9.327
    Vmax(23) = 8.0
    Vmax(24) = 8.0
    Vmax(25) = MR(2)*2.0

    if(tv.ge.10.0) then
        Vmax(1)=Vmax(1)*WR
        Vmax(2:3)=Vmax(2:3)*3.0
        Vmax(8)=Vmax(8)*3.0
        Vmax(16)=Vmax(16)*3.0
        Vmax(17)=Vmax(17)*(1.0+2.0*epi**2.0/(1.0d6+epi**2.0))
```

```
        Vmax(19)=Vmax(19)*(1.0+0.5*epi**2.0/(1.0d6+epi**2.0))
        Vmax(21)=Vmax(21)*3.0
        Vmax(22)=Vmax(22)*3.0
    end if

!Km VALUES
    Km(1) = 0.1                                              !GLC
    Km(2) = 0.2                                              !PYR
    Km(3) = 3.88                                             !LAC
    Km(4) = 0.1                                              !ALA
    Km(5) = 0.015                                            !GLR
    Km(6) = 0.021                                            !FA
    Km(7) = 3.12                                             !TGL
    Km(8) = 7.0d-4                                           !O2
    Km(9) = 20.00                                            !CO2
    Km(10) = 0.171                                           !G6P
    Km(11) = 33.0                                            !GLY
    Km(12) = 0.01                                            !GAP
    Km(13) = 0.29                                            !GRP
    Km(14) = 0.0012                                          !ACoA
    Km(15) = 0.012                                           !CoA
    Km(16) = 0.4                                             !NAD+
    Km(17) = 0.045                                           !NADH
    Km(18) = 3.4                                             !ATP
    Km(19) = 0.02                                            !ADP
    Km(20) = 1.66                                            !Pi
    Km(21) = 8.3                                             !PCR
    Km(22) = 3.5                                             !CR
    Km(23) = Km(16)/Km(17)                                   !NAD/NADH
    Km(24) = Km(17)/Km(16)                                   !NADH/NAD
    Km(25) = Km(18)/Km(19)                                   !ATP/ADP
    Km(26) = Km(19)/Km(18)                                   !ADP/ATP

    call flux(y,Vmax,Km,ptemp,utemp,2)
    P(2,1:22)=ptemp(1:22)
    U(2,1:22)=utemp(1:22)

! Partition coefficients
    s(1) = 4.84                                              !GLC
    s(2) = 0.34                                              !PYR
    s(3) = 0.1392                                            !LAC
    s(4) = 0.0                                               !ALA
    s(5) = 4.6667                                            !GLR
    s(6) = 24.7619                                           !FA
    s(7) = 0.3173                                            !TGL
    s(8) = 3.4683                                            !O2
    s(9) = 1.269                                             !CO2
    s(10:22) = 0.0

! Effective Volumes
    V(2,1:9)=0.93*0.25 + s(1:9)*0.07*0.25
    V(2,10:22)=0.8*0.25

! Uptake/Release rates
    UR(2,1) = Q(2) * (Ca(1) - s(1)*y(1))
    UR(2,2) = Q(2) * (Ca(2) - s(2)*y(2))
    UR(2,3) = Q(2) * (Ca(3) - s(3)*y(3))
```

```
    UR(2,4) = 0.0
    UR(2,5) = Q(2) * (Ca(5) - s(5)*y(5))
    UR(2,6) = Q(2) * (Ca(6) - s(6)*y(6))
    UR(2,7) = 0.0
    UR(2,8) = Q(2) * (Ca(8) - s(8)*y(8))
    UR(2,9) = Q(2) * (Ca(9) - s(9)*y(9))
    UR(2,10:22) = 0.0
    !
    return
    end

!FUNCTION CALL 3 - MUSCLE COMPARTMENT
    subroutine muscle(y)
    double precision y(22), ptemp(22), utemp(22), tv,RMR
    double precision P, U, F, Q, UR, Ca, MR, V,GIR,WR,glyf
    Common /tests/P(7,22),U(7,22),Q(7),UR(7,22),Ca(22),MR(7),Cp(22)
   1             ,V(7,22),GIR,tv,epi,RMR
        Double Precision, Dimension(25) :: Vmax
    Double Precision, Dimension(22) :: s
    Double Precision, Dimension(26) :: Km

    Vmax(1) = 0.398
    Vmax(2) = 0.66
    Vmax(3) = 5.28
    Vmax(4) = 0.0
    Vmax(5) = 0.0
    Vmax(6) = 0.0
    Vmax(7) = 0.5
    Vmax(8) = 0.5*2.0
    Vmax(9) = 174.8387*0.5/0.9091
    Vmax(10) = 253.2427
    Vmax(11) = 0.508
    Vmax(12) = 0.0
    Vmax(13) = 0.0
    Vmax(14) = 0.08
    Vmax(15) = 0.0
    Vmax(16) = 1.3459
    Vmax(17) = 0.44
    Vmax(18) = 0.0
    Vmax(19) = 0.26
    Vmax(20) = 3.048
    Vmax(21) = 9.968
    Vmax(22) = 14.6769
    Vmax(23) = 600.0
    Vmax(24) = 600.0
    Vmax(25) = MR(3)*2.0


    IF(tv.ge.10.00) then
        Vmax(1)=Vmax(1)*(1.0+18.0*epi**2.0/(1.0d6+epi**2.0))
        Vmax(2)=Vmax(2)*RMR
        Vmax(3)=Vmax(3)*RMR
        Vmax(8)=Vmax(8)*RMR/8.0*(1.0+9.0*epi**2.0/(1.0d3+epi**2.0))
        Vmax(14)=Vmax(14)*(1.0+2.0*epi**2.0/(1.0d6+epi**2.0))
        Vmax(16)=Vmax(16)*RMR
        Vmax(17)=Vmax(17)*(1.0+8.0*epi**2.0/(1.0d5+epi**2.0))
        Vmax(19)=Vmax(19)*(1.0+2.5*epi**2.0/(1.0d6+epi**2.0))
```

```
        Vmax(21)=Vmax(21)*RMR !(1.0+39.0*(1.0-dexp(-(tv-10.0)/0.2)))
        Vmax(22)=Vmax(22)*RMR !(1.0+39.0*(1.0-dexp(-(tv-10.0)/0.2)))
    end if

!Km VALUES
    Km(1) = 0.1                                     !GLC
    Km(2) = 0.0775                                  !PYR
    Km(3) = 1.44                                    !LAC
    Km(4) = 1.3                                     !ALA
    Km(5) = 0.064                                   !GLR
    Km(6) = 0.53                                    !FA
    Km(7) = 14.8                                    !TGL
    Km(8) = 7.0d-4                                  !O2
    Km(9) = 15.43                                   !CO2
    Km(10) = 0.24                                   !G6P
    Km(11) = 95.0                                   !GLY
    Km(12) = 0.08                                   !GAP
    Km(13) = 0.147                                  !GRP
    Km(14) = 0.00223                                !ACoA
    Km(15) = 0.0183                                 !CoA
    Km(16) = 0.45                                   !NAD+
    Km(17) = 0.05                                   !NADH
    Km(18) = 6.15                                   !ATP
    Km(19) = 0.02                                   !ADP
    Km(20) = 2.70                                   !Pi
    Km(21) = 20.1                                   !PCR
    Km(22) = 10.45                                  !CR
    Km(23) = Km(16)/Km(17)                          !NAD/NADH
    Km(24) = Km(17)/Km(16)                          !NADH/NAD
    Km(25) = Km(18)/Km(19)                          !ATP/ADP
    Km(26) = Km(19)/Km(18)                          !ADP/ATP

    call flux(y,Vmax,Km,ptemp,utemp,3)
    P(3,1:22)=ptemp(1:22)
    U(3,1:22)=utemp(1:22)

! Partition coefficients
    s(1) = 9.9313                                                   !GLC
    s(2) = 0.8057                                                   !PYR
    s(3) = 0.5725                                                   !LAC
    s(4) = 0.2265                                                   !ALA
    s(5) = 1.1458                                                   !GLR
    s(6) = 1.1488                                                   !FA
    s(7) = 0.0667                                                   !TGL
    s(8) = 12.1723                                                  !O2
    s(9) = 1.5092                                                   !CO2
    s(10:22) = 0.0

! Effective Volumes
    V(3,1:9)=0.93*20.0 + s(1:9)*0.07*20.0
    V(3,10:22)=0.8*20.0

!Uptake/Release rates
    UR(3,1) = Q(3) * (Ca(1) - s(1)*y(1))
    UR(3,2) = Q(3) * (Ca(2) - s(2)*y(2))
    UR(3,3) = Q(3) * (Ca(3) - s(3)*y(3))
    UR(3,4) = Q(3) * (Ca(4) - s(4)*y(4))
```

```
    UR(3,5) = Q(3) * (Ca(5) - s(5)*y(5))
    UR(3,6) = Q(3) * (Ca(6) - s(6)*y(6))
    UR(3,7) = Q(3) * (Ca(7) - s(7)*y(7))
    UR(3,8) = Q(3) * (Ca(8) - s(8)*y(8))
    UR(3,9) = Q(3) * (Ca(9) - s(9)*y(9))
    UR(3,10:22) = 0.0

    return
    end

!FUNCTION CALL 4 - GI COMPARTMENT
    subroutine gi(y)
    double precision y(22), ptemp(22), utemp(22),tv
    double precision P, U, F, Q, UR, Ca, MR, V,GIR,epi,RMR
    Common /tests/P(7,22),U(7,22),Q(7),UR(7,22),Ca(22),MR(7),Cp(22)
   1             ,V(7,22),GIR,tv,epi,RMR
    Double Precision, Dimension(25) :: Vmax
    Double Precision, Dimension(22) :: s
    Double Precision, Dimension(26) :: Km

    Vmax(1) = 0.167
    Vmax(2) = 0.304
    Vmax(3) = 2.432
    Vmax(4) = 0.0
    Vmax(5) = 0.0
    Vmax(6) = 0.0
    Vmax(7) = 0.0
    Vmax(8) = 0.0
    Vmax(9) = 0.8
    Vmax(10) = 0.8
    Vmax(11) = 0.0
    Vmax(12) = 0.0
    Vmax(13) = 0.0
    Vmax(14) = 0.0
    Vmax(15) = 0.0
    Vmax(16) = 1.216
    Vmax(17) = 0.0
    Vmax(18) = 0.0
    Vmax(19) = 0.08
    Vmax(20) = 0.0
    Vmax(21) = 2.432
    Vmax(22) = 3.653
    Vmax(23) = 8.0
    Vmax(24) = 8.0
    Vmax(25) = MR(4)*2.0

    if(tv.ge.10.0) then
        Vmax(19)=Vmax(19)*(1.0+1.0*GIR**2.0/(0.07+GIR**2.0))
    end if

!Km VALUES
    Km(1) = 0.1                                                !GLC
    Km(2) = 0.2                                                !PYR
    Km(3) = 3.88                                               !LAC
    Km(4) = 0.1                                                !ALA
    Km(5) = 0.015                                              !GLR
    Km(6) = 0.021                                              !FA
```

```
    Km(7) = 990.0                                          !TGL
    Km(8) = 7.0d-4                                         !O2
    Km(9) = 15.43                                          !CO2
    Km(10) = 0.171                                         !G6P
    Km(11) = 33.0                                          !GLY
    Km(12) = 0.01                                          !GAP
    Km(13) = 0.29                                          !GRP
    Km(14) = 0.0012                                        !ACoA
    Km(15) = 0.012                                         !CoA
    Km(16) = 0.4                                           !NAD+
    Km(17) = 0.045                                         !NADH
    Km(18) = 3.4                                           !ATP
    Km(19) = 0.02                                          !ADP
    Km(20) = 1.66                                          !Pi
    Km(21) = 8.3                                           !PCR
    Km(22) = 3.5                                           !CR
    Km(23) = Km(16)/Km(17)                                 !NAD/NADH
    Km(24) = Km(17)/Km(16)                                 !NADH/NAD
    Km(25) = Km(18)/Km(19)                                 !ATP/ADP
    Km(26) = Km(19)/Km(18)                                 !ADP/ATP

    call flux(y,Vmax,Km,ptemp,utemp,4)
    P(4,1:22)=ptemp(1:22)
    U(4,1:22)=utemp(1:22)

!Blood/tissue partition coefficients
    s(1) = 4.9309                                              !GLC
    s(2) = 0.34                                                !PYR
    s(3) = 0.1804                                              !LAC
    s(4) = 0.0                                                 !ALA
    s(5) = 7.0909                                              !GLR
    s(6) = 36.6234                                             !FA
    s(7) = 0.000994                                            !TGL
    s(8) = 15.4805                                             !O2
    s(9) = 1.4332                                              !CO2
    s(10:22) = 0.0

! Effective Volumes
    V(4,1:9)=0.93*1.0 + s(1:9)*0.07*1.0
    V(4,10:22)=0.8*1.0

!Uptake/Release rates
    UR(4,1) = Q(4) * (Ca(1) - s(1)*y(1))
    UR(4,2) = Q(4) * (Ca(2) - s(2)*y(2))
    UR(4,3) = Q(4) * (Ca(3) - s(3)*y(3))
    UR(4,4) = 0.0
    UR(4,5) = Q(4) * (Ca(5) - s(5)*y(5))
    UR(4,6) = Q(4) * (Ca(6) - s(6)*y(6))
    UR(4,7) = Q(4) * (Ca(7) - s(7)*y(7))
    UR(4,8) = Q(4) * (Ca(8) - s(8)*y(8))
    UR(4,9) = Q(4) * (Ca(9) - s(9)*y(9))
    UR(4,10:22) = 0.0

    return
    end

!FUNCTION CALL 5 - LIVER COMPARTMENT
```

```
      subroutine liver(y)
      double precision y(22), ptemp(22), utemp(22),tv
      double precision P, U, F, Q, UR, Ca, MR, V,GIR
      Common /tests/P(7,22),U(7,22),Q(7),UR(7,22),Ca(22),MR(7),Cp(22)
     1             ,V(7,22),GIR,tv
      Double Precision, Dimension(25) :: Vmax
      Double Precision, Dimension(22) :: s
      Double Precision, Dimension(26) :: Km

      Vmax(1) = 0.765
      Vmax(2) = 0.68
      Vmax(3) = 5.44
      Vmax(4) = 7.44
      Vmax(5) = 2.082
      Vmax(6) = 1.802
      Vmax(7) = 0.4
      Vmax(8) = 1.92*2.0
      Vmax(9) = 0.84
      Vmax(10) = 1.92
      Vmax(11) = 0.576
      Vmax(12) = 0.0
      Vmax(13) = 0.444
      Vmax(14) = 0.0
      Vmax(15) = 0.64
      Vmax(16) = 0.0
      Vmax(17) = 1.088
      Vmax(18) = 0.896
      Vmax(19) = 0.008
      Vmax(20) = 0.8
      Vmax(21) = 15.616
      Vmax(22) = 22.176
      Vmax(23) = 0.0
      Vmax(24) = 0.0
      Vmax(25) = MR(5)*2.0

      if(tv.ge.10.0) then
      Vmax(4)=Vmax(4)*(1.0+GIR**2.0/(0.07+GIR**2.0))
      Vmax(5)=Vmax(5)*(1.0+0.5*GIR**2.0/(0.07+GIR**2.0))
      Vmax(6)=Vmax(6)*(1.0+0.5*GIR**2.0/(0.07+GIR**2.0))
      Vmax(8)=Vmax(8)*(1.0+3.0*GIR**2.0/(0.07+GIR**2.0))
      Vmax(15)=Vmax(15)*(1.0+GIR**2.0/(0.07+GIR**2.0))
      end if

!Km VALUES
      Km(1) = 10.0                                              !GLC
      Km(2) = 0.37                                              !PYR
      Km(3) = 0.82                                              !LAC
      Km(4) = 0.227                                             !ALA
      Km(5) = 0.07                                              !GLR
      Km(6) = 0.570                                             !FA
      Km(7) = 2.93                                              !TGL
      Km(8) = 7.0d-4                                            !O2
      Km(9) = 15.43                                             !CO2
      Km(10) = 0.2                                              !G6P
      Km(11) = 417                                              !GLY
      Km(12) = 0.108                                            !GAP
      Km(13) = 0.24                                             !GRP
```

```
    Km(14) = 0.035                                          !ACoA
    Km(15) = 0.14                                           !CoA
    Km(16) = 0.45                                           !NAD+
    Km(17) = 0.05                                           !NADH
    Km(18) = 2.74                                           !ATP
    Km(19) = 1.22                                           !ADP
    Km(20) = 4.60                                           !Pi
    Km(21) = 0.1                                            !PCR
    Km(22) = 0.1                                            !CR
    Km(23) = Km(16)/Km(17)                                  !NAD/NADH
    Km(24) = Km(17)/Km(16)                                  !NADH/NAD
    Km(25) = Km(18)/Km(19)                                  !ATP/ADP
    Km(26) = Km(19)/Km(18)                                  !ADP/ATP    !

    call flux(y,Vmax,Km,ptemp,utemp,5)
    P(5,1:22)=ptemp(1:22)
    U(5,1:22)=utemp(1:22)

!Blood/tissue partition coefficients
    s(1) = 0.6796                                               !GLC
    s(2) = 0.1838                                               !PYR
    s(3) = 0.6341                                               !LAC
    s(4) = 0.1615                                               !ALA
    s(5) = 0.0481                                               !GLR
    s(6) = 1.0526                                               !FA
    s(7) = 0.3430                                               !TGL
    s(8) = 218.321                                              !O2
    s(9) = 1.5104                                               !CO2
    s(10:22) = 0.0

! Effective Volumes
    V(5,1:9)=0.93*1.5 + s(1:9)*0.07*1.5
    V(5,10:22)=0.8*1.5

!Uptake/Release rates
    UR(5,1:9) = (Q(4)+Q(5))*(Cp(1:9) - s(1:9)*y(1:9))
    UR(5,10:22) = 0.0

    return
    end

!FUNCTION CALL 6 - ADIPOSE TISSUE COMPARTMENT
    subroutine adipose(y)
    double precision y(22), ptemp(22), utemp(22),tv
    double precision P, U, F, Q, UR, Ca, MR, V,GIR,epi,RMR
    Common /tests/P(7,22),U(7,22),Q(7),UR(7,22),Ca(22),MR(7),Cp(22)
   1             ,V(7,22),GIR,tv,epi,RMR
    Double Precision, Dimension(25) :: Vmax
    Double Precision, Dimension(22) :: s
    Double Precision, Dimension(26) :: Km

    Vmax(1) = 0.079
    Vmax(2) = 0.152
    Vmax(3) = 0.896
    Vmax(4) = 0.0
    Vmax(5) = 0.0
```

```
    Vmax(6) = 0.0
    Vmax(7) = 0.0
    Vmax(8) = 0.0
    Vmax(9) = 0.144
    Vmax(10) = 0.04
    Vmax(11) = 0.0
    Vmax(12) = 0.08
    Vmax(13) = 0.0
    Vmax(14) = 0.0
    Vmax(15) = 0.0
    Vmax(16) = 0.24
    Vmax(17) = 0.160
    Vmax(18) = 0.0
    Vmax(19) = 0.194
    Vmax(20) = 0.480
    Vmax(21) = 1.28
    Vmax(22) = 2.052
    Vmax(23) = 0.0
    Vmax(24) = 0.0
    Vmax(25) = MR(6)*2.0
    if(tv.ge.10.0) then
    Vmax(19) = Vmax(19)*(1.0+4.0*GIR**2.0/(0.07+GIR**2.0))
    end if

!Km VALUES
    Km(1) = 0.1                                          !GLC
    Km(2) = 0.37                                         !PYR
    Km(3) = 0.82                                         !LAC
    Km(4) = 0.1                                          !ALA
    Km(5) = 0.22                                         !GLR
    Km(6) = 0.57                                         !FA
    Km(7) = 990.0                                        !TGL
    Km(8) = 7.0d-4                                       !O2
    Km(9) = 15.43                                        !CO2
    Km(10) = 0.2                                         !G6P
    Km(11) = 0.1                                         !GLY
    Km(12) = 0.108                                       !GAP
    Km(13) = 0.24                                        !GRP
    Km(14) = 0.035                                       !ACoA
    Km(15) = 0.14                                        !CoA
    Km(16) = 0.45                                        !NAD+
    Km(17) = 0.05                                        !NADH
    Km(18) = 2.74                                        !ATP
    Km(19) = 1.22                                        !ADP
    Km(20) = 4.60                                        !Pi
    Km(21) = 0.1                                         !PCR
    Km(22) = 0.1                                         !CR
    Km(23) = Km(16)/Km(17)                               !NAD/NADH
    Km(24) = Km(17)/Km(16)                               !NADH/NAD
    Km(25) = Km(18)/Km(19)                               !ATP/ADP
    Km(26) = Km(19)/Km(18)                               !ADP/ATP

    call flux(y,Vmax,Km,ptemp,utemp,6)
    P(6,1:22)=ptemp(1:22)
    U(6,1:22)=utemp(1:22)

!Blood/tissue partition coefficients
```

```
    s(1) = 1.9269                                                    !GLC
    s(2) = 0.1838                                                    !PYR
    s(3) = 0.9417                                                    !LAC
    s(4) = 0.0                                                       !ALA
    s(5) = 1.5429                                                    !GLR
    s(6) = 2.2349                                                    !FA
    s(7) = 0.000944                                                  !TGL
    s(8) = 270.5761                                                  !O2
    s(9) = 1.4406                                                    !CO2
    s(10:22) = 0.0

! Effective Volumes
    V(6,1:9)=0.93*12.0 + s(1:9)*0.07*12.0
    V(6,10:22)=0.8*12.0

!Uptake/Release terms
    UR(6,1) = Q(6) * (Ca(1) - s(1)*y(1))
    UR(6,2) = Q(6) * (Ca(2) - s(2)*y(2))
    UR(6,3) = Q(6) * (Ca(3) - s(3)*y(3))
    UR(6,4) = 0.0
    UR(6,5) = Q(6) * (Ca(5) - s(5)*y(5))
    UR(6,6) = Q(6) * (Ca(6) - s(6)*y(6))
    UR(6,7) = Q(6) * (Ca(7) - s(7)*y(7))
    UR(6,8) = Q(6) * (Ca(8) - s(8)*y(8))
    UR(6,9) = Q(6) * (Ca(9) - s(9)*y(9))
    UR(6,10:22) = 0.0

    return
    end

!JACOBIAN CALL
      subroutine jex(neq, t, y, j, ia, ja, pdj)
      return
      end

!DFLOAT FUNCTION
      FUNCTION DFLOAT(I)
      IMPLICIT DOUBLE PRECISION(A-H,O-Z)
      DFLOAT=DBLE(FLOAT(I))
      RETURN
      END

! FUNCTION CALL to Flux Rate Equations
    subroutine flux(y,Vmax,Km,P,U,tid)
    double precision y(22),Vmax(25),Km(26),F(25),P(22),U(22)
    double precision rs(2),ps(2),fluxrate,k1,k2
    common/fx/ fluxrate(7,25)
    integer tid

    rs(1) = y(16)/y(17)/(Km(23)+y(16)/y(17))
    rs(2) = y(17)/y(16)/(Km(24)+y(17)/y(16))
    ps(1) = y(18)/y(19)/(Km(25)+y(18)/y(19))
    ps(2) = y(19)/y(18)/(Km(26)+y(19)/y(18))

!FLUX VALUES
!   Flux =Vmax*[Ci/(Km + Ci)][(Ci/Cj)/(k + Ci/Cj)]
```

```
!   Control is based on Michaelis-Menten kinetics
!   of energy transfer components according to the MIMS format.
    F(1) = Vmax(1)*y(1)/Km(1)/(1.0+y(1)/Km(1))*ps(1)
    F(2) = Vmax(2)*y(10)/(Km(10)+y(10))*
   1       (y(19)/y(18))**2.0/(Km(26)**2.0+(y(19)/y(18))**2.0)
    F(3) = Vmax(3)*y(12)*y(20)/Km(12)/Km(20)
   1    /(1.0+y(12)/Km(12)+y(20)/Km(20)+y(12)*y(20)/Km(12)/Km(20))
   1        *rs(1)*ps(2)
    F(4) = Vmax(4)*y(2)/(Km(2)+y(2))*rs(2)*ps(1)
    F(5) = Vmax(5)*y(12)/(Km(12)+y(12))
    F(6) = Vmax(6)*y(10)/(Km(10)+y(10))
    F(7) = Vmax(7)*y(10)/(Km(10)+y(10))*ps(1)
    F(8) = Vmax(8)*y(11)*y(20)/Km(11)/Km(20)
   1    /(1.0+y(11)/Km(11)+y(20)/Km(20)+y(11)*y(20)/Km(11)/Km(20))
    F(8)=F(8)*(y(19)/y(18))**2.0/(Km(26)**2.0+(y(19)/y(18))**2.0)
    k1=0.6
    k2=0.008

    if(tid.eq.3) then
        F(9) = Vmax(9)*y(2)/(0.6+y(2))
   1        *y(17)/y(16)/(Km(24)*0.1+y(17)/y(16))
        F(10) = Vmax(10)*y(3)/(17.0+y(3))
   1        *y(16)/y(17)/(Km(23)+y(16)/y(17))
        F(16) = Vmax(16)*y(2)*y(15)/0.065/Km(15)
   1    /(1.0+y(2)/0.065+y(15)/Km(15)+y(2)*y(15)/0.065/Km(15))
   1        *y(16)/y(17)/(Km(23)+y(16)/y(17))
    else
        F(9) = Vmax(9)*y(2)/(Km(2)+y(2))*rs(2)
        F(10) = Vmax(10)*y(3)/(Km(3)+y(3))*rs(1)
        F(16) = Vmax(16)*y(2)*y(15)/Km(2)/Km(15)
   1    /(1.0+y(2)/Km(2)+y(15)/Km(15)+y(2)*y(15)/Km(2)/Km(15))
   1        *rs(1)
    end if

    F(11) = Vmax(11)*y(5)/(Km(5)+y(5))*ps(1)
    F(12) = Vmax(12)*y(12)/(Km(12)+y(12))*rs(2)
    F(13) = Vmax(13)*y(13)/(Km(13)+y(13))*rs(1)
    F(14) = Vmax(14)*y(2)/(Km(2)+y(2))
    F(15) = Vmax(15)*y(4)/(Km(4)+y(4))
    F(17) = Vmax(17)*y(6)*y(15)/Km(6)/Km(15)*rs(1)
   1    /(1.0+y(6)/Km(6)+y(15)/Km(15)+y(6)*y(15)/Km(6)/Km(15))
    F(18) = Vmax(18)*y(14)/(Km(14)+y(14))*rs(2)*ps(1)
    F(19) = Vmax(19)*y(7)/(Km(7)+y(7))
    F(20) = Vmax(20)*y(13)*y(6)/Km(13)/Km(6)
   1    /(1.0+y(6)/Km(6)+y(13)/Km(13)+y(6)*y(13)/Km(6)/Km(13))
   1        *ps(1)
    F(21) = Vmax(21)*y(14)*y(20)/Km(14)/Km(20)
   1    /(1.0+y(14)/Km(14)+y(20)/Km(20)+y(14)*y(20)/Km(14)/Km(20))
   1        *rs(1)*ps(2)
    F(22) = Vmax(22)*y(8)*y(20)/Km(8)/Km(20)
   1    /(1.0+y(8)/Km(8)+y(20)/Km(20)+y(8)*y(20)/Km(8)/Km(20))
   1        *rs(2)*ps(2)
    F(23) = Vmax(23)*y(21)/(Km(21)+y(21))*ps(2)
    F(24) = Vmax(24)*y(22)/(Km(22)+y(22))*ps(1)
    F(25) = Vmax(25)*y(18)/(Km(18)+y(18))
```

```
!SUBSTRATE PRODUCTION
    P(1) = F(6)
    P(2) = F(3) + F(10) + F(15)
    P(3) = F(9)
    P(4) = F(14)
    P(5) = F(19)
    P(6) = 3.0*F(19) + F(18)/8.0
    P(7) = F(20)/3.0
    P(8) = 0.0
    P(9) = F(16) + 2.0*F(21)
    P(10) = F(1) + F(8) + F(5)/2.0
    P(11) = F(7)
    P(12) = 2.0*F(2) + F(4) + F(13)
    P(13) = F(11)+F(12)
    P(14) = F(16) + 8.0*F(17)
    P(15) = F(21) + F(18)
    P(16) = F(4) + F(9) + 2.0*F(22) + F(12) + 14.0*F(18)/8.0
    P(17) = F(3) + F(10) + F(16) + 4.0*F(21) + 14.0*F(17) + F(13)
    P(18) = 2.0*F(3) + F(21) + 6.0*F(22) + F(23)
    P(19) = F(1) + F(2) + 3.0*F(4) + F(7) + F(11) + 2.0*F(17)
   1            + 7.0*F(18)/8.0 + 2.0*F(20) + F(25) + F(24)
    P(20) = 2.0*F(4) + F(5)/2.0 + F(6) + 2.0*F(7) + 2.0*F(17)
   1        + 7.0*F(18)/8.0 + 7.0/3.0*F(20) + F(25)
    P(21) = F(24)
    P(22) = F(23)

!SUBSTRATE UTILIZATION
    U(1) = F(1)
    U(2) = F(4) + F(9) + F(14) + F(16)
    U(3) = F(10)
    U(4) = F(15)
    U(5) = F(11)
    U(6) = F(17) + F(20)
    U(7) = F(19)
    U(8) = F(22)
    U(9) = 0.0
    U(10) = F(2) + F(6) + F(7)
    U(11) = F(8)
    U(12) = F(3) + F(5) + F(12)
    U(13) = F(13) + F(20)/3.0
    U(14) = F(21) + F(18)
    U(15) = F(16) + 8.0*F(17)
    U(16) = F(3) + F(10) + F(16) + 4.0*F(21) + 14.0*F(17) + F(13)
    U(17) = F(4) + F(9) + 2.0*F(22) + F(12) + 14.0*F(18)/8.0
    U(18) = F(1) + F(2) + 3.0*F(4) + F(7) + F(11) + 2.0*F(17)
   1            + 7.0*F(18)/8.0 + 2.0*F(20) + F(25) + F(24)
    U(19) = 2.0*F(3) + F(21) + 6.0*F(22) + F(23)
    U(20) = F(3) + F(8) + F(21) + 6.0*F(22)
    U(21) = F(23)
    U(22) = F(24)

    fluxrate(tid,1:25)=F(1:25)
    return
```

A-V.2. ADIPOSE TISSUE MODEL FOR INTRAVENOUS EPINEPHRINE INFUSION

The following is the source code (m file) written in MATLAB® in order to simulate the physiological responses in the adipose tissue during intravenous epinephrine infusion. The simulation code utilizes a library from MATLAB®, 'ode15s' to solve a set of ordinary differential equations.

```
%*********************************************************************
% This is the source code for two compartmental model of adipose tissue
% metabolism that is used to simulate the physiological responses
% during intravenous epinephrine infusion.
%*********************************************************************

global URR0 Rflux0 Ca Cb0 Cc0 C0 Cb Cc
global Tmax Mm Lam Vmax Km Kps Krs Ki ...
       CO2bTot CO2cTot SHbO2b O2bTot SMbO2c O2cTot StO2
global V Q UPT REL URR AVD Vvivo Rflux PROD UTIL MRR epi ...
       Vmax0 Tmax0 Lam0
format long

%*********************************************************************
% This section reads mass transport and metabolic reaction fluxes,
% substrate concentration in blood and tissue
% and the kinetic parameters.
%*********************************************************************

Flux0 = zeros(38,1);
URR0 = zeros(9,1);
Rflux0 = zeros(29,1);
Flux0 = dlmread('RestingFluxes.txt');
URR0(1:9) = Flux0(1:9);
Rflux0(1:29) = Flux0(10:38);

Conc0 = zeros(32,1);
Ca = zeros(9,1);
Cb0 = zeros(9,1);
Cc0 = zeros(23,1);
C0  = zeros(32,1);
Conc0 = dlmread('RestingConcentrations.txt');
Ca = Conc0(1:9);
Cc0 = Conc0(10:32);

theta = zeros(113,1);
Mm = zeros(9,1);
Km = zeros(29,1);
Kps = zeros(28,1);
Krs = zeros(28,1);
Ki = zeros(28,1);
theta = dlmread('Parameters.txt');
Kps(1:28)=theta(1:28);
```

```
Krs(1:28)=theta(29:56);
Ki(1:28)=theta(57:84);
Km(1:29)=theta(85:113);

%*********************************************************************
% This section computes the activation factors for Q, V, Tmax, Lam,
% and Vmax.
%*********************************************************************

Q = 0.031;           % Adipose tissue blood flow at fast (l/kg/min)

% Initial values for (venous) blood compartment concentrations
% which can be calculated based on the arterial conc., blood flow and
% uptake-release rate (mass transport flux)

Cb0(1:4)=Ca(1:4)-URR0(1:4)./Q;
Cb0(7:9)=Ca(7:9)-URR0(7:9)./Q;
Cb0(8)=83.3;
Cb0(9)=1247.1;
Cb0(5)=Ca(5)+130;
Cb0(6)=0.58*Ca(6)+336;
%0.58 to convert FFA conc. in plasma to FFA conc. in whole blood

Mm = Cb0;

C0 = [Cb0;Cc0];

[Vmax Tmax Lam]=Adipose_TmaxVmax(Rflux0, URR0, Cb0, Cc0, Km, Ki, ...
                                 Kps,  Krs, Mm, Q);

Cc=Cc0;
Cb=Cb0;
Adipose_Flux;
Vmax0=Vmax;
Tmax0=Tmax;
Lam0=Lam;

%*********************************************************************
% Call to the MATLAB solver,'ODE15S' to solve the stiff system of
% differential equations dC/dt = f(C,t)
%*********************************************************************

% Optimal parameter estimates
p=[0.7165,0.2,0.907,0.2,6.1896,0.2,0.0313;]

Tend=75;
Tspan = [0:0.1:Tend];
options = odeset('RelTol',1e-8, 'AbsTol',1e-8);
[t,C] = ode15s(@Adipose_Cdot_Est,Tspan,C0,options,p);

%*********************************************************************
% Post processing of solutions to create data files and plot figures.
%*********************************************************************

UPT_mat = [];
```

```
REL_mat = [];
URR_mat = [];
AVD_mat = [];
Rflux_mat = [];
PROD_mat = [];
UTIL_mat = [];
MRR_mat = [];
Ca_mat=[];
Cb_mat = [];
Cc_mat = [];
Cbdot_mat=[];
Ccdot_mat=[];
Qrec=[];
epi_rec=[];
Vmax_mat=[];
Vvivo_mat=[];
for j = 1:length(t)
    tj = t(j);
    Cj = C(j,:)';
    [Cdotj] = Adipose_Cdot_Est(tj,Cj,p);
    UPT_mat = [UPT_mat;UPT'];
    REL_mat = [REL_mat;REL'];
    URR_mat = [URR_mat;URR'];
    AVD_mat = [AVD_mat;AVD'];
    Rflux_mat = [Rflux_mat;Rflux'];
    PROD_mat = [PROD_mat;PROD'];
    UTIL_mat = [UTIL_mat;UTIL'];
    MRR_mat = [MRR_mat;MRR'];
    Ca_mat = [Ca_mat; Ca'];
    Cb_mat = [Cb_mat;Cj(1:9)'];
    Cc_mat = [Cc_mat;Cj(10:32)'];
    Cbdot_mat = [Cbdot_mat;Cdotj(1:9)'];
    Ccdot_mat = [Ccdot_mat;Cdotj(10:32)'];
    Qrec = [Qrec; Q];
    epi_rec = [epi_rec; epi];
    Vmax_mat=[Vmax_mat;Vmax'];
    Vvivo_mat=[Vvivo_mat;Vvivo'];
end

%**********************************************************************
% This function computes the new Vmax and Tmax values from the steady
% state uptake-release rates (URR0) and metabolic reaction fluxes with
% the given updated Mm, Km, Kps and Krs values.
% This recalculation of Tmax and Vmax values are important for
% maintaining the resting/steady state conditions.
%**********************************************************************
function [Vmax Tmax Lam]=Adipose_TmaxVmax(Rflux0, URR0, Cb, Cc, Km, Ki,
Kps, Krs, Mm, Q);

format long

%**********************************************************************
% This section computes new Vmax values given the updated Mm, Km, Kps
% and Krs values (passed here through the global statement) and
% resting/steady state conditions (Rflux0 and Cc0 values).
%**********************************************************************
```

```
fact = zeros(29,1);

% Glucose Utilization:  GLC + ATP -> G6P + ADP
ctrl_G6P = 1 / (1 +(Cc(10)/Ki(1)));
fact(1) = ctrl_G6P*Cc(1)*Cc(19)/(Km(1)*(1+Cc(10)/Ki(1))+Cc(1)*Cc(19));

% G6P Breakdown:  G6P + ATP -> 2GA3P + ADP
nH2 = 2;
fact(2) = (Cc(20)/Cc(19))^nH2 / (Kps(2)^nH2 + (Cc(20)/Cc(19))^nH2) ...
          * Cc(10) / (Km(2) + Cc(10));

% GA3P Breakdown:  GA3P + Pi + NAD + 2ADP -> PYR + NADH + 2ATP
nH3=2;
fact(3) = ((Cc(22)/Cc(23)) / (Krs(3) + (Cc(22)/Cc(23))))* ...
        ((Cc(20)/Cc(19))^nH3 / (Kps(3)^nH3 + (Cc(20)/Cc(19))^nH3)) ...
           * Cc(12)*Cc(21) / (Km(3) + Cc(12)*Cc(21));

% Pyruvate Reduction:  PYR + NADH <-> LAC + NAD
fact(4) = (Cc(2) * Cc(23) - Cc(3) * Cc(22) / 1.06e4 ) ...
          / Km(4) / (1+Cc(2)*Cc(23)/Km(4)+Cc(3)*Cc(22)/Ki(4));

% GAP Reduction: GAP + NADH <-> GRP + NAD+
fact(7) = (Cc(12) * Cc(23) - Cc(13)*Cc(22)/ 2.768e8) ...
          / Km(7) / (1+Cc(12)*Cc(23)/Km(7)+Cc(13)*Cc(22)/Ki(7));

% Glyceroneogenesis: PYR + 3ATP + 2NADH -> GR3P + 3ADP + 2NAD + 2Pi
fact(8) = ((Cc(23)/Cc(22)) / (Krs(8) + (Cc(23)/Cc(22))))* ...
   (Cc(19)/Cc(20) / (Kps(8) + Cc(19)/Cc(20)))* Cc(2) / (Km(8) + Cc(2));

% Alanine Utilization:  ALA -> PYR
fact(9) = Cc(4) / (Km(9) + Cc(4));

% Alanine Production:  PYR -> ALA
fact(10) = Cc(2) / (Km(10) + Cc(2));

% Pyruvate Oxidation:  PYR + CoA + NAD -> ACoA + NADH + CO2
fact(11) = ((Cc(22)/Cc(23)) / (Krs(11) + (Cc(22)/Cc(23)))) ...
      * Cc(2)*Cc(16) / (Km(11) + Cc(2)*Cc(16) + Cc(14)*Km(11)/Ki(11));

% FAC Synthesis:  FFA + CoA + 2ATP -> FAC + 2ADP + 2Pi
fact(12) = ((Cc(19)/Cc(20)) / (Kps(12) + (Cc(19)/Cc(20)))) ...
            * Cc(6)*Cc(16) / (Km(12) + Cc(6)*Cc(16));

% FAC Oxidation:  FAC + 7CoA + 14 NAD -> 8ACoA + 14 NADH
fact(13) = ((Cc(22)/Cc(23)) / (Krs(13) + (Cc(22)/Cc(23)))) ...
 * Cc(15)*Cc(16) / (Km(13) + Cc(15)*Cc(16) + Cc(14) * Km(13) / Ki(13));

% TG Breakdown by ATGL:  TGL -> DG + FFA
fact(14) = Cc(7) / (Km(14) + Cc(7));

% TG Breakdown by HSL:  TGL -> DG + FFA
fact(15) = Cc(7) / (Km(15) + Cc(7));

% DG Breakdown by HSL:  DG -> MG + FFA
fact(16) = Cc(17) / (Km(16) + Cc(17));
```

```
% MG Breakdown by MGL:  MG -> GLR + FFA
fact(17) = Cc(18) / (Km(17) + Cc(18));

% MG Breakdown by MGL:  MG -> GLR + FFA
fact(18) = Cc(18) / (Km(18) + Cc(18));

% DG Synthesis:  GR3P + 2FAC -> DG + 2CoA +Pi
fact(20) = Cc(13) * Cc(15) / (Km(20) + Cc(13) * Cc(15));

% TG Synthesis:  DG + FAC -> TG + CoA
fact(21) = Cc(17) * Cc(15) / (Km(21) + Cc(17) * Cc(15));

% Transacylation I: DG + DG -> TG + MG
fact(22) = Cc(17) / (Km(22) + Cc(17));

% Transacylation II: MG + MG -> DG + GLR
fact(23) = Cc(18) / (Km(23) + Cc(18));

% Transacylation III: MG + DG -> TG + GLR
fact(24) = Cc(17) * Cc(18) / (Km(24) + Cc(17) * Cc(18));

% TCA Cycle:  ACoA + ADP + Pi + 4NAD+ -> 2CO2 + CoA + ATP + 4NADH
fact(25) = (Cc(22)/Cc(23)) / (Krs(25) + (Cc(22)/Cc(23))) * ...
           Cc(20)/Cc(19) / (Kps(25) + Cc(20)/Cc(19)) ...
           * Cc(14)*Cc(21) / (Km(25) + Cc(14)*Cc(21));

% Oxygen Consumption:  O2 + 6ADP + 6Pi + 2NADH -> H2O + 6ATP + 2NAD
fact(26) = (Cc(23)/Cc(22)) / (Krs(26) + (Cc(23)/Cc(22))) * ...
           Cc(20)/Cc(19) / (Kps(26) + Cc(20)/Cc(19)) ...
           * Cc(8)*Cc(21) / (Km(26) + Cc(8)*Cc(21));

% ATP Hydrolysis:  ATP -> ADP + Pi
fact(27) = Cc(19) / (Km(27) + Cc(19) + Cc(20) * Cc(21) *  ...
          Km(27)/Ki(27));

% TG Breakdown by LPL: TG -> GLR + 3FFA
fact(28) = Cb(7) / (Km(28) + Cb(7));

% Glycerol Phosphorylation by GK: Glycerol + ATP -> Glycerol-3-P + ADP
fact(29) = Cc(5) * Cc(19) / (Km(29) + Cc(5)*Cc(19));

Vmax=Rflux0./fact;

Tmax=zeros(9,1);
Lam=zeros(9,1);
Tmax(1) = URR0(1)/(Cb(1)/(Mm(1) + Cb(1))-Cc(1)/(Mm(1) + Cc(1)));  % GLC
Tmax(2) = URR0(2)/(Cb(2)/(Mm(2) + Cb(2))-Cc(2)/(Mm(2) + Cc(2)));  % PYR
Tmax(3) = URR0(3)/(Cb(3)/(Mm(3) + Cb(3))-Cc(3)/(Mm(3) + Cc(3)));  % LAC
Tmax(4) = URR0(4)/(Cb(4)/(Mm(4) + Cb(4))-Cc(4)/(Mm(4) + Cc(4)));  % ALA

Lam(5) = URR0(5)/(Cb(5)-Cc(5));                                   % GLR
Lam(6) = URR0(6)/(Cb(6)-Cc(6));                                   % FFA
Lam(8:9) = URR0(8:9)./(Cb(8:9)-Cc(8:9));
```

```
%*********************************************************************
% This section computes the Vvivo values and fluxes for 29 reactions.
% For reactions where a pair of energy metabolites are couples, Vvivo
% is  Vmax times the controller term, else Vvivo = Vmax.
%*********************************************************************

function Adipose_Flux

global URR0 Rflux0 Ca Cb0 Cc0 C0 Cb Cc
global Tmax Mm Lam Vmax Km Kps Krs Ki Sigma_O2 Sigma_CO2
global V Q UPT REL URR AVD Vvivo Rflux PROD UTIL MRR
format long

Vvivo = zeros(29,1); %Initialization of kinetic factors and controllers
Rflux = zeros(29,1); % Initialization of reaction fluxes

% Glucose Utilization:  GLC + ATP -> G6P + ADP
Vvivo(1) = Vmax(1) / (1 +(Cc(10)/Ki(1)));
Rflux(1) = Vvivo(1)*Cc(1)*Cc(19)/(Km(1)*(1+Cc(10)/Ki(1))+Cc(1)*Cc(19));

% G6P Breakdown:  G6P + ATP -> 2GA3P + ADP
Vvivo(2)=Vmax(2)*((Cc(20)/Cc(19))^2/(Kps(2)^2+(Cc(20)/Cc(19))^2));
Rflux(2) = Vvivo(2)*Cc(10) / (Km(2) + Cc(10));

% GA3P Breakdown:  GA3P + Pi + NAD + 2ADP -> PYR + NADH + 2ATP
nH3=2;
Vvivo(3) = Vmax(3) * ((Cc(22)/Cc(23)) / (Krs(3) + (Cc(22)/Cc(23))))* ...
          ((Cc(20)/Cc(19))^nH3 / (Kps(3)^nH3 + (Cc(20)/Cc(19))^nH3));
Rflux(3) = Vvivo(3) * Cc(12)*Cc(21) / (Km(3) + Cc(12)*Cc(21));

% Pyruvate Reduction:  PYR + NADH <-> LAC + NAD
Vvivo(4) = Vmax(4) / Km(4) / (1+Cc(2)*Cc(23)/Km(4)+Cc(3)*Cc(22)/Ki(4));
Rflux(4) = Vvivo(4) * (Cc(2) * Cc(23) - Cc(3) * Cc(22) / 1.06e4 );

% GAP Reduction: GAP + NADH <-> GRP + NAD+
Vvivo(7)=Vmax(7)/Km(7)/(1+Cc(12)*Cc(23)/Km(7)+Cc(13)*Cc(22)/Ki(7));
Rflux(7) = Vvivo(7) * (Cc(12) * Cc(23) - Cc(13)*Cc(22)/ 2.768e8);

% Glyceroneogenesis: PYR + 3ATP + 2NADH -> GR3P + 3ADP + 2NAD + 2Pi
Vvivo(8) = Vmax(8) * ((Cc(23)/Cc(22)) / (Krs(8) + (Cc(23)/Cc(22))))* ...
           (Cc(19)/Cc(20) / (Kps(8) + Cc(19)/Cc(20)));
Rflux(8) = Vvivo(8) * Cc(2) / (Km(8) + Cc(2));

% Alanine Utilization:  ALA -> PYR
Vvivo(9) = Vmax(9);
Rflux(9) = Vvivo(9) * Cc(4) / (Km(9) + Cc(4));

% Alanine Production:  PYR -> ALA
Vvivo(10) = Vmax(10);
Rflux(10) = Vvivo(10) * Cc(2) / (Km(10) + Cc(2));

% Pyruvate Oxidation:  PYR + CoA + NAD -> ACoA + NADH + CO2
Vvivo(11) = Vmax(11) * ((Cc(22)/Cc(23)) / (Krs(11) + (Cc(22)/Cc(23))));

Rflux(11)=Vvivo(11)*Cc(2)*Cc(16)/(Km(11)+Cc(2)*Cc(16) ...
```

```
          +Cc(14)*Km(11)/Ki(11));

% FAC Synthesis:  FFA + CoA + 2ATP -> FAC + 2ADP + 2Pi
Vvivo(12) = Vmax(12) * ((Cc(19)/Cc(20)) / (Kps(12) + (Cc(19)/Cc(20))));
Rflux(12) = Vvivo(12) * Cc(6)*Cc(16) / (Km(12) + Cc(6)*Cc(16));

% FAC Oxidation:  FAC + 7CoA + 14 NAD -> 8ACoA + 14 NADH
Vvivo(13) = Vmax(13) * ((Cc(22)/Cc(23)) / (Krs(13) + (Cc(22)/Cc(23))));
Rflux(13) = Vvivo(13) * Cc(15)*Cc(16) / (Km(13) + Cc(15)*Cc(16) ...
            + Cc(14) * Km(13) / Ki(13));

% TG Breakdown by ATGL:  TGL -> DG + FFA
Vvivo(14) = Vmax(14);
Rflux(14) = Vvivo(14) * Cc(7) / (Km(14) + Cc(7));

% TG Breakdown by HSL:  TGL -> DG + FFA
Vvivo(15) = Vmax(15);
Rflux(15) = Vvivo(15) * Cc(7) / (Km(15) + Cc(7));

% DG Breakdown by HSL:  DG -> MG + FFA
Vvivo(16) = Vmax(16);
Rflux(16) = Vvivo(16) * Cc(17) / (Km(16) + Cc(17));

% MG Breakdown by MGL:  MG -> GLR + FFA
Vvivo(17) = Vmax(17);
Rflux(17) = Vvivo(17) * Cc(18) / (Km(17) + Cc(18));

% MG Breakdown by HSL:  MG -> GLR + FFA
Vvivo(18) = Vmax(18);
Rflux(18) = Vvivo(18) * Cc(18) / (Km(18) + Cc(18));

% DG Synthesis:  GR3P + 2FAC -> DG + 2CoA + Pi
Vvivo(20) = Vmax(20);
Rflux(20) = Vvivo(20) * Cc(13) * Cc(15) / (Km(20) + Cc(13) * Cc(15));

% TG Synthesis:  DG + FAC -> TG + CoA
Vvivo(21) = Vmax(21);
Rflux(21) = Vvivo(21) * Cc(17) * Cc(15) / (Km(21) + Cc(17) * Cc(15));

% Transacylation I: DG + DG -> TG + MG
Vvivo(22) = Vmax(22);
Rflux(22) = Vvivo(22) * Cc(17) / (Km(22) + Cc(17));

% Transacylation II: MG + MG -> DG + GLR
Vvivo(23) = Vmax(23);
Rflux(23) = Vvivo(23) * Cc(18) / (Km(23) + Cc(18));

% Transacylation III: MG + DG -> TG + GLR
Vvivo(24) = Vmax(24);
Rflux(24) = Vvivo(24) * Cc(17) * Cc(18) / (Km(24) + Cc(17) * Cc(18));

% TCA Cycle:  ACoA + ADP + Pi + 4NAD+ -> 2CO2 + CoA + ATP + 4NADH
Vvivo(25)=Vmax(25) * (Cc(22)/Cc(23)) / (Krs(25) + (Cc(22)/Cc(23))) * ...
           Cc(20)/Cc(19) / (Kps(25) + Cc(20)/Cc(19));
Rflux(25) = Vvivo(25) * Cc(14)*Cc(21) / (Km(25) + Cc(14)*Cc(21));
```

```
% Oxygen Consumption:  O2 + 6ADP + 6Pi + 2NADH -> H2O + 6ATP + 2NAD
Vvivo(26) = Vmax(26)*(Cc(23)/Cc(22)) / (Krs(26) + (Cc(23)/Cc(22))) * ...
            Cc(20)/Cc(19) / (Kps(26) + Cc(20)/Cc(19));
Rflux(26) = Vvivo(26) * Cc(8)*Cc(21) / (Km(26) + Cc(8)*Cc(21));

% ATP Hydrolysis:  ATP -> ADP + Pi
Vvivo(27) = Vmax(27);
Rflux(27)=Vvivo(27)*Cc(19)/(Km(27)+Cc(19)+Cc(20)*Cc(21)*Km(27)/Ki(27));

% TG Breakdown by LPL: TG -> GLR + 3FFA
Vvivo(28) = Vmax(28);
Rflux(28) = Vvivo(28) * Cb(7) / (Km(28) + Cb(7));

% Glycerol Phosphorylation by GK: Glycerol + ATP -> Glycerol-3-P + ADP
Vvivo(29) = Vmax(29);
Rflux(29) = Vvivo(29) * Cc(5) * Cc(19) / (Km(29) + Cc(5)*Cc(19));

%**********************************************************************
% This section computes the production of the 30 species
% (the sum of all the reaction fluxes where the species is produced
% scaled by the corresponding stochieometric coefficients)
%**********************************************************************

PROD = zeros(23,1);
PROD(1) = 0;                                    % Glucose
PROD(2) = Rflux(3) + Rflux(9);                  % Pyruvate
PROD(3) = Rflux(4);                             % Lactate
PROD(4) = Rflux(10);                            % Alanine
PROD(5) = Rflux(17)+Rflux(18)+0.5*Rflux(23)+Rflux(24);       % Glycerol
PROD(6) = Rflux(14)+Rflux(15)+Rflux(16)+Rflux(17)+Rflux(18); % FFA
PROD(7) = Rflux(21) + 0.5*Rflux(22) + Rflux(24);   % TG
PROD(8) = 0;                                    % O2
PROD(9) = Rflux(11) + 2*Rflux(25);               % CO2
PROD(10) = Rflux(1) + Rflux(6);                  % Glucose 6-Phosphate
PROD(11) = Rflux(5);                            % Glycogen
PROD(12) = 2*Rflux(2);                      % Glyceraldehyde 3-Phosphate
PROD(13) = Rflux(7) + Rflux(8) + Rflux(29);      % Glycerol 3-Phosphate
PROD(14) = Rflux(11) + 8*Rflux(13);             % Acetyl-CoA
PROD(15) = Rflux(12);                           % Fatty Acyl-CoA
PROD(16) = 2*Rflux(20)+Rflux(21)+Rflux(25);           % CoA
PROD(17) = Rflux(14) + Rflux(15) + Rflux(20) + 0.5*Rflux(23);     % DG
PROD(18) = Rflux(16) + 0.5*Rflux(22);                  % MG
PROD(19) = 2*Rflux(3) + Rflux(25) + 6*Rflux(26);               % ATP
PROD(20) = Rflux(1) + Rflux(2) + Rflux(5) + 3*Rflux(8) ...
         + 2*Rflux(12)+ Rflux(27)+Rflux(29);                   % ADP
PROD(21)=2*Rflux(5)+2*Rflux(8)+2*Rflux(12)+Rflux(20)+Rflux(27);  % Pi
PROD(22)=Rflux(4)+Rflux(7)+2*Rflux(8)+2*Rflux(26);     % NAD+
PROD(23)=Rflux(3)+Rflux(11)+14*Rflux(13)+4*Rflux(25);  % NADH

%**********************************************************************
% This section computes the utilization of the 30 species
% (the sum of all the reaction fluxes where the species is consumed
% scaled by the corresponding stochieometric coefficients).
%**********************************************************************
```

```
UTIL = zeros(23,1);
UTIL(1) = Rflux(1);                                  % Glucose
UTIL(2) = Rflux(4) + Rflux(8) + Rflux(10) + Rflux(11);     % Pyruvate
UTIL(3) = 0;                                         % Lactate
UTIL(4) = Rflux(9);                                         % Alanine
UTIL(5) = Rflux(29);                                         % Glycerol
UTIL(6) = Rflux(12);                                 % Fatty Acid
UTIL(7) = Rflux(14) + Rflux(15);                      % TG
UTIL(8) = Rflux(26);                                 % O2
UTIL(9) = 0;                                         % CO2
UTIL(10) = Rflux(2) + Rflux(5);                       % Glucose 6-Phosphate
UTIL(11) = Rflux(6);                                 % Glycogen
UTIL(12) = Rflux(3) + Rflux(7);                % Glyceraldehyde 3-Phosphate
UTIL(13) = Rflux(20);                                % Glycerol 3-Phosphate
UTIL(14) = Rflux(25);                                % Acetyl-CoA
UTIL(15) = Rflux(13)+2*Rflux(20)+Rflux(21);       % Fatty ACyl CoA
UTIL(16) = Rflux(11) + Rflux(12) + 7*Rflux(13);           % CoA
UTIL(17) = Rflux(16)+Rflux(21)+Rflux(22)+Rflux(24);       % DG
UTIL(18) = Rflux(17) + Rflux(18) + Rflux(23) + Rflux(24);  % MG
UTIL(19) = Rflux(1) + Rflux(2) + Rflux(5) + 3*Rflux(8) ...
         + 2*Rflux(12) + Rflux(27)+Rflux(29);               % ATP
UTIL(20) = 2*Rflux(3) + Rflux(25) + 6*Rflux(26);            % ADP
UTIL(21) = Rflux(3) + Rflux(6) + Rflux(25) + 6*Rflux(26);       % Pi
UTIL(22) = Rflux(3) + Rflux(11) + 14*Rflux(13) + 4*Rflux(25);    % NAD
UTIL(23) = Rflux(4)+ Rflux(7) + 2*Rflux(8) + 2*Rflux(26);       % NADH

%*********************************************************************
% The function Adipose_Cdot_Est lists the system of differential
% equations governing the transport and metabolism of chemical species
% in the adipose tissue.
% It is based on dynamic mass balances of all the species.
%*********************************************************************

function [Cdot] = Adipose_Cdot_Est(t,C,p)

global URR0 Rflux0 Ca Cb0 Cc0 C0 Cb Cc
global Tmax Mm Lam Vmax Km Kps Krs Ki Sigma_O2 Sigma_CO2 ...
       CO2bTot CO2cTot SHbO2b O2bTot SMbO2c O2cTot StO2
global V Q UPT REL URR AVD Vvivo Rflux PROD UTIL MRR epi Vmax0 Tmax0
Lam0
global VbeffO2 VbeffCO2 VceffCO2
format long

%*********************************************************************
% This section sets the capillary blood and tissue cell concentrations
% (Cb and Cc) of all the chemical species at current time and then
% calculates total O2 and CO2 concentrations in ARTERIAL blood,
% CAPILLARY/VENOUS blood, and tissue cells. The calculation for total
% O2 and CO2 concentrations is done using the external functions
% O2Tot_Blood, O2Tot_Cells, CO2Tot_Blood and CO2Tot_Cells.
%*********************************************************************

Cb = zeros(9,1);       % Initialization of Cb
Cc = zeros(23,1);      % Initialization of Cc
Cb = C(1:9);           % Blood species concentrations
Cc = C(10:32);          % Cells species concentrations
```

```
CO2a = Ca(9);     % Free CO2 concentration in arterial blood (mmol/L)
CO2b = Cb(9);     % Free CO2 concentration in venous blood (mmol/L)
CO2c = Cc(9);     % Free CO2 concentration in tissue cells (mmol/L)
O2a = Ca(8);      % Free O2 concentration in arterial blood (mmol/L)
O2b = Cb(8);      % Free O2 concentration in venous blood (mmol/L)
O2c = Cc(8);      % Free O2 concentration in tissue cells (mmol/L)

Vb = 0.07;                    % Blood volume fraction
Visf = 0.13;                  % ISF volume fraction
Vc = 0.8;                     % Cell volume fraction
[SHbCO2a,CHbCO2a,CHCO3a,CO2aTot] = CO2Tot_Blood(CO2a/1000);
[SHbCO2b,CHbCO2b,CHCO3b,CO2bTot] = CO2Tot_Blood(CO2b/1000);
[CHCO3c,CO2cTot] = CO2Tot_Cells(CO2c/1000);
[SHbO2a,CHbO2a,O2aTot] = O2Tot_Blood(O2a/1000);
[SHbO2b,CHbO2b,O2bTot] = O2Tot_Blood(O2b/1000);
Hct = 0.42; CHbTot = 5.2;

% Chnages in blood flow and arterial glycerol and FFA concentrations
if t < 15
    Q=0.031;
    epi=0.1;
    Ca(5)=70;
    Ca(6)=660*0.58;
 %0.58 to convert FFA conc. in plasma to FFA conc. in whole blood
else
    Q=0.031+0.2266*(1-exp(-(t-15)/62.3171));
    epi=(1.4529e-5*(t-15)^3-1.9034e-3*(t-15)^2+6.8374e-2*(t-15)+0.1);
    Ca(5)=70/60*(0.0019*(t-15)^3-0.2198*(t-15)^2+6.839*(t-15)+60);
    Ca(6)=0.58*660.0/620.0*(0.0139*(t-15)^3.0 ...
          -1.8966*(t-15)^2.0+67.9968*(t-15)+620.0);
 %0.58 to convert FFA conc. in plasma to FFA conc. in whole blood
end;

% Vmax modification due to epinephrine infusion, which starts at t=15
% Recalculate flux rate based on the modified Vmax
    Vmax(14)=Vmax0(14)*(1+p(1)*(epi-0.1)^2/(p(2)^2+(epi-0.1)^2));
    Vmax(15)=Vmax0(15)*(1+p(3)*(epi-0.1)^2/(p(4)^2+(epi-0.1)^2));
    Vmax(16)=Vmax0(16)*(1+p(5)*(epi-0.1)^2/(p(6)^2+(epi-0.1)^2));
    Vmax(28)=Vmax0(28)*1001*Q/31/(1+Q/31);

% Update the flux values based on the new maximum rate coefficients
Adipose_Flux;

%*********************************************************************
% This section calculates the uptake (UPT), release (REL),
% uptake-release rates and arterial-venous differences (AVD) of
% the 9 species which undergo blood-tissue exchange.
%*********************************************************************

UPT = zeros(9,1);                          % Initialization of UPT
REL = zeros(9,1);                          % Initialization of REL
URR = zeros(9,1);                          % Initialization of URR
AVD = zeros(9,1);                          % Initialization of AVD

UPT(1) = Tmax(1)*Cb(1)/(Mm(1) + Cb(1));    % Uptake of GLC from blood
REL(1) = Tmax(1)*Cc(1)/(Mm(1) + Cc(1));    % Release of GLC to blood
```

```
UPT(2) = Tmax(2)*Cb(2)/(Mm(2) + Cb(2));    % Uptake of PYR from blood
REL(2) = Tmax(2)*Cc(2)/(Mm(2) + Cc(2));    % Release of PYR to blood
UPT(3) = Tmax(3)*Cb(3)/(Mm(3) + Cb(3));    % Uptake of LAC from blood
REL(3) = Tmax(3)*Cc(3)/(Mm(3) + Cc(3));    % Release of LAC to blood
UPT(4) = Tmax(4)*Cb(4)/(Mm(4) + Cb(4));     % Uptake of ALA from blood
REL(4) = Tmax(4)*Cc(4)/(Mm(4) + Cc(4));     % Release of ALA to blood
UPT(5) = Lam(5)*Cb(5);                     % Uptake of GLR from blood
REL(5) = Lam(5)*Cc(5);                     % Release of GLR to blood
UPT(6) = Lam(6)*Cb(6);                      % Uptake of FFA from blood
REL(6) = Lam(6)*Cc(6);                      % Release of FFA to blood
UPT(7) = 0.0;
REL(7) = 0.0;
UPT(8) = Lam(8)*Cb(8);                     % Uptake of O2 from blood
REL(8) = Lam(8)*Cc(8);           % Release of O2 to blood
UPT(9) = Lam(9)*Cb(9);                     % Uptake of CO2 from blood
REL(9) = Lam(9)*Cc(9);          % Release of CO2 to blood

URR = UPT - REL;                           % URR for all 9 species

AVD(1:7) = Q*(Ca(1:7) - Cb(1:7));          % AVD for 7 species
AVD(9) = Q*(CO2aTot - CO2bTot)*1000;            % AVD for CO2
AVD(8) = Q*(O2aTot - O2bTot)*1000;              % AVD for O2


%*********************************************************************
% This section computes the metabolic reaction rate. This
% section also computes the effective volumes for different species
% in blood and cells (specifically O2 and CO2) and sets the
% differential equations governing the transport and metabolism of
% species in blood and tissue cells.
%*********************************************************************

[VbeffCO2] = VeffCO2_Blood(Vb,Visf,Cb(9)/1000);
[VbeffO2] = VeffO2_Blood(Vb,Visf,Cb(8)/1000);
[VceffCO2] = VeffCO2_Cells(Vc/8,Cc(9)/1000);

Vbeff = (Vb+Visf)*ones(9,1);
Vbeff(9) = VbeffCO2;
Vbeff(8) = VbeffO2;
Vceff = Vc*ones(23,1);
Vceff(9) = VceffCO2;

MRR = zeros(23,1);
MRR = PROD - UTIL;
Cbdot = zeros(9,1);
Ccdot = zeros(23,1);
Cdot  = zeros(32,1);
Cbdot = (AVD - URR)./Vbeff;
Cbdot(5) = Cbdot(5) + Rflux(28)/Vbeff(5);
Cbdot(6) = Cbdot(6) + 3*Rflux(28)/Vbeff(6);
Cbdot(7) = Cbdot(7) - Rflux(28)/Vbeff(7);

% Vceff for TG, DG and MG are equal to the physical tissue volume
Vceff(1:4)=p(7);
Vceff(5:6)=p(7);
Vceff(8)=p(7);
```

```
Vceff(10:16)=p(7);
Vceff(19:23)=p(7);
Ccdot(1:9) = (MRR(1:9) + URR(1:9)) ./ Vceff(1:9);
Ccdot(10:23) = MRR(10:23) ./ Vceff(10:23);
Ccdot(4)=Ccdot(4)+2.649/Vceff(4);
Cdot = [Cbdot;Ccdot];

% END OF DIFFERENTIAL EQUATIONS

%**********************************************************************
% Calculation of total CO2 concentration in blood (pH in plasma
% and RBC is assumed to be constant; equal to 7.4 plasma and 7.24
% in RBC).
%**********************************************************************

function [SHbCO2,CHbCO2,CHCO3,CO2Tot] = CO2Tot_Blood(CO2)

Hct = 0.42;                   % Standard hematocrit
CHbrbc = 5.2;                 % Concentration of hemoglobin in RBC (mM)
CHbCO2Max = 4*Hct*CHbrbc;
% HbCO2 concentration in blood at 100% HbO2 saturation (mM)
pHpl = 7.4;                     % Standard pH in plasma
pHrbc = 7.24;                   % Standard pH in RBC
CHpl = 10^(-pHpl+3);            % H+ concentration in plasma (mM)
CHrbc = 10^(-pHrbc+3);          % H+ concentration in RBC (mM)
Rrbc = CHpl/CHrbc;              % Gibb-Donnan equilibrium constant
KeqCO2hyd = 7.94e-4;      % Equilibrium constant for CO2 hydration (mM)
alphaCO2 = 3.05e-2;             % Solubility of CO2 in blood (mM/mmHg)
P50HbCO2 = 265.0;               % PCO2 at 50% HbCO2 saturation (mmHg)
C50HbCO2 = alphaCO2*P50HbCO2;
% Free CO2 concentration at 50% HbCO2 saturation (mM)
KHbCO2 = 1/C50HbCO2;            % Hill constant for SHbCO2 (mM^-1)

SHbCO2 = KHbCO2*CO2/(1+KHbCO2*CO2); % HbCO2 saturation (unitless)
CHbCO2 = CHbCO2Max*SHbCO2;      % Hb-bound CO2 concentration (mM)
CHCO3pl = KeqCO2hyd*CO2/CHpl;
% Concentration of HCO3 (bicarbonate) in plasma (mM)
CHCO3rbc = Rrbc*CHCO3pl;        % Concentration of HCO3m in RBC (mM)
CHCO3 = (1-Hct)*CHCO3pl + Hct*CHCO3rbc;
% Concentration of HCO3m (mM) in blood
CO2Tot = CO2 + CHbCO2 + CHCO3;  % Total CO2 concentration (mM) in blood

%**********************************************************************
% Calculation of total CO2 concentration in tissue cells (pH in cells
% is assumed to be constant; equal to 7.1).
%**********************************************************************

function [CHCO3,CO2Tot] = CO2Tot_Cells(CO2)

pH = 7.1;                 % standard pH in cells
CH = 10^(-pH+3);          % H+ concentration in cells (mM)
KeqCO2hyd = 7.94e-4;      % Equilibrium constant for CO2 hydration (mM)
CHCO3 = KeqCO2hyd*CO2/CH;
% Concentration of HCO3 (bicarbonate) in cells (mM)
CO2Tot = CO2 + CHCO3;           % Total CO2 concentration in cells (mM)
```

```
%*********************************************************************
% Calculation of total O2 concentration in blood (pH in plasma and RBC
% is assumed to be constant; equal to 7.4 plasma and 7.24 in RBC).
%*********************************************************************

function [SHbO2,CHbO2,O2Tot] = O2Tot_Blood(O2)

Hct = 0.42;                 % Standard hematocrit (unitless)
CHbrbc = 5.2;               % Concentration of hemoglobin in RBC (mM)
CHbO2Max = 4*Hct*CHbrbc;    % HbO2 concentration at 100% HbO2
saturation (mM)
alphaO2 = 1.35e-3;          % Solubility of O2 in plasma (mM/mmHg)
P50HbO2 = 26.8;             % PO2 at 50% HbO2 saturation (mmHg)
C50HbO2 = alphaO2*P50HbO2;
% Free O2 concentration at 50% HbO2 saturation (mM)
nH = 2.7;                   % Hill coefficient for SHbO2 (unitless)
KHbO2 = 1/C50HbO2^nH;       % Hill constant for SHbO2 (mM^-nH)

SHbO2 = KHbO2*O2^nH/(1+KHbO2*O2^nH);  % HbO2 saturation (unitless)
CHbO2 = CHbO2Max*SHbO2;      % Hb-bound O2 concentration in blood (mM)
O2Tot = O2 + CHbO2;          % Total O2 concentration in blood (mM)

function [VbeffCO2] = VeffCO2_Blood(Vb,Visf,CO2)

Hct = 0.42;                 % Standard hematocrit (unitless)
CHbrbc = 5.2;               % Concentration of hemoglobin in RBC (mM)
CHbCO2Max = 4*Hct*CHbrbc;   % HbCO2 concentration in blood at 100%
HbO2 saturation (mM)
pHrbc = 7.24;               % Standard pH in RBC
pHpl  = 7.4;                % Standard pH in plasma
pHisf = 7.2;                % Standard pH in ISF
CHrbc = 10^(-pHrbc+3);      % H+ concentration in RBC (mM)
CHpl  = 10^(-pHpl+3);  % H+ concentration in plasma (mM)
CHisf = 10^(-pHisf+3); % H+ concentration in ISF (mM)
Rrbc = CHpl/CHrbc;     % Gibb-Donnan equilibrium constant for RBC
Rcap = CHpl/CHisf;     % Gibb-Donnan equilibrium constant for capillary
KeqCO2hyd = 7.94e-4;   % Equilibrium constant for CO2 hydration (mM)
alphaCO2 = 3.05e-2;    % Solubility of CO2 in plasma (mM/mmHg)
P50HbCO2 = 265.0;              % PCO2 at 50% HbCO2 saturation (mmHg)
C50HbCO2 = alphaCO2*P50HbCO2;
% Free CO2 concentration at 50% HbCO2 saturation (mM)
KHbCO2 = 1/C50HbCO2;           % Hill constant for SHbCO2 (mM^-1)

% Calculation of derivatives of state variables w.r.t. CO2 and then
% effective blood volume for CO2
DSHbCO2 = KHbCO2/(1+KHbCO2*CO2)^2;
DCHbCO2 = CHbCO2Max*DSHbCO2;
DCHCO3pl = KeqCO2hyd/CHpl;
DCHCO3rbc = Rrbc*DCHCO3pl;
DCHCO3isf = Rcap*DCHCO3pl;
DCHCO3bl = (1-Hct)*DCHCO3pl + Hct*DCHCO3rbc;
VbeffCO2 = Vb*(1+DCHbCO2+DCHCO3bl) + Visf*(1+DCHCO3isf);
```

```
%*********************************************************************
% Calculation of effective cells volume for CO2 accounting for
% different forms of CO2 transport in cells
% (pH in cells is assumed to be constant = 7.1).
%*********************************************************************

function [VceffCO2] = VeffCO2_Cells(Vc,CO2)

pH = 7.1;                          % standard pH in cells
CH = 10^(-pH+3);                   % H+ concentration in cells (mM)
KeqCO2hyd = 7.94e-4;      % Equilibrium constant for CO2 hydration (mM)
alphaCO2 = 3.05e-2;                % Solubility of CO2 in cells (mM/mmHg)
DCHCO3 = KeqCO2hyd/CH;             % dCHCO3/dCO2
VceffCO2 = Vc*(1+DCHCO3);          % Effective cells volume for CO2

%*********************************************************************
% Calculation of effective blood volume for O2 accounting for different
% forms of O2 transport in blood and ISF (pH in plasma and RBC is
% assumed to be constant; equal to 7.4 plasma and 7.24 in RBC ).
%*********************************************************************

function [VbeffO2] = VeffO2_Blood(Vb,Visf,O2)

Hct = 0.42;                        % Standard hematocrit (unitless)
CHbrbc = 5.2;                    % Concentration of hemoglobin in RBC (mM)
CHbO2Max = 4*Hct*CHbrbc;
% HbO2 concentration at 100% HbO2 saturation (mM)
alphaO2 = 1.35e-3;                 % Solubility of O2 in plasma (mM/mmHg)
P50HbO2 = 26.8;                    % PO2 at 50% HbO2 saturation (mmHg)
C50HbO2 = alphaO2*P50HbO2;
% Free O2 concentration at 50% HbO2 saturation (mM)
nH = 2.7;                          % Hill coefficient for SHbO2 (unitless)
KHbO2 = 1/C50HbO2^nH;              % Hill constant for SHbO2 (mM^-nH)

% Calculation of derivatives of state variables w.r.t. O2 and then
% effective blood volume for O2.
DSHbO2 = nH*KHbO2*O2^(nH-1)/(1+KHbO2*O2^nH)^2;
DCHbO2 = CHbO2Max*DSHbO2;
VbeffO2 = Vb*(1+DCHbO2) + Visf;
```

A-V.3. ADIPOSE TISSUE MODEL FOR HYPERINSULINEMIC-EUGLYCEMIC CLAMP SIMULATION

The following is the source code (m file) written in MATLAB® in order to simulate the physiological responses in the adipose tissue during hyperinsulinemic-euglycemic clamp experiment. The simulation code utilizes a library from MATLAB®, 'ode15s' to solve a set of differential equations. The functions that compute the free and bound concentrations of oxygen and carbon dioxide are taken from the source code shown in A-V.2 and are not shown in this section.

```
%*********************************************************************
% This is the main code for two compartmental lumped model of adipose
% tissue metabolism in response to euglycemic-hyperinsulinemic clamp.
%*********************************************************************

global URR0 Rflux0 Ca Cb0 Cc0 C0 Cb Cc
global Tmax Mm Lam Vmax Km Kps Krs Ki ...
       CO2bTot CO2cTot SHbO2b O2bTot SMbO2c O2cTot StO2
global V Q UPT REL URR AVD Vvivo Rflux PROD UTIL MRR ...
       Vmax0 Tmax0 Lam0 CIns
format long

Flux0 = zeros(45,1);
URR0 = zeros(9,1);
Rflux0 = zeros(36,1);
Flux0 = dlmread('RestingFluxes.txt');
URR0(1:9) = Flux0(1:9);
Rflux0(1:36) = Flux0(10:45);

Conc0 = zeros(38,1);
Ca = zeros(9,1);
Cb0 = zeros(9,1);
Cc0 = zeros(29,1);
Conc0 = dlmread('RestingConcentrations.txt');
Ca = Conc0(1:9);
Cc0 = Conc0(10:38);

theta = zeros(136,1);
Mm = zeros(9,1);
Km = zeros(36,1);
Kps = zeros(36,1);
Krs = zeros(36,1);
Ki = zeros(36,1);
theta = dlmread('Parameters.txt');
Kps(1:36)=theta(1:36);
Krs(1:36)=theta(37:72);
```

```
Ki(1:36)=theta(73:108);
Km(1:36)=theta(109:144);

Q = 0.031;           % Adipose tissue blood flow at fast (l/kg/min)

Cb0(1:4)=Ca(1:4)-URR0(1:4)./Q;
Cb0(7)=Ca(7)*0.58-Rflux0(35)./Q;
Cb0(8:9)=Ca(8:9)-URR0(8:9)./Q;
Cb0(8)=65.7;
Cb0(9)=1155.3;
Cb0(5)=Ca(5)+130;
Cb0(6)=0.58*Ca(6)+336;
Rflux0(16)=2.65;
Rflux0(17)=0;
Km(15)=200;
Mm = Cb0;
Mm(3)=10*Cb0(3);
[Vmax Tmax Lam]=Adipose_TmaxVmax(Rflux0, URR0, Cb0, Cc0, Km, ...
                Ki, Kps, Krs, Mm, Q);

Cb=Cb0;
Cc=Cc0;
Adipose_Flux;
Vmax0=Vmax;
Tmax0=Tmax;
Lam0=Lam;
CVmax=Tmax(1);

C0 = [Cb0;Cc0;CVmax];

p=[5.0109;14.6697;0.0233;2.995;];
Tend = 135;
Tspan = [0:0.1:Tend];
options = odeset('RelTol',1e-6, 'AbsTol',1e-6);
[t,C] = ode15s(@Adipose_Cdot_Est,Tspan,C0,options,p);

UPT_mat = [];
REL_mat = [];
URR_mat = [];
AVD_mat = [];
Rflux_mat = [];
PROD_mat = [];
UTIL_mat = [];
MRR_mat = [];
Ca_mat=[];
Cb_mat = [];
Cc_mat = [];
Cbdot_mat=[];
Ccdot_mat=[];
Vmdot_mat=[];
Qrec=[];
epi_rec=[];
Vmax_mat=[];
Vvivo_mat=[];
CIns_mat=[];
for j = 1:length(t)
    tj = t(j);
```

```
    Cj = C(j,:)';
    [Cdotj] = Adipose_Cdot_Est(tj,Cj,p);
    CIns_mat=[CIns_mat; CIns];
    UPT_mat = [UPT_mat;UPT'];
    REL_mat = [REL_mat;REL'];
    URR_mat = [URR_mat;URR'];
    AVD_mat = [AVD_mat;AVD'];
    Rflux_mat = [Rflux_mat;Rflux'];
    PROD_mat = [PROD_mat;PROD'];
    UTIL_mat = [UTIL_mat;UTIL'];
    MRR_mat = [MRR_mat;MRR'];
    Ca_mat = [Ca_mat; Ca'];
    Cb_mat = [Cb_mat;Cj(1:9)'];
    Cc_mat = [Cc_mat;Cj(10:38)'];
    Cbdot_mat = [Cbdot_mat;Cdotj(1:9)'];
    Ccdot_mat = [Ccdot_mat;Cdotj(10:38)'];
    Vmdot_mat = [Vmdot_mat;Cdotj(39)];
    Qrec = [Qrec; Q];
    epi_rec = [epi_rec; epi];
    Vmax_mat=[Vmax_mat;Vmax'];
    Vvivo_mat=[Vvivo_mat;Vvivo'];
end


%**********************************************************************
% This section computes the Vvivo values and fluxes for 36 reactions.
% For reactions where a pair of energy metabolites are couples, Vvivo
% is  Vmax times the controller term, else Vvivo = Vmax.
%**********************************************************************

function Adipose_Flux

global URR0 Rflux0 Ca Cb0 Cc0 C0 Cb Cc
global Tmax Mm Lam Vmax Km Kps Krs Ki Sigma_O2 Sigma_CO2
global V Q UPT REL URR AVD Vvivo Rflux PROD UTIL MRR
format long

Rflux = zeros(36,1);        % Initialization of reaction fluxes

fact = zeros(36,1);

% Glucose Utilization:  GLC + ATP -> G6P + ADP
ctrl_G6P = 1 / (1 +(Cc(10)/Ki(1)));
fact(1)=ctrl_G6P*Cc(1)*Cc(21)/(Km(1)*(1+Cc(10)/Ki(1))+Cc(1)*Cc(21));

% Phosphoglucose Isomerase:  G6P <-> F6P
fact(2) = (Cc(10) - Cc(12)/ 0.33) ...
          / (Km(2)+Cc(10)+Cc(12)*Km(2)/Ki(2));

% F6P Breakdown:  F6P + ATP -> 2GA3P + ADP
nH2 = 2;
fact(3) = (Cc(22)/Cc(21))^nH2 / (Kps(3)^nH2 + (Cc(22)/Cc(21))^nH2) ...
          * Cc(12) / (Km(3) + Cc(12));

% GA3P Breakdown:  GA3P + Pi + NAD + 2ADP -> PYR + NADH + 2ATP
nH3=2;
```

```
fact(4) = ((Cc(24)/Cc(25)) / (Krs(4) + (Cc(24)/Cc(25))))* ...
          ((Cc(22)/Cc(21))^nH3) / (Kps(4)^nH3 +
(Cc(22)/Cc(21))^nH3) ...
          * Cc(14)*Cc(23) / (Km(4) + Cc(14)*Cc(23));

% Pyruvate Reduction:  PYR + NADH <-> LAC + NAD
fact(5) = (Cc(2) * Cc(25) - Cc(3) * Cc(24) / 1.06e4 ) ...
          / Km(5) / (1+Cc(2)*Cc(25)/Km(5)+Cc(3)*Cc(24)/Ki(5));

% Glycogen Synthesis:  G6P + ATP -> GLY + ADP + 2Pi
fact(6) = ((Cc(21)/Cc(22)) / (Kps(6) + (Cc(21)/Cc(22)))) ...
          * Cc(10) / (Km(6) + Cc(10));

% Glycogen Utilization:  GLY + Pi -> G6P
fact(7)=((Cc(22)/Cc(21))^2)/(Kps(7)^2+(Cc(22)/Cc(21))^2) ...
          * Cc(11)*Cc(23) / (Km(7) +  Cc(11)*Cc(23));

% Pentose Phosphate Shunt I:  G6P + 2NADP+ -> R5P + 2NADPH
fact(8) = ((Cc(26)/Cc(27)) / (Krs(8) + (Cc(26)/Cc(27)))) ...
          * Cc(10) / (Km(8) + Cc(10));

% Pentose Phosphate Shunt II:  R5P -> 2/3F6P + 1/3GAP
fact(9) = Cc(13) / (Km(9) + Cc(13));

% GAP Reduction I: GAP1 + NADH <-> G3P1 + NAD+
fact(10) = (Cc(14) * Cc(25) - Cc(15)*Cc(24)/ 2.768e8) ...
          / Km(10) / (1+Cc(14)*Cc(25)/Km(10)+Cc(15)*Cc(24)/Ki(10));

% Glyceroneogenesis: PYR + 3ATP + NADH -> GAP2 + 3ADP + NAD + 2Pi
fact(11) = ((Cc(25)/Cc(24)) / (Krs(11) + (Cc(25)/Cc(24))))* ...
 (Cc(21)/Cc(22) / (Kps(11) + Cc(21)/Cc(22)))* Cc(2) / (Km(11) + Cc(2));

% GAP Reduction II: GAP2 + NADH <-> G3P2 + NAD+
fact(12) = (Cc(28) * Cc(25) - Cc(29)*Cc(24)/ 2.768e8) ...
          / Km(12) / (1+Cc(28)*Cc(25)/Km(12)+Cc(29)*Cc(24)/Ki(12));

% Glycerol Phosphorylation: GLR + ATP -> G3P2 + ADP
fact(13) = ((Cc(21)/Cc(22)) / (Kps(13) + (Cc(21)/Cc(22)))) ...
          * Cc(5) / (Km(13) + Cc(5));

% Alanine Utilization:  ALA -> PYR
fact(14) = Cc(4) / (Km(14) + Cc(4));

% Alanine Production:  PYR -> ALA
fact(15) = Cc(2) / (Km(15) + Cc(2));

% Proteolysis: Protein -> ALA
fact(16)=1;

% Protein Synthesis: ALA -> Protein
fact(17)=1;

% Pyruvate Oxidation:  PYR + CoA + NAD -> ACoA + NADH + CO2
fact(18) = ((Cc(24)/Cc(25)) / (Krs(18) + (Cc(24)/Cc(25)))) ...
      * Cc(2)*Cc(18) / (Km(18) + Cc(2)*Cc(18) + Cc(16)*Km(18)/Ki(18));
```

```
% FAC Synthesis:  FFA + CoA + 2ATP -> FAC + 2ADP + 2Pi
fact(19) = ((Cc(21)/Cc(22)) / (Kps(19) + (Cc(21)/Cc(22)))) ...
            * Cc(6)*Cc(18) / (Km(19) + Cc(6)*Cc(18));

% FAC Oxidation:  FAC + 7CoA + 14 NAD -> 8ACoA + 14 NADH
fact(20) = ((Cc(24)/Cc(25)) / (Krs(20) + (Cc(24)/Cc(25)))) ...
   * Cc(17)*Cc(18)/(Km(20)+Cc(17)*Cc(18) + Cc(16) * Km(20) / Ki(20));

% TG Breakdown by ATGL:  TGL -> DG + FFA
fact(21) = 1;

% TG Breakdown by HSL:  TGL -> DG + FFA
fact(22) = 1;

% DG Breakdown by HSL:  DG -> MG + FFA
fact(23) = Cc(19) / (Km(23) + Cc(19));

% MG Breakdown by MGL:  MG -> GLR + FFA
fact(24) = Cc(20) / (Km(24) + Cc(20));

% MG Breakdown by HSL:  MG -> GLR + FFA
fact(25) = Cc(20) / (Km(25) + Cc(20));

% de novo Lipogenesis: 8ACoA + 14NADPH + 7ATP -> FFA + 8CoA + 14NADP+
% 7ADP + 7Pi
fact(26) = (Cc(27)/Cc(26)) / (Krs(26) + (Cc(27)/Cc(26))) * ...
            Cc(21)/Cc(22) / (Kps(26) + Cc(21)/Cc(22)) ...
            * Cc(16) / (Km(26) + Cc(16));

% DG Synthesis:  G3P1 + 2FAC -> DG + 2CoA + Pi
fact(27) = Cc(29) * Cc(17) / (Km(27) + Cc(29) * Cc(17));

% TG Synthesis:  DG + FAC -> TG + CoA
fact(28) = Cc(19) * Cc(17) / (Km(28) + Cc(19) * Cc(17));

% Transacylation I: DG + DG -> TG + MG
fact(29) = Cc(19) / (Km(29) + Cc(19));

% Transacylation II: MG + MG -> DG + GLR
fact(30) = Cc(20) / (Km(30) + Cc(20));

% Transacylation III: MG + DG -> TG + GLR
fact(31) = Cc(19) * Cc(20) / (Km(31) + Cc(19) * Cc(20));

% TCA Cycle:  ACoA + ADP + Pi + 4NAD+ -> 2CO2 + CoA + ATP + 4NADH
fact(32) = (Cc(24)/Cc(25)) / (Krs(32) + (Cc(24)/Cc(25))) * ...
            Cc(22)/Cc(21) / (Kps(32) + Cc(22)/Cc(21)) ...
            * Cc(16)*Cc(23) / (Km(32) + Cc(16)*Cc(23));

% Oxygen Consumption:  O2 + 6ADP + 6Pi + 2NADH -> H2O + 6ATP + 2NAD
fact(33) = (Cc(25)/Cc(24)) / (Krs(33) + (Cc(25)/Cc(24))) * ...
            Cc(22)/Cc(21) / (Kps(33) + Cc(22)/Cc(21)) ...
            * Cc(8)*Cc(23) / (Km(33) + Cc(8)*Cc(23));
```

```
% ATP Hydrolysis:  ATP -> ADP + Pi
fact(34) = Cc(21) / (Km(34) + Cc(21));

% TG Breakdown by LPL: TG -> GLR + 3FFA
fact(35) = Cb(7) / (Cb0(7) + Cb(7));

% DG Synthesis in Other Cellular Domain:  G3P2 + 2FAC -> DG + 2CoA + Pi
fact(36) = Cc(29) * Cc(17) / (Km(36) + Cc(29) * Cc(17));

Rflux=Vmax.*fact;
%*********************************************************************
% This section computes the production of the 29 species
% (the sum of all the reaction fluxes where the species is produced
% scaled by the corresponding stochieometric coefficients)
%*********************************************************************

PROD = zeros(29,1);
PROD(1) = 0;                                    % Glucose
PROD(2) = Rflux(4) + Rflux(14);                  % Pyruvate
PROD(3) = Rflux(5);                             % Lactate
PROD(4) = Rflux(15)+Rflux(16);                            % Alanine
PROD(5) = Rflux(24)+Rflux(25)+0.5*Rflux(30)+Rflux(31);       % Glycerol
PROD(6)=Rflux(21)+Rflux(22)+Rflux(23)+Rflux(24)+Rflux(25)+Rflux(26)/8;
% Free Fatty Acid
PROD(7) = Rflux(28) + 0.5*Rflux(29) + Rflux(31);   % TG
PROD(8) = 0;                                    % O2
PROD(9) = Rflux(8)+Rflux(18) + 2*Rflux(32);              % CO2
PROD(10) = Rflux(1) + Rflux(7);                  % Glucose 6-Phosphate
PROD(11) = Rflux(6);                            % Glycogen
PROD(12) = Rflux(2)+Rflux(9)*2/3;                % F6P
PROD(13) = Rflux(8);                             % R5P
PROD(14) = 2*Rflux(3)+Rflux(9)/3;    % Glyceraldehyde 3-Phosphate in GC
PROD(15) = Rflux(10);                % Glycerol 3-Phosphate in GC
PROD(16) = Rflux(18) + 8*Rflux(20);             % Acetyl-CoA
PROD(17) = Rflux(19);                           % Fatty Acyl-CoA
PROD(18) =Rflux(26)+2*Rflux(27)+Rflux(28)+Rflux(32)+2*Rflux(36);  % CoA
PROD(19)=Rflux(21)+Rflux(22)+Rflux(27)+0.5*Rflux(30)+Rflux(36); % DG
PROD(20) = Rflux(23) + 0.5*Rflux(29);                  % MG
PROD(21) = 2*Rflux(4) + Rflux(32) + 6*Rflux(33);               % ATP
PROD(22) = Rflux(1) + Rflux(3) + Rflux(6) + 3*Rflux(11) + Rflux(13) ...
           + 2*Rflux(19) + 7/8*Rflux(26) + Rflux(34);          % ADP
PROD(23) = 2*Rflux(6) + 2*Rflux(11) + 2*Rflux(19) + 7/8*Rflux(26) ...
+ Rflux(27) + Rflux(34) + Rflux(36); % Pi
PROD(24) = Rflux(5)+Rflux(10)+Rflux(11)+Rflux(12) + 2*Rflux(33); % NAD+
PROD(25) = Rflux(4) + Rflux(18)+ 14*Rflux(20) + 4*Rflux(32);     % NADH
PROD(26) = 14/8*Rflux(26);                      % NADP+
PROD(27) = 2*Rflux(8);                          % NADPH
PROD(28) = Rflux(11);                           % GAP in OC
PROD(29) = Rflux(12)+Rflux(13);                 % G3P in OC

%*********************************************************************
% This section computes the utilization of the 29 species
% (the sum of all the reaction fluxes where the species is consumed
% scaled by the corresponding stochieometric coefficients).
%*********************************************************************

UTIL = zeros(29,1);
```

```
UTIL(1) = Rflux(1);                                % Glucose
UTIL(2) = Rflux(5) + Rflux(11) + Rflux(15) + Rflux(18);     % Pyruvate
UTIL(3) = 0;                                       % Lactate
UTIL(4) = Rflux(14)+Rflux(17);                             % Alanine
UTIL(5) = Rflux(13);                                       % Glycerol
UTIL(6) = Rflux(19);                               % Fatty Acid
UTIL(7) = Rflux(21) + Rflux(22);                    % TG
UTIL(8) = Rflux(33);                               % O2
UTIL(9) = 0;                                       % CO2
UTIL(10) = Rflux(2) + Rflux(6) + Rflux(8);     % Glucose 6-Phosphate
UTIL(11) = Rflux(7);                               % Glycogen
UTIL(12) = Rflux(3);                               % F6P
UTIL(13) = Rflux(9);                               % R5P
UTIL(14) = Rflux(4) + Rflux(10);    % Glyceraldehyde 3-Phosphate in GC
UTIL(15) = Rflux(27);               % Glycerol 3-Phosphate in GC
UTIL(16) = Rflux(26)+Rflux(32);                              % Acetyl-CoA
UTIL(17) =Rflux(20)+2*Rflux(27)+Rflux(28)+2*Rflux(36); % Fatty ACyl CoA
UTIL(18) = Rflux(18) + Rflux(19) + 7*Rflux(20);             % CoA
UTIL(19) = Rflux(23)+Rflux(28)+Rflux(29)+Rflux(31);         % DG
UTIL(20) = Rflux(24) + Rflux(25) + Rflux(30) + Rflux(31);  % MG
UTIL(21) = Rflux(1) + Rflux(3) + Rflux(6) + 3*Rflux(11)...
         + Rflux(13) + 2*Rflux(19) + 7/8*Rflux(26) + Rflux(34);  % ATP
UTIL(22) = 2*Rflux(4) + Rflux(32) + 6*Rflux(33);             % ADP
UTIL(23) = Rflux(4) + Rflux(7) + Rflux(32) + 6*Rflux(33);       % Pi
UTIL(24) = Rflux(4) + Rflux(18) + 14*Rflux(20) + 4*Rflux(32);    % NAD
UTIL(25) = Rflux(5)+Rflux(10)+Rflux(11)+Rflux(12)+2*Rflux(33); % NADH
UTIL(26) = 2*Rflux(8);                             % NADP+
UTIL(27) = 14/8*Rflux(26);                           % NADPH
UTIL(28) = Rflux(12);                              % GAP in OC
UTIL(29) = Rflux(36);                              % G3P in OC

%*********************************************************************
% This function computes the new Vmax and Tmax values from
% the resting/steady state uptake-release rates (URR0) and metabolic
% reaction fluxes (Rflux0) with the given updated Mm, Km, Kps and Krs
% values. This recalculation of Tmax and Vmax values are important for
% maintaining the resting/steady state conditions.
%*********************************************************************
function [Vmax Tmax Lam]=Adipose_TmaxVmax(Rflux0, URR0, Cb, Cc, Km, Ki,
Kps, Krs, Mm, Q);

format long

%*********************************************************************
% This section computes new Vmax values given the updated Mm, Km, Kps
% and Krs values (passed here through the global statement) and
% resting/steady state conditions (Rflux0 and Cc0 values).
%*********************************************************************

fact = zeros(36,1);

% Glucose Utilization:  GLC + ATP -> G6P + ADP
ctrl_G6P = 1 / (1 +(Cc(10)/Ki(1)));
fact(1)=ctrl_G6P*Cc(1)*Cc(21)/(Km(1)*(1+Cc(10)/Ki(1))+Cc(1)*Cc(21));

% Phosphoglucose Isomerase:  G6P <-> F6P
fact(2) = (Cc(10) - Cc(12)/ 0.33)/(Km(2)+Cc(10)+Cc(12)*Km(2)/Ki(2));
```

```
% F6P Breakdown:  F6P + ATP -> 2GA3P + ADP
nH2 = 2;
fact(3) = (Cc(22)/Cc(21))^nH2 / (Kps(3)^nH2 + (Cc(22)/Cc(21))^nH2) ...
           * Cc(12) / (Km(3) + Cc(12));

% GA3P Breakdown:  GA3P + Pi + NAD + 2ADP -> PYR + NADH + 2ATP
nH3=2;
fact(4) = ((Cc(24)/Cc(25)) / (Krs(4) + (Cc(24)/Cc(25))))* ...
          ((Cc(22)/Cc(21))^nH3)/(Kps(4)^nH3+(Cc(22)/Cc(21))^nH3) ...
          * Cc(14)*Cc(23) / (Km(4) + Cc(14)*Cc(23));

% Pyruvate Reduction:  PYR + NADH <-> LAC + NAD
fact(5) = (Cc(2) * Cc(25) - Cc(3) * Cc(24) / 1.06e4 ) ...
           / Km(5) / (1+Cc(2)*Cc(25)/Km(5)+Cc(3)*Cc(24)/Ki(5));

% Glycogen Synthesis:  G6P + ATP -> GLY + ADP + 2Pi
fact(6) = ((Cc(21)/Cc(22)) / (Kps(6) + (Cc(21)/Cc(22)))) ...
          * Cc(10) / (Km(6) + Cc(10));

% Glycogen Utilization:  GLY + Pi -> G6P
fact(7)=((Cc(22)/Cc(21))^2)/(Kps(7)^2+(Cc(22)/Cc(21))^2) ...
           * Cc(11)*Cc(23) / (Km(7) +  Cc(11)*Cc(23));

% Pentose Phosphate Shunt I:  G6P + 2NADP+ -> R5P + 2NADPH
fact(8) = ((Cc(26)/Cc(27)) / (Krs(8) + (Cc(26)/Cc(27)))) ...
           * Cc(10) / (Km(8) + Cc(10));

% Pentose Phosphate Shunt II:  R5P -> 2/3F6P + 1/3GAP
fact(9) = Cc(13) / (Km(9) + Cc(13));

% GAP Reduction I: GAP1 + NADH <-> G3P1 + NAD+
fact(10) = (Cc(14) * Cc(25) - Cc(15)*Cc(24)/ 2.768e8) ...
           / Km(10) / (1+Cc(14)*Cc(25)/Km(10)+Cc(15)*Cc(24)/Ki(10));

% Glyceroneogenesis: PYR + 3ATP + NADH -> GAP2 + 3ADP + NAD + 2Pi
fact(11) = ((Cc(25)/Cc(24)) / (Krs(11) + (Cc(25)/Cc(24))))* ...
       (Cc(21)/Cc(22)/(Kps(11)+Cc(21)/Cc(22)))*Cc(2)/(Km(11) + Cc(2));

% GAP Reduction II: GAP2 + NADH <-> G3P2 + NAD+
fact(12) = (Cc(28) * Cc(25) - Cc(29)*Cc(24)/ 2.768e8) ...
           / Km(12) / (1+Cc(28)*Cc(25)/Km(12)+Cc(29)*Cc(24)/Ki(12));

% Glycerol Phosphorylation: GLR + ATP -> G3P2 + ADP
fact(13) = ((Cc(21)/Cc(22)) / (Kps(13) + (Cc(21)/Cc(22)))) ...
           * Cc(5) / (Km(13) + Cc(5));

% Alanine Utilization:  ALA -> PYR
fact(14) = Cc(4) / (Km(14) + Cc(4));

% Alanine Production:  PYR -> ALA
fact(15) = Cc(2) / (Km(15) + Cc(2));

% Proteolysis: Protein -> ALA
fact(16)=1;
```

```
% Protein Synthesis: ALA -> Protein
fact(17)=1;

% Pyruvate Oxidation:  PYR + CoA + NAD -> ACoA + NADH + CO2
fact(18) = ((Cc(24)/Cc(25)) / (Krs(18) + (Cc(24)/Cc(25)))) ...
         *Cc(2)*Cc(18)/(Km(18)+Cc(2)*Cc(18)+Cc(16)*Km(18)/Ki(18));

% FAC Synthesis:  FFA + CoA + 2ATP -> FAC + 2ADP + 2Pi
fact(19) = ((Cc(21)/Cc(22)) / (Kps(19) + (Cc(21)/Cc(22)))) ...
            * Cc(6)*Cc(18) / (Km(19) + Cc(6)*Cc(18));

% FAC Oxidation:  FAC + 7CoA + 14 NAD -> 8ACoA + 14 NADH
fact(20) = ((Cc(24)/Cc(25)) / (Krs(20) + (Cc(24)/Cc(25)))) ...
          *Cc(17)*Cc(18)/(Km(20)+Cc(17)*Cc(18)+Cc(16)*Km(20)/Ki(20));

% TG Breakdown by ATGL:  TGL -> DG + FFA
fact(21) = 1;

% TG Breakdown by HSL:  TGL -> DG + FFA
fact(22) = 1;

% DG Breakdown by HSL:  DG -> MG + FFA
fact(23) = Cc(19) / (Km(23) + Cc(19));

% MG Breakdown by MGL:  MG -> GLR + FFA
fact(24) = Cc(20) / (Km(24) + Cc(20));

% MG Breakdown by HSL:  MG -> GLR + FFA
fact(25) = Cc(20) / (Km(25) + Cc(20));

% de novo Lipogenesis: 8ACoA + 14NADPH + 7ATP -> FFA + 8CoA + 14NADP+
% 7ADP + 7Pi
fact(26) = (Cc(27)/Cc(26)) / (Krs(26) + (Cc(27)/Cc(26))) * ...
          Cc(21)/Cc(22)/(Kps(26)+Cc(21)/Cc(22))*Cc(16)/(Km(26)+Cc(16));

% DG Synthesis in Glycolytic Domain:  G3P1 + 2FAC -> DG + 2CoA + Pi
fact(27) = Cc(15) * Cc(17) / (Km(27) + Cc(15) * Cc(17));

% TG Synthesis:  DG + FAC -> TG + CoA
fact(28) = Cc(19) * Cc(17) / (Km(28) + Cc(19) * Cc(17));

% Transacylation I: DG + DG -> TG + MG
fact(29) = Cc(19) / (Km(29) + Cc(19));

% Transacylation II: MG + MG -> DG + GLR
fact(30) = Cc(20) / (Km(30) + Cc(20));

% Transacylation III: MG + DG -> TG + GLR
fact(31) = Cc(19) * Cc(20) / (Km(31) + Cc(19) * Cc(20));

% TCA Cycle:  ACoA + ADP + Pi + 4NAD+ -> 2CO2 + CoA + ATP + 4NADH
fact(32) = (Cc(24)/Cc(25)) / (Krs(32) + (Cc(24)/Cc(25))) * ...
            Cc(22)/Cc(21) / (Kps(32) + Cc(22)/Cc(21)) ...
            * Cc(16)*Cc(23) / (Km(32) + Cc(16)*Cc(23));
```

```
% Oxygen Consumption:  O2 + 6ADP + 6Pi + 2NADH -> H2O + 6ATP + 2NAD
fact(33) = (Cc(25)/Cc(24)) / (Krs(33) + (Cc(25)/Cc(24))) * ...
           Cc(22)/Cc(21) / (Kps(33) + Cc(22)/Cc(21)) ...
           * Cc(8)*Cc(23) / (Km(33) + Cc(8)*Cc(23));

% ATP Hydrolysis:  ATP -> ADP + Pi
fact(34) = Cc(21) / (Km(34) + Cc(21));

% TG Breakdown by LPL: TG -> GLR + 3FFA
fact(35) = 0.5;

% DG Synthesis in Other Cellular Domain:  G3P2 + 2FAC -> DG + 2CoA + Pi
fact(36) = Cc(29) * Cc(17) / (Km(36) + Cc(29) * Cc(17));

Vmax=Rflux0./fact;
Tmax=zeros(9,1);
Lam=zeros(9,1);
Tmax(1) = URR0(1)/(Cb(1)/(Mm(1) + Cb(1))-Cc(1)/(Mm(1) + Cc(1)));  % GLC
Tmax(2) = URR0(2)/(Cb(2)/(Mm(2) + Cb(2))-Cc(2)/(Mm(2) + Cc(2)));  % PYR
Tmax(3) = URR0(3)/(Cb(3)/(Mm(3) + Cb(3))-Cc(3)/(Mm(3) + Cc(3)));  % LAC
Lam(6) = URR0(6)/(Cb(6)-Cc(6));                                   % FFA
Lam(4) = URR0(4)/(Cb(4)-Cc(4));  % ALA
Lam(5) = URR0(5)/(Cb(5)-Cc(5));  % GLR
Lam(8:9) = URR0(8:9)./(Cb(8:9)-Cc(8:9));

%*********************************************************************
% The function Adipose_Cdot_Est lists the system of differential
% equations governing the transport and metabolism of chemical species
% in the adipose tissue.
% It is based on dynamic mass balances of all the species.
%*********************************************************************

function [Cdot] = Adipose_Cdot_Est(t,C,p)

global URR0 Rflux0 Ca Cb0 Cc0 C0 Cb Cc
global Tmax Mm Lam Vmax Km Kps Krs Ki Sigma_O2 Sigma_CO2 ...
       CO2bTot CO2cTot SHbO2b O2bTot SMbO2c O2cTot StO2
global V Q UPT REL URR AVD Vvivo Rflux PROD UTIL MRR epi Vmax0 Tmax0
Lam0 CIns
format long

Cb = zeros(9,1);       % Initialization of Cb
Cc = zeros(29,1);      % Initialization of Cc
Cb = C(1:9);           % Blood species concentrations
Cc = C(10:38);          % Cells species concentrations

Tmax(1)=C(39);



CO2a = Ca(9);          % Free CO2 concentration in arterial blood
CO2b = Cb(9);        % Free CO2 concentration in capillary/venous blood
CO2c = Cc(9);          % Free CO2 concentration in tissue cells
O2a = Ca(8);           % Free O2 concentration in arterial blood
```

```
O2b = Cb(8);          % Free O2 concentration in capillary/venous blood
O2c = Cc(8);           % Free O2 concentration in tissue cells

Vb = 0.07;                      % Blood volume fraction
Visf = 0.13;                    % ISF volume fraction
Vc = 0.8;                       % Cell volume fraction
[SHbCO2a,CHbCO2a,CHCO3a,CO2aTot] = CO2Tot_Blood(CO2a/1000);
[SHbCO2b,CHbCO2b,CHCO3b,CO2bTot] = CO2Tot_Blood(CO2b/1000);
[CHCO3c,CO2cTot] = CO2Tot_Cells(CO2c/1000);
[SHbO2a,CHbO2a,O2aTot] = O2Tot_Blood(O2a/1000);
[SHbO2b,CHbO2b,O2bTot] = O2Tot_Blood(O2b/1000);
[SMbO2c,CMbO2c,O2cTot] = O2Tot_Cells(O2c/1000);
Hct = 0.42; CHbTot = 5.2; CMbTot = 0.5;
StO2 = (Vb*CHbO2b/4 + Vc*CMbO2c)/(Vb*Hct*CHbTot + Vc*CMbTot);

% Vmax modification due to epinephrine infusion
% Recalculate flux rate based on the modified Vmax

CIns0=40*0.21;

if t < 15
    Q=0.031;
    Ca(1)=5000;
    Ca(3)=700;
    Ca(5)=70;
    Ca(6)=660*0.58;
    Ca(7)=990*0.58;
    CIns=CIns0;
    Vmax(1)=Vmax0(1);
    Vmax(3:4)=Vmax0(3:4);
    Vmax(6)=Vmax0(6);
    Vmax(18)=Vmax0(18);
    Vmax(19)=Vmax0(19);
    Vmax(26:28)=Vmax0(26:28);
    Vmax(36)=Vmax0(36);
    Vmax(7)=Vmax0(7);
    Vmax(20:23)=Vmax0(20:23);
    Vmax(25)=Vmax0(25);
    Vmax(16)=Vmax0(16);
    Tmax(1)=Tmax0(1);
else
 Q=0.031*(1+7.764*(1-exp(-(t-15)/20.54))-7.682*(1-exp(-(t-15)/36.48)));
    Ca(1)=5000*(1-1.7716e-1*(t-15)^5.26/((2.2821e1)^5.26+ ...
         (t-15)^5.26)+4.2096e-1*(1-exp(-(t-15)/3.5034e2)));
    Ca(3)=700*(1+0.3891*(t-15)^7.0524/(18.8772^7.0524+(t-15)^7.0524));
    Ca(5)=70*(0.4103 + 0.5906*exp(-(t-15)/10.3844));
    Ca(6)=660*0.58*(0.1175 + 0.8909*exp(-(t-15)/17.219));
    Ca(7)=990*(1-0.0015*(t-15))*0.58;
    CIns=0.21*(40+310*(1-exp(-(t-15)/10)));
    Vmax(1)=Vmax0(1)*(1+p(1)*(CIns-CIns0)^2/(70.6+(CIns-CIns0)^2));
    Vmax(3:4)=Vmax0(3:4).*(1+p(1)*(CIns-CIns0)^2/  ...
              (70.6+(CIns-CIns0)^2));
    Vmax(6)=Vmax0(6)*(1+p(2)*(CIns-CIns0)^2/(70.6+(CIns-CIns0)^2));
    Vmax(18)=Vmax0(18)*(1+p(4)*(CIns-CIns0)^2/(70.6+(CIns-CIns0)^2));
    Vmax(7)=Vmax0(7)*8.4^2/(8.4^2+CIns^2)/0.5;
    Vmax(21)=Vmax0(21)*(8.4*3)^2/((8.4*3)^2+CIns^2)*10/9;
%    Vmax(21)=Vmax0(21)*(8.4)^2/((8.4)^2+CIns^2)/0.5;
```

```
    Vmax(22:23)=Vmax0(22:23)*8.4^2/(8.4^2+CIns^2)/0.5;
    Vmax(16)=Vmax0(16)*8.4^2/(8.4^2+CIns^2)/0.5;
end;

Adipose_Flux;

UPT = zeros(9,1);                          % Initialization of UPT
REL = zeros(9,1);                          % Initialization of REL
URR = zeros(9,1);                          % Initialization of URR
AVD = zeros(9,1);                          % Initialization of AVD

UPT(1) = Tmax(1)*Cb(1)/(Mm(1) + Cb(1));    % Uptake of GLC from blood
REL(1) = Tmax(1)*Cc(1)/(Mm(1) + Cc(1));    % Release of GLC to blood
UPT(2) = Tmax(2)*Cb(2)/(Mm(2) + Cb(2));    % Uptake of PYR from blood
REL(2) = Tmax(2)*Cc(2)/(Mm(2) + Cc(2));    % Release of PYR to blood
UPT(3) = Tmax(3)*Cb(3)/(Mm(3) + Cb(3));    % Uptake of LAC from blood
REL(3) = Tmax(3)*Cc(3)/(Mm(3) + Cc(3));    % Release of LAC to blood
UPT(4) = Lam(4)*Cb(4);                     % Uptake of ALA from blood
REL(4) = Lam(4)*Cc(4);                     % Release of ALA to blood
UPT(5) = Lam(5)*Cb(5);                     % Uptake of GLC from blood
REL(5) = Lam(5)*Cc(5);                     % Release of GLC to blood
UPT(6) = Lam(6)*Cb(6);    % Uptake of FFA from blood
REL(6) = Lam(6)*Cc(6);    % Release of FFA to blood
UPT(7) = 0.0;
REL(7) = 0.0;
UPT(8) = Lam(8)*Cb(8);                     % Uptake of O2 from blood
REL(8) = Lam(8)*Cc(8);            % Release of O2 to blood
UPT(9) = Lam(9)*Cb(9);                     % Uptake of CO2 from blood
REL(9) = Lam(9)*Cc(9);           % Release of CO2 to blood

URR = UPT - REL;                           % URR for all 9 species

AVD(1:7) = Q*(Ca(1:7) - Cb(1:7));          % AVD for 7 species
AVD(9) = Q*(CO2aTot - CO2bTot)*1000;            % AVD for CO2
AVD(8) = Q*(O2aTot - O2bTot)*1000;              % AVD for O2

[VbeffCO2] = VeffCO2_Blood(Vb,Visf,Cb(9)/1000);
[VbeffO2] = VeffO2_Blood(Vb,Visf,Cb(8)/1000);
[VceffCO2] = VeffCO2_Cells(Vc,Cc(9)/1000);
[VceffO2] = VeffO2_Cells(Vc,Cc(8)/1000);

Vbeff = (Vb+Visf)*ones(9,1);
Vbeff(7)=Vb;
Vbeff(9) = VbeffCO2;
Vbeff(8) = VbeffO2;
Vceff = Vc*ones(29,1);
Vceff(1:29) = 0.032;
Vceff(14:15) = 0.016;
Vceff(28:29) = 0.016;
Vceff(7)=0.8;
Vceff(19:20)=0.8;
Vceff(9) = VceffCO2;
Vceff(8) = VceffO2;

MRR = zeros(29,1);
MRR = PROD - UTIL;
```

```
Cbdot = zeros(9,1);
Ccdot = zeros(29,1);
Cdot  = zeros(39,1);
Cbdot = (AVD - URR)./Vbeff;
Cbdot(5) = Cbdot(5) + Rflux(35)/Vbeff(5);
Cbdot(6) = Cbdot(6) + 3*Rflux(35)/Vbeff(6);
Cbdot(7) = Cbdot(7) - Rflux(35)/Vbeff(7);
Ccdot(1:9) = (MRR(1:9) + URR(1:9)) ./ Vceff(1:9);
Ccdot(10:29) = MRR(10:29) ./ Vceff(10:29);
Vmdot = (1+p(3)*CIns-(1+p(3)*CIns0)*C(39)/C0(39));
Cdot = [Cbdot;Ccdot;Vmdot];

% END OF DIFFERENTIAL EQUATIONS
%*********************************************
```

BIBLIOGRAPHY

Abumrad,N.N., A.D.Cherrington, P.E.Williams, W.W.Lacy, and D.Rabin. 1982. Absorption and disposition of a glucose load in the conscious dog. Am. J. Physiol 242:E398-E406.

Ahlborg,G., P.Felig, L.Hagenfeldt, R.Hendler, and J.Wahren. 1974. Substrate turnover during prolonged exercise in man. Splanchnic and leg metabolism of glucose, free fatty acids, and amino acids. J. Clin. Invest 53:1080-1090.

Alberty,R.A. 2003. Thermodynamics of Biochemical Reactions. Wiley & Sons, Hoboken, NJ.

Albright,A.L., and J.S.Stern. 1998. Adipose Tissue. in: T.D.Fay (Ed.), Encyclopedia of Sport Medicine and Science, Internet Society for Sport Science, Internet Society for Sport Science

Arbuckle,M.I., S.Kane, L.M.Porter, M.J.Seatter, and G.W.Gould. 1996. Structure-Function Analysis of Liver-Type (GLUT2) and Brain-Type (GLUT3) Glucose Transporters: Expression of Chimeric Transporters in Xenopus Oocytes Suggests an Important Role for Putative Transmembrane Helix 7 in Determining Substrate Selectivity. Biochemistry 35:16519-16527.

Arner,P., andJ.Bulow. 1993. Assessment of adipose tissue metabolism in man: comparison of Fick and microdialysis techniques. Clin. Sci. (Lond) 85:247-256.

Arner,P., andJ.Ostman. 1974. Mono-acid diacylglycerols in human adipose tissue. Biochim. Biophys. Acta 369:209-221.

Beale,E.G., andE.J.Tishler. 1992. Expression and regulation of cytosolic phosphoenolpyruvate carboxykinase in 3T3-L1 adipocytes. Biochem. Biophys. Res. Commun. 189:925-930.

Beard,D.A. 2005. A biophysical model of the mitochondrial respiratory system and oxidative phosphorylation. PLoS. Comput. Biol. 1:e36.

Belfort,R., L.Mandarino, S.Kashyap, K.Wirfel, T.Pratipanawatr, R.Berria, R.A.DeFronzo, and K.Cusi. 2005. Dose-Response Effect of Elevated Plasma Free Fatty Acid on Insulin Signaling. Diabetes 54:1640-1648.

Bergman,B.C., andG.A.Brooks. 1999. Respiratory gas-exchange ratios during graded exercise in fed and fasted trained and untrained men. J. Appl. Physiol 86:479-487.

Bergman,B.C., G.E.Butterfield, E.E.Wolfel, G.A.Casazza, G.D.Lopaschuk, and

G.A.Brooks. 1999a. Evaluation of exercise and training on muscle lipid metabolism. Am. J. Physiol 276:E106-E117.

Bergman,B.C., G.E.Butterfield, E.E.Wolfel, G.D.Lopaschuk, G.A.Casazza, M.A.Horning, and G.A.Brooks. 1999b. Muscle net glucose uptake and glucose kinetics after endurance training in men. Am. J. Physiol 277:E81-E92.

Bergman,B.C., M.A.Horning, G.A.Casazza, E.E.Wolfel, G.E.Butterfield, and G.A.Brooks. 2000. Endurance training increases gluconeogenesis during rest and exercise in men. Am. J. Physiol Endocrinol. Metab 278:E244-E251.

Bergman,B.C., E.E.Wolfel, G.E.Butterfield, G.D.Lopaschuk, G.A.Casazza, M.A.Horning, and G.A.Brooks. 1999c. Active muscle and whole body lactate kinetics after endurance training in men. J. Appl. Physiol 87:1684-1696.

Bergman,R.N., Y.Z.Ider, C.R.Bowden, and C.Cobelli. 1979. Quantitative estimation of insulin sensitivity. Am. J. Physiol 236:E667-E677.

Bjorkman,O., L.S.Eriksson, B.Nyberg, and J.Wahren. 1990. Gut exchange of glucose and lactate in basal state and after oral glucose ingestion in postoperative patients. Diabetes 39:747-751.

Boden,G., X.Chen, R.A.Desantis, and Z.Kendrick. 1993. Effects of insulin on fatty acid reesterification in healthy subjects. Diabetes 42:1588-1593.

Boden,G., X.Chen, J.Ruiz, J.V.White, and L.Rossetti. 1994. Mechanisms of fatty acid-induced inhibition of glucose uptake. J Clin. Invest 93:2438-2446.

Bodenlenz,M., L.A.Schaupp, T.Druml, R.Sommer, A.Wutte, H.C.Schaller, F.Sinner, P.Wach, and T.R.Pieber. 2005. Measurement of interstitial insulin in human adipose and muscle tissue under moderate hyperinsulinemia by means of direct interstitial access. Am. J Physiol Endocrinol. Metab 289:E296-E300.

Bradbury,M.W. 2006. Lipid metabolism and liver inflammation. I. Hepatic fatty acid uptake: possible role in steatosis. Am. J. Physiol Gastrointest. Liver Physiol 290:G194-G198.

Brasaemle,D.L., B.Rubin, I.A.Harten, J.Gruia-Gray, A.R.Kimmel, and C.Londos. 2000. Perilipin A increases triacylglycerol storage by decreasing the rate of triacylglycerol hydrolysis. J. Biol. Chem. 275:38486-38493.

Brito,S.C., W.L.Festuccia, N.H.Kawashita, M.F.Moura, A.R.Xavier, M.A.Garofalo, I.C.Kettelhut, and R.H.Migliorini. 2006. Increased glyceroneogenesis in adipose tissue from rats adapted to a high-protein, carbohydrate-free diet: role of dietary fatty acids. Metabolism 55:84-89.

Brooks,G.A. 2007. Lactate: link between glycolytic and oxidative metabolism. Sports Med. 37:341-343.

Brooks,G.A., andJ.Mercier. 1994. Balance of carbohydrate and lipid utilization during exercise: the "crossover" concept. J. Appl. Physiol 76:2253-2261.

Cabrera,M.E., G.M.Saidel, and S.C.Kalhan. 1998. Role of O2 in regulation of lactate dynamics during hypoxia: mathematical model and analysis. Ann. Biomed. Eng 26:1-27.

Cabrera,M.E., G.M.Saidel, and S.C.Kalhan. 1999. Lactate metabolism during exercise: analysis by an integrative systems model. Am. J. Physiol 277:R1522-R1536.

Carmen,G.Y., andS.M.Victor. 2006. Signalling mechanisms regulating lipolysis. Cell Signal. 18:401-408.

Casazza,J.P., andR.L.Veech. 1986. The interdependence of glycolytic and pentose cycle intermediates in ad libitum fed rats. J Biol. Chem. 261:690-698.

Chang,T.J., W.J.Lee, H.M.Chang, K.C.Lee, and L.M.Chuang. 2008. Expression of subcutaneous adipose tissue phosphoenolpyruvate carboxykinase correlates with body mass index in nondiabetic women. Metabolism 57:367-372.

Chen,J., andP.D.Gollnick. 1994. Effect of exercise on hexokinase distribution and mitochondrial respiration in skeletal muscle. Pflugers Arch. 427:257-263.

Clifford,G.M., C.Londos, F.B.Kraemer, R.G.Vernon, and S.J.Yeaman. 2000. Translocation of hormone-sensitive lipase and perilipin upon lipolytic stimulation of rat adipocytes. J. Biol. Chem. 275:5011-5015.

Coppack,S.W., K.N.Frayn, and S.M.Humphreys. 1989a. Plasma triacylglycerol extraction in human adipose tissue in vivo: effects of glucose ingestion and insulin infusion. Eur. J. Clin. Nutr. 43:493-496.

Coppack,S.W., K.N.Frayn, S.M.Humphreys, H.Dhar, and T.D.Hockaday. 1989b. Effects of insulin on human adipose tissue metabolism in vivo. Clin. Sci. (Lond) 77:663-670.

Coppack,S.W., K.N.Frayn, S.M.Humphreys, P.L.Whyte, and T.D.Hockaday. 1990. Arteriovenous differences across human adipose and forearm tissues after overnight fast. Metabolism 39:384-390.

Coppack,S.W., M.Persson, and J.M.Miles. 1996. Phenylalanine kinetics in human adipose tissue. J. Clin. Invest 98:692-697.

Crofford,O.B., andA.E.Renold. 1965. GLUCOSE UPTAKE BY INCUBATED RAT EPIDIDYMAL ADIPOSE TISSUE. RATE-LIMITING STEPS AND SITE OF INSULIN ACTION. J. Biol. Chem. 240:14-21.

Dash,R.K., andJ.B.Bassingthwaighte. 2006a. Simultaneous blood-tissue exchange of oxygen, carbon dioxide, bicarbonate, and hydrogen ion. Ann. Biomed. Eng 34:1129-1148.

Dash,R., andJ.Bassingthwaighte. 2006b. Simultaneous blood-tissue exchange of oxygen, carbon dioxide, bicarbonate and hydrogen ion. Ann. Biomed. Eng. 34:1129-1148.

DeFronzo,R.A., E.Jacot, E.Jequier, E.Maeder, J.Wahren, and J.P.Felber. 1981. The effect of insulin on the disposal of intravenous glucose. Results from indirect calorimetry and hepatic and femoral venous catheterization. Diabetes 30:1000-1007.

Denton,R.M., andM.L.Halperin. 1968. The control of fatty acid and triglyceride synthesis in rat epididymal adipose tissue. Roles of coenzyme A derivatives, citrate and L-glycerol 3-phosphate. Biochem. J. 110:27-38.

Denton,R.M., R.E.Yorke, and P.J.Randle. 1966. Measurement of concentrations of metabolites in adipose tissue and effects of insulin, alloxan-diabetes and adrenaline. Biochem. J. 100:407-419.

DiGirolamo,M., F.D.Newby, and J.Lovejoy. 1992. Lactate production in adipose tissue: a regulated function with extra-adipose implications. FASEB J. 6:2405-2412.

Edens,N.K., R.L.Leibel, and J.Hirsch. 1990a. Lipolytic effects on diacylglycerol accumulation in human adipose tissue in vitro. J. Lipid Res. 31:1351-1359.

Edens,N.K., R.L.Leibel, and J.Hirsch. 1990b. Mechanism of free fatty acid re-esterification in human adipocytes in vitro. J. Lipid Res. 31:1423-1431.

Ekberg,K., B.R.Landau, A.Wajngot, V.Chandramouli, S.Efendic, H.Brunengraber, and J.Wahren. 1999. Contributions by kidney and liver to glucose production in the postabsorptive state and after 60 h of fasting. Diabetes 48:292-298.

Elia,M., C.Zed, G.Neale, and G.Livesey. 1987. The energy cost of triglyceride-fatty acid recycling in nonobese subjects after an overnight fast and four days of starvation. Metabolism 36:251-255.

Franckhauser,S., S.Munoz, A.Pujol, A.Casellas, E.Riu, P.Otaegui, B.Su, and F.Bosch. 2002. Increased fatty acid re-esterification by PEPCK overexpression in adipose tissue leads to obesity without insulin resistance. Diabetes 51:624-630.

Frayn,K.N. 2001. Adipose tissue and the insulin resistance syndrome. Proc. Nutr. Soc. 60:375-380.

Frayn,K.N. 2002. Adipose tissue as a buffer for daily lipid flux. Diabetologia 45:1201-1210.

Frayn,K.N., S.W.Coppack, S.M.Humphreys, and P.L.Whyte. 1989. Metabolic characteristics of human adipose tissue in vivo. Clin. Sci. (Lond) 76:509-516.

Frayn,K.N., S.M.Humphreys, and S.W.Coppack. 1995. Fuel selection in white adipose tissue. Proc. Nutr. Soc. 54:177-189.

Frayn,K.N., F.Karpe, B.A.Fielding, I.A.Macdonald, and S.W.Coppack. 2003. Integrative physiology of human adipose tissue. Int. J. Obes. Relat Metab Disord. 27:875-888.

Frayn,K.N., K.Khan, S.W.Coppack, and M.Elia. 1991. Amino acid metabolism in human subcutaneous adipose tissue in vivo. Clin. Sci. (Lond) 80:471-474.

Frayn,K.N., S.Shadid, R.Hamlani, S.M.Humphreys, M.L.Clark, B.A.Fielding, O.Boland, and S.W.Coppack. 1994. Regulation of fatty acid movement in human adipose tissue in the postabsorptive-to-postprandial transition. Am. J. Physiol 266:E308-E317.

Friedlander,A.L., G.A.Casazza, M.A.Horning, M.J.Huie, and G.A.Brooks. 1997. Training-induced alterations of glucose flux in men. J. Appl. Physiol 82:1360-1369.

Friedlander,A.L., G.A.Casazza, M.A.Horning, A.Usaj, and G.A.Brooks. 1999. Endurance training increases fatty acid turnover, but not fat oxidation, in young men. J. Appl. Physiol 86:2097-2105.

Galbo,H., E.A.Richter, J.Hilsted, J.J.Holst, N.J.Christensen, and J.Henriksson. 1977. Hormonal regulation during prolonged exercise. Ann. N. Y. Acad. Sci. 301:72-80.

Geers,C., andG.Gros. 2000. Carbon dioxide transport and carbonic anhydrase in blood and muscle. Physiol Rev. 80:681-715.

Gerich,J.E. 1993. Control of glycaemia. Baillieres Clin. Endocrinol. Metab 7:551-586.

Gerich,J.E. 2000. Physiology of glucose homeostasis. Diabetes Obes. Metab 2:345-350.

Granneman,J.G., H.P.Moore, R.L.Granneman, A.S.Greenberg, M.S.Obin, and Z.Zhu. 2007. Analysis of lipolytic protein trafficking and interactions in adipocytes. J. Biol. Chem. 282:5726-5735.

Grimmsmann,T., K.Levin, M.M.Meyer, H.Beck-Nielsen, and H.H.Klein. 2002. Delays in insulin signaling towards glucose disposal in human skeletal muscle. J. Endocrinol. 172:645-651.

Haemmerle,G., A.Lass, R.Zimmermann, G.Gorkiewicz, C.Meyer, J.Rozman, G.Heldmaier, R.Maier, C.Theussl, S.Eder, D.Kratky, E.F.Wagner, M.Klingenspor, G.Hoefler, and R.Zechner. 2006. Defective lipolysis and altered energy metabolism in mice lacking adipose triglyceride lipase. Science 312:734-737.

Haemmerle,G., R.Zimmermann, M.Hayn, C.Theussl, G.Waeg, E.Wagner, W.Sattler, T.M.Magin, E.F.Wagner, and R.Zechner. 2002. Hormone-sensitive lipase deficiency in mice causes diglyceride accumulation in adipose tissue, muscle, and testis. J. Biol. Chem. 277:4806-4815.

Harvey,W.D., G.R.Faloona, and R.H.Unger. 1974. The effect of adrenergic blockade on exercise-induced hyperglucagonemia. Endocrinology 94:1254-1258.

Henderson,G.C., M.A.Horning, S.L.Lehman, E.E.Wolfel, B.C.Bergman, and G.A.Brooks. 2004. Pyruvate shuttling during rest and exercise before and after endurance training in men. J. Appl. Physiol 97:317-325.

Himwich,H.E., andL.H.Nahum. 1932. THE RESPIRATORY QUOTIENT OF THE BRAIN. Am J Physiol 101:446-453.

Hirsch,I.B., J.C.Marker, L.J.Smith, R.J.Spina, C.A.Parvin, J.O.Holloszy, and P.E.Cryer. 1991. Insulin and glucagon in prevention of hypoglycemia during exercise in humans. Am. J. Physiol 260:E695-E704.

Honnor,R.C., G.S.Dhillon, and C.Londos. 1985. cAMP-dependent protein kinase and lipolysis in rat adipocytes. II. Definition of steady-state relationship with lipolytic and antilipolytic modulators. J. Biol. Chem. 260:15130-15138.

Hundal,R.S., M.Krssak, S.Dufour, D.Laurent, V.Lebon, V.Chandramouli, S.E.Inzucchi, W.C.Schumann, K.F.Petersen, B.R.Landau, and G.I.Shulman. 2000. Mechanism by which metformin reduces glucose production in type 2 diabetes. Diabetes 49:2063-2069.

Jansson,P.A., A.Larsson, U.Smith, and P.Lonnroth. 1994. Lactate release from the subcutaneous tissue in lean and obese men. J. Clin. Invest 93:240-246.

Jensen,M.D. 2002. Adipose tissue and fatty acid metabolism in humans. J. R. Soc. Med. 95 Suppl 42:3-7.

Jensen,M.D., K.Ekberg, and B.R.Landau. 2001. Lipid metabolism during fasting. Am. J. Physiol Endocrinol. Metab 281:E789-E793.

Jensen,M.D., M.W.Haymond, R.A.Rizza, P.E.Cryer, and J.M.Miles. 1989. Influence of body fat distribution on free fatty acid metabolism in obesity. J Clin. Invest 83:1168-1173.

Jurczak,M.J., A.M.Danos, V.R.Rehrmann, M.B.Allison, C.C.Greenberg, and M.J.Brady. 2007. Transgenic overexpression of protein targeting to glycogen markedly increases adipocytic glycogen storage in mice. Am. J. Physiol Endocrinol. Metab 292:E952-E963.

Kahn,S.E., R.L.Hull, and K.M.Utzschneider. 2006. Mechanisms linking obesity to insulin resistance and type 2 diabetes. Nature 444:840-846.

Kanda,H., S.Tateya, Y.Tamori, K.Kotani, K.Hiasa, R.Kitazawa, S.Kitazawa, H.Miyachi, S.Maeda, K.Egashira, and M.Kasuga. 2006. MCP-1 contributes to macrophage infiltration into adipose tissue, insulin resistance, and hepatic steatosis in obesity. J Clin. Invest 116:1494-1505.

Karpe,F., B.A.Fielding, J.L.Ardilouze, V.Ilic, I.A.Macdonald, and K.N.Frayn. 2002. Effects of insulin on adipose tissue blood flow in man. J. Physiol 540:1087-1093.

Karpe,F., T.Olivecrona, G.Olivecrona, J.S.Samra, L.K.Summers, S.M.Humphreys, and K.N.Frayn. 1998. Lipoprotein lipase transport in plasma: role of muscle and adipose tissues in regulation of plasma lipoprotein lipase concentrations. J. Lipid Res. 39:2387-2393.

Kemp,B.E., K.I.Mitchelhill, D.Stapleton, B.J.Michell, Z.P.Chen, and L.A.Witters. 1999. Dealing with energy demand: the AMP-activated protein kinase. Trends Biochem. Sci. 24:22-25.

Kershaw,E.E., J.K.Hamm, L.A.Verhagen, O.Peroni, M.Katic, and J.S.Flier. 2006. Adipose triglyceride lipase: function, regulation by insulin, and comparison with adiponutrin. Diabetes 55:148-157.

Kim,J., G.M.Saidel, and M.E.Cabrera. 2007. Multi-scale computational model of fuel homeostasis during exercise: effect of hormonal control. Ann. Biomed. Eng 35:69-90.

Kim,J., G.M.Saidel, and S.C.Kalhan. 2008. A computational model of adipose tissue metabolism: evidence for intracellular compartmentation and differential activation of lipases. J. Theor. Biol. 251:523-540.

Klein,S., andR.R.Wolfe. 1990. Whole-body lipolysis and triglyceride-fatty acid cycling in cachectic patients with esophageal cancer. J. Clin. Invest 86:1403-1408.

Korzeniewski,B., andP.Liguzinski. 2004. Theoretical studies on the regulation of anaerobic glycolysis and its influence on oxidative phosphorylation in skeletal muscle. Biophys. Chem. 110:147-169.

Krebs,H.A., R.Hems, M.J.Weidemann, and R.N.Speake. 1966. The fate of isotopic carbon in kidney cortex synthesizing glucose from lactate. Biochem. J. 101:242-249.

Krudys,K.M., M.G.Dodds, S.M.Nissen, and P.Vicini. 2005. Integrated model of hepatic and peripheral glucose regulation for estimation of endogenous glucose production during the hot IVGTT. Am. J. Physiol Endocrinol. Metab 288:E1038-E1046.

Lambeth,M.J., andM.J.Kushmerick. 2002. A computational model for glycogenolysis in skeletal muscle. Ann. Biomed. Eng 30:808-827.

Landau,B.R., J.Wahren, V.Chandramouli, W.C.Schumann, K.Ekberg, and S.C.Kalhan. 1995. Use of 2H2O for estimating rates of gluconeogenesis. Application to the fasted state. J. Clin. Invest 95:172-178.

Langin,D., andP.Arner. 2006. Importance of TNFalpha and neutral lipases in human adipose tissue lipolysis. Trends Endocrinol. Metab 17:314-320.

Large,V., P.Arner, S.Reynisdottir, J.Grober, H.Van, V, C.Holm, and D.Langin. 1998. Hormone-sensitive lipase expression and activity in relation to lipolysis in human

fat cells. J. Lipid Res. 39:1688-1695.

Large,V., O.Peroni, D.Letexier, H.Ray, and M.Beylot. 2004. Metabolism of lipids in human white adipocyte. Diabetes Metab 30:294-309.

Lewis,G.F., K.D.Uffelman, L.W.Szeto, and G.Steiner. 1993. Effects of acute hyperinsulinemia on VLDL triglyceride and VLDL apoB production in normal weight and obese individuals. Diabetes 42:833-842.

Londos,C., D.L.Brasaemle, J.Gruia-Gray, D.A.Servetnick, C.J.Schultz, D.M.Levin, and A.R.Kimmel. 1995. Perilipin: unique proteins associated with intracellular neutral lipid droplets in adipocytes and steroidogenic cells. Biochem. Soc. Trans. 23:611-615.

Londos,C., D.L.Brasaemle, C.J.Schultz, J.P.Segrest, and A.R.Kimmel. 1999. Perilipins, ADRP, and other proteins that associate with intracellular neutral lipid droplets in animal cells. Semin. Cell Dev. Biol. 10:51-58.

Lund,S., G.D.Holman, O.Schmitz, and O.Pedersen. 1995. Contraction stimulates translocation of glucose transporter GLUT4 in skeletal muscle through a mechanism distinct from that of insulin. Proc. Natl. Acad. Sci. U. S. A 92:5817-5821.

Luyckx,A.S., andP.J.Lefebvre. 1974. Mechanisms involved in the exercise-induced increase in glucagon secretion in rats. Diabetes 23:81-93.

Mann,F.C., andW.M.Boothby. 1928. STUDIES ON THE PHYSIOLOGY OF THE LIVER: XVI. The Respiratory Quotient and Basal Metabolic Rate Following Removal of the Liver and Injection of Glucose. Am J Physiol 87:486-496.

Martin,G., K.Schoonjans, A.M.Lefebvre, B.Staels, and J.Auwerx. 1997. Coordinate regulation of the expression of the fatty acid transport protein and acyl-CoA synthetase genes by PPARalpha and PPARgamma activators. J Biol. Chem. 272:28210-28217.

Martin,W.H., III, G.P.Dalsky, B.F.Hurley, D.E.Matthews, D.M.Bier, J.M.Hagberg, M.A.Rogers, D.S.King, and J.O.Holloszy. 1993. Effect of endurance training on plasma free fatty acid turnover and oxidation during exercise. Am. J. Physiol 265:E708-E714.

McLean,P., A.L.Greenbaum, J.Brown, and K.R.Greenslade. 1967. Influence of hormones on the nicotinamide nucleotide coenzymes of adipose tissue. Biochem. J 105:1013-1018.

Michelson,S. 2006. The impact of systems biology and biosimulation on drug discovery and development. Mol. Biosyst. 2:288-291.

Miyoshi,H., J.W.Perfield, S.C.Souza, W.J.Shen, H.H.Zhang, Z.S.Stancheva, F.B.Kraemer, M.S.Obin, and A.S.Greenberg. 2007. Control of adipose triglyceride lipase action

by serine 517 of perilipin A globally regulates protein kinase A-stimulated lipolysis in adipocytes. J Biol. Chem. 282:996-1002.

Miyoshi,H., G.I.Shulman, E.J.Peters, M.H.Wolfe, D.Elahi, and R.R.Wolfe. 1988. Hormonal control of substrate cycling in humans. J. Clin. Invest 81:1545-1555.

Moore,H.P., R.B.Silver, E.P.Mottillo, D.A.Bernlohr, and J.G.Granneman. 2005. Perilipin targets a novel pool of lipid droplets for lipolytic attack by hormone-sensitive lipase. J. Biol. Chem. 280:43109-43120.

Muretta,J.M., I.Romenskaia, and C.C.Mastick. 2008. Insulin releases Glut4 from static storage compartments into cycling endosomes and increases the rate constant for Glut4 exocytosis. J Biol. Chem. 283:311-323.

Musi,N., andL.J.Goodyear. 2003. AMP-activated protein kinase and muscle glucose uptake. Acta Physiol Scand. 178:337-345.

Newsholme,E.A., andB.Crabtree. 1976. Substrate cycles in metabolic regulation and in heat generation. Biochem. Soc. Symp. 61-109.

Nye,C.K., R.W.Hanson, and S.C.Kalhan. 2008. Glyceroneogenesis is the dominant pathway for triglyceride glycerol synthesis in vivo in the rat. J Biol. Chem. (*Submitted*).

Odland,L.M., G.J.Heigenhauser, D.Wong, M.G.Hollidge-Horvat, and L.L.Spriet. 1998. Effects of increased fat availability on fat-carbohydrate interaction during prolonged exercise in men. Am. J. Physiol 274:R894-R902.

Okazaki,H., J.Osuga, Y.Tamura, N.Yahagi, S.Tomita, F.Shionoiri, Y.Iizuka, K.Ohashi, K.Harada, S.Kimura, T.Gotoda, H.Shimano, N.Yamada, and S.Ishibashi. 2002. Lipolysis in the absence of hormone-sensitive lipase: evidence for a common mechanism regulating distinct lipases. Diabetes 51:3368-3375.

Okuno,A., H.Tamemoto, K.Tobe, K.Ueki, Y.Mori, K.Iwamoto, K.Umesono, Y.Akanuma, T.Fujiwara, H.Horikoshi, Y.Yazaki, and T.Kadowaki. 1998. Troglitazone increases the number of small adipocytes without the change of white adipose tissue mass in obese Zucker rats. J Clin. Invest 101:1354-1361.

PASTAN,I., V.WILLS, B.HERRING, and J.B.FIELD. 1963. Pyridine Nucleotides in the Thyroid. I. A Method for the Measurement of Oxidized and Reduced Triphosphopyridine Nucleotides with the Use of 6-Pphosphogluconate-1-C14. J Biol. Chem. 238:3362-3365.

Patterson,B.W., J.F.Horowitz, G.Wu, M.Watford, S.W.Coppack, and S.Klein. 2002. Regional muscle and adipose tissue amino acid metabolism in lean and obese women. Am. J. Physiol Endocrinol. Metab 282:E931-E936.

Pellerin,L., G.Pellegri, P.G.Bittar, Y.Charnay, C.Bouras, J.L.Martin, N.Stella, and P.J.Magistretti. 1998. Evidence supporting the existence of an activity-dependent

astrocyte-neuron lactate shuttle. Dev. Neurosci. 20:291-299.

Petersen,K.F., M.Krssak, V.Navarro, V.Chandramouli, R.Hundal, W.C.Schumann, B.R.Landau, and G.I.Shulman. 1999. Contributions of net hepatic glycogenolysis and gluconeogenesis to glucose production in cirrhosis. Am. J. Physiol 276:E529-E535.

Petersen,K.F., T.Price, G.W.Cline, D.L.Rothman, and G.I.Shulman. 1996. Contribution of net hepatic glycogenolysis to glucose production during the early postprandial period. Am. J. Physiol 270:E186-E191.

Popel,A.S. 1989. Theory of oxygen transport to tissue. Crit Rev. Biomed. Eng 17:257-321.

Qvisth,V., E.Hagstrom-Toft, E.Moberg, S.Sjoberg, and J.Bolinder. 2007. Lactate release from adipose tissue and skeletal muscle in vivo: defective insulin regulation in insulin-resistant obese women. Am. J. Physiol Endocrinol. Metab 292:E709-E714.

Randle,P.J., P.B.Garland, C.N.Hales, and E.A.Newsholme. 1963. The glucose fatty-acid cycle. Its role in insulin sensitivity and the metabolic disturbances of diabetes mellitus. Lancet 1:785-789.

Reshef,L., andR.W.Hanson. 1972. The interaction of catecholamines and adrenal corticosteroids in the induction of phosphopyruvate carboxylase in rat liver and adipose tissue. Biochem. J 127:809-818.

Reshef,L., R.W.Hanson, and F.J.Ballard. 1969. Glyceride-glycerol synthesis from pyruvate. Adaptive changes in phosphoenolpyruvate carboxykinase and pyruvate carboxylase in adipose tissue and liver. J Biol. Chem. 244:1994-2001.

Reshef,L., Y.Olswang, H.Cassuto, B.Blum, C.M.Croniger, S.C.Kalhan, S.M.Tilghman, and R.W.Hanson. 2003. Glyceroneogenesis and the triglyceride/fatty acid cycle. J. Biol. Chem. 278:30413-30416.

Richter,E.A., J.N.Nielsen, S.B.Jorgensen, C.Frosig, and J.F.Wojtaszewski. 2003. Signalling to glucose transport in skeletal muscle during exercise. Acta Physiol Scand. 178:329-335.

Rigden,D.J., A.E.Jellyman, K.N.Frayn, and S.W.Coppack. 1990. Human adipose tissue glycogen levels and responses to carbohydrate feeding. Eur. J Clin. Nutr. 44:689-692.

Rothman,D.L., R.G.Shulman, and G.I.Shulman. 1992. 31P nuclear magnetic resonance measurements of muscle glucose-6-phosphate. Evidence for reduced insulin-dependent muscle glucose transport or phosphorylation activity in non-insulin-dependent diabetes mellitus. J. Clin. Invest 89:1069-1075.

Saggerson,E.D., andA.L.Greenbaum. 1970. The regulation of triglyceride synthesis and fatty acid synthesis in rat epididymal adipose tissue. Biochem. J 119:193-219.

Salem,J.E., G.M.Saidel, W.C.Stanley, and M.E.Cabrera. 2002. Mechanistic model of myocardial energy metabolism under normal and ischemic conditions. Ann. Biomed. Eng 30:202-216.

Samols,E., andG.C.Weir. 1979. Adrenergic modulation of pancreatic A, B, and D cells alpha-Adrenergic suppression and beta-adrenergic stimulation of somatostatin secretion, alpha-adrenergic stimulation of glucagon secretion in the perfused dog pancreas. J. Clin. Invest 63:230-238.

Samra,J.S., E.J.Simpson, M.L.Clark, C.D.Forster, S.M.Humphreys, I.A.Macdonald, and K.N.Frayn. 1996. Effects of epinephrine infusion on adipose tissue: interactions between blood flow and lipid metabolism. Am. J. Physiol 271:E834-E839.

Saunders,P.T., J.H.Koeslag, and J.A.Wessels. 1998. Integral rein control in physiology. J. Theor. Biol. 194:163-173.

Saunders,P.T., J.H.Koeslag, and J.A.Wessels. 2000. Integral rein control in physiology II: a general model. J. Theor. Biol. 206:211-220.

Schweiger,M., R.Schreiber, G.Haemmerle, A.Lass, C.Fledelius, P.Jacobsen, H.Tornqvist, R.Zechner, and R.Zimmermann. 2006. Adipose triglyceride lipase and hormone-sensitive lipase are the major enzymes in adipose tissue triacylglycerol catabolism. J. Biol. Chem. 281:40236-40241.

Serlie,M.J., J.H.de Haan, C.J.Tack, H.J.Verberne, M.T.Ackermans, A.Heerschap, and H.P.Sauerwein. 2005. Glycogen synthesis in human gastrocnemius muscle is not representative of whole-body muscle glycogen synthesis. Diabetes 54:1277-1282.

Shen,W.J., S.Patel, V.Natu, and F.B.Kraemer. 1998. Mutational analysis of structural features of rat hormone-sensitive lipase. Biochemistry 37:8973-8979.

Shulman,G.I. 2004. Unraveling the cellular mechanism of insulin resistance in humans: new insights from magnetic resonance spectroscopy. Physiology. (Bethesda.) 19:183-190.

Shulman,G.I., P.W.Ladenson, M.H.Wolfe, E.C.Ridgway, and R.R.Wolfe. 1985. Substrate cycling between gluconeogenesis and glycolysis in euthyroid, hypothyroid, and hyperthyroid man. J. Clin. Invest 76:757-764.

Shulman,R.G., andD.L.Rothman. 1996. Enzymatic phosphorylation of muscle glycogen synthase: a mechanism for maintenance of metabolic homeostasis. Proc. Natl. Acad. Sci. U. S. A 93:7491-7495.

Sigal,R.J., G.P.Kenny, D.H.Wasserman, and C.Castaneda-Sceppa. 2004. Physical activity/exercise and type 2 diabetes. Diabetes Care 27:2518-2539.

Sokoloff,L. 1973. Metabolism of ketone bodies by the brain. Annu. Rev. Med. 24:271-280.

Staples,J., andR.Suarez. 1997. Honeybee flight muscle phosphoglucose isomerase: matching enzyme capacities to flux requirements at a near-equilibrium reaction. J Exp. Biol. 200:1247-1254.

Stralfors,P., andR.C.Honnor. 1989. Insulin-induced dephosphorylation of hormone-sensitive lipase. Correlation with lipolysis and cAMP-dependent protein kinase activity. Eur. J Biochem. 182:379-385.

Strawford,A., F.Antelo, M.Christiansen, and M.K.Hellerstein. 2004. Adipose tissue triglyceride turnover, de novo lipogenesis, and cell proliferation in humans measured with 2H2O. Am. J. Physiol Endocrinol. Metab 286:E577-E588.

Stumvoll,M., S.Jacob, H.G.Wahl, B.Hauer, K.Loblein, P.Grauer, R.Becker, M.Nielsen, W.Renn, and H.Haring. 2000. Suppression of systemic, intramuscular, and subcutaneous adipose tissue lipolysis by insulin in humans. J. Clin. Endocrinol. Metab 85:3740-3745.

Summers,L.K. 2006. Adipose tissue metabolism, diabetes and vascular disease--lessons from in vivo studies. Diab. Vasc. Dis. Res. 3:12-21.

Sztalryd,C., G.Xu, H.Dorward, J.T.Tansey, J.A.Contreras, A.R.Kimmel, and C.Londos. 2003. Perilipin A is essential for the translocation of hormone-sensitive lipase during lipolytic activation. J. Cell Biol. 161:1093-1103.

Tansey,J.T., C.Sztalryd, J.Gruia-Gray, D.L.Roush, J.V.Zee, O.Gavrilova, M.L.Reitman, C.X.Deng, C.Li, A.R.Kimmel, and C.Londos. 2001. Perilipin ablation results in a lean mouse with aberrant adipocyte lipolysis, enhanced leptin production, and resistance to diet-induced obesity. Proc. Natl. Acad. Sci. U. S. A 98:6494-6499.

Tiessen,R.G., M.M.Rhemrev-Boom, and J.Korf. 2002. Glucose gradient differences in subcutaneous tissue of healthy volunteers assessed with ultraslow microdialysis and a nanolitre glucose sensor. Life Sci. 70:2457-2466.

Tordjman,J., G.Chauvet, J.Quette, E.G.Beale, C.Forest, and B.Antoine. 2003. Thiazolidinediones block fatty acid release by inducing glyceroneogenesis in fat cells. J. Biol. Chem. 278:18785-18790.

Trayhurn,P., andJ.H.Beattie. 2001. Physiological role of adipose tissue: white adipose tissue as an endocrine and secretory organ. Proc. Nutr. Soc. 60:329-339.

Trimmer,J.K., J.M.Schwarz, G.A.Casazza, M.A.Horning, N.Rodriguez, and G.A.Brooks. 2002. Measurement of gluconeogenesis in exercising men by mass isotopomer distribution analysis. J. Appl. Physiol 93:233-241.

Vicini,P., J.J.Zachwieja, K.E.Yarasheski, D.M.Bier, A.Caumo, and C.Cobelli. 1999. Glucose production during an IVGTT by deconvolution: validation with the tracer-to-tracee clamp technique. Am. J. Physiol 276:E285-E294.

Wahren,J., P.Felig, G.Ahlborg, and L.Jorfeldt. 1971. Glucose metabolism during leg

exercise in man. J. Clin. Invest 50:2715-2725.

Wahren,J., L.Hagenfeldt, and P.Felig. 1975. Splanchnic and leg exchange of glucose, amino acids, and free fatty acids during exercise in diabetes mellitus. J. Clin. Invest 55:1303-1314.

Wang,S.P., N.Laurin, J.Himms-Hagen, M.A.Rudnicki, E.Levy, M.F.Robert, L.Pan, L.Oligny, and G.A.Mitchell. 2001. The adipose tissue phenotype of hormone-sensitive lipase deficiency in mice. Obes. Res. 9:119-128.

Warram,J.H., B.C.Martin, A.S.Krolewski, J.S.Soeldner, and C.R.Kahn. 1990. Slow glucose removal rate and hyperinsulinemia precede the development of type II diabetes in the offspring of diabetic parents. Ann. Intern. Med. 113:909-915.

Wasserman,D.H., andJ.E.Ayala. 2005. Interaction of physiological mechanisms in control of muscle glucose uptake. Clin. Exp. Pharmacol. Physiol 32:319-323.

Wasserman,D.H., andA.D.Cherrington. 1991. Hepatic fuel metabolism during muscular work: role and regulation. Am. J. Physiol 260:E811-E824.

Wasserman,D.H., andA.E.Halseth. 1998. An overview of muscle glucose uptake during exercise. Sites of regulation. Adv. Exp. Med. Biol. 441:1-16.

Wasserman,D.H., andM.Vranic. 1986. Interaction between insulin and counterregulatory hormones in control of substrate utilization in health and diabetes during exercise. Diabetes Metab Rev. 1:359-384.

Way,J.M., W.W.Harrington, K.K.Brown, W.K.Gottschalk, S.S.Sundseth, T.A.Mansfield, R.K.Ramachandran, T.M.Willson, and S.A.Kliewer. 2001. Comprehensive messenger ribonucleic acid profiling reveals that peroxisome proliferator-activated receptor gamma activation has coordinate effects on gene expression in multiple insulin-sensitive tissues. Endocrinology 142:1269-1277.

Welch,G.R., andJ.S.Easterby. 1994. Metabolic channeling versus free diffusion: transition-time analysis. Trends Biochem. Sci. 19:193-197.

Xiang,S.Q., K.Cianflone, D.Kalant, and A.D.Sniderman. 1999. Differential binding of triglyceride-rich lipoproteins to lipoprotein lipase. J Lipid Res. 40:1655-1663.

Yang,Y.J., I.D.Hope, M.Ader, and R.N.Bergman. 1989. Insulin transport across capillaries is rate limiting for insulin action in dogs. J Clin. Invest 84:1620-1628.

Zechner,R., J.G.Strauss, G.Haemmerle, A.Lass, and R.Zimmermann. 2005. Lipolysis: pathway under construction. Curr. Opin. Lipidol. 16:333-340.

Zhou,L., J.E.Salem, G.M.Saidel, W.C.Stanley, and M.E.Cabrera. 2005. Mechanistic model of cardiac energy metabolism predicts localization of glycolysis to cytosolic subdomain during ischemia. Am. J. Physiol Heart Circ. Physiol 288:H2400-H2411.

Zimmermann,R., J.G.Strauss, G.Haemmerle, G.Schoiswohl, R.Birner-Gruenberger, M.Riederer, A.Lass, G.Neuberger, F.Eisenhaber, A.Hermetter, and R.Zechner. 2004. Fat mobilization in adipose tissue is promoted by adipose triglyceride lipase. Science 306:1383-1386.